Long-Acting Release Implants for Local Fenretinide Delivery and Oral Cancer Chemoprevention

by

Kari Jo Nieto

A dissertation submitted in partial fulfillment
of the requirements for the degree of
Doctor of Philosophy
(Pharmaceutical Sciences)
in the University of Michigan
2017

Doctoral Committee:

Professor Steven P. Schwendeman, Chair
Professor Susan R. Mallery, Ohio State University
Professor Naír Rodríguez-Hornedo
Professor Gustavo Rosania

Kari J. Nieto

kariblai@umich.edu

ORCIDiD 0000-0002-1955-2361

DEDICATION

To my number one and husband Abel Nieto, and parents Kevin and Karen Blain.

ACKNOWLEDGEMENTS

Abel, you have been a good listener and offered suggestions when I was struggling, including teaching yourself calculus to help me with my painstaking biophysics homework. Thank you Dad and Mom for teaching me the importance of hard work, discipline, and attitude. I have done my best to stay as busy, productive, and get as much done as you. Thank you to my mother and father-in law whom have welcomed me with open arms into their family as Abel and I married the first year of graduate school. Thank you to my sister and brother-in-law and their full of life family, whom have been a major source of fun and joy.

And finally, thank you to all of the unnamed individuals who have believed in me and helped me along this journey. Life is full of teachers and lessons, and I have been so fortunate to have learned from the best. I will leave you with a final quote by the great mind Albert Einstein;

"Logic will take you from A to B. Imagination will take you everywhere."

TABLE OF CONTENTS

CHAPTERS

LIST OF FIGURES

LIST OF TABLES

LIST OF APPENDICES

ABSTRACT

The synthetic vitamin A derivative, fenretinide (4HPR) was developed in the 1970's as a means to induce retinoid cancer preventive effects in cells and tissues devoid of the retinoic acid receptor, and has become an important compound for chemoprevention of a variety of cancers such as oral squamous cell carcinoma (OSCC). However, OSCC chemoprevention clinical trials with orally delivered 4HPR have been unsuccessful likely due to extensive first pass metabolism, systemic toxicity, and sub-therapeutic levels of 4HPR at the target site. Local 4HPR delivery vehicles have the potential to deliver therapeutic doses while alleviating any systemic side effects. Limited penetration distance of the drug in tissues, however, is one of the most prevalent challenges with the local delivery approach. To overcome these limitations and to increase drug exposure at the site of action, solubilizers and permeation enhancers were combined with 4HPR in local delivery depots, and their drug release kinetics *in vivo* and 4HPR's tissue uptake in presence of solubilizers *ex vivo* were evaluated. Long-acting release of 4HPR from injectable millicylindrical implants were prepared with poly(lactic-*co*-glycolic acid) and polyvinyl alcohol (PVA)/sucrose matrices as a function of drug loading and the presence of various excipients to enhance the release of the water-insoluble 4HPR. 4HPR was released from PLGA implants much slower *in vivo* than in the Tween 80-solubilizing media *in vitro*, with a 3-week lag phase followed by continuous release of >2 months, and showed some release enhancement by addition of solubilizers. The water-soluble PVA/sucrose implant provided continuous drug release for up to 6 weeks *in vivo*. These 4HPR-PLGA formulations were further evaluated in an oral cancer xenograph mouse model, and shown to be effective at reducing rate of tumor growth

over 10 days. A remarkable solubility enhancing formulation was achieved with 4HPR amorphous solid dispersions (ASDs) prepared with polvinylpyrrolidone (PVP) polymer. The PVP-4HPR ASD was loaded into PLGA implants and evaluated *in vivo*, and found to substantially improve release kinetics from previous crystalline 4HPR formulations. Tissue binding kinetics was characterized in buccal epithelia and subcutaneous tissues in presence of various solubilizing and permeation enhancing media. Time of exposure, but not solubilizer or permeation enhancers, affected uptake and 4HPR exhibited a five-fold greater binding affinity to buccal epithelia relative to subcutaneous connective tissues. These optimized long-acting 4HPR millicylindrical implants were further evaluated *in vivo* over 2 weeks in rabbit buccal epithelia, for their ability to enhance drug-tissue distribution. Quantitative Raman spectroscopic imaging was utilized to measure drug-tissue concentration gradients in excised tissue sections. The implants released much faster in the mouth compared to our previous studies in s.c. tissue, and the drug penetration in the buccal tissues (i.e. distance to reach 10% of concentration at implant surface, or C_{10}) was on the order of 0.5- 8 mm for all formulations. The ASD of 4HPR in PLGA provided the greatest drug penetration through tissues, likely as a result of supersaturated drug concentrations next to the implant. Hence, these approaches may be useful for local delivery of 4HPR and OSCC chemoprevention.

Chapter 1: Introduction

1.1. Oral Cancer Disease State and Treatment

Oral squamous cell carcinoma (OSCC) is a worldwide health concern, and in 2016, ~50,000 Americans were newly diagnosed with oral or pharyngeal cancer(1). The risk factors associated with OSCC include smoking, alcohol consumption, human papillomavirus (HPV) infection, and Epstein-Barr virus(EBV) (2). The vast majority of oral cancers arise from malignant transformation of preneoplastic surface epithelial lesions(3). Despite treatment advances that include intraoperative radiation, the 5-year survival rates of persons with OSCC is discouraging low (50%) (2). Following initial therapy, oral cancer patients are managed by close clinical follow-up often supplemented with imaging studies. Despite vigilant monitoring and well-recognized risk factors for recurrence, over one third of patients develop life-threatening and often untreatable recurrent OSCCs (4). Replacement of the current "watchful waiting" strategy with well-tolerated and effective secondary OSCC chemoprevention could make a significant clinical impact for these individuals. As OSCC management requires extensive, often disfiguring surgery, treated OSCC patients often experience depression and reduced motivation.

Development of an implantable delivery system capable of providing therapeutic drug levels while alleviating systemic side effects and improving patient compliance issues could advance secondary OSCC chemoprevention. The synthetic vitamin A derivative, 4-hydroxy(phenyl)retinamide [fenretinide (4HPR)] was developed in the 1970s as a means to

induce retinoid cancer preventive effects in cells and tissues devoid of the retinoic acid receptor (5). Previous studies from our labs have demonstrated that 4HPR inhibits focal adhesion kinase (FAK)-ECM interactions and significantly reduces invasion, which is the ultimate step in OSCC development(6). To address OSCC's redundant signaling cascades, secondary OSCC chemoprevention will ultimately require complementary agents (7). Based on fenretinide's multiple mechanisms of action including growth regulation and suppression of gratuitous signaling (8), it is our intention to include fenretinide (4-HPR) in the secondary chemopreventive formulation.

1.2. Fenretinide (4HPR) for Oral Cancer Chemoprevention

1.2.1. 4HPR Clinical Trial Results

One of the first studies utilizing 4HPR as a chemopreventive was done in 1994 by Tradati *et* al, where topical application (100 mg b.i.d. x 2 months) for treatment of oral leukoplakia/lichen planus resulted in regression of lesions, with no adverse side effects and minimal systemic drug levels (9). The clinical trials (2005) with oral administration of 4HPR at low doses (100 mg p.o. b.i.d.), showed that 4-HPR protected against recurrent lesions, but its overall efficacy was unclear. An additional study of low dose (200 mg p.o. q.d. x 3 months) given to non-excised oral epithelia dysplasia (OED) lesions showed reduction of lesion size in 34% of patients (10). In high dose studies (900 mg/m^2 p.o. b.i.d. in 3 weeks cycles), low response rates led to discontinuation of the study (11). Despite some promising results of decreased lesion size in these clinical trials, the orally dosed route failed due to inability to achieve therapeutic levels, even at high doses(4). These high doses often were associated with severe side effects, including nyctalopia, hyperlipidemia, and dry skin. These studies also

failed to fully evaluate local pharmacokinetic (PK) parameters including tissue concentrations, metabolite formation, and drug stability and release kinetics(4).

1.2.2. 4HPR Pharmacological Mechanisms

I*n vitro,* 4HPR demonstrated extensive cancer prevention (chemopreventive) promise by its abilities to induce terminal differentiation and/or apoptosis in a variety of epithelial and neural origin premalignant and malignant cells (12, 13). *In vitro* efficacy did not translate, however, to clinical efficacy (14-16) where human OSCC chemoprevention clinical trials using oral/systemic 4-HPR delivery were unsuccessful (4). These findings likely reflect extensive 4HPR inactivation during first pass metabolism coupled with an inability to achieve therapeutic levels in the oral cavity(4), while systemic side effects e.g. mucositis, nyctalopia and increased sera lipids were observed (16, 17). 4HPR can bind with high affinity to selected proteins e.g. retinol binding protein, focal adhesion kinase (6, 18), STAT3 (7), which opens the prospect that tissue bound 4HPR could serve as a local drug reservoir. Furthermore, for optimal cancer prevention efficacy, 4HPR also needs to induce tumor suppressive effects on the connective tissue stroma and infiltrating inflammatory cells as well as the premalignant lesional cells (19). 4HPR has the antineoplastic effects of Vitamin A, but also has a decreased resistance-induction and toxicology profile (20). 4HPR has been shown to modulate thiol dependent proteins that are responsible for redox-signaling and growth regulation are important in chemoprevention (21-23). Long-term efficacy with 4HPR is plausible due to its receptor-independent induction of apoptosis. It has been shown *in vitro* that high 4HPR concentrations (10 μM) induced apoptosis through a receptor-independent pathway, and low concentration (1 μM) promoted epithelial differentiation through a receptor-mediated pathway (20).

1.2.3. 4HPR Physiochemical Properties and Pharmacokinetics

4HPR (Fig.1-1) is a highly lipophilic compound, with a logP of 6.31(24). 4HPR is nearly insoluble in aqueous solutions, making it a cumbersome compound to develop into an effective drug product. 4HPR has a phenyl-amide group that possesses three proton-accepting sites as well as two proton donors, that is connected to the parent retinoid structure of a conjugated poly-olefin chain and cyclohexenyl ring. This highly conjugated molecule gives rise to its bright yellow color, strong UV absorption at 365 nm with molar absorptivity (ε) of 47,900 $M^{-1} \cdot cm^{-1}$. The phenyl-amide group gives 4HPR more surface activity than other retinoids (25). Discrepancies may arise from observed versus predicted solubilities due to tendency of retinoids to aggregate (25). Additional formulation challenges can arise during *in vitro* experiments when high levels of surfactants are used for 4HPR solubilization, which do not produce physiologically meaningful data (26, 27). Therefore it becomes difficult to predict release and tissue distribution behavior based on standard *in vitro* testing methods. In addition to its low aqueous solubility, 4HPR is subject to photodegradation and oxidative degradation which is most pronounced in organic solvents. 4-HPR is stable in its solid state(24) and multiple polymorphs do exist.(28)
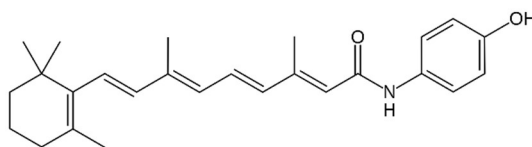
Figure 1-1. Fenretinide (4HPR) chemical structure, a chemotherapeutic molecule.

Human pharmacokinetic (PK) data obtained from previous 4-HPR clinical trials with 200-1000 mg daily oral dosing demonstrated that 4HPR is retained in tissues (20%)(29), rapid equilibrium occurs in plasma (<24 h)(29), has greater preference for tissue than plasma, max plasma levels are achieved after 4 h (Tmax) (15), half live ($t_{1/2}$) is 12-24 h (14-16) and is

detected in blood even 6 mo. post-treatment indicating bioaccumulation (16). When dosed

orally, 4HPR exhibits high first pass metabolism into its primary metabolites including the

oxidized 4HPR (4-oxo-HPR), hydroxyl-4HPR (4-OH-HPR), methylated 4HPR (4-MPR), and

glucuronidated 4-HPR. 4-MPR is inactive and is the primary outcome of 4-HPR as it passes

through the liver. While the human oral cavity does not contain enzymes that can methylate 4-

HPR, it does possess the enzymes capable of oxidative bioactivation and the glucuroniated

metabolite capable of enteric recycling. Nude mouse tissue, however, may be capable of

methylating 4-HPR. The 4-oxo-HPR metabolite is active and has been shown to have

chemotherapeutic properties. Additionally, little or no free retinol, retinaldehyde or retinoyl

esters are excreted from body following intravenous (IV) injection of 4HPR, indicating

extensive metabolic degradation is occurring(30).

Poor therapeutic tissue levels of 4HPR can be related to its physicochemical properties

and non-specific binding to tissue components. Highly lipophilic drugs generally have greater

tissue permeability due to partitioning and accumulation into the cells phospholipid bilayer.

However, for extremely lipophilic drugs (logP >3.5), the permeation is actually decreased due

to high aqueous insolubility and excessive accumulation in the subcutaneous (SC) fat deposits

(29). 4HPR across Caco-2 monolayers was investigated, and where it was suspect that many

factors could contribute to poor oral absorption of 4HPR, including low solubility/dissolution,

paracellular transport component of passive diffusion, drug efflux by the transporter p-

glycoprotein (P-gp), transport via saturatable carrier-mediated transporters, degradation and

metabolism, and accumulation in the cell membrane.(31) The results of that study showed that

transport of 4HPR through Caco-2 cells occurs by transcellular passive diffusion, and poor

permeation of 4HPR was attributed to its accumulation in the lipophilic cell membrane and poor partitioning into the receiver medium (solubility issues)(31).

Biological molecules, such as sera protein albumin, can stabilize drugs and prevent their clearance from tissue. The high propensity of 4HPR to precipitate with plasma proteins leads to a decrease of active drug at the target site. This high plasma binding is characteristic of retinoids, such as retinol, where little to no free retinol is transported in the body, due to its exclusive binding to the carrier protein retinol binding protein (RBP) present on cell surfaces (30). 4HPR displaces vitamin A on sera retinol binding protein with 100-fold greater affinity (17), results that demonstrate 4HPR is capable of high-affinity protein binding. RBP then forms a complex with pre-albumin to prevent loss by ultrafiltration in the kidney, thereby contributing to slower clearance of the drug-protein complex (30).

1.3. Oral Cavity Properties and Drug Formulation Considerations

1.3.1. Oral Epithelium Properties

The oral cavity is an attractive site for local and systemic drug delivery routes due to a high degree of vascularization leading to greater permeability. In particular, the non-keratinized tissues of the oral mucosa are preferred over keratinized sites. Nearly all compounds are capable of traversing these tissues, yet their rate depends upon their size and chemical nature. The permeability of the oral mucosa is protected by several barriers, including intercellular boundaries caused by membrane coated granules in stratified squamous epithelium, basement membranes, lipids, and saliva containing high molecular weight mucins (MG1) (32). The mucosal layer functions include: clearance mechanisms, water balance, ion transport and regulation, lubrication, diffusion barrier, creating a barrier to drug absorption (33).

The surface area of the human oral mucosa is 200 cm^2 and is highly vascularized, multi-stratified, and is either keratinized or non-keratinized contingent upon location. Drug permeation through the mucosa occurs via both transcellular and paracellular routes (34). The buccal region has three distinct tissue layers (Fig. 1-2): epithelium, basement membrane, and connective tissue. The thickness of the buccal epithelium (in humans) is 500-800 μm, or 8-10 cells, and its turnover rate is 28 days (32). The mucus coating the buccal epithelium is 0.1-0.7 mm thick. Three types of overlying stratified epithelium is present in different regions including: masticatory mucosa, lining mucosa, and buccal mucosa(32). Masticatory mucosa covers the gingival and hard palate and consists of keratinized epithelium closely resembling the epidermis of skin. It is usually tightly attached to collagenous connective tissue. Lining mucosa covers all other regions except the dorsal surface of tongue, and has the ability to stretch, and is composed on non-keratinized stratified squamous epithelium. Lining epithelium is attached by loose, elastic connective tissue underlying structures. The buccal mucosa epithelium is the least permeable site, while the floor of the mouth has the highest permeability, and most extensive vascularity, hence it is a popular delivery site for sublingual medications. The lining regions of the floor of mouth and lateral border of tongue have been deemed high risk sites for OSCC. Additional layers of the epithelium in oral cavity include the corium and submucosa that contain minor salivary glands and other secretory glands, blood vessels, fat, fibrous tissue, and white blood cells. The types of cells present in healthy oral epithelium include melanocyte, Langerhans cells, and Merkel cells. Following local trauma, infection, or an immune response, granulocytes, histiocytes and lymphocytes are also present.
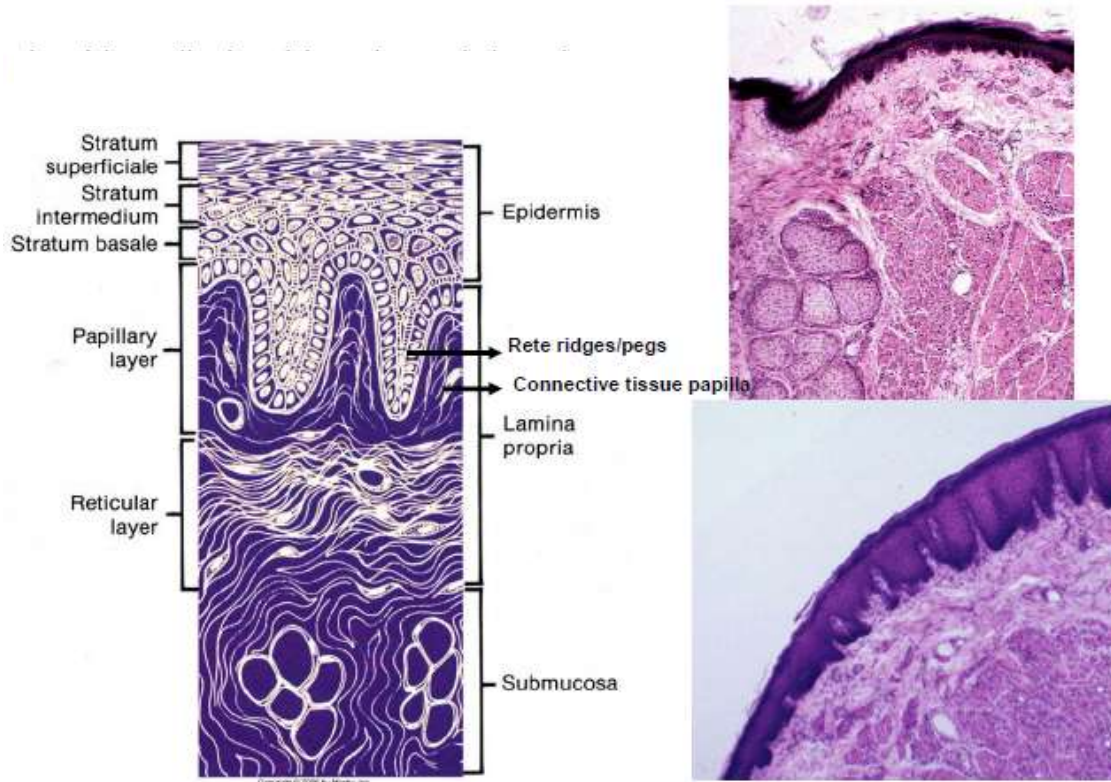
Figure 1-2. Structure of the oral mucosa, including the overlying oral epithelium and underlying connective tissue (lamina propria and submucosa) (32).

1.3.2.   Factors Affecting Oral Mucosa Permeability

The permeability of the mucosa may be increased under certain circumstances, and is most often observed in undifferentiated epithelial cells that may be present near the teeth, during consumption of alcohol, through use of toothpastes containing surfactants, or in lesions that facilitate uptake of water.(32) Although premalignant oral lesions are most often seen in tobacco users, persons with negative social histories are still susceptible. Depending upon the lesion grade, 4 to 95% of the lesions can undergo malignant transformation(32). Inflammation is a common condition that can occur in the mouth, and can lead to reduced keratinization, and subsequently greater permeability. Age of an individual can affect the characteristics of the oral epithelium, and concerns of whether thinning skin or other changes can lead to decreased

permeability are debatable. Cancer therapies including chemotherapeutics and radiation can limit the proliferative capacity of the epithelium making it thinner or ulcerated, as well as reduction of salivary mucins, both compromising barrier function(32). Permeability of some drugs through the buccal mucosa was found to increase when their carrier system decreased the pH of the mucosa (35).

1.3.3. Animal Models for Studying Oral Drug Delivery

Rabbits, dogs, and pig animal models are ideal for studying delivery to oral cavity due to the histological similarities to humans (36). The mucosa in rabbits and dogs is non-keratinized and the thickness of rabbit mucosa (600 µm) is similar to humans. The epithelial cheek pouch in rabbits differs slightly from humans in that it is slightly keratinized, and the identification and isolation of non-keratinized regions can be difficult. Nonetheless, the rabbit model provides ample surface area to work with and are more economical to use than dogs. Rats and mice are less ideal models to use due to a greater abundance of keratinized tissues present. Although the oral epithelium of dogs and monkeys is non-keratinized, it is much thinner than humans, and therefore more permeable. Pig buccal mucosa is frequently used due to its similar molecular composition to human, as well as its ease and low cost of tissue acquisition (34). Separation of pig buccal mucosa epithelium from connective tissue results in epithelium thickness of 150 µm(34). Table 1-1 below outlines the various characteristics of buccal mucosa in different mammals.

Table 1-1. Comparison of buccal mucosa of different mammals (34)

Animal Model	Tissue structure	Buccal membrane thickness (µm)	Permeability constant for titrated water (x 10^7 cm/min)
Human	Non-keratinized	580 ± 90	579 ± 122
Dog	Non-keratinized	126 ± 30	1045 ± 37
Hamster	Keratinized	115.3 ± 11.5	n.d.
Pig	Non-keratinized	772 ± 150	634 ± 40
Rabbit	Partially keratinized	600	n.d.
Rat	Keratinized	n.d.	n.d.
Monkey	Non-keratinized	271 ± 50	1025 ± 154

n.d.= not determined
Data represents mean ± SD

1.4. Local Drug Delivery Systems

Some cancers can metastasize throughout the body, making systemic drug administration necessary, while other types of cancer such as OSCC, are bound to specific visible locations and would most likely benefit from local delivery of chemotherapeutics. Notably, local delivery formulations provide a pharmacologic advantage via provision of therapeutic levels to the target site without eliciting systemic effects. One of the challenges of delivering a drug locally is the drug's limited penetration distance in tissue. Previous research done by the Saltzman group(37-41) found that the penetration distance of a the drug released from an implantable polymer device in the brain was at most 3 mm from center of the device, while the highest concentrations occurred at a penetration distance of only 1 mm. In this research, we will be formulating millicylindrical implants for local delivery, so we will limit the discussion of types of local delivery vehicles to the following sections.

1.5. Factors Affecting Drug-Tissue Distribution

1.5.1. Overview

Limited penetration distance is the most prevalent challenge encountered during local drug delivery (39, 42). Not surprisingly, there are many factors that govern drug distribution in tissues including: rates of diffusion, convection, elimination, protein binding, cellular uptake, capillary permeation, degradation and permeability into cell and subcellular components (which may lead to bioaccumulation), and finally intracellular metabolism and efflux (43). Upon administration of an implantable/injectable device, the drug moves from the devices' matrix to the extracellular space (ECS) along a concentration gradient, or by convecting interstitial fluid. Consumption of molecules occurs via binding to tissue elements (including target receptors and non-specific), which can then be internalized or metabolized. Additionally, drug molecules can permeate blood vessels and then be transported into systemic circulation, leading to biotransformation, or elimination. Diffusion through tissue interstitium is a slow process, and during this period of migration extensive metabolism or clearance can occur(43). As a result, the volume of tissue exposed to the delivered drug is small. A drug's fate can be described in detail in terms of absorption, distribution, metabolism, and elimination also known as ADME.

1.5.2. Drug Absorption

Regardless of the route of administration, a drug must cross several cell or basement membranes before it reaches its target tissue. Drugs and other molecules move across cellular membranes by several processes such as: bulk flow or convection, passive diffusion, facilitated or active transport, and pinocytosis. Of these, passive diffusion and convection is most

important in xenobiotics. Diffusion mediated processes are governed by movement of drug along a concentration gradient, while convection occurs along a bulk flow of a liquid. Convection processes have a significant effect on drug delivery to tumor vascular space. The change in concentration can be expressed as a sum of diffusion and convection processes in Ficks 2nd law:

$$\frac{\partial c}{\partial t} = D \frac{\partial^2 c}{\partial x^2} + v \frac{\partial c}{\partial t}$$

Small hydrophilic drugs (100-200 Da) generally travel through epithelium via paracellular transport (between adjacent cells), and movement of molecules is limited by presence of tight junctions (44). Permeation enhancers are often used to allow paracellular absorption of large hydrophillic molecules (44). Hydrophobic drugs are most likely to pass via a transcellular pathway (through the cells) (44). Once the hydrophobic drug has partitioned into the cell membrane, it can be absorbed transcellularly via passive diffusion or by specialized transporters, such as P-glycoprotein (P-gp). In some cases drugs can be absorbed by transcytosis, a process by which exogenous substances are engulfed into vesicles of polarized cells and released at other side of cell. If, in this process, the vesicle fuses with lysosomes, the drug will be degraded. Alternatively, a drug exhibiting similar structural homology to endogenous compounds, could bind to a receptor, resulting in endocytosis, and eventually leading to drug degradation.

1.5.3. Drug Distribution

Upon parenteral delivery of a drug, it comes into contact immediately with a vast number of capillaries. Most of the 10^{13} cells in the body are within a few cell diameters of a blood vessel, thereby making delivery of oxygen and nutrients to and from tissues possible

(45). Notably, while the human oral surface epithelia is directly exposed to oxygen it is avascular and therefore dependent upon the underlying connective tissue vasculature for nutrients. Blood vessel properties affecting clearance include: total surface area, average separation between blood vessels, wall thickness (permeability), volume/blood flow profile in skin, and variability in these properties can occur at given depths of skin (46). Highly lipophilic drugs will have high capillary permeability, leading to a greater drug elimination from injection site. Solutes traverse the pores in the capillary wall by a combination of 2 processes: diffusion and filtration. Diffusion is the primary mode of transport for lipid-insoluble molecules. Most drugs can rapidly permeate capillaries at a rate much faster than they can traverse other membranes, and thus the rate limiting step for the movement of molecules through tissue is based on rate of blood flow rather than capillary permeability.

Understanding and elucidating the microvascular patterns in regular and irregular tissues is important for prediction of drug delivery to those tissues. The vascular network of oral mucosa was characterized by analysis of space-filing properties (local fractal dimension, D), tortuosity (fractal dimension of the minimum path, Dmin), and randomness (47). Blood microvessels distribution in normal skin is most abundant approximately 0.1 mm below skin surface (46). Total blood vessel area was found to decrease quasi-exponentially to a depth of approx. 0.75 mm, but can vary between sites.

Absorption of an injected drug usually occurs within 30 min, however absorption can be delayed in presence of s.c. fat, which act as barriers to transport. Both the human buccal fat pad and the fatty zone of the anterior hard palate are lipid rich sites in the oral cavity. The rate of absorption can be prolonged by incorporation of vasoconstrictors, conversion of drug into a less soluble form, injection of depots or implants, or administration of insoluble

microcrystalline suspension(48). Cell membranes and macromolecules in extracellular space (ECS) are transport barriers that increase diffusion path length. Therefore, differences are expected between free diffusion coefficient in solution (D_f) and apparent diffusion coefficient in tissue (D_b). The ratio of D_f to D_b is defined as the square of the tortuosity (t^2), and increases when more barriers to drug traveling through ECS are present. Other factors that can affect diffusion include molecular size and shape, electrostatic interactions, and protein binding.

After absorption into the blood stream, drugs can be distributed to all parts of the body. Compounds that can permeate freely through membranes are distributed in body water to both extracellular and intercellular fluids. Compounds that are only able to permeate capillaries are only distributed into the extracellular space. Often times, a drug is highly protein bound, and remains in the intravascular space after injection. Drugs can be readily redistributed in the body where there is a rich vascular supply, such as the brain or within the tumor environment. Over time, the plasma concentration falls, and the drug diffuses back into circulation for redistribution. The drug can also accumulate in lipid-rich tissues with poor blood supplies, and is especially true for highly lipophilic drugs. Often, drugs are not distributed equally within the body, but rather accumulate in specific tissues. For example, basic drugs tend to concentrate in areas with pH lower than the pKa and acidic drugs tend to concentrate in areas with a greater pH than the pKa.

Drug-protein binding can enhance or detract from the drugs bioavailability and performance. Only unbound drugs are able to freely move from one compartment to another and exert their pharmacological effect. Drugs may bind to a wide variety of plasma proteins including: most commonly albumin, but also lipoproteins, glycoproteins, and globulins.

Albumin is an alkaloid, so it will bind neutral or acidic molecules, but once it becomes

saturated, molecules will begin to bind to lipoproteins. Basic molecules are likely to bind to α1

acid glycoproteins. Generally, drugs that have low protein binding are able to penetrate the

tissue better than those that have high protein binding, however lower binding can lead to

faster clearance. As a rule of thumb, if drug-protein binding is < 90%, then it is likely to have

good performance, however if it is >99% bound, it is likely to significantly impact

performance. For drugs that undergo slow metabolism, changes in unbound fraction of drug

directly influence the clearance of the drug. Changes in level of free drug change the volume

of distribution (V_d) because free drug may distribute into tissue and lead to a decrease in

plasma concentration. The fraction of drug unbound (fu) can be expressed in terms of free

drug [D] and drug-protein complex [DP]:

$$fu = \frac{[D]}{[D] + [DP]}$$

1.5.4. Drug Elimination

Drugs can be eliminated from the active site by capillary transport and by cellular

uptake leading to drug degradation or metabolism. As already discussed, drugs with high

binding affinity have slower elimination rates and longer half-lives due to the ability to evade

clearance mechanisms. An advantage of local drug delivery is the ability to bypass extensive

degradation by eliminating the first-pass effect. When a foreign molecule enters the cell, the

cell has mechanisms for detoxifying and degrading it such as pH dependent degradation or

enzymatic degradation. The purpose of metabolic processes it to render the drug more

hydrophilic and less potent so that it may be excreted from the system. Degradation process

can occur by either Phase 1 or Phase 2 metabolism; by oxidative/reductive reactions with

CYP450 or other enzymes or through conjugation reactions (glucuronidation, sulfation, acetylation) respectively.

1.5.5. Drug-Tissue Penetration Equations

Penetrability is defined as the ability of an agent to migrate through tissue, or more specifically, the ability of drug molecules deposited in interstitial space to navigate through tissue without loss of activity (43). Drug penetration is a function of dispersivity and elimination. Dispersivity can be characterized by the diffusion coefficient, rate of fluid flow in tissue, and extent of tissue binding. The relationship between these factors can be summarized by the diffusivity/elimination modulus, φ, and is an effective way to characterize drug penetration (49):

$$\varphi = L \times \sqrt{\frac{k}{D}}$$

where L is the half thickness of delivery device, k is the elimination rate constant, and D is the dispersivity constant. Additionally, the effectiveness of local drug delivery (η) can be calculated based on the diffusion/elimination modulus(49):

$$\eta = \frac{1}{\varphi}[1 - \exp(-\varphi)]$$

In vivo studies conducted to determine the drug penetration distance often involves determining drug concentration in thinly sliced tissue sections. Using the semi-infinite slab model(50), the drug concentration in tissue sections can be transformed into infinite homogeneous space (where C_o is the concentration tissue/device interface):

$$C(x) = C_0 e^{-x(\frac{k}{D})^{1/2}}$$

The penetration distance is related to elimination/diffusivity modulus (φ). At large φ values, elimination dominates over diffusion, while a lower φ favors diffusion, and consequently a larger penetration distance. The modulus φ can be related to the treatment area, for example to find the area where drug concentration is greater than 10% of maximum value ($C > 0.1C_0$), then the penetration distance equation becomes:

$$Penetration\ distance = x - L = \frac{ln10}{\sqrt{\frac{k}{D}}}$$

For most drugs, the concentrations decreases exponentially the further away from implanted medical device, and is typically on the order of 1-3 mm(50). Research by Saltzman studied the penetration distance of the cytotoxic drug carmustine from a polymeric implant in a rat brain for glioblastoma treatment, and found the drug penetration distance is maximized with a lower φ values, (diffusion is faster than elimination) with distances ranging from 1 mm to 6 mm, shown in Fig 1-3(43).
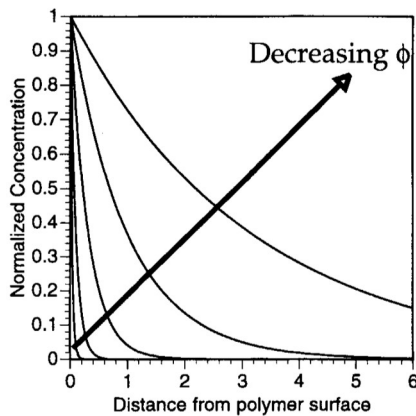
Figure 1-3. Drug (carmustine) tissue-penetration from locally delivered polymeric implant in rat brain, as a function of elimination/diffusion modulus (φ).

In some cases, a three compartment pharmacokinetic model is used to describe distribution to the tissue adjacent to the delivery device including; extracellular matrix (ECM), intracellular space (ICS), and cellular membrane (CM). The molar concentration of drug per total tissue volume, **C,** can be expressed as:(41)

$$C = \alpha \cdot C_{ECM}^{O} + \beta \cdot C_{ICS}^{O} + (1 - \alpha - \beta) \cdot C_{CM}^{O}$$

Where α and β are the volume fractions of ECS and ICS, respectively; C_{ECS}^{0}, C_{ICS}^{0} and C_{CM}^{0} indicate the moles of drug per phase volume. Water soluble drugs distribute most readily in ECM and are therefore able to efficiently diffuse around cells.(45) Conversely, lipid soluble drugs are usually able to have greater penetration into lipid membranes and be transported intracellularly.

1.6. Tumor Targeting

The local environment of a tumor makes it difficult to target for drug delivery, due to its lack of vascular density, and thereby the cell's distance from blood vessels which supply nutrients and also transport drugs, is vastly larger (>100 µm) than normal tissue. The rapid proliferation of tumor cells force blood vessels apart, leading to irregular blood flow, compression of blood and lymphatic vessels by cancer cells, and ultimately hypoxic regions in the tumor(45). Additionally, this poor organization of vasculature can cause increased interstitial fluid pressure (IFP), and decreased movement of molecules through the ECM due to reduced convection(45). The ECM is known to have a rapid turnover rate, so modification of the ECM has the potential to alter penetration of drugs through tissue. To target the tumor extravascularly by the enhanced permeation and retention (EPR) effect, particles should be in the size range of 200-400 nm.

It is expected that drug release rate from a local delivery vehicle into the tumor will be influenced by the type of tumor environment due to expansion or compression exerted on the implant (non-necrotic tumor > necrotic tumor > SC > in vitro) (51). The convective forces *in vivo* are likely to increase solvent and drug efflux, leading to a greater release *in vivo* than *in vitro*. Differences in tissue perfusion will also affect drug release rates, and is expected that the relatively avascular network of necrotic tumor will be slower than the more vascularized subcutaneous space due to increased drug elimination and a larger concentration gradient.

1.7. Solubilization Strategies for Hydrophobic Drugs

Many techniques have been employed in attempt to increase aqueous solubility of a poorly soluble drug molecule, including 4HPR and other retinoid derivatives, including: micellar solubilization(25, 52) reduction in particle size via milling, conjugation with amphilphilic moieties(53, 54), complexation to dextrans(55), PEGylation(52), encapsulation into PLGA polymeric systems including microparticles (24,56,57), liposomes(58,59), lipid-based emulsions, formation of drug-salt (54), or formation of co-crystals (60) to name a few (61). Previous work by our lab had determined 4HPR solubility parameters in selected organic solvents along with various excipients (24, 26, 27). A comprehensive compilation of 4HPR solubility in organic solvents, surfactants, polymers and proteins can be found in Appendix 1. Solubilization agents are classified as those that inhibit crystal formation by forming drug complexes (PVP, β-cyclodextran, PEG 8000), or micelle forming nonionic surfactants with high HLB values such as Tween80 and citrate esters (35). The potential for excipient related toxicity should be taken into consideration, and pharmaceutical excipients acceptable for human use can be referenced in the *Handbook of Pharmaceutical Excipients* (by Rowe, Sheskey and Weller, 4th ed, 2003), or commercial approved product references such as USP

30/NF 25 (2006), *Physician's Desk Reference* (57th ed 2003), FDA's website on inactive ingredient guide (IIG), or deemed *Generally Regarded as Safe* (GRAS) by FDA. When dosing SC, stricter guidelines must be followed compared to IV, such as smaller volumes, isotonicity, narrow pH range (4-8), and lower concentration of cosolvents (62).

1.8. Permeation Enhancing Excipients

Permeation or tissue penetration enhancers aim to increase the drug flux into the targeted tissues. The mechanisms to achieve higher permeation include: changing mucus rheology (in mucoadhesive systems), increasing fluidity of lipid bilayer, acting on components and tight junctions, overcoming enzyme barriers, and increasing thermodynamic activity of drugs (35). A list of penetration enhancer classes, examples, and their mechanisms of action can be found in Table 1-2, and include the classes of surfactants, bile salts, fatty acids, chelators, cyclodextrins, anionic polymers, and cationic compounds. The concentration of the permeation enhancer must be such that it facilitates the transport of drug, but does not cause intercellular swelling or edema of epithelium.

Table 1-2 Penetration enhancers and their mechanisms of action

Class	Examples	Mechanism of action
Surfactants	Anionic: Sodium lauryl sulfate Cationic: Cetyl pyridinium chloride Nonionic: Poloxamer, Brij, Span, Myrj, Tween	Solubilization and perturbation of intercellular lipids and protein domain integrity
Bile salts	Sodium deoxycholate	
Fatty acids	Oleic acid, Caprylic acid, Lauric acid, Lyso phosphatidyl choline, Phosphatidyl choline	Increase fluidity of phospholipid bilayer
Cyclodextrins	α, β, γ, Cyclodextrin, methylated β – cyclodextrins	Inclusion of membrane compounds
Chelators	EDTA, Citric acid, Sodium salicylate, Methoxy salicylates	Interfere with Ca^{2+} open tight junctions, decrease trans. epith. elect. resis. (TEER)
Anionic Polymers	Carbopol, polyacrylic acid	
Cationic Polymers & Compounds	Chitosan, Trimethyl chitosan Poly-L-arginine, L-lysine	Ionic interaction with negative charge on the mucosal surface

1.9. Millicylinders Implants for Controlled Release (CR) Local Drug Delivery

Local CR drug delivery systems are presumed advantageous over daily oral dosage forms in that the once monthly dosing could lead to better treatment outcomes, elimination of first-pass effect and patient compliance issues, lowered risk of systemic toxicity, and increased drug stability. Preformed implants, including millicylinders are injectable delivery vehicles, and can be manufactured by extrusion or compression forces to design implants of various shapes and sizes. The shape of the implant plays a large role in the release of the drug due to available surface area for pore formation and drug diffusion routes through the implant matrix. Preformed implants' reproducible size lead to release profiles that can be easily controlled. The process of extruding can either utilize solvent extrusion or hot melt extrusion processes. Hot melt extrusion is useful for low solubility or amorphous drugs with low melting points (63). A major factor dictating the drug release profile is the homogeneity of drug encapsulated in the polymer matrix. For controlled release drug delivery over 1-6 mo., implants can be prepared from bioerodible polymers, such as poly(lactic-*co*-glycolic acid) (PLGA), and are useful for both local and systemic delivery of a large range of drugs including small molecules and biologics. However, it is known that the dissolution of a hydrophobic drug solid can be a slow, thermodynamic process, resulting in intrinsic controlled release properties of the drug, and so therefore polymer-free implants loaded with hydrophobic drug could exert the intended long-acting release profiles as well. Currently, there are several injectable FDA approved drug products that exhibit long-acting release based on dissolution including psychotropics and corticosteroids.

1.9.1.   Rationale for Controlled Release PLGA Implants

PLGA and poly-lactic acid (PLA) are still the biodegradable controlled release (CR) polymers of choice in injectable depots owing to its safety, biodegradability, ease of processing, and tailorable release by adjusting its molecular weight, end-group capping, and ratio of lactide:glycolide monomers, as shown in Fig. 1-4 (64-66). To date, the FDA has approved several PLGA CR drug products including both systemic delivery products such as the Lupron Depot (leuprolide acetate microspheres for prostate cancer) and local delivery formulations including Ozurdex® (dexamethasone intravitreal implant for macular edema), and Atridox (doxycycline in situ forming implants [ISFIs] for periodontitis)(67). For our studies we chose to formulate 4-HPR in PLGA millicylinders due to the ability to achieve high drug loading, lower burst release compared to microspheres and ISFIs developed previously for systemic delivery (24, 56). Additionally, the millicylinder formulations are desirable for future evaluation of *in vivo* tissue penetration and efficacy studies, and will allow for precise drug-tissue distribution measurements from point of origin, and will stay in place so as to better target the local pre-cancerous region. Due to the small size of millicylinders (~ 5 mg, 0.8 mm i.d. x 1 cm), they can be easily injected through a trocar syringe or surgically implanted.
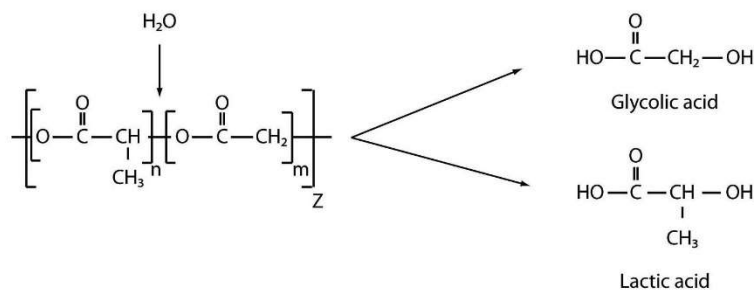
Figure 1-4. Chemical structure of PLGA or poly(lactic-co-glycolic) acid, showing bio-erosion by hydrolysis into its monomer units.

1.9.2.   PLGA Chemical Properties Provide Tailorable Drug Release

In aqueous environments, PLGA can readily undergo hydrolysis and degrade into its glycolic acid and lactic acid counterparts which are later biodegraded in the citric acid cycle. The polymer properties, water uptake and degradation time, can be adjusted by careful selection of a polymer based on the following criteria: molecular weight, polymer end-capping group, lactide/glycolide ratio, and crystallinity (D or L isomers) (64). The composition of the ratio of glycolic: lactic acid monomer chains in PLGA are critical aspects for controlled release properties. Common PLGA ratios are 50:50, 75:25, 85:15 or 100% lactic acid (PLA). Formulations with higher content of lactic acid have slower degradation due to having greater hydrophobicity than glycolic acid. Degradation of 40-70% PLGA is the fastest, and 50% PLGA is most commonly used for 2 month release applications. There are 2 different stereoisomer forms of PLGA/PLA, D and L. The D isomer is amorphous, while the L isomer is semi-crystalline and also has slower degradation. Common formulations use a mixture of D and L PLGA isomers. Hydrolysis occurs faster in amorphous parts of polymer matrix, due to greater mobility of the chains. However, the oligomers formed during degradation have the ability to crystallize, and slow the drug release.

The molecular weight of PLGA, proportionally related to viscosity, can affect its degradation profile. Common molecular weights range from 10-200 kDa, and higher molecular weight polymers result in slower degradation, but higher burst release due to a greater free volume between the polymer chains(68). Water uptake is faster in lower molecular weight polymers which leads to formation of pores where the drug can diffuse through. Polymer blends have been used to facilitate drug release of a hydrophobic drug, such as combinations of higher molecular weight polymers blended with a small amount of low molecular weight

polymer. A low molecular weight polymer may be desirable for a hydrophobic drug to minimize the lag phase(64).

PLGA polymers can also be tailored by varying the end-capping of the polymer chains, most commonly with ester or carboxyl groups. PLGA is a moderately hydrophobic molecule, with very low aqueous solubility, and hydrophilic end-capping can induce plasticization of the polymer. Carboxylated PLGA's have greater swelling than esters, and therefore lead to faster polymer degradation and drug release(69). The polymer acidic microenvironment is due to the buildup of lactic and glycolic acid monomers formed from polymer hydrolytic degradation. The acidic microenvironment has been shown to stabilize certain hydrophobic drugs with maximum stability below pH 4(64).

The polymer concentration in the carrier solvent affects the drug release as well. The initial burst release is inversely proportionate to polymer concentration, and a higher concentration of polymer can lead to slower drug release. Common carrier solvents used for formation of PLGA based delivery systems due to PLGA's high solubility in include: dichloromethane (DCM), ethyl acetate (EtOAc), tetrohydrofuran (THF), n-methylpyrrolidone (NMP), and acetone. The toxicity of the solvent is important for the operator, patient and regulatory approval of the drug product. Permissible levels of residual solvent are specified by the United States Pharmacopeia (USP) classifications.

1.9.3. Drug Release Mechanisms from PLGA

Drug release profiles from bioerodible PLGA systems are characterized by triphasic release patterns: an initial high rate of drug release in the burst release, followed by a slow lag

phase where by drug release is controlled by diffusion, and finally by an increased drug release the occurs when the polymer erodes. Transport through pores is the most common route for release, and can further be described as diffusion controlled or convection controlled (through osmotic pumping) (66). Table 1-3 outlines the processes that may occur to influence release kinetics from PLGA matrices, and the characteristics of the triphasic drug release will be discussed in detail in the following sections *(38)*.

Table 1-3. Processes that influence the rate of drug release from bioerodible matrices

Process	Possible effect	Effect on the release rate
Hydrolysis	Auto-catalysis	Increase
	Erosion and pore formation	
	Plasticizing effect of oligomers	
	Crystallization of oligomers	Decrease
	Polymer chain mobility and pore closure	
	Drug–drug and polymer–drug interactions	
Erosion	Pore formation	Increase
	Loss of catalytic effect of acidic degradation products	Decrease
Water absorption	Hydrolysis	Increase
	Pore formation	
	Increased pH	Decrease
	Polymer chain mobility and pore closure	
Collapse of the polymer structure	Cracks and new surfaces	Increase
	Decreased porosity	Decrease

Phase 1: Burst Release

The first phase of drug release from polymer matrix is considered the burst release, and can be defined as the quantity of drug that escapes the polymeric delivery system prior to onset of polymer erosion-mediated drug release(68). The rate and extent of burst release is an interplay of drug solubility (thermodynamic) and transport (diffusion) properties of the system. Burst release is due to rapid release of drug molecules on the surface of the polymer, or those that are close to the surface and are easily accessible by hydration, and therefore correlates with the particle surface area. The surface area can be affected by particle size distribution, irregularities in shapes, and cracks that serve as channels to increase effective surface area.(68)

Phase 2: Drug Diffusion

Following the initial burst release phase, the drug release in Phase 2 is often the slow release or lag phase. During this phase, the drug diffuses slowly out of the denser polymer matrix through the few existing pores. It is a function of drug diffusivity through polymer matrix, drug loading, drug solubility, matrix dimensions (surface area), and porosity and tortuosity of diffusion pathway (70). In the early stages of release, the polymer becomes hydrated and swells and the pore formation process begins. Initially, these pores are small, so little drug is able to diffuse out. Over time, a pore network begins to form and drug can diffuse from matrix. Another component of drug release in this phase is drug diffusion through the polymer matrix, and is dependent upon the molecule size and matrix tortuosity.

Phase 3: Polymer Degradation and Erosion

In the last phase of drug release, polymer degradation and erosion govern the rate of drug release. This phase is characterized by the onset of matrix erosion, and release rate is greater than the diffusion controlled release in Phase 2. Polymer degradation refers to hydration and erosion of the polymer matrix. During degradation, physical changes occur such as softening, pore creation/closure, pH changes, and crystallization.(70) Factors that influence polymer degradation include amount of water uptake, pH, polymer chemical bond type, and copolymer composition. Degradation of biodegradable polymers occurs as the polymer begins to swell by water uptake, which can be accelerated in the presence of osmotic solutes within the polymer matrix. When the water enters the PLGA matrix, chemical degradation occurs as the polymeric matrix hydrolytically cleaves into its monomers and oligomers. Simultaneously, pores begin to form within the polymer matrix, through which the oligomers/monomers can escape and thereby reduce the mass of the particle.   It is known that the micro-environment of

PLGA microspheres are acidic due to buildup of glycolic and lactic acid within the matrix during degradation. This low micro-environment pH can further lead to the autocatalysis of the PLGA/PLA matrices. The hydrolysis of PLGA and PLA can be acid or base catalyzed.(69) Addition of basic, pore forming salts (such as $MgCO_3$ and $Mg(OH)_2$) increase water uptake leading to increased polymer degradation, and consequently increases drug release.   These basic salts also aide in neutralization of PLGA's low micro-environment pH and slow autocatalysis, whereas addition of carboxylic acid anhydrides showed the opposite trend (69, 71).

Polymer erosion is more complex than degradation because it depends upon other processes such as depredation, swelling, dissolution and diffusion of oligomer, and morphological changes, all leading to a decrease in molecular weight.(72) For PLGA, the mass loss of the polymeric device occurs at a critical molecular weight of ~1 kDa irrespective of the lactic/glycolic acid ratio. The erosion of biodegradable polymers can occur by two different mechanisms: surface erosion or bulk homogeneous erosion. Surface erosion occurs faster than bulk homogeneous erosion due to intrusion of water into the polymer bulk, and erosion of the outer layer begins first (69). Large polymer matrices have slower drug release kinetics due to slower release of formed oligomers. Higher molecular weight polymers are more subjected to heterogeneous erosion and autocatalysis. Crystallization of insoluble salts can occur on the outer shell of polymer due to accumulation of PLGA degradation products contacting buffers or salts (70). When bulk erosion occurs, the polymer degrades slower because water uptake is much faster than the degradation, and results in homogeneous degradation (69). Polymers that are built from very reactive functional groups degrade by surface erosion, where as those made from less reactive functional groups such as PLA or

PLGA degrade by bulk erosion mechanisms. PLA's slower degradation rate can also be attributed to steric effects, due to the alkyl group that hinders the attack of water (72).

1.10.   Scope of Research

The scope of this research is to develop long acting local 4HPR millicylindrical implants for secondary oral cancer chemoprevention (Fig. 1-5). These 4HPR millicylinder formulations should be capable of delivering high levels of drug at the lesional target site, while eliminating 4HPR's extensive first pass metabolic degradation and toxic side effects associated with high dose systemic delivery routes. Our aim is to utilize CR PLGA millicylinders to provide steady therapeutic drug levels over 1-2 months. Equally as important as developing local 4HPR formulations, is evaluating 4HPR's tissue disposition. To date, there are no data that depict 4HPR's tissue binding affinity during local delivery. Limited penetration distance is the most prevalent challenge encountered during local drug delivery, which is further exacerbated by the fat deposit's barrier action due to 4HPR affinity for lipid rich regions. To overcome 4HPR extreme aqueous insolubility, solubility enhancing strategies will need to be employed, while permeation enhancer may be necessary to overcome limited tissue dispersivity. The following paragraphs outline the steps taken to achieve these objectives.

Figure 1-5: Millicylinders for local long-acting oral cancer chemoprevention.

In Chapter 2, 4HPR will be formulated into PLGA millicylinders for long-acting local delivery and evaluated *in vitro* and in vivo for their release, implant water uptake, and polymer erosion. The challenges addressed include 4HPR limited aqueous solubility and incomplete drug release from the PLGA millicylinders. We have selecting a continuously eroding PLGA polymer that will target the 1-2 month delivery period, however the potential for the hydrophobic 4HPR to precipitate over time was quite apparent. Initial formulation steps optimized 4HPR loading, addition of solubilizers, and pore forming agents to promote 4HPR release. The *in vivo* evaluation 4HPR PLGA millicylinders in rat SC tissues was compared to drug release from an immediate dissolving sugar matrix, to determine if the controlled release of 4HPR was dictated by PLGA or by dissolution of the hydrophobic drug. An initial efficacy study in mouse xenograph oral cancer model was performed. The findings of these *in vivo* release studies will be the motivation for further elucidating of the unusually slow 4HPR release from PLGA into the aqueous tissue environment. Results of that mechanistic 4HPR-PLGA investigation can be found in Appendix 2.

In Chapter 3, the limitations of the initial PLGA-4HPR millicylinder formulations were realized, and therefore creation of amorphous drug systems for solubility enhancement was investigated. A robust PVP-4HPR ASD showed incredible solubility enhancement over 1 week, and was loaded into PLGA millicylinders, and release was evaluated *in vitro* and *in vivo*. The *in vivo* release of the amorphous drug far outperformed the crystalline drug release from our implants in proceeding experiments.

In Chapter 4, 4HPR tissue binding kinetics and partitioning into blood/plasma components was assessed *ex vivo*, and will be useful to determine factors that may influence 4HPR's tissue dispersion. The effect of 4HPR uptake by addition of various solubilizing and permeation enhancing excipients will be evaluated. A comparison of the 4HPR uptake in subcutaneous connective and buccal epithelia tissue types was also performed. 4HPR's binding to cell membrane components was also evaluated, to determine factors responsible for 4HPR's high non-specific tissue binding.

In Chapter 5, 4HPR's tissue penetration after release from long-acting millicylinders was evaluated in rabbit buccal epithelia. This is the first time that the spatial distribution of 4HPR has been evaluated, and results from this study will have huge clinical impact on development of these local delivery systems for widespread treatment of pre-cancerous regions. Quantitative Raman spectroscopic imaging methods were established using calibration standards that were prepared with excised buccal tissues incubated in drug solutions. The 4HPR tissue levels was reported as a function of the diffusion distance, with the aim that these formulations prepared in Chapters 2 and 3 will enhance the penetration distance compared to the solid drug control in the immediately dissolving sugar matrix.

1.11. References

1. Foundation TOC. Information - Support - Advocacy-Research... and Hope 2016 [updated 1-6-17Jan. 2017]. Available from: http://oralcancerfoundation.org/facts/.

2. Foundation OC. [5/6/2014]. Available from: http://oralcancerfoundation.org.

3. Reibel J. Prognosis of oral pre-malignant lesions: significance of clinical, histopathological, and molecular biological characteristics. Critical reviews in oral biology and medicine : an official publication of the American Association of Oral Biologists. 2003;14(1):47-62. Epub 2003/05/24. PubMed PMID: 12764019.

4. Holpuch A, Desai K-G, Schwendeman S, Mallery S. Optimizing therapeutic efficacy of chemopreventive agents: A critical review of delivery strategies in oral cancer chemoprevention clinical trials2011 January 1, 2011. 23- p.

5. Berni R, Formelli F. In vitro interaction of fenretinide with plasma retinol-binding protein and its functional consequences. FEBS Letters. 1992;308(1):43-5. doi: http://dx.doi.org/10.1016/0014-5793(92)81046-O.

6. Han BB, Li S, Tong M, Holpuch AS, Spinney R, Wang D, et al. Fenretinide Perturbs Focal Adhesion Kinase in Premalignant and Malignant Human Oral Keratinocytes. Fenretinide's Chemopreventive Mechanisms Include ECM Interactions. Cancer Prevention Research. 2015;8(5):419-30. doi: 10.1158/1940-6207.capr-14-0418.

7. Mallery SR, Wang D, Santiago B, Pei P, Schwendeman S, Nieto K, et al. Benefits of Multifaceted Chemopreventives in the Suppression of the Oral Squamous Cell Carcinoma (OSCC) Tumorigenic Phenotype. Cancer Prevention Research. 2016. doi: 10.1158/1940-6207.capr-16-0180.

8. Han BB, Li S, Tong M, Holpuch AS, Spinney R, Wang D, et al. Fenretinide Perturbs Focal Adhesion Kinase in Premalignant and Malignant Human Oral Keratinocytes. Fenretinide's Chemopreventive Mechanisms Include ECM Interactions. Cancer prevention research (Philadelphia, Pa). 2015;8(5):419-30. Epub 2015/02/26. doi: 10.1158/1940-6207.capr-14-0418. PubMed PMID: 25712051; PubMed Central PMCID: PMC4417376.

9. Tradati N, Chiesa F, Rossi N, Grigolato R, Formelli F, Costa A, et al. Successful topical treatment of oral lichen planus and leukoplakias with fenretinide (4-HPR). Cancer letters. 1994;76(2-3):109-11. Epub 1994/01/30. PubMed PMID: 8149338.

10. Lippman SM, Lee JJ, Martin JW, El-Naggar AK, Xu X, Shin DM, et al. Fenretinide activity in retinoid-resistant oral leukoplakia. Clinical cancer research : an official journal of the American Association for Cancer Research. 2006;12(10):3109-14. Epub 2006/05/19. doi: 10.1158/1078-0432.ccr-05-2636. PubMed PMID: 16707609.

11. William WN, Jr., Lee JJ, Lippman SM, Martin JW, Chakravarti N, Tran HT, et al. High-dose fenretinide in oral leukoplakia. Cancer prevention research (Philadelphia, Pa). 2009;2(1):22-6. Epub 2009/01/14. doi: 10.1158/1940-6207.capr-08-0100. PubMed PMID: 19139014.

12. Uray IP, Dmitrovsky E, Brown PH. Retinoids and rexinoids in cancer prevention: from laboratory to clinic. Seminars in oncology. 2016;43(1):49-64. Epub 2016/03/13. doi: 10.1053/j.seminoncol.2015.09.002. PubMed PMID: 26970124; PubMed Central PMCID: PMC4789177.

13. di Masi A, Leboffe L, De Marinis E, Pagano F, Cicconi L, Rochette-Egly C, et al. Retinoic acid receptors: from molecular mechanisms to cancer therapy. Molecular aspects of medicine. 2015;41:1-115. Epub 2014/12/30. doi: 10.1016/j.mam.2014.12.003. PubMed PMID: 25543955.

14. Garaventa A, Luksch R, Lo Piccolo MS, Cavadini E, Montaldo PG, Pizzitola MR, et al. Phase I trial and pharmacokinetics of fenretinide in children with neuroblastoma. Clinical cancer research : an official journal of the American Association for Cancer Research. 2003;9(6):2032-9. Epub 2003/06/11. PubMed PMID: 12796365.

15. Peng YM, Dalton WS, Alberts DS, Xu MJ, Lim H, Meyskens FL, Jr. Pharmacokinetics of N-4-hydroxyphenyl-retinamide and the effect of its oral administration on plasma retinol concentrations in cancer patients. International journal of cancer Journal international du cancer. 1989;43(1):22-6. Epub 1989/01/15. PubMed PMID: 2521335.

16. Formelli F, Clerici M, Campa T, Di Mauro MG, Magni A, Mascotti G, et al. Five-year administration of fenretinide: pharmacokinetics and effects on plasma retinol concentrations. Journal of clinical oncology : official journal of the American Society of Clinical Oncology. 1993;11(10):2036-42. Epub 1993/10/01. PubMed PMID: 8410127.

17. Radu RA, Han Y, Bui TV, Nusinowitz S, Bok D, Lichter J, et al. Reductions in Serum Vitamin A Arrest Accumulation of Toxic Retinal Fluorophores: A Potential Therapy for Treatment of Lipofuscin-Based Retinal Diseases. Investigative Ophthalmology & Visual Science. 2005;46(12):4393-401. doi: 10.1167/iovs.05-0820.

18. Mallery SR, Budendorf DE, Larsen MP, Pei P, Tong M, Holpuch AS, et al. Effects of Human Oral Mucosal Tissue, Saliva, and Oral Microflora on Intraoral Metabolism and Bioactivation of Black Raspberry Anthocyanins. Cancer Prevention Research. 2011;4(8):1209-21. doi: 10.1158/1940-6207.capr-11-0040.

19. van Gelderen P, de Vleeschouwer MHM, DesPres D, Pekar J, van Zijl PCM, Moonen CTW. Water diffusion and acute stroke. Magnetic Resonance in Medicine. 1994;31(2):154-63. doi: 10.1002/mrm.1910310209.

20. Holpuch AS, Hummel GJ, Tong M, Seghi GA, Pei P, Ma P, et al. Nanoparticles for local drug delivery to the oral mucosa: proof of principle studies. Pharm Res. 2010;27(7):1224-36. Epub 2010/04/01. doi: 10.1007/s11095-010-0121-y. PubMed PMID: 20354767; PubMed Central PMCID: PMC2883929.

21. Huber K, Patel P, Zhang L, Evans H, Westwell AD, Fischer PM, et al. 2-[(1-methylpropyl)dithio]-1H-imidazole inhibits tubulin polymerization through cysteine oxidation. Molecular cancer therapeutics. 2008;7(1):143-51. Epub 2008/01/19. doi: 10.1158/1535-7163.mct-07-0486. PubMed PMID: 18202017.

22. Janssen-Heininger YM, Poynter ME, Baeuerle PA. Recent advances towards understanding redox mechanisms in the activation of nuclear factor kappaB. Free radical biology & medicine. 2000;28(9):1317-27. Epub 2000/08/05. PubMed PMID: 10924851.

23. Wouters MA, Iismaa S, Fan SW, Haworth NL. Thiol-based redox signalling: rust never sleeps. The international journal of biochemistry & cell biology. 2011;43(8):1079-85. Epub 2011/04/26. doi: 10.1016/j.biocel.2011.04.002. PubMed PMID: 21513814.

24. Wischke C, Zhang Y, Mittal S, Schwendeman SP. Development of PLGA-based injectable delivery systems for hydrophobic fenretinide. Pharm Res. 2010;27(10):2063-74. Epub 2010/07/30. doi: 10.1007/s11095-010-0202-y. PubMed PMID: 20668921.

25. Li C-Y, Zimmerman C, Wiedmann T. Solubilization of Retinoids by Bile Salt/ Phospholipid Aggregates. Pharmaceutical Research. 1996;13(6):907-13. doi: 10.1023/a:1016013414457.

26. Desai KG, Mallery SR, Holpuch AS, Schwendeman SP. Development and in vitro-in vivo evaluation of fenretinide-loaded oral mucoadhesive patches for site-specific chemoprevention of oral cancer. Pharm Res. 2011;28(10):2599-609. Epub 2011/06/16. doi: 10.1007/s11095-011-0489-3. PubMed PMID: 21674264; PubMed Central PMCID: PMC3171589.

27. Wu X, Desai KG, Mallery SR, Holpuch AS, Phelps MP, Schwendeman SP. Mucoadhesive fenretinide patches for site-specific chemoprevention of oral cancer: enhancement of oral mucosal permeation of fenretinide by coincorporation of propylene glycol and menthol. Mol Pharm. 2012;9(4):937-45. Epub 2012/01/28. doi: 10.1021/mp200655k. PubMed PMID: 22280430; PubMed Central PMCID: PMC3687357.

28. Edgar M, Lichter J, Mata NL. Compositions and methods for treating ophthalmic conditions. Google Patents; 2013.

29. Swanson BN, Zaharevitz DW, Sporn MB. Pharmacokinetics of N-(4-hydroxyphenyl)-all-trans-retinamide in rats. Drug Metabolism and Disposition. 1980;8(3):168-72. doi: 10.1124/dmd.8.3.168.

30. Allen JG, Bloxham DP. The pharmacology and pharmacokinetics of the retinoids. Pharmacology & Therapeutics. 1989;40(1):1-27. doi: http://dx.doi.org/10.1016/0163-7258(89)90071-5.

31. Kokate A, Li X, Jasti B. Transport of a novel anti-cancer agent, fenretinide across Caco-2 monolayers. Invest New Drugs. 2007;25(3):197-203. doi: 10.1007/s10637-006-9026-3.

32. Squier CA. The permeability of oral mucosa. Critical reviews in oral biology and medicine : an official publication of the American Association of Oral Biologists. 1991;2(1):13-32. Epub 1991/01/01. PubMed PMID: 1912142.

33. Khanvilkar K, Donovan MD, Flanagan DR. Drug transfer through mucus. Advanced Drug Delivery Reviews. 2001;48(2–3):173-93. doi: http://dx.doi.org/10.1016/S0169-409X(01)00115-6.

34. Patel VF, Liu F, Brown MB. Modeling the oral cavity: In vitro and in vivo evaluations of buccal drug delivery systems. Journal of Controlled Release. 2012;161(3):746-56. doi: http://dx.doi.org/10.1016/j.jconrel.2012.05.026.

35. Chinna Reddy P, Chaitanya KS, Madhusudan Rao Y. A review on bioadhesive buccal drug delivery systems: current status of formulation and evaluation methods. Daru. 2011;19(6):385-403.

36. Dali MM, Moench PA, Mathias NR, Stetsko PI, Heran CL, Smith RL. A rabbit model for sublingual drug delivery: comparison with human pharmacokinetic studies of propranolol, verapamil and captopril. J Pharm Sci. 2006;95(1):37-44. Epub 2005/11/25. doi: 10.1002/jps.20312. PubMed PMID: 16307454.

37. Fung L, Shin M, Tyler B, Brem H, Saltzman WM. Chemotherapeutic Drugs Released from Polymers: Distribution of 1,3-bis(2-chloroethyl)-l-nitrosourea in the Rat Brain. Pharmaceutical Research. 1996;13(5):671-82. doi: 10.1023/a:1016083113123.

38. During MJ, Freese A, Sabel BA, Saltzman WM, Deutch A, Roth RH, et al. Controlled release of dopamine from a polymeric brain implant: In vivo characterization. Annals of Neurology. 1989;25(4):351-6. doi: 10.1002/ana.410250406.

39. Fleming AB, Saltzman WM. Pharmacokinetics of the carmustine implant. Clinical pharmacokinetics. 2002;41(6):403-19. Epub 2002/06/21. doi: 10.2165/00003088-200241060-00002. PubMed PMID: 12074689.

40. Fung LK, Ewend MG, Sills A, Sipos EP, Thompson R, Watts M, et al. Pharmacokinetics of Interstitial Delivery of Carmustine, 4-Hydroperoxycyclophosphamide, and Paclitaxel from a Biodegradable Polymer Implant in the Monkey Brain. Cancer research. 1998;58(4):672-84.

41. Fung LK, Saltzman WM. Polymeric implants for cancer chemotherapy. Advanced Drug Delivery Reviews. 1997;26(2–3):209-30. doi: http://dx.doi.org/10.1016/S0169-409X(97)00036-7.

42. Strasser JF, Fung LK, Eller S, Grossman SA, Saltzman WM. Distribution of 1,3-bis(2-chloroethyl)-1-nitrosourea and tracers in the rabbit brain after interstitial delivery by biodegradable polymer implants. The Journal of pharmacology and experimental therapeutics. 1995;275(3):1647-55. Epub 1995/12/01. PubMed PMID: 8531140.

43. Haller M, Saltzman WM. Localized Delivery of Proteins in the Brain: Can Transport Be Customized? Pharmaceutical Research. 1998;15(3):377-85. doi: 10.1023/a:1011911912174.

44. Pepić I, Lovrić J, Filipović-Grčić J. How do polymeric micelles cross epithelial barriers? European Journal of Pharmaceutical Sciences. 2013;50(1):42-55. doi: http://dx.doi.org/10.1016/j.ejps.2013.04.012.

45. Minchinton AI, Tannock IF. Drug penetration in solid tumours. Nat Rev Cancer. 2006;6(8):583-92.

46. Cevc G, Vierl U. Spatial distribution of cutaneous microvasculature and local drug clearance after drug application on the skin. Journal of Controlled Release. 2007;118(1):18-26. doi: http://dx.doi.org/10.1016/j.jconrel.2006.10.022.

47. Bianciardi G, Traversi C, Cattaneo R, De Felice C, Monaco A, Tosi G, et al. Phase transition of the microvascular network architecture in human pathologies. Theoretical biology forum. 2012;105(1):37-45. Epub 2012/12/01. PubMed PMID: 23193796.

48. Manual M. Disposition and Fate of Drugs [8/7/2014]. Available from: www.merckmanual.com.

49. Stroh M, Zipfel WR, Williams RM, Webb WW, Saltzman WM. Diffusion of Nerve Growth Factor in Rat Striatum as Determined by Multiphoton Microscopy. Biophysical Journal. 2003;85(1):581-8. doi: http://dx.doi.org/10.1016/S0006-3495(03)74502-0.

50. Fleming AB, Haverstick K, Saltzman WM. In Vitro Cytotoxicity and in Vivo Distribution after Direct Delivery of PEG−Camptothecin Conjugates to the Rat Brain. Bioconjugate Chemistry. 2004;15(6):1364-75. doi: 10.1021/bc034180o.

51. Patel RB, Solorio L, Wu H, Krupka T, Exner AA. Effect of injection site on in situ implant formation and drug release in vivo. Journal of Controlled Release. 2010;147(3):350-8. doi: http://dx.doi.org/10.1016/j.jconrel.2010.08.020.

52. Orienti I, Zuccari G, Falconi M, Teti G, Illingworth NA, Veal GJ. Novel micelles based on amphiphilic branched PEG as carriers for fenretinide. Nanomedicine: Nanotechnology, Biology and Medicine. 2012;8(6):880-90. doi: http://dx.doi.org/10.1016/j.nano.2011.10.008.

53. Orienti I, Zuccari G, Bergamante V, Carosio R, Gotti R, Cilli M, et al. Fenretinide-polyvinylalcohol Conjugates: New Systems Allowing Fenretinide Intravenous Administration. Biomacromolecules. 2007;8(10):3258-62. doi: 10.1021/bm7005592.

54. Orienti I, De MMR, Zeuner AP. Fenretinide complexes. Google Patents; 2016.

55. Orienti I, Zuccari G, Carosio R, G. Montaldo P. Improvement of aqueous solubility of fenretinide and other hydrophobic anti-tumor drugs by complexation with amphiphilic dextrins. Drug Delivery. 2009;16(7):389-98. doi: doi:10.1080/10717540903101655. PubMed PMID: 19624248.

56. Ying Zhang CW, Sachin Mittal, Amitava Mitra, Steven P. Schwendeman. Design of controlled release PLGA microspheres for hydrophobic fenretinide. Molecular Pharmaceutics. in press.

57. Graves RA, Ledet GA, Glotser EY, Mitchner DM, Bostanian LA, Mandal TK. Formulation and evaluation of biodegradable nanoparticles for the oral delivery of fenretinide. European Journal of Pharmaceutical Sciences. 2015;76(0):1-9. doi: http://dx.doi.org/10.1016/j.ejps.2015.04.024.

58. Trapasso E, Cosco D, Celia C, Fresta M, Paolino D. Retinoids: new use by innovative drug-delivery systems. Expert Opin Drug Deliv. 2009;6(5):465-83. Epub 2009/05/06. doi: 10.1517/17425240902832827. PubMed PMID: 19413455.

59. Parchment RE, Jasti BR, Boinpally RR, Rose SE, Holsapple ET. Liposomal nanoparticles and other formulations of fenretinide for use in therapy and drug delivery. Google Patents; 2014.

60. Almarsson Ö, Hickey MB, Peterson ML, Zaworotko MJ, Moulton B, Rodriguez-Hornedo N. Pharmaceutical co-crystal compositions. Google Patents; 2011.

61. Strickley R. Solubilizing Excipients in Oral and Injectable Formulations. Pharmaceutical Research. 2004;21(2):201-30. doi: 10.1023/b:pham.0000016235.32639.23.

62. Li P, Zhao L. Developing early formulations: Practice and perspective. International Journal of Pharmaceutics. 2007;341(1–2):1-19. doi: http://dx.doi.org/10.1016/j.ijpharm.2007.05.049.

63. Desai K, Mallery S, Schwendeman S. Formulation and Characterization of Injectable Poly(dl-lactide-co-glycolide) Implants Loaded with N-Acetylcysteine, a MMP Inhibitor. Pharmaceutical Research. 2008;25(3):586-97. doi: 10.1007/s11095-007-9430-1.

64. Wischke C, Schwendeman SP. Principles of encapsulating hydrophobic drugs in PLA/PLGA microparticles. Int J Pharm. 2008;364(2):298-327. Epub 2008/07/16. doi: 10.1016/j.ijpharm.2008.04.042. PubMed PMID: 18621492.

65. Hyon SH. Biodegradable poly (lactic acid) microspheres for drug delivery systems. Yonsei Med J. 2000;41(6):720-34.

66. Fredenberg S, Wahlgren M, Reslow M, Axelsson A. The mechanisms of drug release in poly(lactic-co-glycolic acid)-based drug delivery systems—A review. International Journal of Pharmaceutics. 2011;415(1–2):34-52. doi: http://dx.doi.org/10.1016/j.ijpharm.2011.05.049.

67. Wang Y, Wen, Q., Choi, S. FDA's Regulatory Science Program for Generic PLA/ PLGA-Based Drug Products2016 1/24/17]. Available from: http://www.americanpharmaceuticalreview.com.

68. Allison SD. Analysis of initial burst in PLGA microparticles. Expert Opin Drug Deliv. 2008;5(6):615-28. Epub 2008/06/06. doi: 10.1517/17425247.5.6.615. PubMed PMID: 18532918.

69. Siepmann J, Göpferich A. Mathematical modeling of bioerodible, polymeric drug delivery systems. Advanced Drug Delivery Reviews. 2001;48(2–3):229-47. doi: http://dx.doi.org/10.1016/S0169-409X(01)00116-8.

70. Parent M, Nouvel C, Koerber M, Sapin A, Maincent P, Boudier A. Plga In Situ Implants Formed By Phase Inversion: Critical Physicochemical Parameters To Modulate Drug Release. Journal of controlled release : official journal of the Controlled Release Society. 2013. Epub 2013/09/05. doi: 10.1016/j.jconrel.2013.08.024. PubMed PMID: 24001947.

71. Shumway BS, Kresty LA, Larsen PE, Zwick JC, Lu B, Fields HW, et al. Effects of a Topically Applied Bioadhesive Berry Gel on Loss of Heterozygosity Indices in Premalignant Oral Lesions. Clinical Cancer Research. 2008;14(8):2421-30. doi: 10.1158/1078-0432.ccr-07-4096.

72. Gopferich A. Mechanisms of polymer degradation and erosion. Biomaterials. 1996;17(2):103-14. Epub 1996/01/01. PubMed PMID: 8624387.

Chapter 2: Formulate 4HPR into PLGA millicylinders for CR local delivery and

evaluate release *in vitro* and *in vivo*

2.1.   Abstract

Local, long-acting release fenretinide (4HPR) millicylindrical implants were prepared and evaluated for their release kinetics *in vivo* and their ability to suppress oral cancer tumor explant growth. Poly(lactic-*co*-glycolic acid)(PLGA) implants were prepared as a function of drug loading and the presence of various excipients (pore-formers, solubilizers, crystallization inhibitors) to enhance release of the insoluble 4HPR. Release kinetics and bioerosion of PLGA were monitored both *in vitro* in a PBS/Tween 80 buffer and *in vivo* by recovery of the drug remaining at the injection site. 4HPR was released from PLGA implants much slower *in vivo* than in the drug solubilizing media *in vitro*, with a 3-week lag phase and continuous release of >2 months, but showed some release enhancement by addition of solubilizers. Water-soluble PVA/sucrose implants for release of 4HPR served to determine if drug dissolution provided suitable controlled release without the PLGA, and this formulation showed continuous drug release over 6 weeks *in vivo.* Placement of PLGA-4HPR implants adjacent to oral cancer tumor murine xenografts showed inhibition of tumor growth relative to sham implants, indicating the potential for the local 4HPR delivery approach to be useful for oral cancer chemoprevention.

2.2.   Introduction

Oral squamous cell carcinoma (OSCC) is a worldwide health concern, and in 2016, ~50,000 Americans were newly diagnosed with oral or pharyngeal cancer

(http://oralcancerfoundation.org). The vast majority of oral cancers arise from malignant transformation of preneoplastic surface epithelial lesions (1). Despite treatment advances that include intraoperative radiation, the 5-year survival rates of persons with OSCC is discouraging low (50%). Following initial therapy, HNSCC patients are managed by close clinical follow up often supplemented with imaging studies. Despite vigilant monitoring and well-recognized risk factors for recurrence, over one third of patients develop life-threatening and often untreatable recurrent OSCCs (2). Replacement of the current "watchful waiting" strategy with well-tolerated and effective secondary OSCC chemoprevention could make a significant clinical impact for these individuals. As OSCC management requires extensive, often disfiguring surgery, treated OSCC patients often experience depression and reduced motivation. Development of an implantable delivery system to provide therapeutic drug levels without systemic effects and eliminate patient compliance issues could advance secondary OSCC chemoprevention. Previous studies from our labs have demonstrated that fenretinide (4HPR) inhibits focal adhesion kinase- extracellular matrix (FAK-ECM) interactions and significantly reduces invasion, which is the ultimate step in OSCC development (3). To address OSCC's redundant signaling cascades, secondary OSCC chemoprevention will ultimately require complementary agents (4). Based on 4HPR's multiple mechanisms of action including growth regulation and suppression of gratuitous signaling (5), it is our intention to include 4HPR in the secondary chemopreventive formulation.

Here, we chose to formulate 4HPR local controlled release (CR) implants using biodegradable poly(lactic-*co*-glycolic acid) (PLGA) to provide continuous release for >30 days. Local CR drug delivery systems are presumed advantageous over daily oral dosage forms in that the once monthly dosing could lead to better treatment outcomes, elimination of

first-pass effect and patient compliance issues, lowered risk of systemic toxicity, and increased drug stability. PLGA is still the biodegradable controlled release polymer of choice in injectable depots owing to its safety, biodegradability, ease of processing, and tailorable release by adjusting its molecular weight, end-group capping, and ratio of lactide:glycolide monomers(6, 7,8). To date, the FDA has approved several PLGA CR drug products including both systemic delivery products such as the Lupron Depot (leuprolide acetate microspheres for prostate cancer) and local delivery formulations including Ozurdex® (dexamethasone intravitreal implant for macular edema), and Atridox (doxycycline in situ forming implants [ISFIs] for periodontitis)(9). For our studies we chose to formulate 4HPR in millicylinders due to the ability to achieve high drug loading, and lower burst release compared to microspheres and ISFIs developed previously for systemic delivery(10,11). Additionally, the millicylinder formulations are desirable for future evaluation of *in vivo* tissue penetration and efficacy studies, and will allow for precise drug-tissue distribution measurements from the point of origin, and are expected to remain in place for better targeting of the local pre-cancerous region. Due to the small size of millicylinders (~ 5 mg, 0.8 mm i.d. x 1 cm), they can be easily injected through a trocar syringe or surgically implanted.

Previous work has been done by our lab in formulating local 4HPR drug delivery systems including PLGA microspheres, ISFIs, and buccal mucoadhesive patches as well as determining 4HPR solubility in various PLGA solubilizing solvents, release media compositions, and selected surfactants (10, 12). In previous pharmacokinetic (PK) studies, we compared serum levels of 4HPR encapsulated in PLGA microspheres and ISFIs relative to a control drug suspension dosed subcutaneously (SC) in rats, and found that PLGA CR formulations were successful at strongly reducing the burst release compared to the control

suspension (13). However, after 15 days, the amount of 4HPR released from the PLGA

formulations coincided with those of the drug suspension and showed a steady decline for

more than a month. Based on this data, after 2 weeks it was unclear whether the actual drug

was exhibiting controlled release properties due to dissolution into surrounding interstitial

fluid, or slow release from tissue lipid "reservoirs" where 4HPR could have accumulated after

fast dissolution.

These studies extended our previous work to include sustained duration (1-2 months) *in*

vitro and *in vivo* of 4HPR encapsulated in PLGA CR millicylinders. Local delivery of

hydrophobic 4HPR presents a significant challenge owing to its extreme water insolubility,

with a logP of 6.31. We have selecting a continuously eroding PLGA polymer that will target

the 1-2 month delivery period, although we considered the potential for the hydrophobic 4HPR

to precipitate over time causing dissolution rate-controlled release instead of typical PLGA-

erosion control. Initial parameters assessed included varying 4HPR loading (10, 20, 30%),

along with selected solubilizers and penetration enhancers *in vitro* and *in vivo*. We have

previously shown that the addition of a basic salt, magnesium carbonate ($MgCO_3$), to the

millicylinder can lead to more favorable release kinetics due to its slow pore forming

capabilities (14), similar to what was originally patented for release of proteins(15). To

facilitate the release of the hydrophobic drug into aqueous interstitial fluid, we co-encapsulated

4HPR with PLGA and solubility enhancing excipients including sodium deoxycholate (NaDC)

via micelle formation and beta-cyclodextran (β-CD) via inclusion complexes. Other excipients

were also investigated based on their ability to inhibit drug crystallization and aide in implant

disintegration including polyvinylpyrollidone (PVP K30) (16, 17, 18), and hydroxypropyl

methylcellulose (HPMC K4M) (19, 20). HPMC has also been utilized to facilitate drug release

due to its swelling behavior that promotes pore formation. All excipients studied have been categorized as generally regarded as safe (GRAS) by the US FDA, and many are currently used in FDA approved drug products (21).

2.3. Materials and Methods

2.3.1. Materials

50:50 acid end-capped PLGA 503H (24-38 kDa), was purchased from Evonik, 4HPR was generously supplied by Merck Co, and acitretin was used as an internal standard (analytical grade, Sigma-Aldrich). Excipients used were sodium deoxycholate, (NaDC, 99% pure, Acros), polyvinylpyrrolidone (PVP K30, 40 kDa, BASF), hydroxypropyl methylcellulose K4M (HPMC K4M, Dow Chemical, Midland, MI), and β-CD (Sigma-Aldrich). Water-soluble implants were composed of polyvinyl alcohol (PVA, 9-10 kDa, 80% hydrolyzed, Sigma-Aldrich) and D-sucrose (Sigma-Aldrich). All other materials were reagent grade or better including: $MgCO_3$, acetone, ethanol (EtOH), tetrahydrofuran (THF), and Tween 80. Solvents for UPLC-UV and MS analysis were HPLC or MS grade including acetonitrile (ACN), methanol (MeOH), double distilled water (ddH_2O), phosphoric acid (H_3PO_4), ammonium formate (NH_4COO) and formic acid (HCOOH). Silicon tubing (0.8 mm i.d.,) was purchased from BioRad Laboratories. Ethylenediaminetetraacetic acid (EDTA, analytical standard, LECO, St. Joseph, MI) and Bovine Serum Albumin (BSA, 99% pure, heat shock fraction, Sigma-Aldrich) were used as standards for nitrogen analysis.

2.3.2. 4HPR Millicylinder Preparation

To prepare PLGA millicylinders, 60% w/w 50:50 acid end-capped PLGA (24-38 kDa) was dissolved in acetone at room temperature by slowly vortexing in a capped 2 mL Eppendorf tube. 4HPR and excipients were added to the polymer mixture, and those excipients that were

insoluble in acetone (including $MgCO_3$ and NaDC) were cryomilled (Retsch swing mill cryomill, PN 20.749.001) and sieved to < 90 μm prior to their addition to the formulation. The solids were incorporated into polymer solution by stirring with a spatula. Additional acetone was added and recorded to obtain a solution with an extrudable viscosity. Note, that solutions with low viscosity result in hollow implants, and therefore the highest extrudable viscosity was sought to obtain non-hollow and dense implants. Next, the resulting gel solution was loaded into a 3 mL syringe equipped with an 18 g blunt end needle attached to silicone rubber tubing (0.8 mm i.d.), and slowly extruded. The implants were dried at room temperature for 2 days, and then transferred to vacuum oven and dried at 40 °C for an additional 2 days, after which the tubing was carefully removed and implants were cut to the desired length of 1 cm. Efforts were taken in all 4HPR experiments to minimize light exposure due to the drug's known photo-instability.

Formulation efforts were necessary to accelerate 4HPR release rates. Initial studies optimized the 4HPR loading level (10, 20, 30% w/w). To improve release kinetics additional excipients were added including 20% NaDC or CaDC, along with investigating the effects of varying the concentration of the pore former $MgCO_3$ (3, 10, 15 % w/w). Other excipients were added to accelerate release, aid in drug solubilization, and prevent drug crystallization and included β-CD, HPMC K4M, and PVP K30. For the *in vivo* studies, a water soluble matrix 4HPR millicylinder was prepared with a PVA/ D-sucrose (40%, 30% w/v respectively in ddH_2O) matrix with and without excipients, followed by extrusion and drying in the same fashion as PLGA implants.

2.3.3. NaDC and CaDC PLGA Millicylinders

Design of CR of solubilizer of deoxycholic acid was attempted via preparation of the less soluble calcium salt of deoxycholic acid and compared to NaDC. To prepare the CaDC, 10 mL of 2 mM $CaCl_2 \cdot 2H_2O$ in ddH_2O (pH adjusted to 9 with 0.1 N sodium hydroxide) was added to 10 mL of 10 mM NaDC in ddH_2O (pH 7.7), and stirred at room temperature for 3 h, during which the CaDC salt formed and precipitated. The reaction mixture was centrifuged, and supernatant removed and discarded. The CaDC salt was freeze dried, cryomilled and sieved to < 90 μM. PLGA millicylinders were prepared using polymers 503 and 503H and loading with either 20% CaDC or 20% NaDC. In vitro releases performed by placing 1 implant in 1 mL PBST 0.02% Tween80 and assayed by LC-MS.

2.3.4. 4HPR Solubility in the presence of Selected Excipients

Solubility studies were performed with selected excipients including NaDC, HPMC, β-CD, and PVP K30 at levels of 1, 2, 5, 10, 20% w/v in double distilled water (ddH_2O). For all studies, 2 mg of 4HPR was added to 1 mL of solution and incubated at 37° C while rotating, and protected from light with aluminum foil covered vials. The resulting suspension was centrifuged and the supernatant was analyzed by UPLC/UV and day 7 solubility was reported. Previous work by our lab has determined 4HPR solubility parameters in selected organic solvents used in our assays and in presence of other solubilizing excipients[10]. In addition to these selected excipients, a comprehensive compilation of 4HPR solubility from previous solubility studies from our lab, literature sources, and my data, can be referenced in Appendix 1.

2.3.5. 4HPR Implant Loading

To determine the amount to 4HPR loaded into the implant, one millicylinder was weighed into a 15 mL centrifuge tube, PLGA and 4HPR were co-dissolved by addition of 0.5 mL THF, followed by precipitation of PLGA by addition of 9.5 mL EtOH. Next, the sample was centrifuged, and supernatant was assayed by UPLC/UV. Encapsulation efficiency was invariable and ranged from 97-103%.

2.3.6. 4HPR *In vitro* release

4HPR *in vitro* release from millicylinders was determined by placing one millicylinder (5-7 mg) in 5 mL eppindorf tube containing 4 mL PBS pH 7.4 + 2% Tween 80, necessary to maintain sink conditions, and incubating at 37 °C on a shaking platform (200 rpms). The solutions were sampled by complete media replacement, until nearly 100% release, after which a mass balance accounting was done by determining the amount of 4-HPR remaining in millicylinder using the loading assay described above.

2.3.7. 4HPR *In vivo* release

To evaluate 4HPR release *in vivo*, millicylinders were weighed and implanted subcutaneously (SC) in the flanks of male Sprague Dawley rats using a 12 g trocar. Each rat could receive up to 6 implants. For each formulation, 3 implants were implanted in each rat, and 1 rat per time point (days 1, 7, 14, 28, 42, 60) was sacrificed. Millicylinders were carefully harvested to ensure complete removal and release from encompassing tissues. The wet millicylinders were weighed, dried by vacuum for 2 days, and weighed again to determine the mass loss and water uptake, and SEM images acquired. The amount of 4HPR released was determined by assaying the amount of 4HPR remaining in recovered millicylinder by loading assay

2.3.8. 4HPR UPLC-UV Assay

4-HPR levels in *in vitro* release media and millicylinders digests were determined by UPLC/UV. Because of 4HPR's high extinction coefficient (47,900 M^{-1}-cm^{-1} at 365 nm), excellent sensitivity was achieved via UPLC/UV with a LLOQ of 5 ng/mL. The reverse phase UPLC/UV analyses were carried out with a Waters Acquity UPLC system and Empower software under the following conditions: Acquity BEH C18 2.1x100 mm column, mobile phase 80:20 ACN: ddH_2O + 0.1% H_3PO_4, isocratic flow rate 0.65 mL/min, UV detection at 365 nm, and total analysis time of 2 min. 4HPR calibration standards were prepared in mobile phase (0.5-100 µg/mL) from a 0.5 mg/mL 4HPR stock solution in ACN, which reflects the large linear dynamic calibration range.

2.3.9. CaDC/NaDC UPLC-MS Assay

A UPLC-MS assay for NaDC and CaDC was developed using Waters Acquity UPLC-MS (quadrupole mass analyzer, Acquity QDa) system and Empower software under the following conditions: Acquity BEH C18 2.1x100 mm column, mobile phase 37.5:37.5: 25 MeOH: ACN: 0.02 M NH_4COO pH adjusted to 4.3 with HCOOH, isocratic flow rate 0.4 mL/min, and total analysis time of 3 min. MS was operated in positive ion mode and the molecular ion m/z 392.5 (dexoxycholic acid) was monitored. NaDC calibration standards were prepared by dissolving a stock solution 5 mg/mL NaDC in PBS, and working standards prepared in the range of 10-500 µg/mL.

2.3.10. Millicylinder Morphology via Scanning Electron Microscopy

The morphology of millicylinders was examined by scanning electron microscopy (SEM) using a Phillips XL FEG SEM. The millicylinders were dried, sputter coated with gold

for 90 sec, then imaged using 3 kV electric beam. Cross section and surfaces of millicylinders were imaged and inspected for 4HPR crystallization or solubilization in polymer matrix.

2.3.11. Protein content in PLGA after *in vivo* Release by LECO Nitrogen Analysis

The amount of protein infused into 4HPR PLGA millicylinders after *in vivo* release was determined by nitrogen analysis on LECO instrumentation (TruSpec CHN Micro, PN200-716, St. Joseph, MI). The LECO instrument was calibrated by weighing EDTA standards ranging from 0.2 -3 mg, and percent nitrogen content was determined upon incineration of sample. To prepare samples for the protein analysis, the PLGA millicylinders (20% 4HPR + 20% NaDC+15% $MgCO_3$ + 1% PVP) were carefully removed from SC tissue after 28 and 42 days of *in vivo* release with minimal excess tissue encasing the implant. The drug was extracted from implant using the 4HPR loading assay (section 2.4), supernatant was removed, and 4HPR levels determined. The remaining precipitate (likely composed of PLGA and proteins, both of which are insoluble after the loading assay) was dried at 40 °C x 2 days in a vacuum oven, and dried mass was recorded. The percent nitrogen in the PLGA-protein pellet was measured, and percent protein was estimated by normalizing to the model protein BSA (16% w/w nitrogen), as albumin is the most abundant serum protein. To summarize this mass balance quantitation, the total composition of the millicylinder was determined by: 1) percent 4HPR by loading assay, 2) percent protein by nitrogen analysis, and 3) PLGA calculated from total mass of dried implant - (4HPR + protein).

2.3.12. Effects of 4HPR Implants on OSCC Tumor Nude Mice Xenografts

The efficacy of 4HPR-PLGA millicylinders designed for 30-day controlled release dosing were tested by their effect on OSCC tumor xenografts. These studies were conducted at Ohio State University animal facility in accordance to ULAR regulations. For tumor induction,

1×10^6 SCC2095sc human oral squamous cell carcinoma (OSCC) tumor cells were injected into right-back flank side athymic nude mice. OSCC tumor masses were developed for 7 days after OSCC cell injection. Mice were randomly assigned to two groups (n=4), including: 1) control sham- PLGA millicylinder and 2) two CR 4HPR-PLGA millicylinders implanted alongside of tumor, with treatment duration of 10 days. All mice were weighed and tumor volume was recorded each day. On day 10, mice were euthanized, 4HPR millicylinders were removed, wet mass recorded, then dried to obtain percent water uptake, then assayed for percent 4HPR release by loading assay. Statistical analysis was performed to analyze differences in the control sham-PLGA to the 4HPR-PLGA formulations on tumor growth inhibition using an unpaired t-test analysis.

4HPR levels in tumors were quantified via tumor homogenization followed by drug extraction. The wet mass of tumor was recorded, internal standard was spiked into tissue (50 µL of 5 µg/mL acitretin), and 2 mL ice cold RIPA lysis buffer (to lyse contents of cells) was added to the tumor and homogenized using mechanical homogenizer (10,000 rpms x 1 min). Next, 3 mL ice cold ACN was added, homogenates sonicated on ice for 10 min, followed by centrifugation at 10,000 rpm x 10 min at 4 °C. The supernatant was assayed by UPLC/UV and normalized by internal standard recovery. 4HPR levels in serum were determined by spiking 10 µL 5 µg/mL acitretin into 50 µL serum, adding 140 µL ice cold ACN, sonicating on ice x 10 min, followed by centrifugation, and assaying supernatant by UPLC.

2.4.   Results and Discussion

2.4.1. Effect of 4HPR Loading on *in vitro* Release

To determine the maximum drug loading that would allow for the most continuous and complete release, we selected PLGA 503H for controlled release of 4HPR based on our

previous work with formulating 4HPR into microspheres and ISFIs (10). The free-acid low molecular weight PLGA continuously erodes at physiological conditions to allow continuous release (22). Also, we have found a positive effect upon addition of a poorly soluble basic salt (i.e. solubilizes upon pH lowering like antacids) on release of proteins and hydrophobic small molecules from PLGA millicylinders, which is attributed to pore formation and neutralization of PLGA monomers that have degraded within the bulk polymer (23). Based on these considerations, 4HPR was encapsulated in PLGA 503H millicylinders containing 3% $MgCO_3$. Loading levels of 4HPR were varied at 10, 20 and 30% and *in vitro* release was evaluated (as shown in Fig. 2-1). In the higher 4HPR loading levels (20, 30%) a 2-week lag phase was present, whereas 10% 4HPR had a more continuous release and released the greatest percentage after day 28 (53%). Therefore the 10% 4HPR-loaded implant formulation containing 3% $MgCO_3$ was selected for *in vivo* release and characterization as described below.
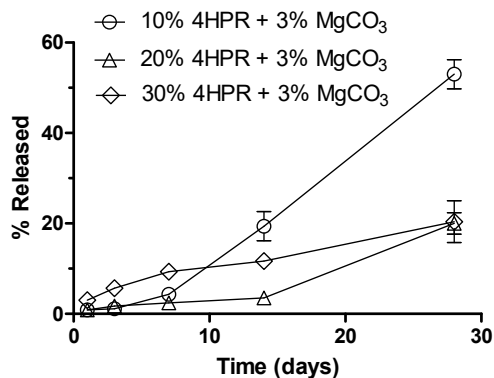
Figure 2-1: Effect of 4-HPR loading on *in vitro* release. The implants were composed of PLGA 503H + 3% $MgCO_3$ + 10, 20 or 30% 4HPR. Values represent mean ± SE (n=3).

2.4.2. In *vivo* release of 4HPR-PLGA Millicylinders with Pore Forming Agent

The optimal releasing implant from Fig. 2-1 containing a pore forming agent was evaluated after SC implantation in rats. Kinetics of drug release, implant erosion, and water uptake were examined as shown in Fig. 2-2a. Although the 10% 4HPR with 3% $MgCO_3$ pore-forming solubilizing base formulation performed well *in vitro*, very little if any controlled release was observed *in vivo*, with much less drug released by day 28 (18% *in vivo* vs. 53% *in vitro*). This *in vivo/in vitro* discrepancy may reflect the presence of high levels of Tween 80 solubilizer present in the *in vitro* release media. The PLGA *in vivo* erosion kinetics is shown in Fig. 2-2b for the 4HPR formulation and the no-drug sham control (i.e. PLGA + 3% $MgCO_3$). Polymer erosion was nearly complete after day 28, however, 82% of drug remained. Moreover, most of 4HPR release occurred on the first day. The erosion rates of drug and sham formulations were similar, with slightly faster erosion in the sham, which indicates that 4HPR does not significantly alter the PLGA 503H millicylinder standard erosion profile. As seen in the figure, there was a significant polymer mass loss that occurred between 14-28 days, which is consistent with expected PLGA 503H erosion kinetics from the dense implant. SEM images showing the erosion over 28 days for both the drug and sham implants can be found in Supplemental Information Figure S2-1. The incomplete release from the implant along with the high PLGA erosion rate confirms our suspicion that the polymer has little effect on the late stage 4HPR release, and it is highly likely release is governed by the slow dissolution of the solid drug itself.

A in vitro 10% 4HPR+ 3% MgCO$_3$
in vivo 10% 4HPR+ 3% MgCO$_3$

% Released

B in vivo no-drug sham control
in vivo 4HPR

% Erosion

C in vivo no-drug sham control
in vivo 4HPR

% Water Uptake
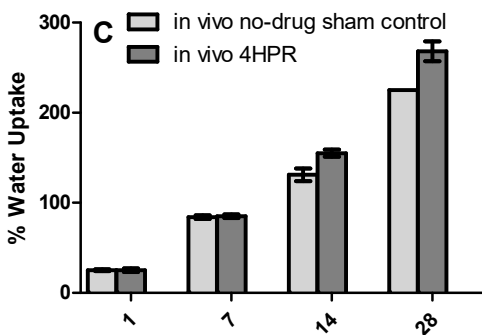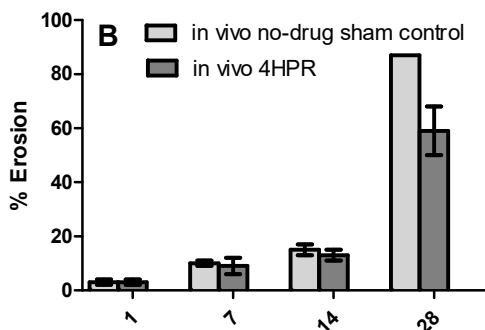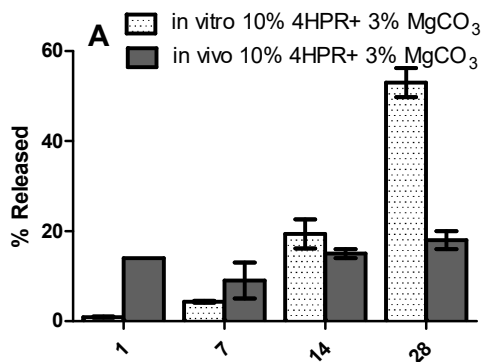
Figure 2-2. In vivo performance of 4HPR PLGA millicylinder formulation without solublizers (10% 4HPR + 3% MgCO$_3$). a) 4HPR release in vivo vs. in vitro (in a solubilizing media containing PBS+ 2%Tween), b) in vivo erosion of 4HPR PLGA implants compared to sham implants (PLGA + 3% MgCO$_3$ only), and c) *in vivo* water uptake in 4HPR PLGA implants and sham PLGA implants. Values represent mean ± SE (n=3).

The water uptake kinetics (Fig. 2-2c) of both the drug and sham implant were also similar, with 225% and 228% water uptake respectively. Water uptake is therefore not affected by the presence or absence of drug in the implant.

2.4.3. Solubility and Release Enhancing Excipients

Previous studies from our group indicated that 4HPR's poor aqueous solubility adversely affected a 4HPR controlled release during the 1 month study [13]. To enhance 4HPR solubility and polymer drug release, we introduced several solubilizing excipients, crystallization inhibitors, and disintegrants for co-encapsulation with the drug and PLGA. NaDC selection was based on numerous studies on the solubilization and permeation enhancing behavior of bile salts(24,25, 26) inclusive of retinoid solubilization (27,28). The

aqueous solubility of 4HPR at 37 ˚C in the presence of excipients is shown in Fig. 2-3. NaDC provided the best solubilization with 20% NaDC providing 1030 µg/mL 4HPR solubility, i.e., a 200:1 mass ratio of NaDC: 4HPR. β-CD resulted in a 40 µg/ml 4HPR solubility at 20% excipient level. The crystallization inhibitor/pore forming agent HPMC did not solubilize 4HPR, while the disintegrant/crystallization inhibitor PVP K30 provided only minimal solubility enhancement of 0.66 µg/mL at 20% PVP compared to 0.2 µg/ml 4HPR aqueous solubility without excipients. Despite little solubility enhancement achieved with HPMC and PVP, these agents were still pursued as they could improve release kinetics by alternative aforementioned mechanisms.

We have proceeded to develop 4HPR-PLGA millicylinders that were capable of accelerating *in vitro* release (Supporting Information, Fig. S2-2) by 1) increasing 4HPR solubility by addition of 20% NaDC, and 2) increasing PLGA porosity to aid in drug diffusion by increasing ($MgCO_3$). The addition of the 20% NaDC allowed us to achieve a 20% drug loading, while decreasing the 3-week lag phase. In this solubilized formulation (20% NaDC), increasing $MgCO_3$ from 3% to 15% further enhanced the extent of 4HPR release after 28 days from 50% to 71%. Next the effects of specialized excipients (β-CD, HPMC, and PVP) added to PLGA +20% 4HPR + 20% NaDC + 15% $MgCO_3$ millicylinders were examined *in vit*ro and *in vivo* as shown in the following section.
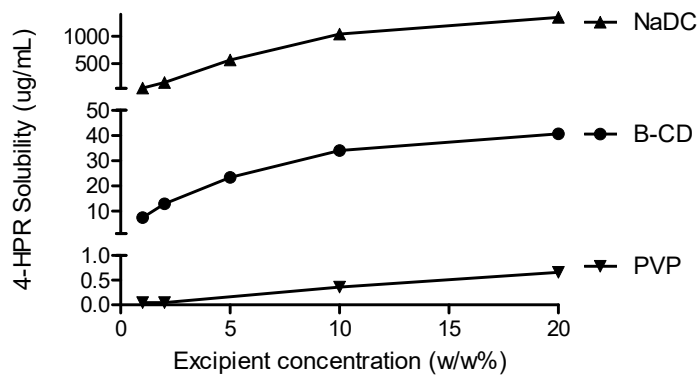
Figure 2-3. Effect of excipient concentration on 4HPR solubility in deionized water at 37 °C.

2.4.4. In vivo Release from 4HPR-PLGA millicylinders with Solubilizers and Crystallization Inhibitors

The next set of PLGA millicylinders formulations aimed to increase 4HPR release *in vivo* by co-incorporating a high level of solubilizers, pore forming agents, and specialized excipients. The baseline formulation tested was 20% 4HPR + 20% NaDC + 15% $MgCO_3$. The specialized excipients included: 5% β-CD to enhance solubility by formation of an inclusion complex with 4HPR, 1% HPMC K4M to promote swelling, aide in pore formation, and inhibit crystallization, and 1% PVP K30 to enhance solubility, inhibit crystallization, and aid in disintegration. The *in vivo*/*in vitro* release with these specialized excipients is shown in Fig. 2-4a. Much slower release was observed *in vivo* for all compared to *in vitro* (day 28 release was ~25% vs. ~80%), and release *in vivo* in these cases was only slightly improved compared to the initial formulation containing 10% 4HPR+ 3% $MgCO_3$ (Fig. 2a) without solubilizers (25% vs 18% by day 28). Inclusion of the crystallization inhibitor PVP to the baseline formulation was effective at providing controlled release of 4HPR, whereas the other excipients additives had an initial burst release with no further drug release until after 4 weeks.

52

The PLGA erosion was evaluated, and all these formulations showed similar erosion profiles, which were unaffected by HPMC, β-CD, or PVP (Fig 4b). The erosion profiles were as follows: 0-15% of eroded on day 1, 15-25% eroded by day 7, and 20-30% eroded by day 28. Greater variability on day 28 likely reflects the extent of millicylinder-attached to surrounding connective tissue. Higher connective tissue levels could result in an overestimate of mass (and underestimate of PLGA erosion). On day 28, these implants containing high levels of $MgCO_3$ and NaDC had significantly less PLGA erosion compared to the non-solubilized implant (30% vs 60%), but nonetheless released more drug. These findings are consistent with the *in vitro* mechanistic data provided in the Supplemental Information (Fig. S2-3), which showed that NaDC and $MgCO_3$ inhibit PLGA erosion, but also promote implant water uptake due to their osmotic properties. These results indicate that 4HPR release from PLGA implants *in* vivo is not an erosion-controlled process over the 28 day period.

Implant water uptake was evaluated as shown in Figure 2-4c, and was similar for these 4 formulations, where all excipients (B-CD, HPMC, and PVP) promoted same level of water uptake as the baseline formulation containing 20% NaDC and 15% $MgCO_3$, yielding $\sim 75\%$, 150%, 250% water uptake on days 1, 7, 28 respectively. When compared to the initial formulation without solubilizers (Fig. 2-2c), we see that the presence of these osmotic agents only significantly increased water uptake on day 1, while after 7 and 28 days, they behaved similarly (25%, 155%, 225%), but was much less compared to in vitro (>500% after 28 days), indicating that the tissue environment decreases implant water uptake. This again confirms that that drug release *in vivo* from PLGA implants is not driven by implant water uptake.
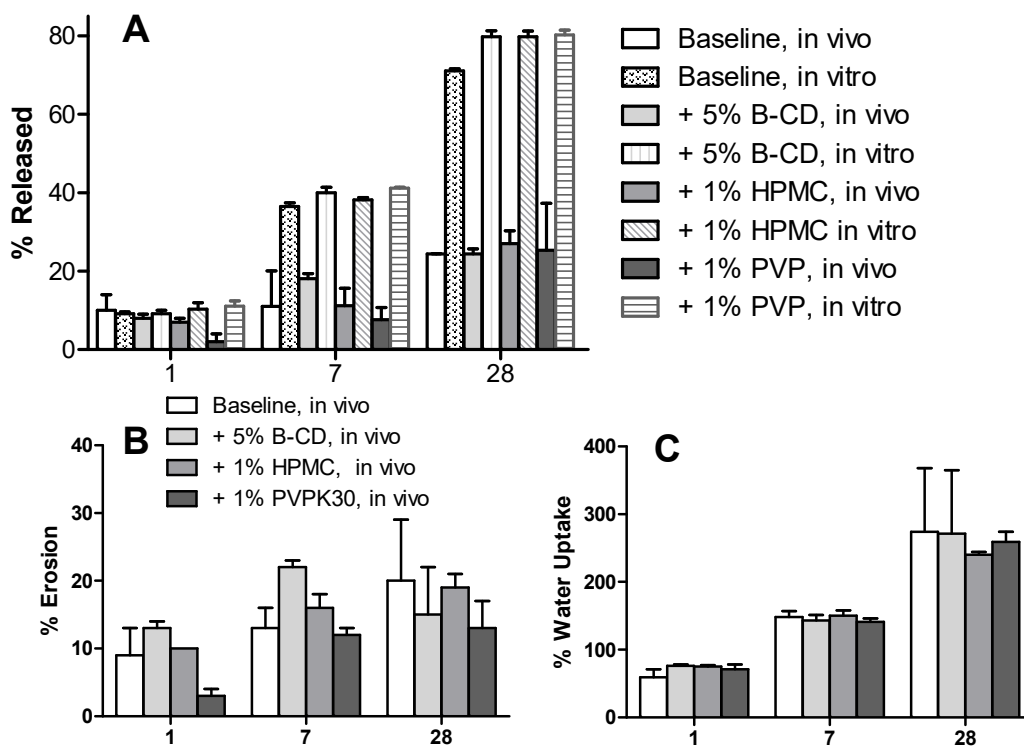
Figure 2-4. a) *In vivo /in vitro* release for PLGA 503H + 20% 4HPR + 15% MgCO3 + 20% NaDC (baseline) and specialized excipients including 5% B-CD, 1% HPMC K4M, and 1% PVP K30. b) Implant erosion, and c) implant water uptake *in vivo*. (mean ± SE, n=3)

Thus far we have shown that addition of solubilizing, pore forming agents and specialized excipients to the PLGA implants, while effective *in vitro* at accelerating 4HPR release, had little effect *in vivo* on accelerating 4HPR release after 4 weeks (~25% drug release). Furthermore, we have concluded from these two *in vivo* experiments (with and without solubilizers) that neither PLGA erosion rate nor implant water uptake can explain the slow *in vivo* drug release. Therefore, the likely cause is very slow dissolution of the drug. To test this, 4HPR *in vivo* release from PLGA implants with solubilizers was compared to a water-soluble matrix implant (PVA/sucrose) over 2 months. In addition, a second PVA/sucrose formulation incorporated a solubilizer and crystallization inhibitor (NaDC, PVP). Two salt forms of deoxycholic acid (sodium and calcium) were utilized in the PLGA formulations, with

the intent that the less water soluble CaDC would be released slower, and help facilitate 4HPR

release out of implant at later time points. A water-soluble matrix implant was prepared in a

PVA/sucrose vehicle with and without solubilizers (20% 4HPR+ 20% NaDC + 1% PVP), and

compared to PLGA formulation previously shown to have the most desirable release (Fig. 2-4,

20% 4HPR + 15 % $MgCO_3$ + 1% PVPK30+ 20% NaDC or CaDC). The *in vivo* evaluation

(Fig. 2-5a) shows a controlled 4HPR release over 2 months for the PLGA formulations, and

that the effect of bile salt type (sodium vs. less soluble calcium salt) had little effect on the rate

of 4HPR release, which exhibited a 3-week lag period. Notably, both bile salts showed nearly

identical 4HPR release profiles, despite achieving a slower release of the deoxycholic acid

(DC-) solubilizer over 14 days with the calcium salt, compared to an 80% burst release with

NaDC (Fig. 2-5c). These results indicate that 4HPR release from PLGA millicylinders may not

be controlled by solubilization, at least not by NaDC.

When examining the drug release from the water soluble PVA/sucrose implants, we

observed that 4HPR was released steadily during the first 3 weeks, then a large surge in drug

release, followed by a controlled release pattern similar to the PLGA implants in weeks 4-6

(Fig. 2-5a). The additional solubilizing excipients in this PVA/sucrose implant led to an

accelerated 4HPR release after 28 days, where 78% was released vs. 59% for those without the

extra excipients. In the PLGA CR formulations, only 32% 4HPR was released after 1 month,

and the presence of the 3-week lag phase is likely due to the rate of PLGA erosion, where we

have previously shown (Fig. 2-4c) that PLGA did not exhibit appreciable erosion *in vivo* until

after 2 weeks. After 1 month, the water-soluble excipients would have dissipated from the

implantation site, leading us to the logical conclusion that the controlled release is due to

dissolution of the hydrophobic drug solid into the surrounding aqueous tissues. After 6 weeks,

both water soluble PVA/sucrose implants formulations (with and without solubilizers) had performed similarly, and released ~90% 4HPR, whereas the PLGA only released ~50% 4HPR. Similarities in the release slopes of PLGA and PVA/sucrose implants between weeks 4-6 suggests that late stage release of 4HPR from PLGA is controlled by dissolution of the drug.

The images of the implants after a month *in vivo* release in rat SC tissue are shown in Figure 2-5b, and we see that the PLGA implants maintained their cylindrical shapes, with no apparent yellow 4HPR diffusion into the surrounding tissue. The PVA/sucrose implants were no longer in their millicylindrical form, and the addition of the NaDC and PVP solubilizers enabled greater 4HPR tissue dispersion. We further note that the two implants (PVA/sucrose, PLGA) could potentially be used together for further extended release as the water soluble PVA/sucrose formulation can be used to overcome the initial lag phase, while PLGA can provide a 2+ month long acting release of 4HPR.

These data from 4HPR *in vivo* release from millicylinders align with results from our previous PK study, where a slow and continuous release of 4HPR from a SC injected drug suspension occurred after 2 weeks, following a large burst release, confirming that the controlled release properties are due to the dissolution of the hydrophobic drug. The fact that 4HPR release from PVA/sucrose water-soluble matrix formulation is faster than the PLGA and different from the solid control used in PK study, suggests that perhaps the PVA/sucrose formulation may release faster than pure 4HPR crystals. We were unable to test 4HPR crystals here because we could not collect them to determine the fraction drug remaining, but future PK analyses could be used to determine this question.
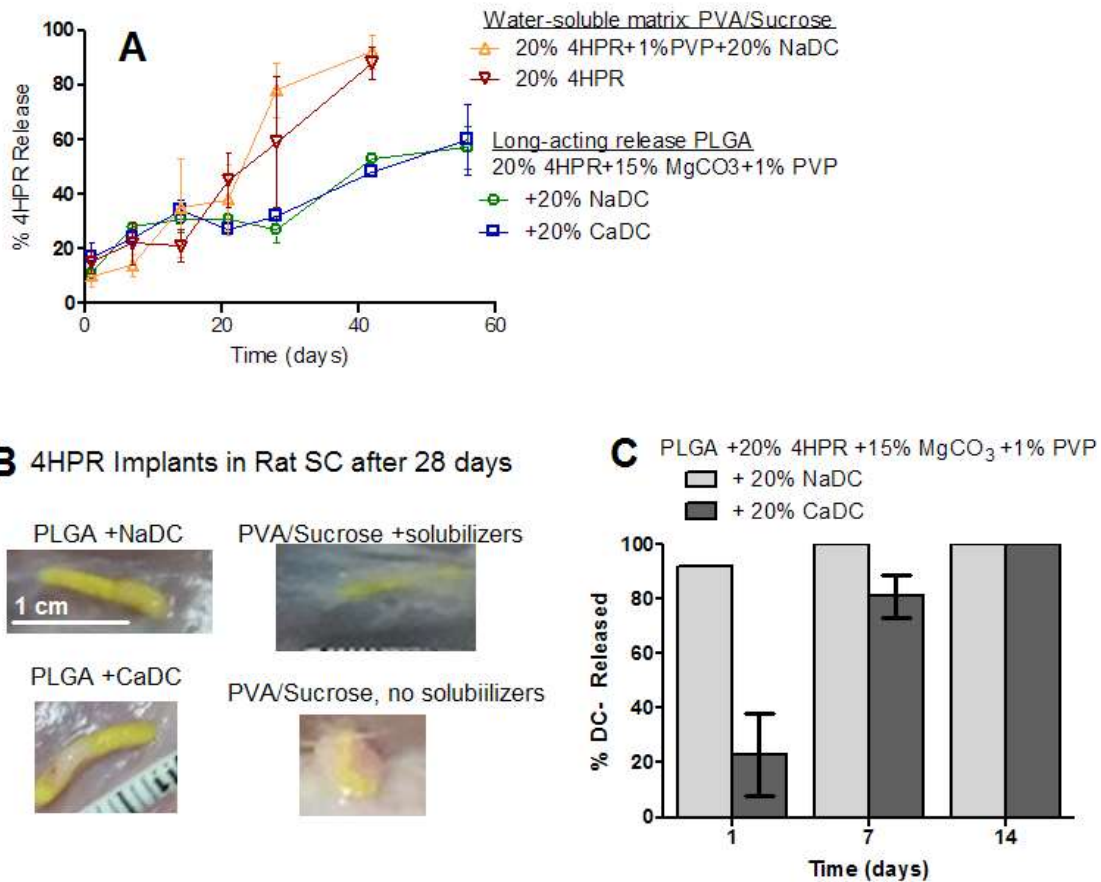
Figure 2-5 a) *In vivo* release of 4HPR from CR PLGA millicylinders vs. water soluble matrix PVA/sucrose implants with and without solubilizers. The PLGA implants contained 20% 4HPR + 15% MgCO3 + 1% PVP+ 20% NaDC or CaDC, while the PVA/sucrose implants contained either 20% 4HPR or additional solubilizer and crystallization inhibitor (20% NaDC + 1% PVP). b) Implant images prior to harvesting from rat SC tissue on day 28 (yellow represents 4HPR). C) *In vivo* release of sodium and calcium deoxycholic acid (DC-) from PLGA millicylinders. *(*mean ± SE, n=3)

These PLGA-4HPR millicylinders were further examined to determine what other physiological factors besides polymer properties were hindering drug release and dispersion into tissue. These tests included SEM images of tissue-millicylinder interactions and nitrogen analysis to estimate protein levels within the millicylinders. The SEM images of a PLGA millicylinder (20% 4HPR + 15% $MgCO_3$ + 1% PVP+ 20% NaDC) after 28 days in the SC environment are displayed in Figure 2-6. In these micrographs, the tissue binding to the

millicylinders is quite apparent, where the millicylinder has become completely encased within a fibrous tissue capsule. The resistance exerted by this tissue encasing could be partially responsible for the inhibition of drug release from the millicylinders. Upon harvesting of the millicylinder, the tissue encasement was removed and the extracted millicylinder (Fig. 2-6 c,d) was further examined. Observation of the implant cross sections shows mostly crystalline species, perhaps drug or protein, along with remnants of the porous PLGA matrix. The low local pH within the PLGA implant could be contributing to plasma protein precipitation. The composition of this drug-polymer-protein mass was investigated after removing from the tissue encasement and the amount of protein was estimated via LECO nitrogen analysis. After 28 days, the extracted millicylinder contained $23 \pm 1\%$ w/w 4HPR of the extracted mass, similar to the initial drug loading of 20%. From the LECO analysis, the estimated percent protein (normalized to BSA) bound in this extracted mass was $25 \pm 4\%$, and PLGA was calculated to be $52 \pm 5\%$, which aligns well with the *in vitro* erosion data for this formulation of 60%. After 42 days, this extracted PLGA-4HPR-protein was composed of 16% 4HPR, ~55% protein, and ~29% PLGA. From this analysis, we observe high levels of protein within the PLGA-4HPR implant, which could play a role in the drug release.
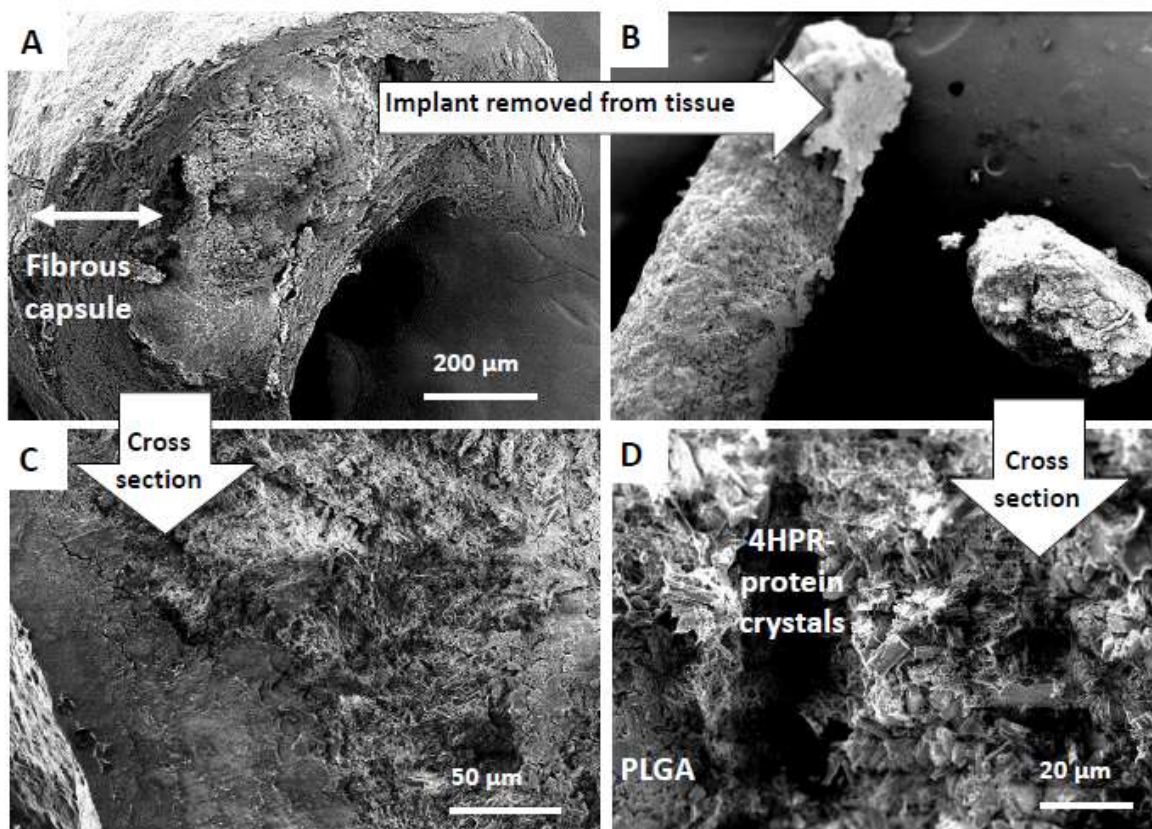
Figure 2-6. SEM images depicting 4HPR-PLGA millicylinders interactions with the tissue environment after 28 days in vivo. PLGA millicylinder shown was composed of 20% 4HPR + 15% $MgCO_3$ + 1% PVP+ 20% NaDC. a) Cross section of millicylinder encased with tissue, b) zo zoomed in to show tissue growth into millicylinder, c) 4HPR-PLGA millicylinder removed from tissue encasing, and d) cross section (zoomed in to show precipitated 4HPR, permeated tissue components, and remaining PLGA matrix).

2.4.5. Evaluation of *in vivo* Efficacy

The optimized and characterized formulation of 503H+ 20% 4HPR+ 20% NaDC + 15% $MgCO_3$ + 1% PVP was tested *in vivo* in tumor xenographed mice for the ability to decrease the rate of tumor growth compared to control blank PLGA millicylinders + PBS injections. Spatial dependency of the tumor growth suppression effects of polymer implants on tumor growth were assessed by daily caliper measurements. As shown in Figure 2-7, the PLGA-4HPR millicylinders were effective at reducing the rate of tumor growth over 10 days (1.3 ± 0.3 fold increase in volume from initial, n =3) compared to the control Sham PLGA

millicylinder (2.0 ± 0.3 fold increase, n=2) (Note: smaller sample sizes were used than desired due to lack of tumor xenograph uptake initially, and therefore statistical analysis could not be performed). The efficacy of 4HPR-PLGA millicylinder in these studies served as proof of concept for our full studies that were sufficiently statistically powered and showed that 4HPR was effective in combination with other chemotherapeutic agents tocilizumab, and 2-methoxyestradial at reducing rate of tumor growth (4). Furthermore, H&E stained tissue sections demonstrated tumor necrosis in close proximity to the 4HPR implant, while tumor tissue proliferated a few millimeters from the implants (*data not shown*). Therapeutic efficacious 4HPR levels (>10 μM) of 90 ± 76 μM were achieved in tumor after CR delivery with 4HPR PLGA millicylinders, although levels were highly variable as reflected in the large standard error of the mean. 4HPR was not detected in serum, which is a favorable aspect that local drug delivery is capable of alleviating potentially toxic systemic side effects.

The release performance of the PLGA-4HPR after implantation alongside the perimeter of the tumor is listed in Table 2-1. The PLGA-4HPR millicylinders released 16.0 ± 2.0% of their load after 10 days equating to ~160 μg 4HPR (x 2 millicylinders = 320 μg dosed), which was approximately double of the released amount of the same formulation implanted in flanks of rats (7.5 ± 2.8% released on day 7). This difference could be due to the different properties of tissue environments, where the tissue surrounding the tumor may have greater blood flow and acidic pH compared to the SC tissue. The 4HPR-PLGA implants had greater water uptake compared to the sham PLGA implants (367% vs. 197%, Table 2-1), which aligns well with our mechanistic characterization studies.

Table 2-1. Tumor efficacy study with 4HPR-PLGA millicylinders. Mean $\pm$ SE, n=3

Group	Water Uptake in implant	4HPR release (day 10)	4HPR level in tumor (μM)
Sham PLGA	367 ± 21 %	-	-
4HPR-PLGA	197 ± 22 %	16 ± 2%	90 ± 76
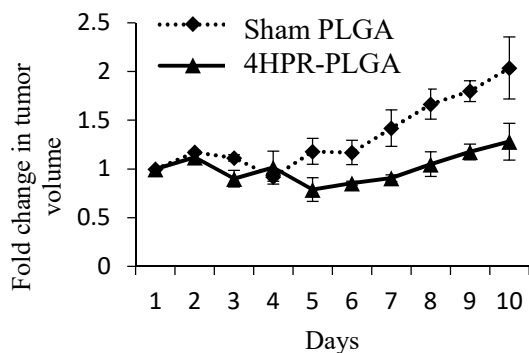
Figure 2-7: Efficacy of 4HPR PLGA millicylinders (503H + 20% 4HPR +20% NaDC+ 15% $MgCO_3$ + 1% PVP) in reducing tumor mass of SCC2095sc human OSCC tumor cells xenographed in Athymic nude mice relative to sham PLGA implants without 4HPR.

2.5. Conclusions

Here we describe our approach to control the release of 4HPR in SC tissues and tumor environments. We found that 4HPR releases from PLGA millicylinders much slower *in vivo* compared to *in vitro,* likely due to difference in solubilization in the *in vitro* release media compared to *in vivo*. After exhibiting a significant lag phase *in vivo*, PLGA implants that included various excipients provide release to proceed continuously for at least 2 months. The lag phase can be obviated by formulating a millicylinder without PLGA but with soluble components (PVA/sucrose/PVP/NaDC) to promote dissolution and crystallization inhibition. Indeed, the shorter and longer acting formulations could be useful in the future as a combination, as the overlapping release may be desired. Initial evaluations of the efficacy of the PLGA implants demonstrate inhibition of OSCC tumor xenographs with local controlled release. Therefore, these data motivate further development of the local controlled release approach for chemoprevention with 4HPR.

2.6. SUPPLEMENTAL INFORMATION

2.6.1. Supplemental Methods

Effects of Implant Erosion, Water Uptake, and Percent Solids on Release kinetics

A mechanistic study was carried out *in vitro* to determine the effects of formulation variables (4HPR loading, $MgCO_3$ levels, presence of NaDC) had on drug release including polymer erosion and water uptake. The *in vitro* release assay was utilized as previously described. Accurate PLGA mass loss was corrected for implant mass loss due to NaDC and 4HPR released at given time points. The following equations were used:

$$Implant\ Erosion = \frac{Initial\ mass - final\ dry\ mass}{inital\ mass} \ x\ 100\%$$

$$Water\ Uptake = \frac{Final\ wet\ mass - final\ dry\ mass}{final\ dry\ mass} \ x\ 100\%$$

Additionally, the effect of percent solids (4HPR, $MgCO_3$, NaDC) initially present in PLGA millicylinders was correlated with the drug burst release on day 1.

CaDC synthesis and PLGA-CaDC and NaDC millicylinders

The CaDC synthesis method was adapted from literature methods (24). Briefly, to 10 mL of 10 mM NaDC in ddH_2O (pH 7.7), 10 mL of 2 mM $CaCl_2 \cdot 2H_2O$ in ddH_2O (pH adjusted to 9 with 0.1 N sodium hydroxide) was added and stirred at room temperature for 3 h, during which the CaDC salt formed and precipitated. The reaction mixture was centrifuged, and supernatant removed and discarded. The CaDC salt was freeze dried, cryomilled and sieved to < 90 μm. Validation of CaDC synthesis was done by inspecting crystal structure via SEM imaging, and comparing to literature CaDC crystal structures (24, 26), which depicts thin filament mesh-like structures identical to those in the literature.

CaDC and NaDC (20%) PLGA millicylinders were prepared in PLGA 503H and 503 implants, and release evaluated *in vitro* by placing 1 implant into 1 mL PBST 0.02% Tween80. Release media sampled up to 1 month and assayed by LC-MS.

2.6.2. Supplemental Results

Morphology of PLGA-4HPR millicylinders with pore forming agents after in vivo release

The morphology of the initial formulation of PLGA + 10% 4HPR + 3% $MgCO_3$ after *in vivo* release was examined by SEM and compared to a no-drug sham PLGA control (+ 3% $MgCO_3$) (Fig. S2-1), and shows the progression of pore formation and polymer erosion. On day 1, both the no-drug sham and 4HPR implants were folded and had begun to curl. The sham was slightly more porous, but overall they had very smooth surfaces. On day 7, both the sham and 4HPR implants look similar and show an increase in pore size. On day 14, the 4HPR implants have developed a larger pore network and crystals (likely 4HPR) on surface, while the sham-PLGA implants are folded and have a smoother surface. On day 28, both the 4HPR and sham-PLGA have broken apart, showing high polymer erosion, consistent with the erosion loss data in Fig. 2-2c (60% and 85% eroded respectively).

	Day1	Day 7	Day 14	Day 28
10% 4HPR-PLGA				
4HPR 200x				
Sham-PLGA				
Sham 200X				
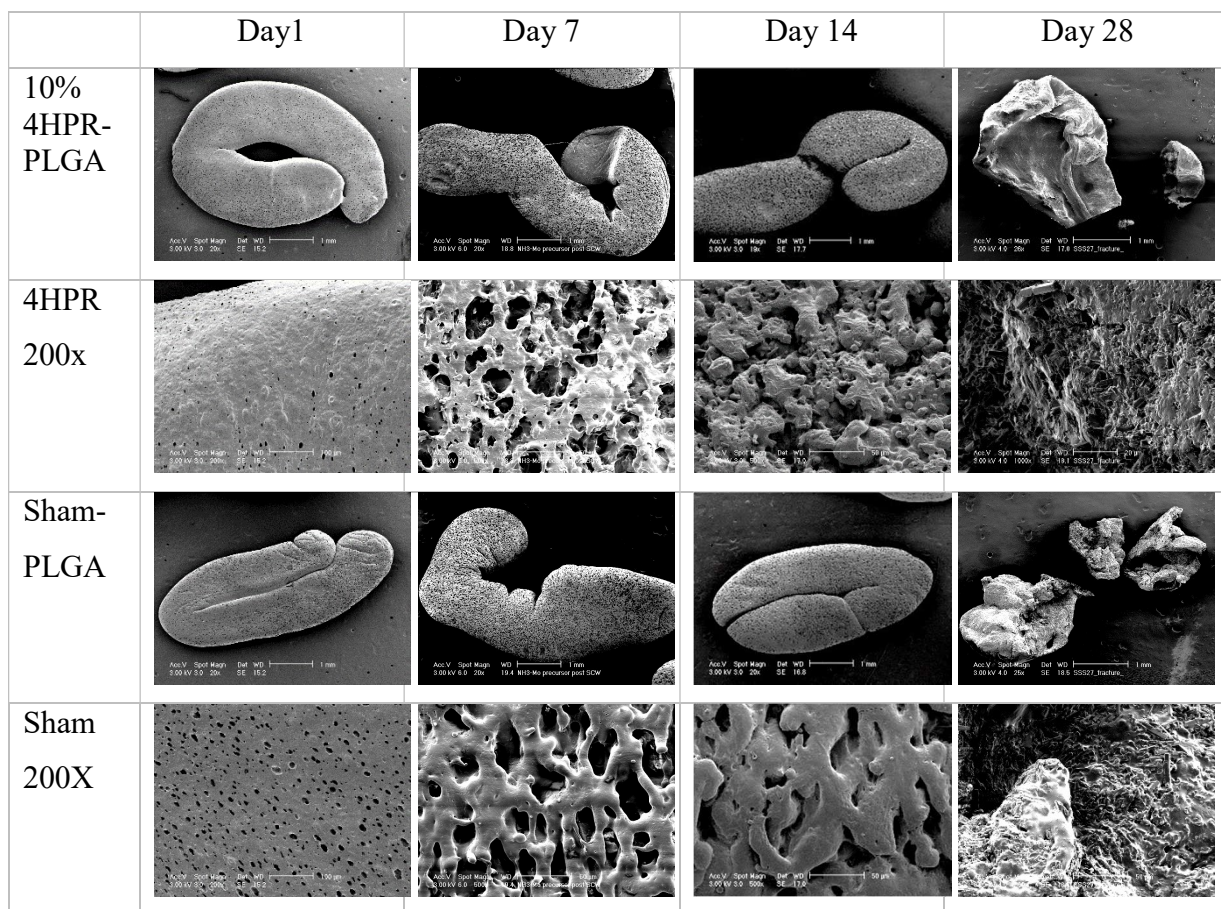
Figure S2- 1. Implant morphology via SEM after in vivo release on days 1, 7, 14, and 28 of PLGA 503H + 10% 4HPR + 3% MgCO3 millicylinders compared to a no-drug sham PLGA + 3% $MgCO_3$ implants.

Optimizing 4HPR Release In vitro By Addition of Excipients

The *in vivo* release profile of implants containing 10% 4HPR + 3% $MgCO_3$ had

incomplete drug release (< 20% 4HPR after 28 days) and lacked controlled release properties.

Therefore, two approaches were taken to accelerate release and evaluated *in vitro*: 1) increase

4HPR solubility by addition of solubilizers, and 2) increase diffusion pathways through

polymer by increasing the level of pore forming agent ($MgCO_3$). Increasing 4HPR solubility

could potentially allow for greater drug loading which would be useful at increasing drug

levels at target site, so 10% and 20% 4HPR + 20% NaDC in PLGA + 3% $MgCO_3$ were

evaluated *in vitro* (Fig. S2-2a). The 10% 4HPR implant performed the same with and without

NaDC, however, substantial increase in percent release was observed with 20% 4HPR + 20%

NaDC. Although the addition of 20% NaDC improved release kinetics substantially by

decreasing the 21 day lag phase, still only ~50% drug was released after 28 days, and therefore

further release enhancement was necessary. The next release enhancement strategy increased

the amount of pore-former $MgCO_3$ (3, 10, 15%) to the solubilized formulation (PLGA + 20%

4HPR + 20% NaDC). As shown in Fig. S2-2b, increasing $MgCO_3$ from 3% to 10% is relatively

ineffective, however, 15% $MgCO_3$ substantially enhances drug released after 28 days from

50% to 71% 4HPR for 10% and 15% $MgCO_3$ respectively. These formulation strategies

proved successful *in vitro* and allowed for greater drug loading to be achieved, resulting in at

75% drug release after 28 days. The effect of these high levels of additives in PLGA

millicylinders will be investigated in the following section.
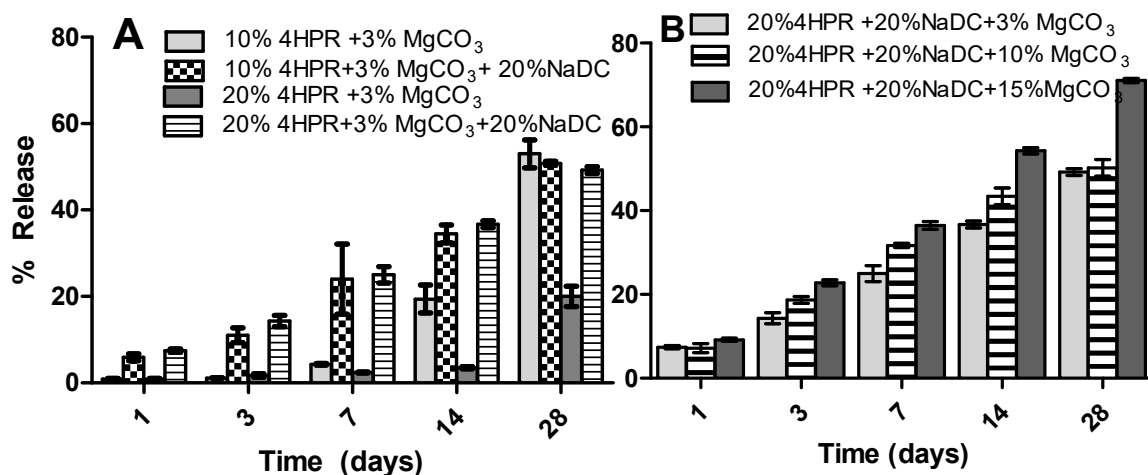
Figure S2- 2. Optimizing in vitro release of PLGA-4HPR millicylinders via solubilization and pore formation. a)
Effect of addition of 20% NaDC to 10% and 20% 4HPR PLGA 503H implants. b) Effect of amount of pore-
forming agent MgCO3 loading (3, 10, or 15%) in PLGA 503H+20% 4HPR + 20% NaDC millicylinders. Values
represent mean ± SE (n=3).

In vitro Mechanistic Evaluation of Parameters affecting 4HPR release: Polymer Erosion, Water Uptake, and Percent Solids

The purpose of these *in vitro* mechanistic evaluations was to elucidate the mechanism(s) of 4HPR release from PLGA millicylinders and delineate the effects of drug loading, $MgCO_3$ level, NaDC, and total percent solids initially present in implant had on implant erosion, water uptake, and the extent of 4HPR release. The formulations that were evaluated are listed in table S2-1.

Table S2- 1. Representative formulations for *in vitro* characterization study

Formulation #	4HPR (%)	$MgCO_3$ %	NaDC%
1	10	3	
2	20	3	-
1 & 2 sham	-	3	-
3	20	3	20
3 sham	-	3	20
4 sham	-	15	20
5 sham	-	15	-

First, effect of 4HPR, NaDC, or $MgCO_3$ on polymer erosion was evaluated (Fig S2-3a). No differences in PLGA erosion was observed at different 4HPR loading levels (10% [#1] and 20% [#2], 54%, and 59% respectively), but was slightly greater than the corresponding no-drug formulation (47%). The addition of 20% NaDC (to the 3% $MgCO_3$+ 20% 4HPR implant [#2]) resulted in significantly less erosion compared to its corresponding sham control #3 (27% vs 58%). The no-drug sham #3 with 20% NaDC+ 3% $MgCO_3$ had similar erosion to implants containing 4HPR without NaDC (#1,2). When $MgCO_3$ is increased from 3% to 15% in implants containing 20% NaDC (#3 vs #4), the erosion significantly slows from 58% to 40%. When NaDC is removed from these implants (#5), the erosion is further decreased to only 33%. To summarize, increasing 4HPR loading slightly increased implant erosion, while NaDC

slightly prolongs erosion, and increasing $MgCO_3$ levels to 15% dramatically decreased the erosion rate.

Another parameter that can affect the rate of drug release from implant is the extent of water uptake, which drives PLGA hydrolysis and erosion. Because 4HPR is hydrophobic, increased water uptake may facilitate faster drug precipitation within the implant and hinder drug release. As shown in Figure S3b, increasing the drug loading from 10% to 20% (#1 and #2) resulted in a substantial uptake in water after 28 days (505% vs. 159%), and both were greater than the corresponding sham formulation (119%). We can conclude that 4HPR draws water into implant over time. Both NaDC and $MgCO_3$ substantial increased implant water uptake, as expected due to their osmotic properties. On day 7, the greatest water uptake occurred with the sham +15% $MgCO_3$ (#5), which had 4x's more water uptake than the sham +3% $MgCO_3$ (#1, 2), but only 2x's greater water uptake than sham implants containing 20% NaDC + 15% $MgCO_3$ (#4 sham). It can be concluded that the extent of water uptake in PLGA implants is influenced by $MgCO_3$ > NaDC > 4HPR. Although positive release effects via solubilizers and pore forming agents are observed in early stage release, erosion inhibition and excessive implant water uptake could negatively impact later stage drug release due to precipitation of 4HPR within the implant.
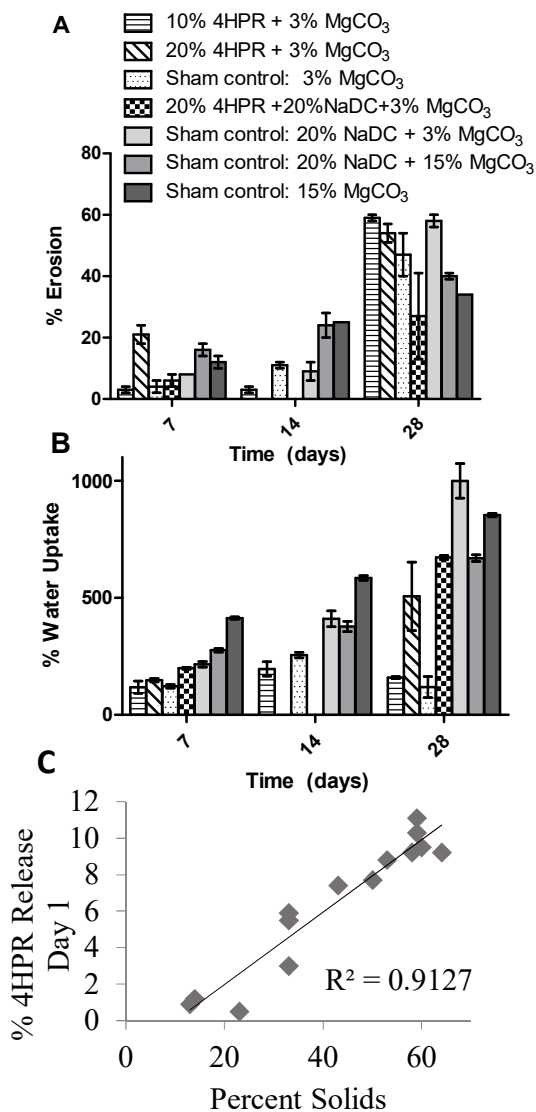
Figure S2- 3. Mechanistic *in vitro* evaluation of formulation variables (4HPR loading, $MgCO_3$ levels, and NaDC) on: a) PLGA implant erosion, and b) water uptake. C) Effect of percent solids on amount of 4HPR burst release on day 1.

Next, the effect of percent solids (4HPR, $MgCO_3$, NaDC) initially present in PLGA millicylinders was correlated with the extent of drug burst release on day 1 (Fig. S2-3c), and show that greater percent solids lead to greater burst release (r^2=0.91), likely due to formation of pores as the water soluble excipients escape the implant. Some formulations contained > 60% solids, leaving less than 40% PLGA matrix to govern the controlled release.

Astonishingly, although only 40% PLGA was present, only a small amount of 4HPR was released (<10%) after day 1, further validating that 4HPR release is a dissolution controlled mechanism, rather than controlled release from its PLGA matrix.

CaDC Synthesis and In vitro Release from PLGA millicylinders

We hypothesized that the solubilizer NaDC would be almost completely released from the implant within the first week due to its high aqueous solubility, and therefore drug release would halt once the solubilizer was gone. This was the case in both *in vitro* and *in vivo* release of NaDC (80% released after 1 day, Fig. 2-5c). In attempt to provide slow the CR of this solubilizer, the calcium salt of deoxycholic acid (CaDC) was synthesized, due to its lower aqueous solubility. Validation of CaDC salt was confirmed by SEM image in Fig. S2-4a, showing the filament mesh-like crystal structures similar to literature. The results from the *in vitro* release from PLGA millicylinder (Fig. S2-4b) shows that CaDC releases much slower than NaDC in PLGA 503H, whereby 29% released by day 28 compared to 72% for NaDC. Also, slower CaDC release was observed in the 503H formulation compared to 503 (29% vs 87% by day 28), indicating that the acid end-capped polymer will provide the most controlled release of this bile salt. Contrary to our suspicions, CaDC from the ester capped PLGA released much faster than acid-capped PLGA, where we suspected that the calcium ions would bind strongly to carboxylic acid end-capped PLGA.
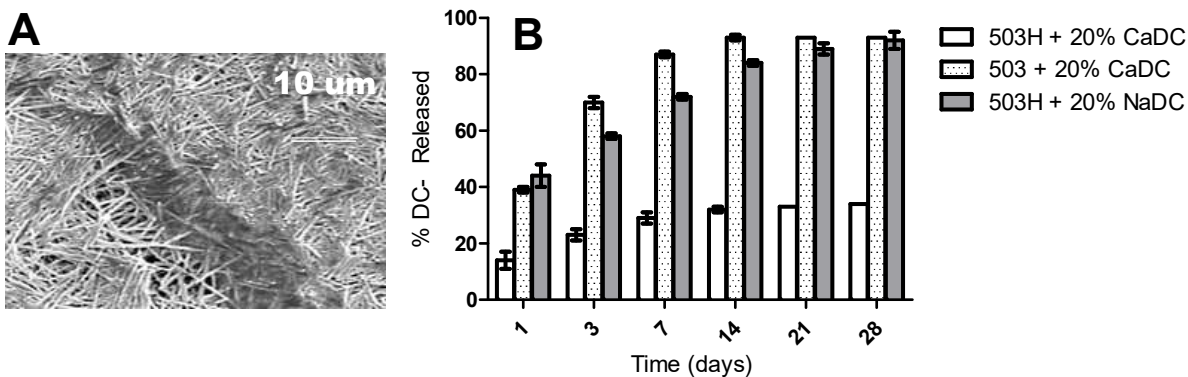
Figure S2- 4.a) SEM image of CaDC crystals, and b) in vitro release of 20% NaDC and CaDC from PLGA 503 and 503H millicylinders in PBST 0.02% pH 7.4 (mean ±SE, n=3).

4HPR Tumor Levels after 4HPR-PLGA Millicylinder Dosing

A sample chromatogram trace of 4HPR extracted from the OSCC tumor after PLGA-4HPR millicylinder delivery is shown Figure S2-5. Acitretin, a synthetic retinoid, served as the internal standard and was added prior to tissue extraction. Known peaks are labeled.
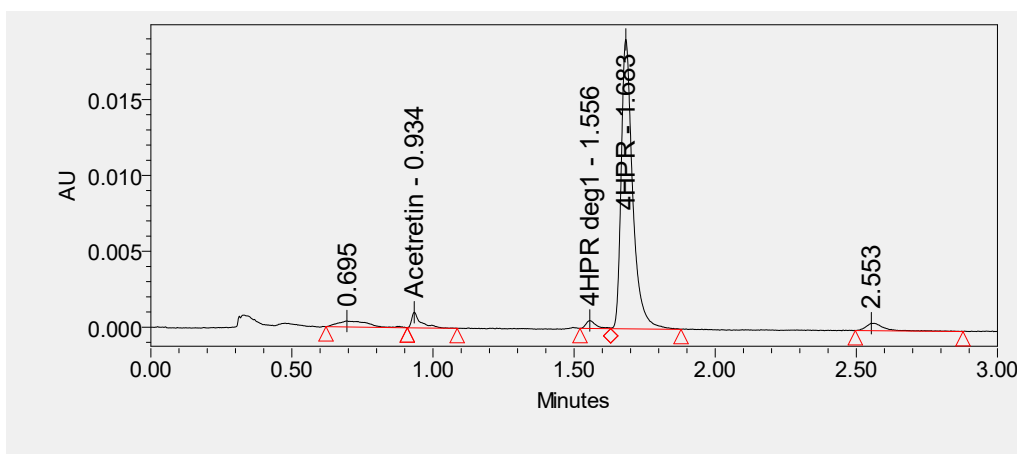
Figure S2- 5. UPLC-UV Chromatogram of 4HPR dosed OSCC tumor extract, showing the recovery of the internal standard acitretin, 4HPR's major degradation product, and 4HPR peak.

2.7. References

1. Reibel, J., Prognosis of oral pre-malignant lesions: significance of clinical, histopathological, and molecular biological characteristics. *Critical reviews in oral biology and medicine : an official publication of the American Association of Oral Biologists* **2003,** *14* (1), 47-62.
2. Holpuch, A.; Desai, K.-G.; Schwendeman, S.; Mallery, S., *Optimizing therapeutic efficacy of chemopreventive agents: A critical review of delivery strategies in oral cancer chemoprevention clinical trials*. 2011; Vol. 10, p 23-23.
3. Han, B. B.; Li, S.; Tong, M.; Holpuch, A. S.; Spinney, R.; Wang, D.; Border, M. B.; Liu, Z.; Sarode, S.; Pei, P.; Schwendeman, S. P.; Mallery, S. R., Fenretinide Perturbs Focal Adhesion Kinase in Premalignant and Malignant Human Oral Keratinocytes. Fenretinide's Chemopreventive Mechanisms Include ECM Interactions. *Cancer Prevention Research* **2015,** *8* (5), 419-430.
4. Mallery, S. R.; Wang, D.; Santiago, B.; Pei, P.; Schwendeman, S.; Nieto, K.; Spinney, R.; Tong, M.; Koutras, G.; Han, B. B.; Holpuch, A. S.; Lang, J. C., Benefits of Multifaceted Chemopreventives in the Suppression of the Oral Squamous Cell Carcinoma (OSCC) Tumorigenic Phenotype. *Cancer Prevention Research* **2016**.
5. Han, B. B.; Li, S.; Tong, M.; Holpuch, A. S.; Spinney, R.; Wang, D.; Border, M. B.; Liu, Z.; Sarode, S.; Pei, P.; Schwendeman, S. P.; Mallery, S. R., Fenretinide Perturbs Focal Adhesion Kinase in Premalignant and Malignant Human Oral Keratinocytes. Fenretinide's Chemopreventive Mechanisms Include ECM Interactions. *Cancer prevention research (Philadelphia, Pa.)* **2015,** *8* (5), 419-30.
6. Wischke, C.; Schwendeman, S. P., Principles of encapsulating hydrophobic drugs in PLA/PLGA microparticles. *Int J Pharm* **2008,** *364* (2), 298-327.
7. Hyon, S. H., Biodegradable poly (lactic acid) microspheres for drug delivery systems. *Yonsei Med J* **2000,** *41* (6), 720-734.
8. Fredenberg, S.; Wahlgren, M.; Reslow, M.; Axelsson, A., The mechanisms of drug release in poly(lactic-co-glycolic acid)-based drug delivery systems—A review. *International Journal of Pharmaceutics* **2011,** *415* (1–2), 34-52.
9. Wang, Y., Wen, Q., Choi, S. FDA's Regulatory Science Program for Generic PLA/ PLGA-Based Drug Products 2016. http://www.americanpharmaceuticalreview.com.
10. Wischke, C.; Zhang, Y.; Mittal, S.; Schwendeman, S. P., Development of PLGA-based injectable delivery systems for hydrophobic fenretinide. *Pharm Res* **2010,** *27* (10), 2063-74.
11. Ying Zhang, C. W., Sachin Mittal, Amitava Mitra, Steven P. Schwendeman, Design of controlled release PLGA microspheres for hydrophobic fenretinide. *Molecular Pharmaceutics* **in press**.
12. (a) Holpuch, A. S.; Phelps, M. P.; Desai, K. G.; Chen, W.; Koutras, G. M.; Han, B. B.; Warner, B. M.; Pei, P.; Seghi, G. A.; Tong, M.; Border, M. B.; Fields, H. W.; Stoner, G. D.; Larsen, P. E.; Liu, Z.; Schwendeman, S. P.; Mallery, S. R., Evaluation of a mucoadhesive fenretinide patch for local intraoral delivery: a strategy to reintroduce fenretinide for oral cancer chemoprevention. *Carcinogenesis* **2012,** *33* (5), 1098-105; (b) Wu, X.; Desai, K. G.; Mallery, S. R.; Holpuch, A. S.; Phelps, M. P.; Schwendeman, S. P., Mucoadhesive fenretinide patches for site-specific chemoprevention of oral cancer:

enhancement of oral mucosal permeation of fenretinide by coincorporation of propylene glycol and menthol. *Mol Pharm* **2012,** *9* (4), 937-45.

13. Zhang, Y.; Wischke, C.; Mittal, S.; Mitra, A.; Schwendeman, S. P., Design of Controlled Release PLGA Microspheres for Hydrophobic Fenretinide. *Molecular Pharmaceutics* **2016,** *13* (8), 2622-2630.

14. (a) Kang, J.; Schwendeman, S. P., Comparison of the effects of Mg(OH)2 and sucrose on the stability of bovine serum albumin encapsulated in injectable poly(d,l-lactide-co-glycolide) implants. *Biomaterials* **2002,** *23* (1), 239-245; (b) Kang, J.; Lambert, O.; Ausborn, M.; Schwendeman, S. P., Stability of proteins encapsulated in injectable and biodegradable poly(lactide-co-glycolide)-glucose millicylinders. *International Journal of Pharmaceutics* **2008,** *357* (1–2), 235-243.

15. Schwendeman, S. P.; SHAH, R. B.; GILES, M. B.; Chang, R. S.; SCHWENDEMAN, A. A., Efficient aqueous encapsulation and controlled release of bioactive agents. Google Patents: 2015.

16. Srinarong, P.; Kouwen, S.; Visser, M. R.; Hinrichs, W. L. J.; Frijlink, H. W., Effect of drug-carrier interaction on the dissolution behavior of solid dispersion tablets. *Pharmaceutical Development and Technology* **2010,** *15* (5), 460-468.

17. Parchment, R. E.; Jasti, B. R.; Boinpally, R. R.; Rose, S. E.; Holsapple, E. T., Liposomal nanoparticles and other formulations of fenretinide for use in therapy and drug delivery. Google Patents: 2014.

18. SURMAN, P.; BINNIE, F. C.; VOS, M. G., Pharmaceutical methods and topical compositions containing acitretin. Google Patents: 2013.

19. Siepmann, J.; Peppas, N. A., Modeling of drug release from delivery systems based on hydroxypropyl methylcellulose (HPMC). *Advanced Drug Delivery Reviews* **2001,** *48* (2–3), 139-157.

20. Do, M. P.; Neut, C.; Metz, H.; Delcourt, E.; Siepmann, J.; Mäder, K.; Siepmann, F., Mechanistic analysis of PLGA/HPMC-based in-situ forming implants for periodontitis treatment. *European Journal of Pharmaceutics and Biopharmaceutics* **2015,** *94*, 273-283.

21. Strickley, R., Solubilizing Excipients in Oral and Injectable Formulations. *Pharmaceutical Research* **2004,** *21* (2), 201-230.

22. Hirota, K.; Doty, A. C.; Ackermann, R.; Zhou, J.; Olsen, K. F.; Feng, M. R.; Wang, Y.; Choi, S.; Qu, W.; Schwendeman, A. S.; Schwendeman, S. P., Characterizing release mechanisms of leuprolide acetate-loaded PLGA microspheres for IVIVC development I: In vitro evaluation. *Journal of Controlled Release* **2016,** *244, Part B*, 302-313.

23. Desai, K. G. H.; Mallery, S. R.; Schwendeman, S. P., Effect of formulation parameters on 2-methoxyestradiol release from injectable cylindrical poly(dl-lactide-co-glycolide) implants. *European Journal of Pharmaceutics and Biopharmaceutics* **2008,** *70* (1), 187-198.

24. (a) Gu, J. J.; Hofmann, A. F.; Ton-Nu, H. T.; Schteingart, C. D.; Mysels, K. J., Solubility of calcium salts of unconjugated and conjugated natural bile acids. *Journal of Lipid Research* **1992,** *33* (5), 635-646; (b) D'Archivio, A. A.; Galantini, L.; Gavuzzo, E.; Giglio, E.; Mazza, F., Calcium Ion Binding to Bile Salts. *Langmuir* **1997,** *13* (12), 3090-3095.

25. Reis, S.; Moutinho, C. G.; Matos, C.; de Castro, B.; Gameiro, P.; Lima, J. L. F. C., Noninvasive methods to determine the critical micelle concentration of some bile acid salts. *Analytical Biochemistry* **2004,** *334* (1), 117-126.

26. Lichtenberg, D.; Younis, N.; Bor, A.; Kushnir, T.; Shefi, M.; Almog, S.; Nir, S., On the solubility of calcium deoxycholate: kinetics of precipitation and the effect of conjugated bile salts and lecithin. *Chemistry and Physics of Lipids* **1988,** *46* (4), 279-291.

27. Mohapatra, M.; Mishra, A. K., Effect of Submicellar Concentrations of Conjugated and Unconjugated Bile Salts on the Lipid Bilayer Membrane. *Langmuir* **2011,** *27* (22), 13461-13467.

28. Li, C.-Y.; Zimmerman, C.; Wiedmann, T., Solubilization of Retinoids by Bile Salt/ Phospholipid Aggregates. *Pharmaceutical Research* **1996,** *13* (6), 907-913.

CHAPTER 3: 4HPR solubility enhancement by PVP-4HPR amorphous solid dispersions and release from PLGA millicylinders

3.1. Abstract

Purpose: The goal of this study was to develop long-acting 4HPR PLGA millicylinder implants for oral cancer chemoprevention. Due to 4HPR's extreme hydrophobicity, formation of 4HPR- polyvinylpyrrolidone (PVP) amorphous solid dispersions (ASD) were investigated as a solubility enhancement technique.

Methods: PVP-4HPR ASDs were prepared by co-dissolving in methanol to form a thin film, then cryomilled into particles. Dissolutions tests determined solubility enhancement. The PVP-4HPR particles were loaded into PLGA millicylinders and drug release was evaluated *in vitro* and *in vivo* in s.c. tissues.

Results: The optimal ratio was 9/1 w/w PVP-4HPR, which sustained a 50 to 1000-fold solubility enhancement in water over 1 week. Initial formulations of PLGA millicylinders loaded with PVP-4HPR showed rapid release of PVP, yet only 10% drug released *in vitro* after 28 days. Addition of the plasticizer triethyl-o-acetyl-citrate (TEAC) into PVP-4HPR ASDs resulted in a 5.6-fold increase in 4HPR released *in vitro* from PLGA millicylinders, and showed a dramatic improvement of *in vivo* drug release from our previous PLGA-4HPR millicylinders, with nearly complete and continuous release over 1 month.

Conclusions: Extreme 4HPR solubility enhancement was achieved with robust PVP-4HPR ASDs. The addition of TEAC to PVP-4HPR ASDs enabled complete and continuous release from PLGA millicylinders over 1 month *in vivo.*

3.2. Introduction

The synthetic analogue of all-trans retinoic acid (ATRA), fenretinide (4HPR), is a highly active and promising chemopreventive agent for oral cancer. Despite the known therapeutic effects of 4HPR, clinical trials using systemic delivery has shown poor efficacy due to significant drug inactivation by first pass metabolism and lack of drug accessibility to the target site[1]. Local delivery of 4HPR may therefore prove to be beneficial, and designing a long–acting release drug depot may be favorable for improved patient compliance in their lifelong chemoprevention therapy. However formulation of 4HPR presents a significant challenge due to its extreme water insolubility, with a logP of 6.31. Many techniques have been employed in attempt to increase aqueous solubility of a poorly soluble drug molecule, including 4HPR and other retinoid derivatives, including: micellar solubilization(2, 3), reduction in particle size via milling, conjugation with amphiphilic moieties(4, 5), complexation to dextrans (6), PEGylation(2), encapsulation into PLGA microparticles (7-9), liposomes(10, 11), formation of drug-salt(5), formation of co-crystals(12), or preparation of amorphous solid dispersions (ASD's) to name a few. Addition of solubilizers can enhance drug solubility by formation of micelles, however often times large amounts of solubilizers are necessary to achieve the desired drug loading, which may not be feasible to incorporate that amount into the delivery vehicle. For example, we have found that the bile salt sodium deoxycholate (NaDC) greatly enhanced 4HPR solubility to 1 mg/mL however, it required 200x's more solubilizer than drug. Our lab has also screened many 4HPR solubility and

permeation enhancing excipients including: Tween, polyvinyl alcohol, Soluplus, ASD's with PEG, and cosolvent systems to name a few (8,13,14). Although these were capable of solubilizing 4HPR, their high water solubility led to an immediate release, which is not amenable to the design of a long-acting release local delivery system. This prompted us to explore other solubilization options for this poorly water-soluble crystalline drug.

The 4HPR solubility in this enhancement technique investigated study was formation of an amorphous solid dispersion (ASD) with the polymer polyvinylpyrolidone (PVP). Amorphous solids are not crystalline because arrangement of molecules is disordered. The ASD's can greatly enhance drug solubility and bioavailability, and are prepared by dispersing drug molecules in a polymer such that the drug solubility in polymer is much greater than its crystalline solubility. Upon contact with water, the amorphous drug dissolves much more quickly than the crystalline form due to absence of a crystalline lattice, and also due to the water solubility of the polymer (15). With ASD's, the drug is able to reach a super-saturated concentration, but the solubility decreases over time due to liquid-liquid phase separation and eventually drug precipitation. Therefore, the ability to maintain the super-saturation over time is a measure of the ASD robustness, and can be addressed by optimizing the polymer type, polymer molecular weight and chain length, and mass ratio of polymer to drug.

PVP has been widely used in pharmaceutical, cosmetic, food, and industrial applications since 1938 when first discovered, owing its usefulness to its ability to readily dissolve in a variety of solvents including water, alcohols, amides, chlorinated hydrocarbons. It is odorless, colorless, non-irritating to skin, non-ionic, absorbs large amounts of water, and has adhesive and thickening properties(16). Interestingly, PVP debuted as a blood plasma substitute that helped to save lives in World War Two. PVP's chemical properties are exploited

in the beer and wine industry for stabilization of polyphenols, where the interactions between PVP's carbonyl groups and hydroxyl groups of polyphenols is well known and characterized(17,18). PVP could potentially exhibit the same interactions between 4HPR's redox-reactive phenol group as well. PVP has been shown to adsorb onto the hydroxyl surface groups of oxides by acid-base interactions with the carbonyl bond in the PVP backbone(19), which acts as a Lewis base in aqueous solutions(20). One disadvantage is that the presence of large quantities of salt may lead to precipitation of PVP(19). In the pharmaceutical industry, PVP is used to form films for tablet coatings, a disintegrate in tablets, and crystallization inhibitor by complexing with insoluble precipitates, and generally regarded as safe (GRAS) by the US FDA(21). In the FDA approved topical tretinoin (retinoic acid) gel formulations, 0.06% PVP is added as a crystallization inhibitor(22). Recently, Laurent Pharmaceuticals developed PVP-4HPR solid dispersions for oral dosing and found that it enhanced 4HPR's bioavailability(23). Another group prepared PVP-4HPR nanoparticles and found that the ratio of 4:1 PVP-4HPR provided greatest cell uptake in CaCO2 cells(24).

The aim of this work was to (A) enhance 4HPR solubility by formation of PVP-4HPR ASD and (B) provide controlled release dosing over 1-2 mo. of this solubilized form of 4HPR from poly-(lactic-co glycolic acid) (PLGA) millicylinders for local delivery applications. Delivering solubilized 4HPR to the local tissue environment may help facilitate widespread tissue distribution, which is a hurdle in local delivery systems. Previously we have reported that in vivo release of 4HPR from PLGA millicylinders has similar release rates to the solid drug depot alone, due to slow dissolution of the precipitated drug even after 56 days. To accomplish these objectives, PVP-4HPR ASD particles were prepared at different drug loading levels by co-dissolving in methanol, forming a thin film, then cryomilling into particles < 90

µm. The solubility enhancement and robustness of these PVP-4HPR particles was evaluated in water and PBST buffer systems, and the optimum drug-polymer ratio was determined. The PVP-4HPR ASD's were characterized using differential scanning calorimetry (DSC), thermogravimetric analysis (TGA), isothermal titration calorimetry (ITC), and scanning electron microscopy (SEM). Next, various PLGA millicylinder preparation methods were investigated to circumvent the issue of incomplete release of hydrophobic 4HPR into aqueous media, including: loading cryomilled PVP-4HPR particles into PLGA, co-dissolving the drug and polymers in DCM, coating PVP-4HPR core implants with PLGA, and investigating use of the plasticizer triethyl-o-acetyl-citrate (TEAC) to enhance release. Our results show that PVP-4HPR-TEAC 9/1/1 particles loaded into PLGA implants were able to achieve in a 5.6-fold increase (35%) in total 4HPR released after 28 days compared to a similar formulation without TEAC. Furthermore, this optimized ASD formulation showed a dramatic improvement from our previous in vivo release from PLGA-4HPR millicylinders, with nearly complete and continuous release over 1 month. These formulations will have future applicability for lifelong oral cancer chemoprevention measures.

3.3.   Materials and Methods

3.3.1. Materials

PLGAs (50:50) were purchased from Evonik, including 503H and 503 (24-38 kDa, acid and ester end-capped respectively), 4HPR was generously supplied by Merck Co. Excipients utilized included: polyvinylpyrrolidone polymer (PVP K30, 40 kDa, BASF) and triethyl-o-acetyl-citrate (TEAC, Sigma-Aldrich.). See Figure 3-1 for chemical structures of these materials. All other materials were reagent grade or better including: $MgCO_3$, acetone, dichloromethane (DCM), ethanol (EtOH), tetrahydrofuran (THF), and Tween 80. Solvents for

UPLC-UV and LC-MS analysis were HPLC or MS grade including acetonitrile (ACN), methanol (MeOH), double distilled water (ddH$_2$0), phosphoric acid (H$_3$PO$_4$). Millicylinders were extruded through silicon tubing (0.8 mm i.d., BioRad Laboratories). Additional media for the solubility study included fetal bovine serum (FBS, Life Technologies) and Dulbecco's Modified Eagle Medium (DMEM, Life Technologies, Cat# 11995065).
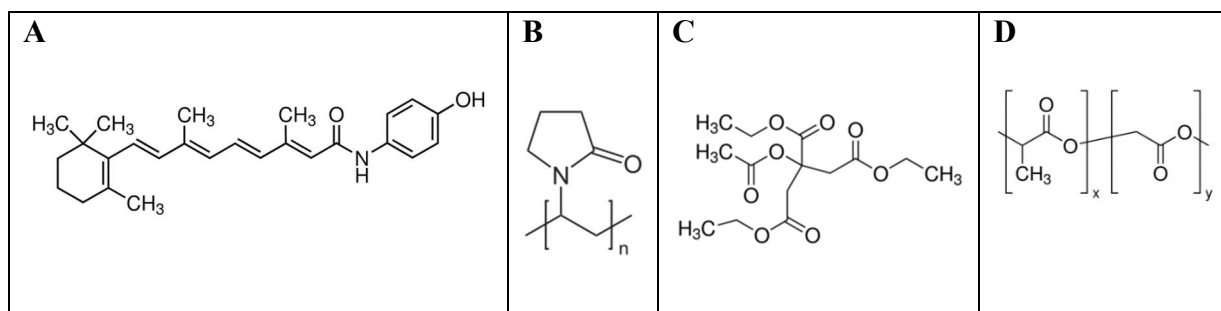
Figure 3-1. Chemical structures of a) 4HPR, b) PVP, c) Triethyl-o-acetyl-citrate (TEAC), and d) PLGA.

3.3.2. Solubilization and Crystallization Inhibition of 4HPR by PVP

4HPR solubility in PVP aqueous solutions (1, 2, 5, 10, and 20% w/v in ddH$_2$0) was evaluated by adding 2 mg of 4HPR to 1 mL of PVP solution, incubating at 37° C on a rotator in the dark, and was sampled after 1 and 7 days. Prior to sampling, the samples were centrifuged and 10 µL of supernatant was assayed by UPLC-UV, and re-dispersed for the day 7 time point.

PVP's drug crystallization inhibition properties were evaluated by spiking a solubilized 4HPR in acetone (0.5 ml of 10 mg/mL) into 2 mL of 1% or 10% w/v PVP in ddH$_2$0, or a ddH$_2$0 control in an open glass vial, and stirred at room temperature at 350 rpm for 24 h to allow for acetone evaporation. The solutions were filtered, and 4HPR concentration assayed by UPLC. The solid 4HPR precipitate was examined for crystalline character by scanning

electron microscopy (SEM) and compared to the crystal structures of 4HPR without any treatment and 4HPR recrystallized from acetone.

3.3.3. Formation of PVP-4HPR Amorphous Solid Dispersions

PVP-4HPR ASD's particles were prepared by co-dissolving 4HPR with PVP in MeOH. Briefly, PVP (50% w/w) was dissolved in MeOH, then 4HPR was added at mass ratios of 9/1, 8/2, or 7/3 PVP-4HPR. Later studies incorporated TEAC into the films at a mass ratio of 9/1/1 PVP-4HPR-TEAC. The solutions were vigorously mixed, shaken for 2 h to maximize polymer-drug interactions, poured into a Teflon-lined petri dish to form a thin film, slowly dried at RT for 2 days, then further dried in vacuum oven at 40° C for 2 days. The film was cryomilled (Retsch swing mill cryomill, PN 20.749.001) at a frequency of 1/30 sec for 30 min, and particles were sieved to < 90 μm. The film morphology was inspected for drug crystallization via light microscopy prior to cryomilling, and the cryomilled particles were imaged via SEM. The 4HPR loading in cryomilled films was determined by dissolving 2 mg PVP-4HPR cryomilled particles in 1 mL MeOH, diluting into mobile phase, centrifuging, and 4HPR assayed by UPLC-UV.

3.3.4. 4HPR-PVP Dissolution Studies to determine Solubilization Enhancement

Dissolution studies were conducted with PVP-4HPR particles (9/1, 8/2, 7/3, all <90 μm) compared to control 4HPR by adding 5 mg of solids to 1 mL of dissolution media (ddH$_2$0, PBST 0.02%, or PBST 2% pH 7.4) and incubating on a shaking platform at 37 °C in the dark. Media were sampled after 1, 6, and 12 h, then daily up to 7 days by removing 10 μL aliquots, diluting in mobile phase, and assaying for 4HPR by UPLC-UV. The solubility enhancement was calculated by dividing the concentration of 4HPR from PVP-4HPR complex ($C_{s, PVP-4HPR}$)

by 4HPR's intrinsic solubility ($C_{s, 4HPR}$). Additionally, the solubility of 9/1 PVP-4HPR particles was determined in cell based media (5% FBS/DMEM) after 24 h.

$$\text{Solubilty Enhancement} = \frac{C_{s,PVP-4HPR}}{C_{s,4HPR}}$$

3.3.5. Formulation of Controlled Release PLGA PVP-4HPR ASD Millicylinder Implants

The goal of these PLGA millicylinder formulations was to provide a controlled release of the solublized 4HPR prepared in the PVP-4HPR ASD. Because hydrophilic PVP and hydrophobic PLGA are not soluble in similar organic solvents, unique approaches were taken to load PVP-4HPR ASDs into PLGA millicylinders. All implants contained 5% 4HPR theoretical loading, and the formulation strategies are outlined in Table 3-1. Care was take in all experiments to minimize light exposure to the drug by covering with foil.

Table 3-1. Formulation Strategies for Controlled Release PLGA 4HPR-PVP ASD Millicylinders

Batch#	Preparation Methods	Rationale
1-5	Load varying ratios of PVP-4HPR particles into PLGA dissolved in acetone	Maximize 4HPR loading Determine optimum PLGA type
6	Co-dissolve PVP, 4HPR, PLGA in DCM Coat with PLGAs	DCM solubilizes all components, CR of PVP
7,8	Coat PVP-4HPR and PVP-4HPR-TEAC core implants with PLGAs	Reservoir of solubilized drug
9-11	PVP-4HPR-TEAC (9/1/1) particles loaded into PLGA Compare to control PLGA-TEAC-4HPR	TEAC keeps PVP-4HPR ASD intact

The initial formulations (#1-5) investigated the ratio of PVP-4HPR particles (9/1, 8/2 or 7/3) and polymer type (acid or ester end-capped). Briefly, 60% PLGA 503H or 503 was dissolved in acetone, and required amount of PVP-4HPR particles to obtain 5% 4HPR loading was added to the PLGA solution and vigorously stirred. Note, different PVP-4HPR ratios resulted in different levels of PLGA and PVP in the implants. The resulting solution was

loaded into a 3 mL syringe equipped with an 18 g blunt end needle attached to silicon tubing (0.8 mm i.d.) and slowly extruded. The implants were dried at room temperature for 2 days, and then transferred to vacuum oven and dried at 40 °C for an additional 2 days, after which the tubing was carefully removed and implants were cut to the desired size of 1 cm.

The next formulation (#6) attempted to provide controlled release of PVP from PLGA implant by co-dissolving all compounds in DCM with same composition as #1 (PLGA/PVP/4HPR 45/50/5). PLGA 503H was dissolved in DCM (60%), PVP and 4HPR were added and vigorously stirred, shaken at RT for 2 h in a capped tube to allow for complete mixing, then extruded and dried as previously described. Some implants were coated with PLGA to further slow the release of PVP, and left inside the silicon tubing for the coatings. Three different PLGA coatings were tested: PLGA 503H, PLGA 503H + 3% $MgCO_3$ (a basic pore forming salt), and PLGA 503 + 3% $MgCO_3$. Briefly, PLGA coatings were prepared by dissolving 50% PLGA in acetone and adding $MgCO_3$, then extruded into the tubing containing the dried implants, and allowed to dry for 2 days at 40 °C in a vacuum oven. The final implants removed from tubing, cut to 1 cm.

The next set of formulations (#7, 8), PVP-4HPR (9/1) or PVP-4HPR-TEAC (9/1/1) core implants were coated with PLGAs. To prepare PVP-4HPR millicylinders, PVP was dissolved at 60% w/v in MeOH, then 4HPR and TEAC was added and vigorously stirred. The implants were extruded as previously described, dried for 2 days at RT, coated 2 times with PLGA's as described for formulation #6, and dried for 2 days at 40 °C.

The final set of formulations (#9-11) incorporated PVP-4HPR-TEAC particles into PLGA and compared to control PLGA-4HPR-TEAC implants. PVP-4HPR-TEAC 9/1/1 particles were added to PLGA 503H dissolved in acetone with a total implant composition of

PLGA/PVP/4HPR/TEAC 40/50/5/5. A control formulation (#10) was prepared by adding 7.5% TEAC and 5% 4HPR to PLGA 503H + 4HPR, which is representative of the PLGA-TEAC ratio (11:1) in formulation #9. In attempt to further accelerate release, additional 4% TEAC (#11) was added to the PLGA solution prior to adding the PVP-4HPR-TEAC 9/1/1 particles.

3.3.6. 4HPR Loading Assays in PLGA Millicylinders

To determine the amount to 4HPR loaded into the implant, one millicylinder was weighed into a 15 mL centrifuge tube, PLGA and 4HPR were co-dissolved by addition of 0.5 mL THF, followed by precipitation of PLGA by addition of 9.5 mL EtOH. Next, the sample was centrifuged, and supernatant was assayed by UPLC/UV. Encapsulation efficiency was invariable and ranged from 97-103%.

3.3.7. In vitro Release of 4HPR and PVP from PLGA-PVP Millicylinders

4HPR and PVP in vitro release from millicylinders was performed by incubating 1 millicylinder (5-7 mg) in a non-solubilizing buffer of 4 mL PBS pH 7.4 + 0.02% Tween80 at 37 °C on a shaking platform (200 rpm) while covering vials with aluminum foil to protect from light. The solutions were sampled by complete media replacement up to 6 weeks.

3.3.8. *In vivo* Release of 4HPR from PLGA-PVP Millicylinders

To evaluate 4HPR release in vivo, millicylinders were weighed and implanted subcutaneously (s.c.) in the dorsal region of male Sprague Dawley rats using a 12 g trocar. Each rat could receive up to 6 implants. For each formulation, 3 implants were implanted in each rat, and 1 rat per time point (days 1, 14, 28) was sacrificed. Millicylinders were carefully harvested to ensure complete removal and release from encompassing tissues. The amount of

4HPR released was determined by assaying the amount of 4HPR remaining in recovered millicylinder by loading assay.

3.3.9. 4HPR UPLC-UV Assay

4HPR levels in PVP-4HPR particles, millicylinder loading, and in vitro release media was determined by UPLC/UV. The reverse phase UPLC/UV analysis utilized a Waters Acquity UPLC system and Empower software under the following conditions: Acquity BEH C18 2.1x100 mm column, mobile phase 80:20 ACN: ddH_2O + 0.1% H_3PO_4, isocratic flow rate 0.65 mL/min, UV detection at 365 nm, and total analysis time of 2 min. 4HPR calibration standards were prepared in mobile phase (0.5-100 μg/mL) from a 0.5 mg/mL 4HPR stock solution in ACN, and reflects the large linear dynamic calibration range.

3.3.10. PVP UPLC-UV SEC Assay

PVP levels in in vitro release media was determined by UPLC/UV size exclusion chromatography (SEC). The PVP assay was adopted from Johnson &Johnson[25] and utilized a Waters Acquity UPLC system and Empower software under the following conditions: Acquity BEH H125 1.7 μm 4.6x150 mm column, mobile phase 80:20 0.1 M sodium acetate buffer in ddH_2O: MeOH, isocratic flow rate 0.7 mL/min, UV detection at 220 nm, and total analysis time of 4 min.

3.3.11. Particle and Millicylinder Morphology via Scanning Electron Microscopy (SEM)

The morphology of 4HPR, 4HPR-PVP cryomilled film particles, and millicylinder cross sections were examined by scanning electron microscopy (SEM) using a Phillips XL FEG SEM. All samples were completely dried, sputter coated with gold for 90 sec, then imaged using 3 kV electric beam.

3.3.12. Differential Scanning Calorimetry (DSC) and Thermogravimetric Analysis (TGA)

Glass transition temperature's (T_g) of the PVP-4HPR particles and millicylinders were determined via DSC (Discovery, TA instruments). Briefly, 2-3 mg of the PVP-4HPR particles or millicylinders were added to a hermetic pan, and samples were heated with a modulating temperature program from -10 °C to 180 °C. The amount of residual solvent trapped in the cryomilled films and millicylinders after drying was determined by Thermogravimetric Analysis (TGA, Discovery, TA instruments). The following temperature ramping profile was used: 10 °C/min until 300° C, then 20 °C/min till 600° C.

3.3.13. Isothermal Titration Calorimetry (ITC) for PVP-4HPR Affinity Stoichiometry

ITC was used to measure the stoichiometry of interactions between 4HPR and PVP, using a nano-ITC (TA instruments), equipped with a low volume gold sample cell. 300 µL of 0.2% 4HPR (in MeOH) was loaded into sample cell, stirred at 250 rpms at 25 ˚C, and 20 x 2.5 µL aliquots of 10% PVP (in MeOH) were titrated into the 4HPR solution. The reference cell was filled with 100% MeOH, and a blank isotherm for MeOH injections into MeOH was subtracted from the sample measurements.

3.4. Results

3.4.1. 4HPR Solubility in PVP Solutions and Crystallization Inhibition

The results from the 4HPR solubility in PVP solutions is shown in Fig. 3-2a. The initial solubility studies show that PVP aqueous solutions were not capable of significantly increasing 4HPR solubility, where even at 20% PVP, only 0.7 µg/mL 4HPR was solubilized. The PVP crystallization inhibition study showed that PVP was slightly effective at preventing 4HPR precipitation upon addition of 4HPR/acetone solution to PVP solutions, and both the 1% and 10% PVP solutions resulted in cloudy solutions, while the control ddH_2O solution showed

aggregation of hydrophobic drug that adhered to the walls of the glass vessel. Based on these observations, PVP appeared to be functioning as a surfactant or wetting agent. The solubility of 4HPR/acetone in PVP solutions increased 10-fold compared to PVP solutions without acetone, likely due to the solubility enhancement from acetone, which may have not completely evaporated. The stability of these solutions after 4 mo. of light exposure at RT shows that PVP prevents photo-degradation as evident by the yellow color of 4HPR solids compared to the orange solids in ddH$_2$O (Fig. 3-2b). The morphology of 4HPR crystals (no treatment), 4HPR recrystallized in acetone, and 4HPR precipitated in 10% PVP and ddH$_2$O are displayed in (Fig. 3-2c-f), and show that 4HPR recrystallization in acetone(Fig. 2d) lead to a more disordered crystal structure from the original cuboidal shaped 4HPR crystals (Fig. 3-2c). When 4HPR had precipitated from the PVP solutions (Fig. 3-2e), it appears that 4HPR has adhered to PVP surface, and looks very different from 4HPR precipitation in ddH$_2$0 (Fig. 3-2f).
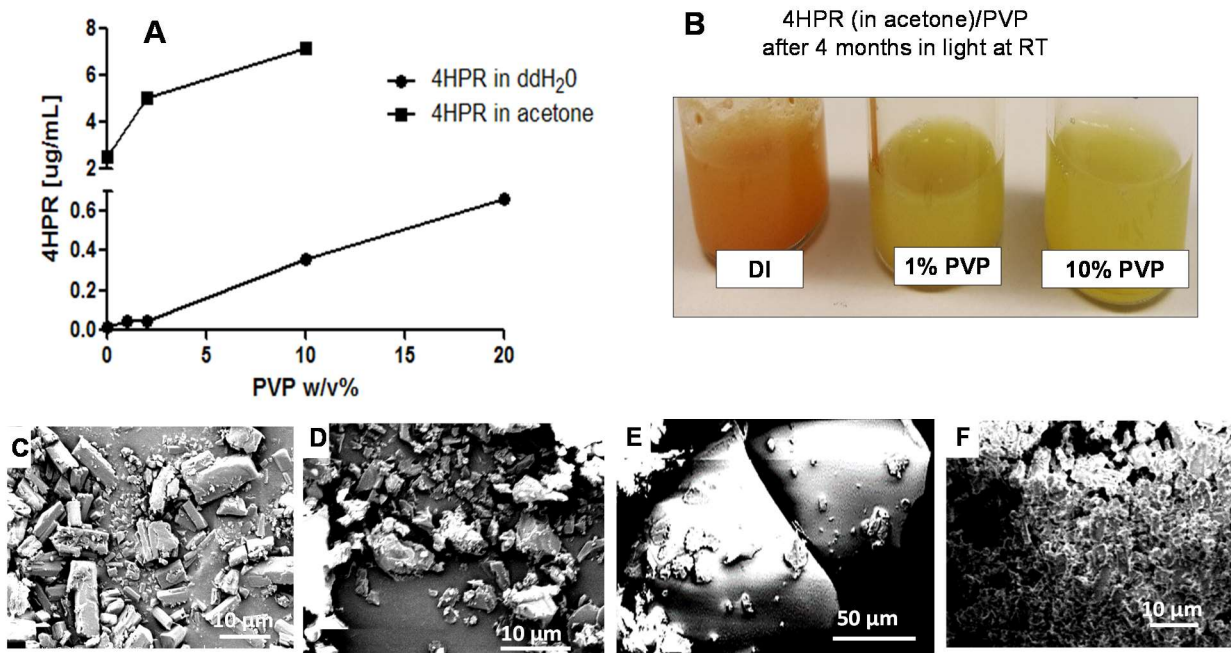
Figure 3-2. 4HPR solubility, stability, and morphology in solid state and PVP and PVP-acetone solutions. A) 4HPR solubility in 1-20% PVP after 7 days at 37 °C compared to 4HPR dissolved in acetone (0.5 mL of 10 mg/mL) added to PVP solutions and stirred uncapped at RT x 1 d, b) Photo-stability enhancement by PVP from crystallization inhibition experiment (4HPR in acetone) after 4 mo. light exposure at RT. C-E) are SEM images of c) 4HPR solid, d) 4HPR recrystallized in acetone, e) 4HPR dissolved in acetone then precipitated in 10% PVP aqueous solution, f) 4HPR dissolved in acetone, then precipitated in ddH$_2$O.

3.4.2. Formation of PVP-4HPR ASDs

Although the results from the PVP solubility and crystallization inhibition study did not show PVP's effectiveness of increasing 4HPR solubility, the literature shows the utility of PVP in increasing hydrophobic drug solubility by formation of ASDs. Ledet and coworkers increased 4HPR solubility by formulating PVP-4HPR (16-20% 4HPR) nanoparticles by preparing films that were homogenized and then lyophilized, and resulted in an increased uptake in CaCO2 cells[24]. Laurent Pharmaceuticals prepared PVP-4HPR (20-60% 4HPR) ASDs for oral dosage which increased bioavailability of 4HPR compared to a corn oil formulation[23]. Because PVP is a hydrophilic polymer, it will dissolve quickly in aqueous solutions, resulting in a large burst release of the excipient, which may contribute to dissociation of the drug-PVP

ASD. A literature search revealed that PVP melting could be delayed by addition of dibutyl phthalate (DBP) to beeswax/ PVP implants for veterinary therapies(26). Due to the known health risks of phthalates, TEAC has been listed as suitable substitute for DBP in a wide range of applications(27), and was added to the PVP-4HPR ASD's.

In our studies, a film was prepared by co-dissolving 4HPR at different loading levels in PVP and MeOH. In Figure 3-3(a-b), the light microscopy shows the translucentness of the PVP-4HPR system after drying, indicating that 4HPR was solubilized in PVP. The cracks in the film are apparent and are due to the brittle character of PVP. The SEM images (Fig. 3-3c-f) of the cryomilled PVP-4HPR particles shows the interaction between PVP and 4HPR, where 4HPR's regular cuboidal crystal structure (Fig. 3-2c) is no longer present. No noticeable difference in morphology of 9/1 and 8/2 PVP-4HPR particles, but slightly less adherence of 4HPR to PVP surface in the 7/3 PVP-4HPR particles was observed. The 9/1/1 PVP-4HPR-TEAC particles were noticeably different from the 9/1 PVP-4HPR particles. The 4HPR loadings in the PVP-4HPR particles are listed in Table 3-2.

Table 3-2. 4HPR loading in PVP-4HPR particles. Mean ± SE, n=3.

Film Composition	% 4HPR
9/1 PVP-4HPR	9.7 ± 0.0
8/2 PVP-4HPR	18.3 ± 0.3
7/3 PVP-4HPR	26.1 ± 0.4
9/1/1 PVP-4HPR-TEAC	9.2 ± 0.2
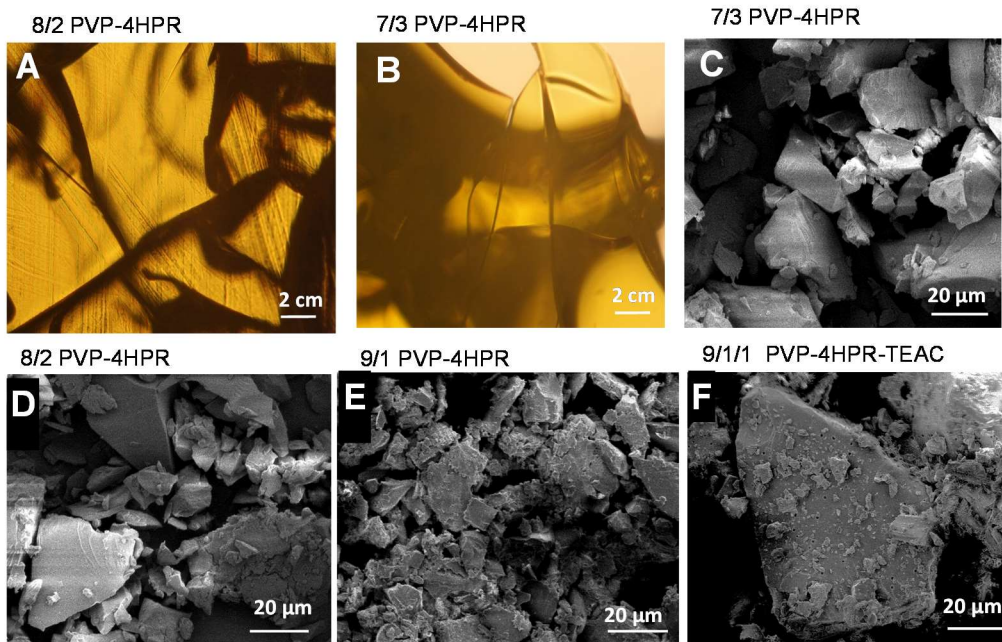
Figure 3-3. Morphology via light microscopy of films (a,b) and SEM images of PVP-4HPR cryomilled film particles (<90 μm) (c-f) with varying ratios of PVP-4HPR as noted on figure.

3.4.3.4HPR Dissolution and Solubility Enhancement with PVP-4HPR particles

The solubility enhancement of the different ratios of PVP-4HPR particles (<90 μm) were evaluated in water and PBST's (Fig. 3-4). It should be noted that the net PVP concentration in all studies was < 0.5% w/v upon dissolving the complex, and based on the previous PVP solubility study, it should have negligible effect on solubility when in aqueous phase, and therefore the solubility enhancement is an indication of the robustness of the ASD system. By far the greatest solubility was achieved with 9/1 PVP-4HPR, where >300 μg/mL 4HPR was maintained in ddH$_2$O for 7 days, equating to a 50 to 1000-fold solubility enhancement. In the higher drug loaded ASD's (8/2 and 7/3 PVP-4HPR), little solubility enhancement (2.4, 1.3-fold increase respectively) was observed after 7 days in ddH$_2$O. The solubility enhancement of 4HPR with PVP-4HPR ASDs was significantly less in PBS buffer

with 0.02% or 2% Tween, likely due to disruption of polymer-drug interactions by salts, as this is a known phenomenon with PVP ASD's. In 0.02% PBST, the 8/2 and 9/1 PVP-4HPR performed the similar and had sustained a 170 to 50-fold solubility enhancement over 7 days, but much less enhancement with 7/3 PVP-4HPR ASDs. In 2% PBST, all compositions have limited solubility advantage (1 to 6-fold) due to the extensive solubilization by Tween. Here, 4HPR solubility trend is reversed in 2% PBST: 7/3 > 8/2 > 9/1 PVP-4HPR up to 24 h, which suggests a competition between micellar solubilization by Tween and PVP-4HPR ASD. After 24 h in PBST 2%, the solubility steeply declines until day 4, where equilibrium had been reach and all have equivalent solubility to the drug alone. In respect to dissolution time to reach max solubility: in ddH$_2$0 PVP-4HPR 9/1 took 6 h, 8/2 and 7/3 took 48 h, and in PBST's all took 6 h.

For translation into *in vivo* applications, it is expected that there will be plasma proteins, fats, sugars, and other surfactants present that may affect the solubility of the PVP-4HPR ASD, and could either aid in solubilization of 4HPR, or interruption of the drug-polymer interactions. To test this, 5 mg of 9/1 PVP-4HPR was dissolved in 1 mL of a cell based media of 5% FBS in DMEM (containing plasma proteins and glucose) and solubility after 24 h was 337 $\pm$ 11 ug/mL 4HPR equating to 87 $\pm$ 3% solubilized (data not shown). The sustained solubility enhancement (>7 days) will be useful for our local controlled release drug delivery applications, and possibly enhance 4HPR tissue dispersion.
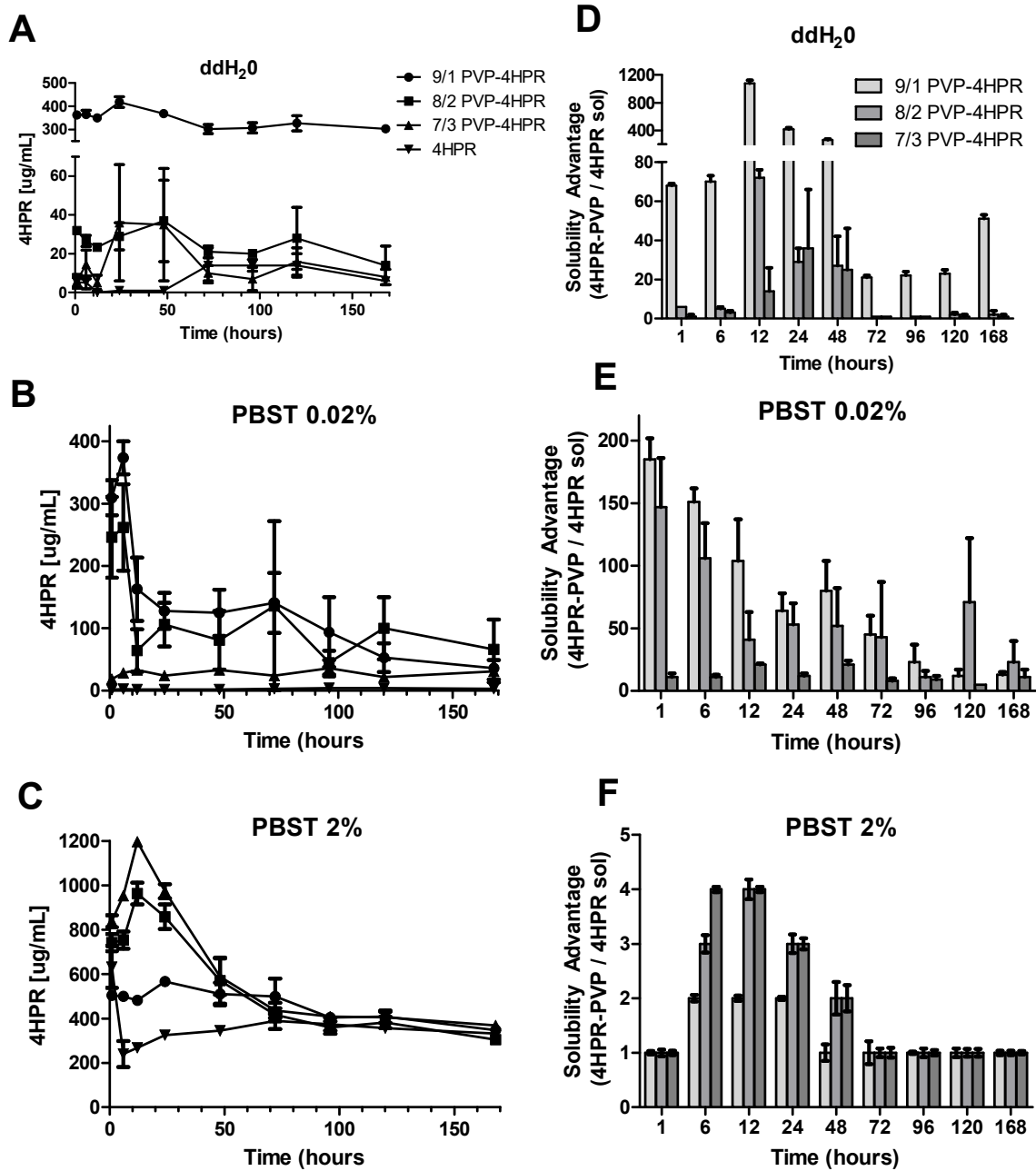
Figure 3-4. Dissolution and solubility enhancement of 4HPR from PVP-4HPR ASDs at various drug loading levels evaluated in different levels of micellar solubilizing and non-solubilizing media over 1 week. A-C) Show4HPR concentrations and D-F) shows the calculated solubility enhancement compared to control 4HPR. (Media are denoted on figure, 5 mg particles added to 1 mL media, data represents mean ±SE, n=3).

3.4.4. Characterization of PVP-4HPR ASDs by Microcalorimetry: DSC, TGA, ITC

The extent of drug solubility in the polymer is an important aspect of ASD's, and the level of solubility can be measured by measuring the Tg of the system via DSC, and drug activity can be obtained and used calculate the Flory-Huggins interaction parameter (X)(28). While this data is useful for selection of the optimum polymer for ASD's, it is not within the scope of this paper. The Tg of a mixture can be calculated according to the Fox equation:

$$\frac{1}{T_{g,mix}} = \frac{w_1}{T_{g1}} + \frac{w_2}{T_{g2}}$$

where $T_{g,mix}$ is the glass transition temperature of the mixture (in Kelvin), and w is the weight fraction of each component. A limitation of the Fox equation is that it can only be applied to blends with weak intermolecular interactions. Factors affecting the Tg include molecular size and shape, and extent and strength of hydrogen bonding, all of which can affect the packing or free volume. It is likely that PVP and 4HPR exhibit strong hydrogen bonding, and therefore this equation may not lead to accurate predictions. It is important to note that any residual water present can act as a plasticizer (Tg = -138 ˚C) and leads to a decrease in T_g. For example, if 5% water (Tg = -138 ˚C) is present in 100% PVP (T_g=164 ˚C), the Tg of the hydrated excipient will decrease to 120 ˚C. Because the Tm of 4HPR and Tg of PVP are so similar, 164 °C and 174 °C respectively, the heat flow peaks cannot be resolved, and DSC cannot be used for calculation of ratios.

The results from the Tg measurements of 4HPR, PVP, and the PVP-4HPR particles are shown in Fig. 3-5a, where presence of only one Tg would be indicative of formation of an ASD. When comparing the Tg's of the different ratios of PVP-4HPR particles the 9/1 ratio has the greatest Tg (155 °C) vs. the 8/2 and 7/3 films (131, 133 °C respectively), which are both

lower than the Tm of 4HPR (174 °C) and Tg of PVP (164 °C). These lower Tg's would likely

be due to less crystalline solids, while the 9/1 PVP-4HPR particles have an excess of

crystalline PVP. Nonetheless, only one Tg is present with all PVP-4HPR ASD's, which

suggests an amorphous system. When the plasticizer TEAC is included PVP-4HPR particles

(PVP-4HPR-TEAC 9/1/1), the Tg dramatically decreases to 91 °C, as expected. The TGA

analysis showed that all of these PVP-4HPR particles had been sufficiently dried with residual

solvent levels of 1-6% based on mass loss reading at 100 °C (representative TGA spectra in

Supplemental Information, Fig. S3-1). The results of the ITC binding experiment shows an

inflection point of the heat flow versus PVP injections into 4HPR solution after 10 injections,

equating to an interaction stoichiometry of PVP:4HPR of 4.58:1, or ~9/2 or 18% 4HPR (Fig. 4-

5b).

DSC data comparing Tg's of 9/1 PVP-4HPR particles loading into PLGA

millicylinders can be referenced in Supplemental Information Fig. S3-2, and discusses how the

Tg may indicate PLGA and PVP-4HPR phase miscibility.
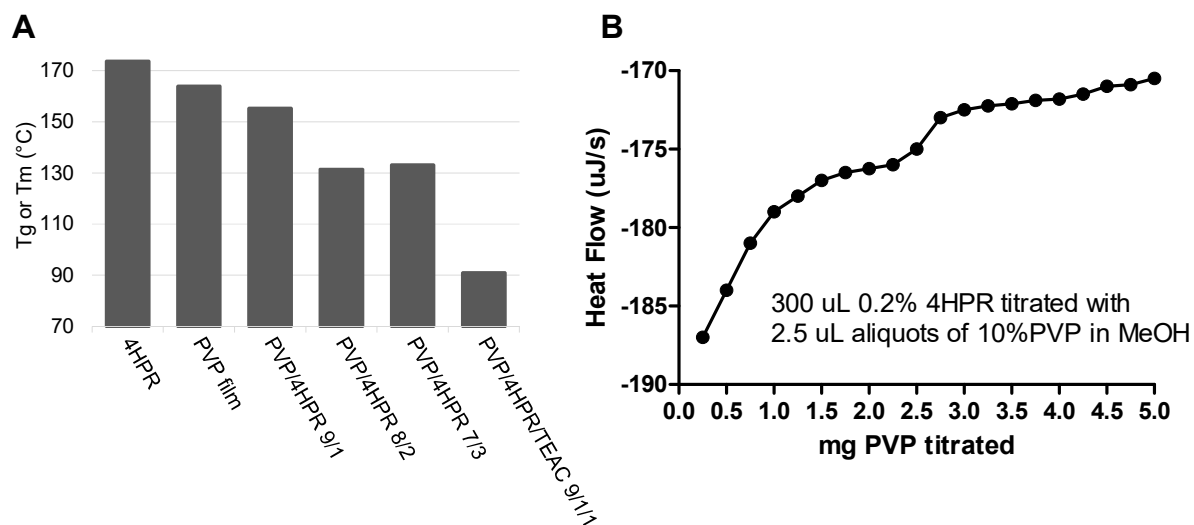
Figure 3-5. a) Effect of 4HPR loading and TEAC plasticizer in PVP ASD's on Tg compared to 4HPR and PVP alone. b) PVP-4HPR interaction stoichiometry by ITC reveals optimum ratio of 4.58:1 PVP-4HPR or 18% 4HPR, as indicated by the inflection point in heat flow after 10 injections of PVP into 4HPR solution (300 μL 0.2% 4HPR titrated with 2.5 μL injections of 10% PVP in MeOH. 10 aliquots of PVP=2.5mg PVP into 0.6 mg 4HPR).

3.4.5. *In vitro* and *In vivo* Evaluation of PVP-4HPR PLGA Millicylinders

3.4.5.1. Effect of Polymer Type and PVP/4HPR Ratios

The first set of formulations (#1-5,) investigated the different ratios of PVP-4HPR particles loaded into either PLGA 503H or 503, with goal of using the lower ratio of PVP-4HPR (i.e. 8/2 or 7/3) to achieve a greater drug loading in PLGA implant. As shown in Fig 3-6, the 9/1 PVP-4HPR PLGA implants (#1) outperformed the others with a 10-fold increase in amount of 4HPR released after 28 days (7.7% vs. 0.7-4.2%), results that correlate with the dissolution studies, yet this is still not at the desired release level. This formulation also had a large PVP burst release (>80% after 3 days), likely due to greater percent solids or less PLGA in implant compared to the other ratios. The ester-capped PLGA 503 (#4,5) released more 4HPR than the 503H with similar PVP-4HPR composition. The overall trend was that greater PVP level had a more favorable 4HPR release, but a higher PVP burst. These opposition of trends for desired 4HPR and PVP release profiles make it challenging to co-formulate into one

system, and will require more creative strategies. See Table 4-3 for a summary of results of all

PLGA-PVP-4HPR millicylinder performances, which includes the composition, 4HPR loading

and day 28 release, and time to 80% PVP release.
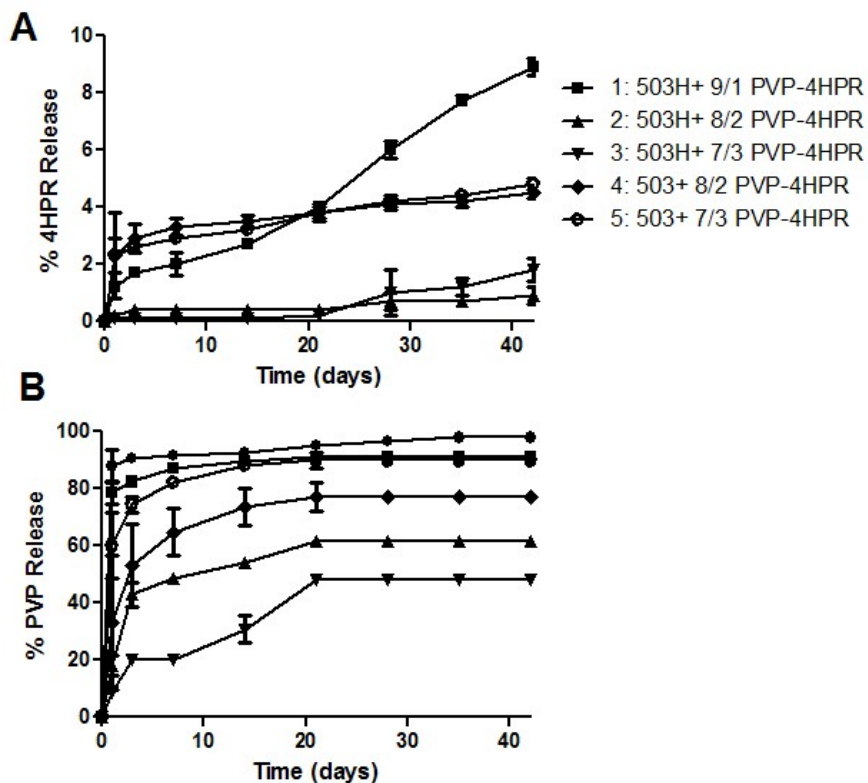
Figure 3-6. Effects of PVP-4HPR ratio and polymer type on in vitro release of a) 4HPR and b) PVP from PLGA implants (mean ±SE, n=3). PLGA implants were prepared by loading either PLGA 503 or 503H with PVP-4HPR (9/1, 8/2, 7/3) ASD particles to yield implants containing 5% 4HPR.

The morphology of formulations #1-5 was examined by SEM prior to and after 28 days

of *in vitro* release (Fig. 3-7). From these images, we can observe the initial crystallinity and

miscibility of 4HPR or PVP in PLGA, and also the extent of implant erosion after 28 days. The

greatest implant homogeneity is observed in #1 (PLGA 503H+ 9/1 PVP-4HPR), but as the

PVP/4HPR ratio decreases (requiring a lesser amount of the ASD to be loaded into implant to

achieve 5% 4HPR loading in #2 and 3), more crystals (likely 4HPR precipitation) are present.

In #4 and #5, more crystallinity is observed in PLGA 503 ester end-capped, which is a

reflection of insolubility of both PVP and 4HPR in PLGA 503, and correlates with the faster

4HPR and PVP release. On day 28, it appears that the PLGA 503H implant erosion rate

increases as the PVP level decreases. This trend is opposite of expected, where the *in vitro*

release shows PVP released more slowly in the 7/3 and 8/2 PVP-4HPR compared to the 9/1

complex. Upon visual inspection, the lower PVP-4HPR ratio loaded implants had greater

swelling (for 503H formulations), slower erosion, and released PVP and 4HPR slower. Also

on day 28, the PLGA 503 implants (#4, 5) did not show any erosion, but the formation of a

pore network was present.
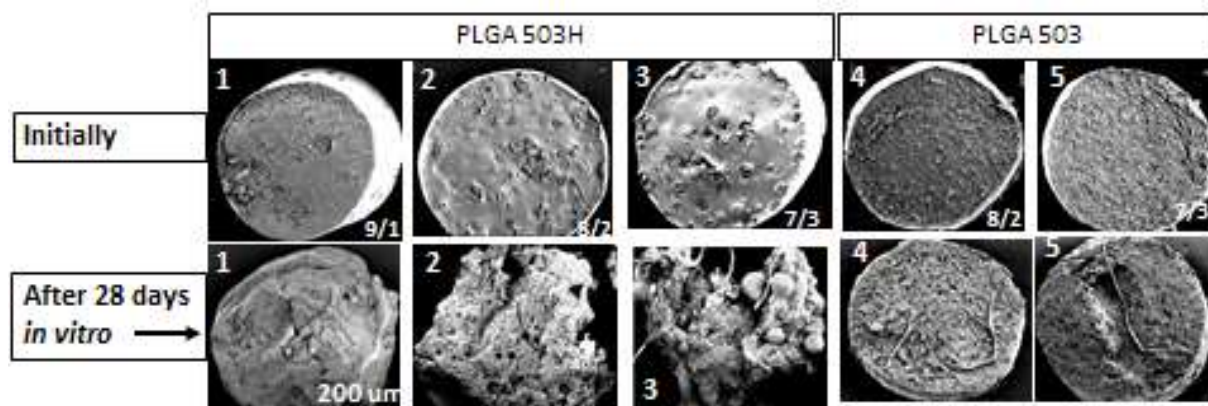
Figure 3-7. SEM images of cross sections of PLGA millicylinder implants (#1-5) loaded with PVP-4HPR particles with varying ratios prior to and after 28 days in in vitro release media. Numbers correspond to formulations#1-3 prepared with PLGA 503H, and #4, 5 with PLGA 503. #1: PVP/4HPR 9/1 particles, #2, 4: PVP/4HPR 8/2 particles, #3, 5: PVP/4HPR 7/3 particles.

3.4.5.2. **PLGA-PVP-4HPR millicylinders co-dissolved in DCM +PLGA Coatings**

In the previous experiment, nearly complete PVP release was observed after the first

few days, which left the insolubilized drug in the implant. In the next set of formulations (#6a-

d), we hypothesized that co-dissolving PVP, 4HPR, and PLGA in DCM would slow the release

of PVP due to physical entanglement of PVP's and PLGA's polymer chains, and thus provide

controlled release of the PVP-4HPR ASD. Additionally, these millicylinders were coated with

different PLGA's, including acid and ester end-capped, with and without pore forming agent (503H, 503H+3% $MgCO_3$, or 503+ 3%$MgCO_3$) to provide an additional diffusion barrier to slow PVP release. The results of *in vitro* releases of (Fig. 3-8) shows that the uncoated implant (#6d) released 4HPR the fastest and had the best PVP release profile, yet still the desired 4HPR release kinetics were still not achieved, with only 10% released after 42 days. This could be attributed to the inability of PVP to interact with 4HPR in presence in PLGA, and therefore no 4HPR solubility enhancement occurred. However, the hypothesis was true that PVP release can be controlled by physical entanglement of the polymer chains using DCM solvent. The coatings did slow 4HPR and PVP release as expected, with the slowest release with coating 503H and 503 +3% $MgCO_3$. The slowest PVP release occurred in uncoated implants, while the fastest was with 503H + 3% $MgCO_3$ coating, results that suggest that PLGA repels PVP from implant.
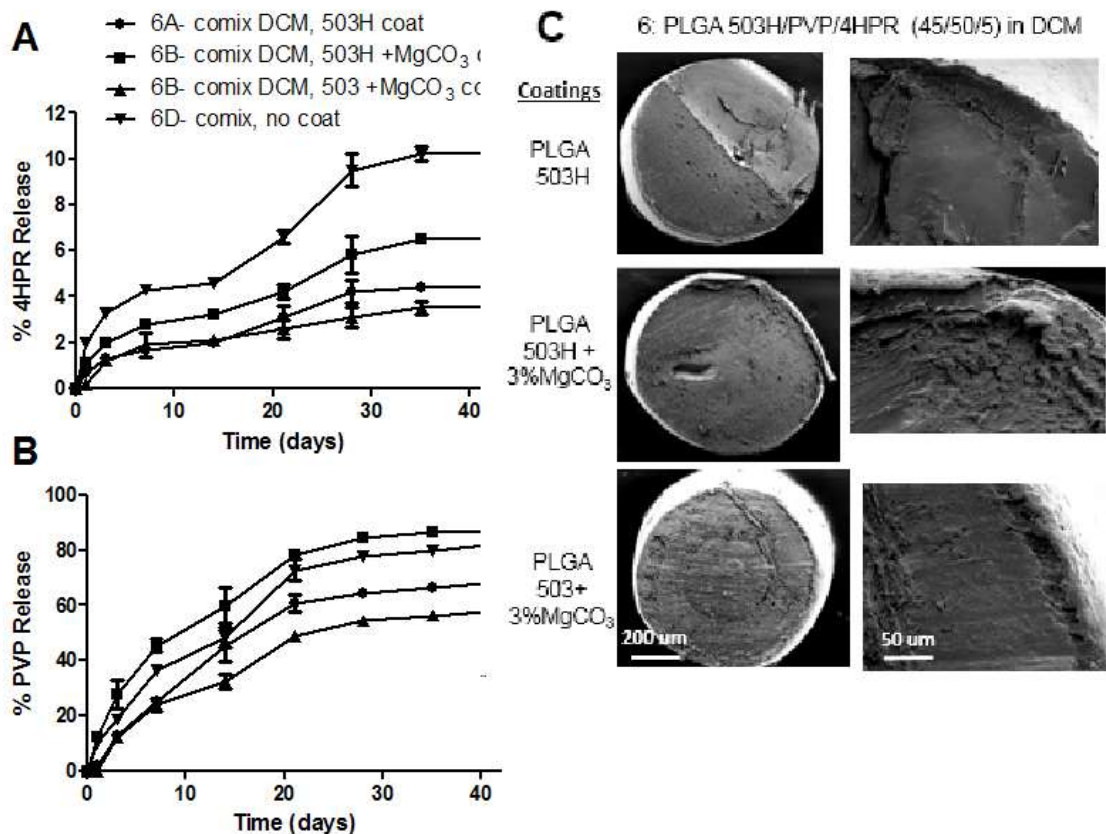
Figure 3-8. 4HPR (a) and PVP (b) in vitro release from PLGA coated millicylinder #6 (PLGA 503H/PVP/4HPR 45/50/5, all commixed in DCM) (mean ±SE, n=3). C) SEM's show cross-sectional morphology of #6 PLGA coated implants, including a close up of the coating-core edge for each implant.

3.4.5.3. PLGA coated PVP-4HPR and PVP-4HPR-TEAC core implants

In the next set of millicylinder formulations, we sought to create a reservoir of the soluble drug by preparing core implants with PVP-4HPR (#7) and PVP-4HPR-TEAC (#8), and coating with PLGAs to slowly release the solubilized drug. These millicylinders had open ends, providing a port for drug release. It was postulated that the addition of TEAC to the PVP implant (#8), would aid in keeping the PVP-4HPR ASD intact, facilitate slower release of PVP, leading to controlled release of a soluble form of 4HPR. TEAC is not soluble in PVP, but soluble in PLGA. The *in vitro* releases of these PLGA coated PVP-4HPR and PVP-4HPR-TEAC implants (Fig 9a-d), shows similar release rates with 10% 4HPR release after 28 days,

however, slightly slower 4HPR release was observed when TEAC added to implant. We observed that the PVP-4HPR core implant melts immediately, resulting in rapid PVP release, leaving behind crystallized 4HPR in PLGA coatings. The effect of the PLGA coatings on 4HPR release was: 503 + 3% $MgCO_3$ > 503H > 503H + 3% $MgCO_3$.

The effect of the PLGA coatings on PVP release shows the slowest releases when coated with PLGA 503H (3 days for 80% release), and addition of the basic pore forming salt $MgCO_3$ accelerated PVP release. This effect of $MgCO_3$ accelerating PVP release was also observed in #6 PLGA coated formulations. This could be attributed to $MgCO_3$'s neutralization of PLGA's acidic end groups, which may play a role in hydrogen bonding of PVP and adhering the coating to the implant. The least favorable coating for delaying PVP release was PLGA 503, and nearly 100% PVP was released after first day, likely due to similar phenomenon, where ester end-capped PLGA had less hydrogen bonding with PVP, and exhibited a greater repulsion for each other. In the SEM images (Fig. 4-8c),the PLGA coatings containing 3% $MgCO_3$ do not adhere as tightly to the PVP-4HPR-TEAC implant compared to the PVP-4HPR implant, suggesting that TEAC may play a role in repulsion of PVP to PLGA or of 4HPR to PLGA. Although these formulations (#7, 8) did not perform well *in vitro*, insight was gained into how PLGAs and TEAC affect the release rate of the PVP-4HPR complex.
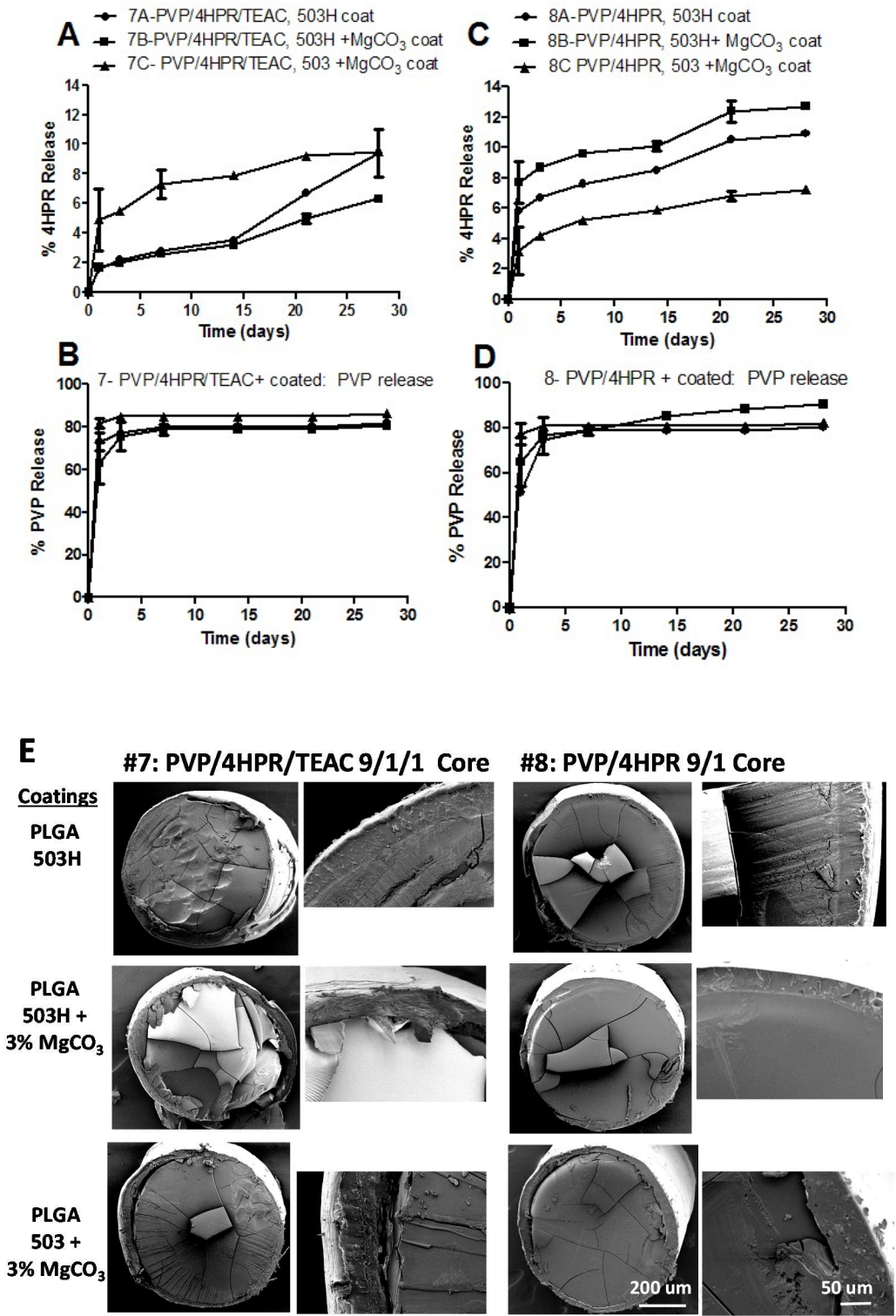
Figure 3-9. In vitro release of 4HPR (a,c) and PVP (b,d) from PVP-4HPR-TEAC 9/1/1 (a,b) or PVP-4HPR 9/1 (c,d) core implants coated with PLGA (503H, 503H + 3% MgCO3 or 503+ 3% MgCO3) (mean± SE, n=3). E) SEM's show cross-sectional morphology of #7 and #8 PLGA coated implant, including a close up of the coating-core edge for each implant.

3.4.5.4. PLGA millicylinders loaded with PVP-4HPR-TEAC ASDs enhance 4HPR release

The aim of the next formulations (#9-11) was to utilize TEAC to keep the ASD intact. In the previous PLGA coated PVP-4HPR-TEAC cores, the TEAC was only slightly effective at slowing the release of PVP. Also, it was suspected that the PVP-4HPR ASD was dissociating in the presence of PLGA due to chemical interactions, and it was postulated that addition of TEAC would inhibit this interaction due to masking PLGA's carboxylic acid end groups (See chemical structures in Fig. 3-1). As shown in Fig. 3-10, the PLGA millicylinder loaded with TEAC-PVP-4HPR particles 9/1/1 (#9), and resulted in a 5.6-fold increase in 4HPR release after 28 days (34% vs 6% 4HPR respectively) compared to formulation #1 without TEAC. To determine if TEAC's plasticizing effects on PLGA was responsible for the favorable 4HPR release from #9, a control implant without PVP was evaluated (#10: PLGA 503H+4% TEAC+ 5% 4HPR), and did not perform well with only 0.5% released after 28 days. Furthermore, in the last formulation #11, TEAC was added to PLGA prior to addition of the PVP-4HPR-TEAC ASD to further enhance 4HPR release, if in fact the favorable drug release was due to PLGA plasticization. This formulation released slightly less than #9, (23% after day 28), so it could be established that the TEAC is likely exerting its effects by allowing the PVP-4HPR complex to remain intact, rather than due to the PLGA plasticization. The solubility of each of these components in PLGA can be seen in SEM cross-sectional images (Fig. 4-10c). The PVP-4HPR-TEAC ASD is not soluble in the PLGA (#9), TEAC is soluble in PLGA (#10), and the additional TEAC in PLGA prior to addition of the PVP-4HPR-TEAC ASD (#11) resulted in poor implant formation with holes present.

Next, this optimized formulation (#9) or PLGA+ PVP-4HPR-TEAC, was evaluated *in vivo* after SC implantation and compared to an immediately dissolving PVP-4HPR (9/1)

implant. The *in vivo* release shows slow and continuous release over 30 days (Fig. 3-10d), and

the controlled release PLGA formulation out-performed the completely amorphous ASD. This

is a significant improvement from our previous PLGA-4HPR millicylinder implants, where we

found that only 25% drug could be release after 30 days *in vivo.*
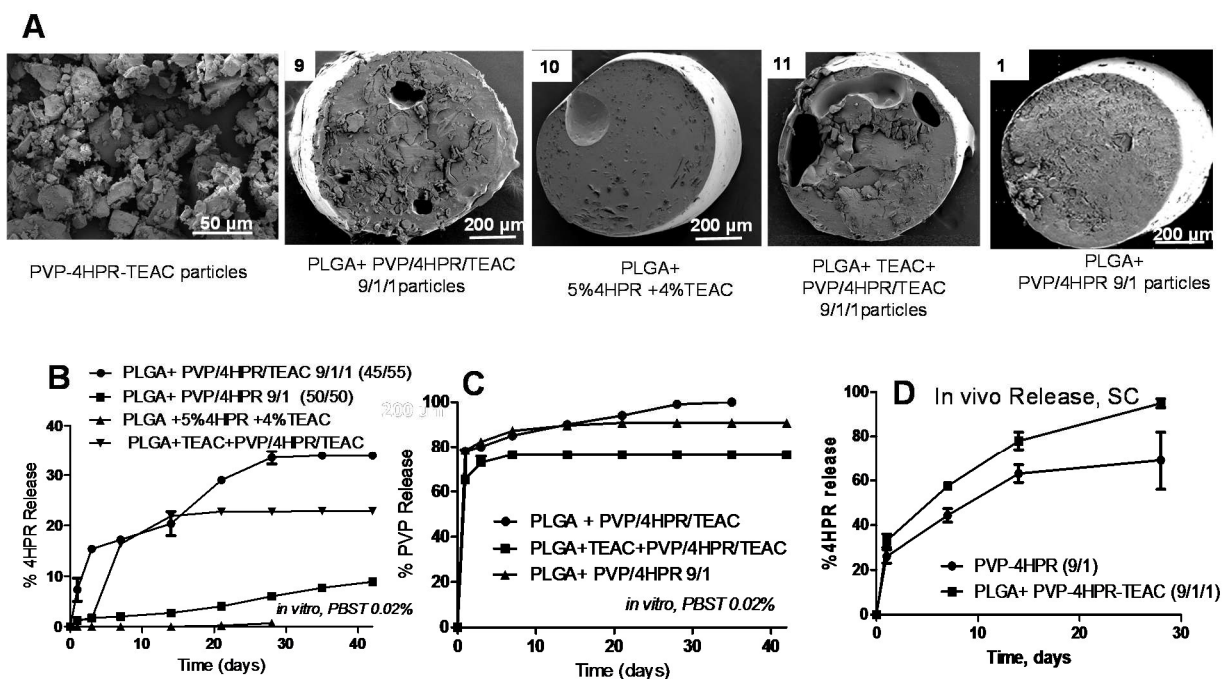
Figure 3-10. Effects addition of TEAC to PVP-4HPR particles loaded into PLGA implants on *in vitro* and *in vivo* releases. A) SEM images PVP-4HPR-TEAC particles and implant cross section show PVP-4HPR-TEAC particles are more intact in PLGA than PVP-4HPR particles, and TEAC is insoluble in PLGA. b) *in vitro* release of 4HPR accelerated by TEAC, c) in vitro release of PVP not affected by TEAC (#10), and d) Desirable 4HPR release kinetics achieved *in vivo* in SC region of rats with PLGA+ 4HPR-PVP-TEAC, which outperformed the completely amorphous PVP formulation. Mean ± SE, n=3.

Table 3-3. PVP-4HPR-PLGA millicylinder implant compositions and *in vitro* performances

Batch	Preparation Method	PLGA type	Theoretical Loadings				Experimental Data			
			% PLGA	% 4HPR	% PVP	% TEAC	% 4HPR	% PLGA coating	Day 28 % 4HPR released	Time 80% PVP release (days)
1	PLGA +9/1 PVP-4HPR particles	503H	50	5	45	--	4.1 ± 0.5	--	7.7 ± 0.2	3
2	PLGA +8/2 PVP-4HPR particles	503H	75	5	20	--	3.5 ± 0	--	0.7 ± 0.3	>35
3	PLGA +7/3 PVP-4HPR particles	503H	83	5	12	--	3.1 ± 0.3	--	1.0 ± 0.8	>35
4	PLGA +8/2 PVP-4HPR particles	503	75	5	20	--	2.3 ± 0.6	--	4.1 ± 0.2	28
5	PLGA +7/3 PVP-4HPR particles	503	83	5	12	--	3.1 ± 0.1	--	4.2 ± 0.2	7
6a	Co-dissolve PLGA (503H), PVP, 4HPR in DCM *coated with PLGAs	Coat 503H	45	5	50	--	3.4	<0.1	4.2 ± 0.5	>42
b		Coat 503H+ 3%MgCO$_3$					2.9	0.3	5.8 ± 0.8	28
c		Coat 503+ 3%MgCO$_3$					3.1	0.1	3.1 ± 0.4	>42
d		503H, no coat					3.2	--	9.5 ± 0.7	35
7a	PVP-4HPR-TEAC (9/1/1) *core coated with PLGAs	Coat 503H	--	9	82	9	5.9	1.7	9.4 ± 1.6	7
b		Coat 503H+ 3%MgCO$_3$					5.8	1.8	6.3 ± 0.2	28
c		Coat 503+ 3%MgCO$_3$					5.8	1.9	9.5 ± 0.0	1
d		--					7.6	--	--	--
8a	PVP-4HPR (9/1) *core coated with PLGAs	Coat 503H	--	10	90	--	7.0	--	10.9 ± 0.2	28
b		Coat 503H+ 3%MgCO$_3$					7.2	2.1	12.7 ± 0.2	14
c		Coat 503+ 3%MgCO$_3$					7.1	2.0	7.2 ± 0.2	3
d		--					9.1	2.1	--	--
9	PLGA+ PVP-4HPR-TEAC (9/1/1)	503H	--	5	45	5	5.5	--	33.5 ± 1.3	3
10	PLGA+ TEAC (11/1) + 4HPR	503H	87.5	5	--	7.5	$5.9 \pm 0.4\%$	--	0.7 ± 0.2	--
11	PLGA+ TEAC (11/1) + PVP-4HPR-TEAC(9/1/1) particles	503H	41	5	45	9	$2.7 \pm 0\%$	--	22.8 ± 0	7

- All percentages are expressed as w/w.
- Note: in #6-8, only 1 millicylinder was used for 4HPR loading determination due to the limited supply.

3.5. Discussion

The initial solubilization studies showed that PVP aqueous solutions are not effective at solubilizing 4HPR. When 4HPR is first dissolved in acetone prior to adding to the PVP solution however, its solubility is enhanced. PVP acted as a wetting agent and formed a cloudy colloidal drug suspension, and also reduced 4HPR's photo-sensitivity by maintaining 4HPR's yellow color. Next, amorphous PVP-4HPR complexes were prepared, and the 9/1 PVP-4HPR complex resulted in a 50-fold solubility enhancement of 4HPR was achieved (in ddH$_2$0) and sustained over 7 days.

One of the advantages of amorphous molecules is faster dissolution and greater apparent solubility for extended periods of time. One of the disadvantages of amorphous molecules is that they can have decreased physical stability, and can form different crystal structures after recrystallization. This was evident in our 4HPR acetone recrystallization studies where different crystal structures were observed, and confirms the presence of multiple polymorphic states, as described in literature where two polymorphs of 4HPR are known, with Tm's of 173-175 °C and 178-180 °C (9). Stability of co-amorphous drug systems is influenced by their Tg and intermolecular interactions (26, 27). PVP's high Tg (174 °C) gives rise to better stability of the PVP-4HPR amorphous solid dispersion due to hindered drug diffusion and inhibition of drug precipitation in the glassy matrix. A nearly completely amorphous and highly homogeneous dispersed drug can be validated by having a single glass transition temperature, indicating a high degree of homogeneity (23). Based on the long duration of sustained solubility from the 9/1 PVP-4HPR complex shown in the dissolution study, which was tested months later, we see that this is a very stable system.

Further investigation into the PVP-4HPR interactions by ITC revealed that the optimum mass ratios of ~9/2 PVP-4HPR (or 18% 4HPR), which requires half the amount of PVP we found necessary for superior 4HPR solubility enhancement. These results agree with the optimal PVP-4HPR ratios found by Ledet and coworkers (20% 4HPR)(24) and Laurent Pharmaceuticals (20% 4HPR)(23). It is suspected that out 9/1 PVP-4HPR ratio performed the best by providing excess PVP to prevent PVP-4HPR dissociation or to increase hydrogen bonding. This is also consistent with the study of molecular mobility of PVP-nifedipine glassy dispersions that found that PVP mobility was delayed by increasing strength of hydrogen bonding along with increasing PVP concentration which contributed to the stability of the complex (28). The most likely mechanism of PVP-4HPR ASD stability is due to hydrogen bonding between PVP's carbonyl and 4HPR's hydroxyl group.

Next, PLGA millicylinders were prepared using different methods for loading of PVP-4HPR ASDs into the implant. Solubility considerations of the components in various solvents and PLGA matrix were important for delivery of the intact PVP-4HPR complex. The challenge here was to design a system that accounted for the different chemical properties of hydrophobic 4HPR and hydrophilic PVP which had differing affinities for hydrophobic PLGA matrix. This inherently led to rapid release of PVP, leaving behind precipitated 4HPR shielded from aqueous environment in PLGA. PLGA is soluble in the organic solvents DCM and acetone (typically used in preparations because of their high volatility needed for drying of implants), PVP is insoluble in acetone, but soluble in DCM and MeOH, and 4HPR solubility in these solvents is as follows: acetone > MeOH > DCM(8). For our *in vitro* release studies, a non-solublilizing buffer system was used (PBS 0.02% pH 7.4), and therefore any appreciable amount of 4HPR released will be indicative of release of the solubilizing 4HPR-PVP complex.

Our first experiments (#1-5) loaded different ratios of PVP-4HPR particles into PLGA dissolved in acetone, and yielded poor 4HPR release kinetics, (<10% after 28 days), due to rapid and nearly complete release of PVP after 3 days. This confirms the challenge of co-delivery of drugs and excipients with different chemical properties. The next set of formulations (#6) used DCM as a co-solvent, where all three components were solubilized, and successfully provided PVP controlled release by entanglement of PVP and PLGA polymer chains, however it impaired PVP-4HPR interactions and resulted in incomplete 4HPR release (10% after 6 weeks). Additionally, #6 was coated with PLGA's, but did not have a significant positive affect on 4HPR release kinetics, but did slow PVP release as expected.

Because PVP is a hydrophilic polymer, it will dissolve quickly in aqueous solutions, resulting in a large burst release of the excipient, which may contribute to dissociation of the drug-PVP ASD. A literature search revealed that PVP melting could be delayed by addition of dibutyl phthalate (DBP) to beeswax/ PVP implants for veterinary therapies (29). Due to the known health risks of phthalates, TEAC has been listed as suitable substitute for DBP in a wide range of applications (30), and was added to the PVP-4HPR ASD's. Next an attempt was made to create millicylinder systems that contained core PVP-4HPR or PVP-4HPR-TEAC complexes coated with PLGAs to provide controlled release of the ASD. The results of these *in vitro* release studies were disappointing, where nearly all of the core had dissolved after the first few days, and >90% of the precipitated drug was left behind in the PLGA coatings. However, we did learn a few things: PLGA coatings containing 3% $MgCO_3$ do not adhere as tightly to the PVP-4HPR-TEAC implant compared to the PVP-4HPR implant, suggesting that TEAC may play a role in repulsion of PVP to PLGA or of 4HPR to PLGA. An important question is what is the

preference of 4HPR in PLGA vs. PVP? By decreasing the amount of PLGA, we may be able to limit 4HPR partition into PLGA, and remain in the PVP-4HPR solubilizing complex.

The final formulation utilize PVP-4HPR-TEAC particles and was suspected that TEAC was enhancing drug release by insulating PVP-4HPR ASD and inhibit its dissociation by PLGA. This was the most favorable release, with 35% released after 28 days, equating to a 5.6-fold increase in release compared to the formulation without TEAC. Furthermore, this optimized ASD formulation showed a dramatic improvement from our previous *in vivo* release from PLGA-4HPR millicylinders, with nearly complete and continuous release over 1 month.

3.6. Conclusions

Here we show that 4HPR solubility can be significantly enhanced by formation of PVP-4HPR ASDs at the optimum ratio of 9/1. We have formulated this solubilized form of 4HPR-PVP ASD into long-acting release PLGA millicylinders for local delivery. By incorporating the plasticizer TEAC into the PVP-4HPR particles, a 5.6-fold increase on 4HPR *in vitro* release was observed compared to those implants without TEAC. The *in vivo* release of 4HPR from the PLGA PVP-4HPR-TEAC implants have shown remarkable controlled release properties over 1 month. These results shows the utility of PVP-4HPR ASD into controlled release local drug delivery and will be beneficial for life-long oral cancer chemoprevention applications.

3.7. Supplemental Information

3.7.1. Tg's of PVP-4HPR particles and PLGA-PVP-4HPR +TEAC Millicylinders

The glass transition temperature (T_g) of the PVP-4HPR particles was measured to determine if a complex had formed, which would could be confirmed by verification of one Tg. The Tg of the dried PLGA-PVP-4HPR millicylinders was also measured to determine if PVP or 4HPR affected the Tg of PLGA implying miscibility of the components.

- Tg 1 is a reflection of PLGA and excipient miscibility.

- Tg 2 is a reflection of the percent amorphous PVP-4HPR in system, likely the Tg from PVP (163 °C) or Tm of 4HPR (174 °C), due to dilution by amorphous PVP-4HPR.

Figure S1 shows Tg's of representative PLGA-PVP-4HPR millicylinder formulation with and without TEAC, compared to the PVP-4HPR particles all having complex ratios of 9/1. The Tg's of #8A and 8C (PVP-4HPR coated with 503H or 503+3%MgCO$_3$) are similar, 126 and 121 °C respectively, but an additional Tg is present with #8A at 34 ˚C, representing PLGA 503H. These PVP-4HPR 9/1 cores have a much lower Tg than the corresponding particles (155 °C), possibly due to residual solvent or water present. The PVP-4HPR-TEAC core coated with PLGA 503H (#7a), has Tg's at 30 °C and 97 °C, while the corresponding particles has a Tg of 87 °C, and the 10 °C difference could be due to precipitation of the PVP in presence of the PLGA coating and TEAC. And finally formulation #7 contained the PVP-4HPR-TEAC 9/1/1 particles loaded into PLGA 503H, and has Tg's at 37 °C and 140 °C. The later Tg is much greater than the corresponding particles (87 °C) and the core implant coated with PLGA 503H (97 °C). These elevated Tgs in formulations #9 and the 9/1 PVP-4HPR particles (compared to the 8/2 and 7/3 ratios) may play a role in the favorable release and solubility enhancement.
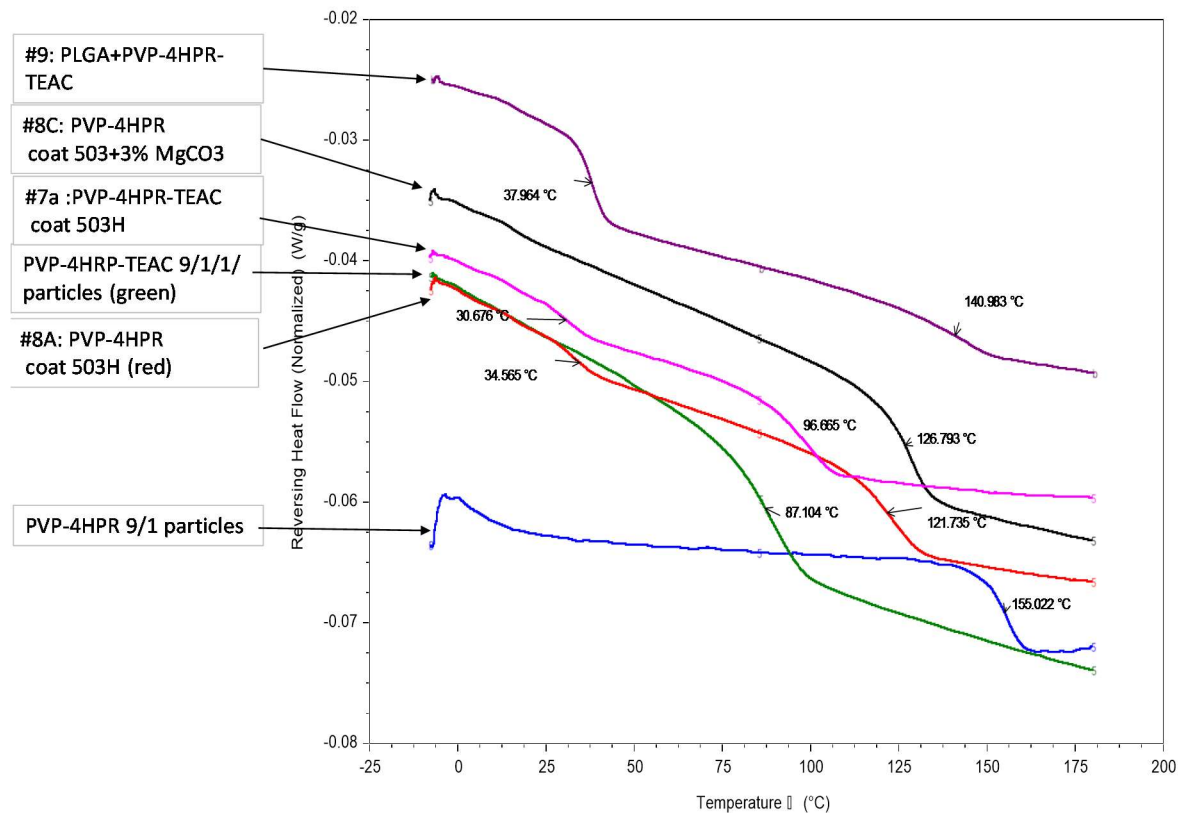
Figure S3- 1. Overlay of Tg's by DSC of PLGA-PVP millicylinder formulations (#7A, #8A,C, #9) and compared them to the Tg's of the PVP-4HPR 9/1 or PVP-4HPR-TEAC 9/1/1 particles.

3.7.2. TGA Analysis

The TGA analysis shows <5% residual solvent present after drying implant after ready mass loss at 100 °C.

109
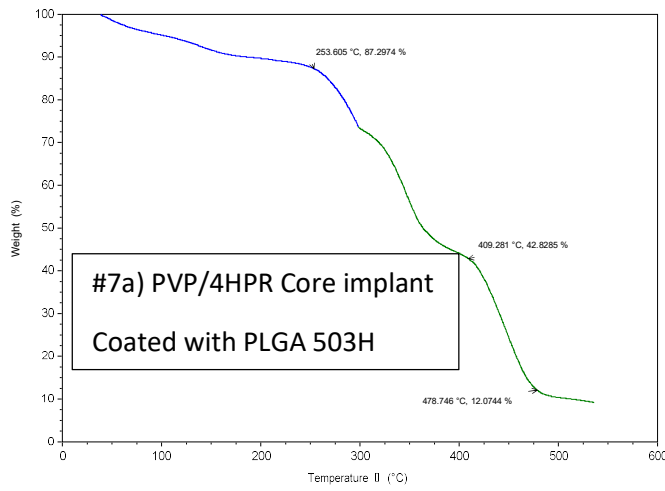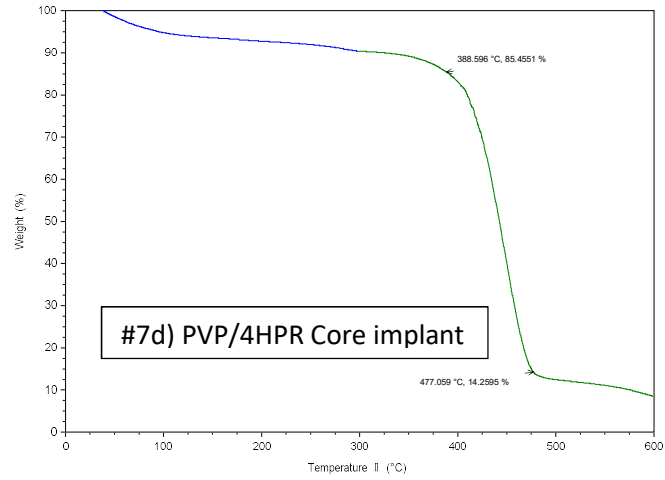
Figure S3- 2. TGA spectra of (a) #7d PVP-4HPR 9/1 core (uncoated) vs (b) #7a coated with PLGA 503H.

3.8. References

1. Holpuch, A., Desai, K.-G., Schwendeman, S. & Mallery, S. Optimizing therapeutic efficacy of chemopreventive agents: A critical review of delivery strategies in oral cancer chemoprevention clinical trials (2011).
2. Orienti, I. et al. Novel micelles based on amphiphilic branched PEG as carriers for fenretinide. *Nanomedicine: Nanotechnology, Biology and Medicine* **8**, 880-890 (2012).
3. Li, C.-Y., Zimmerman, C. & Wiedmann, T. Solubilization of Retinoids by Bile Salt/ Phospholipid Aggregates. *Pharmaceutical Research* **13**, 907-913 (1996).
4. Orienti, I. et al. Fenretinide-polyvinylalcohol Conjugates: New Systems Allowing Fenretinide Intravenous Administration. *Biomacromolecules* **8**, 3258-3262 (2007).
5. Orienti, I., De, M.M.R. & Zeuner, A.P. (Google Patents, 2016).
6. Orienti, I., Zuccari, G., Carosio, R. & G. Montaldo, P. Improvement of aqueous solubility of fenretinide and other hydrophobic anti-tumor drugs by complexation with amphiphilic dextrins. *Drug Delivery* **16**, 389-398 (2009).
7. Ying Zhang, C.W., Sachin Mittal, Amitava Mitra, Steven P. Schwendeman. Design of controlled release PLGA microspheres for hydrophobic fenretinide. *Molecular Pharmaceutics* (in press).
8. Wischke, C., Zhang, Y., Mittal, S. & Schwendeman, S.P. Development of PLGA-based injectable delivery systems for hydrophobic fenretinide. *Pharm Res* **27**, 2063-74 (2010).
9. Graves, R.A. et al. Formulation and evaluation of biodegradable nanoparticles for the oral delivery of fenretinide. *European Journal of Pharmaceutical Sciences* **76**, 1-9 (2015).
10. Trapasso, E., Cosco, D., Celia, C., Fresta, M. & Paolino, D. Retinoids: new use by innovative drug-delivery systems. *Expert Opin Drug Deliv* **6**, 465-83 (2009).
11. Parchment, R.E., Jasti, B.R., Boinpally, R.R., Rose, S.E. & Holsapple, E.T. (Google Patents, 2014).
12. Almarsson, Ö. et al. (Google Patents, 2011).
13. Wu, X. et al. Mucoadhesive fenretinide patches for site-specific chemoprevention of oral cancer: enhancement of oral mucosal permeation of fenretinide by coincorporation of propylene glycol and menthol. *Mol Pharm* **9**, 937-45 (2012).
14. Desai, K.G., Mallery, S.R., Holpuch, A.S. & Schwendeman, S.P. Development and in vitro-in vivo evaluation of fenretinide-loaded oral mucoadhesive patches for site-specific chemoprevention of oral cancer. *Pharm Res* **28**, 2599-609 (2011).
15. Chen, Y. et al. Initial Drug Dissolution from Amorphous Solid Dispersions Controlled by Polymer Dissolution and Drug-Polymer Interaction. *Pharm Res* **33**, 2445-58 (2016).
16. BASF. (ed. BASF) (2009).
17. Magalhães, P.J. et al. Isolation of phenolic compounds from hop extracts using polyvinylpolypyrrolidone: Characterization by high-performance liquid chromatography–diode array detection–electrospray tandem mass spectrometry. *Journal of Chromatography A* **1217**, 3258-3268 (2010).
18. Durán-Lara, E.F. et al. Experimental and theoretical binding affinity between polyvinylpolypyrrolidone and selected phenolic compounds from food matrices. *Food Chemistry* **168**, 464-470 (2015).
19. Pattanaik, M. & Bhaumik, S.K. Adsorption behaviour of polyvinyl pyrrolidone on oxide surfaces. *Materials Letters* **44**, 352-360 (2000).

20. Cohen Stuart, M.A., Fleer, G.J. & Bijsterbosch, B.H. Adsorption of poly(vinyl pyrrolidone) on silica. II. The fraction of bound segments, measured by a variety of techniques. *Journal of Colloid and Interface Science* **90**, 321-334 (1982).
21. FDA. (01/07/2016).
22. Farng, R.K., Gendimenico, G.J., Mezick, J.A., Ng, S.M. & Wrobel, S.B. (Google Patents, 1998).
23. Laurent, P., BETANCOURT, A., Lemieux, M. & Thibert, R. (Google Patents, 2016).
24. Ledet, G.A., Graves, R.A., Glotser, E.Y., Mandal, T.K. & Bostanian, L.A. Preparation and in vitro evaluation of hydrophilic fenretinide nanoparticles. *Int J Pharm* **479**, 329-37 (2015).
25. Tavlarakis, P., Urban, J.J. & Snow, N. Determination of total polyvinylpyrrolidone (PVP) in ophthalmic solutions by size exclusion chromatography with ultraviolet-visible detection. *J Chromatogr Sci* **49**, 457-62 (2011).
26. R, A.W., William, D. & Anthony, P. (Google Patents, 1969).
27. Maag, J., Lassen, C., Brandt, U.K. (ed. Danish Ministry of the Environment, E.P.A.) (Denmarck, 2010).
28. Sun, Y., Tao, J., Zhang, G.G.Z. & Yu, L. Solubilities of Crystalline Drugs in Polymers: An Improved Analytical Method and Comparison of Solubilities of Indomethacin and Nifedipine in PVP, PVP/VA, and PVAc. *Journal of Pharmaceutical Sciences* **99**, 4023-4031 (2010).
29. Alhnan, M.A. & Basit, A.W. In-process crystallization of acidic drugs in acrylic microparticle systems: influence of physical factors and drug-polymer interactions. *J Pharm Sci* **100**, 3284-93 (2011).
30. Yao, J., Shi, N.Q. & Wang, X.L. [The development of co-amorphous drug systems]. *Yao Xue Xue Bao* **48**, 648-54 (2013).
31. Mehta, M., McKenna, G.B. & Suryanarayanan, R. Molecular mobility in glassy dispersions. *Journal of Chemical Physics* **144** (2016).

Chapter 4: 4HPR's Binding Kinetics to Tissue and Cell Membrane Components

4.1. Abstract

Fenretinide (4HPR) tissue binding kinetics were characterized using varied *ex vivo* tissues (intact, thinly sliced, homogenates), *in vivo* sites [buccal epithelia and subcutaneous (s.c.) tissue] with concurrent assessment of varied solubilizer and permeation enhancer levels. Effects of tissue-composition i.e. lipid on 4HPR interactions were also assessed. 4HPR tissue uptake was evaluated as a function of free-drug level and drug-tissue aqueous partitioning coefficients (Kp_u) were calculated. These results show that time of exposure, but not solubilizer or permeation enhancers, affected tissue uptake. Furthermore, 4HPR exhibited a fifteen-fold greater binding affinity to buccal epithelia relative to s.c. connective tissues. Obtaining 4HPR solubility in aqueous solutions was the limiting factor for tissue uptake. While the majority of non-specific tissue binding likely reflects lipid interactions, it is well known that 4HPR also demonstrates high affinity protein binding. To conclude, this study found that 4HPR-tissue binding revealed an apparent lack of saturation, as tissue uptake rates remained comparable even at highest 4HPR levels. 4HPR's tissue binding propensity introduces the prospect of 4HPR-mediated tumor-stromal chemoprevention.

4.2. Introduction

The lipophilic vitamin A derivative, 4-hydroxy(phenyl)retinamide [fenretinide (4HPR)] was developed in the 1970's to elicit retinoid chemopreventive effects in cells devoid of the retinoic acid receptor (1). I*n vitro,* 4HPR demonstrated extensive cancer-preventive potential via its induction of terminal differentiation and/or apoptosis in a variety of premalignant and

malignant cells (2). As a result of 4HPR's poor bioavailability, however, *in vitro* efficacy did not translate to clinical efficacy (3). Another complication is 4HPR's extensive first pass metabolic inactivation during systemic delivery. In contrast, local delivery can delivery therapeutic 4HPR doses to target tissue without adverse effects e.g. nyctalopia (4). 4HPR binds with high affinity to several proteins including kinases associated with gratuitous signaling e.g. focal adhesion kinase (5) and STAT3 (6). Such 4HPR-protein interaction extend 4HPR's tumor suppressive effects beyond lesional to stromal and inflammatory cells (7). Pharmacokinetic (PK) data from previous 4-HPR clinical trials (100-200 qd oral) demonstrated 4HPR's tissue retention (20%), rapid equilibrium in plasma (<24 h) (8), greater preference for tissue than plasma, max plasma levels achieved after 4 h (Tmax) (3), half live ($t_{1/2}$) is 12-24 h (3,4,9), and bioaccumulates in blood (detected 6 mo, post-treatment)(4).

While 4-HPR's dispersion through lesional tissue is essential for chemoprevention, 4HPR's tissue binding affinity during local delivery has not been evaluated. Notably, limited penetration distance is the most prevalent challenge encountered during local drug delivery (10). A variety of factors govern tissue-drug distribution including diffusion rates, convection, elimination, protein binding, cellular uptake, capillary permeation, degradation and entrance into cell and subcellular components and intracellular metabolism and efflux (11). Following subcutaneous delivery (s.c.), diffusion and convection enable a drug's entrance to the extracellular space, while elimination can occur via local metabolism or clearance. Locally delivered drugs can enter systemic circulation via capillary flow or lymphatic uptake. Due to their enhanced permeability, lipophilic drugs like 4HPR are cleared from the local site within the first 30 min. Due to the ease of drug-capillary diffusion, the rate-limiting step in systemic distribution is blood flow. Also, the microvasculature patterns vary, and are most abundant 0.1

mm below skin. Barriers to interstitial space diffusion include presence of lipids, proteins, or blood vessels, in contrast to molecular diffusion in a boundary free medium which depends only on molecular size, the temperature, and medium viscosity, and results from random or Brownian motion of particles (12). Additionally, drug binding to tissue components such as lipids or proteins, can prevent drug clearance and keep more drug at the target site. While it is widely held that only unbound drug is active, stromal protein bound 4HPR can serve as a tissue reservoir and also elicit chemopreventive effects. Provided these extensive parameters, there is likely an optimal chemoprevention "sweet spot" between binding and clearance. A final local delivery consideration is that that retinoids, including 4HPR, exhibit high binding affinities to lipid rich cell membranes and plasma proteins(13) that can limit its ability to permeate throughout the treatment site.

These studies characterized 4HPR tissue binding kinetics using a variety of *ex vivo* tissues, delivery sites [buccal vs. s.c.], tissue preparations (intact, homogenate, or thinly sliced), with inclusion of solubilizers and permeation enhancers in medias. Buccal mucosa is known to have greater permeation than s.c. (4-4,000 fold), contingent upon the molecule, lipid profiles and local blood flow (14). Thinly sectioned tissues and tissue homogenates could augment greater binding due to increased binding site exposure. Comparative competitive binding experiments with another retinoid molecule, acitretin, whose tissue and plasma protein interactions have been well characterized (15) were performed. 4HPR solutions were incubated with isolated cell membrane fractions to assess 4HPR's lipid binding affinity. Aqueous drug- tissue partition coefficients (Kp) were calculated for each tissue type and solubilizing media. Our results show 4HPR exhibits very high non-specific tissue binding. Further, comparable rates of drug-tissue

uptake occurred even at the highest 4HPR levels, which imply that 4HPR solubility as opposed to tissue saturation limits 4HPR-tissue uptake.

4.3. Materials

4HPR was generously supplied by Merck Co. Acitretin was purchased from Sigma-Aldrich. Polyvinylpyrrolidone polymer (PVP K30, 40 kDa) was purchased from BASF. All other materials were reagent grade or better including ethanol (EtOH), dimethylsulfoxide (DMSO) and Tween 80. Solvents for UPLC/UV analysis were HPLC grade including acetonitrile (ACN), double distilled water (ddH$_2$0), and phosphoric acid (H$_3$PO$_4$). Tissues were sectioned using optimum cutting temperature compound (OCT, Tissue Tek), and adhered to poly-lysine coated glass slides. Phosphate buffer saline (PBS) for tissue incubation media and radioimmunoprecipitation assay buffer (RIPA) to lyse cells and tissues, were prepared in house according to standard recipes. Naïve rat SC tissue, and porcine buccal tissues were used.

4.4. Methods

An overview of the 4HPR binding studies and purposes are listed in Table 4-1, followed by complete experimental descriptions.

Table 4-1. Overview of 4HPR Binding Studies

Purpose	Parameter(s)	Rationale
Binding to tissues	Binding (μg 4HPR/ g tissue) vs. free drug concentration:	Examine effects of each listed parameter on drug-tissue uptake:
	Effects of Tween and other solubilizers	• Evaluate extent of solubilization on uptake • Addition of tween and/or other solubilizers to media is necessary for 4HPR solubility during *in vitro* studies
	Effects of penetration enhancers	• Permeation enhancers should allow drug to access more binding sites
	Buccal epithelia vs. s.c. tissue	• Buccal epithelia 4-4000x's greater permeability due to buccal fat pad which alters lipid profile • Does tissue site affect 4HPR binding affinities?
	Intact tissue, tissue homogenates, and thinly sectioned tissue	• Thinly sectioned and homogenized tissues will have greater exposure of binding sites, and potentially greater uptake • Comparing each of these will address drug-tissue penetration depth and tissue saturation
	Competitive binding with another synthetic retinoid (acitretin) and 4HPR	• Competition with another retinoid may decrease 4HPR binding, due to occupying binding sites
	Time & concentration dependence	• Equilibrium binding time determined • Determine if tissue saturation is achieved, and if uptake linear
	Aqueous phase-Tissue partitioning (Kp_u)	• Compare effects of tissue types, incubation media, and drug concentration has on uptake
Binding to cell membranes	Binding (μg 4HPR/ g cell membrane components) vs. free drug concentration	• Effects of 4HPR's established high affinity lipid binding on bioaccumulation

4.4.1. Tissue Binding

4.4.1.1. 4HPR Uptake in Buccal Epithelial (Intact and Homogenates) as a Function of Solubilization by Tween

Porcine buccal tissue was freed from connective tissue (70-100 mg wet mass) and incubated at 37 °C in 0.5 mL of 40 μg/mL(~100 μM) 4HPR prepared in PBS pH 7.4 + 0.02, 0.5, 1, or 2% Tween 80 (n=5 each). Epithelial tissues were homogenized (75-100 mg in 0.5 mL of 0.5% PBST, n=5) at 10,000 rpm x 2 min. Media were sampled (20 μL) at 0, 6, and 24 h and the

percent 4HPR uptake was determined by disappearance of 4HPR compared to starting concentration using the UPLC assay listed below. The amount of 4HPR (µg) uptake per g of wet tissue mass was reported after 6 h and 24 h, along with percent bound.

$$Percent\ Bound = \frac{C_i - C_f}{C_i}\ x\ 100$$

4.4.1.2. 4HPR uptake in Intact s.c. Tissue with Solubilizers, Permeation Enhancers, and Competitive Ligands

Intact rat s.c. tissue was cut (1x1 cm^2), weighed, and incubated with 10 mL of 4HPR solutions containing solubilizers and permeations enhancers. In the first experiment, tissues were incubated in PBS + 2% Tween + 0.1% DMSO (0, 2.5, 5, 12.5, 25, 50 µg/mL 4HPR) for 24 h at 37 °C on a shaking platform. In one sample, tissue was co-incubated with competitive ligand acitretin (5 µg/mL) and 5 µg/mL 4HPR solution. The percent uptake was determined by sampling incubation media before and after incubation, assaying 4HPR by UPLC. Drug-tissue extractions on thinly sliced incubated tissues were performed to obtain concentration penetration depth profiles. After 24 h, the intact tissues were removed from media, rinsed 2x's in 0.02% PBST, snap frozen, and cryosectioned (Leica 3050S cryostat) into 60 µm sections (n=6). Blank tissue was also collected for analyte extraction recovery controls (see tissue extraction methods). 4HPR was extracted from tissues using the extraction method listed below, and 4HPR tissue uptake was expressed as µg 4HPR/mg tissue and plotted against free drug concentration. For the competitive binding between acitretin and 4HPR, the relative percent uptake of each was compared.

The second experiment evaluated the effect of the solubilizing complex of PVP-4HPR on tissue uptake. PVP-4HPR amorphous complex (9/1 w/w) was prepared by solvent casting in

MeOH, followed by cryomilling (Retsch swing mill cryomill, PN 20.749.001) and sieving particles < 90 μm. Rat SC intact tissue sections (1x1 cm^2) were incubated with 10 mL of PVP-4HPR solutions (5-150 μg/mL [12-380 μM] 4HPR) for 24 h and solutions assayed for 4HPR level before and after incubations. A mass balance to account for drug precipitation was performed by quantifying 4HPR tissue levels after extraction.

4.4.1.3. 4HPR uptake in s.c. Thin Tissue Sections: Time and Concentration Dependence

Rat SC tissues were snap frozen, a 1x1 cm^2 tissue block was cryosectioned into 20 μm sections and thaw mounted on poly-lysine coated glass slides. A representative tissue mass was recorded by averaging 3 tissue section masses collected intermittently throughout the relatively homogeneous tissue block. The tissues sections were pretreated by incubating in PBS + 0.5% Tween for 30 min. To determine equilibrium binding time, tissues were incubated in 4 or 40 μg/mL (10 or 100 μM) 4HPR in PBST 0.5% for 1, 2, 4, 6, 12, and 24 h (n=2 each time point). At each time point, tissues were washed in PBS x 2 then ddH$_2$0, 4HPR was extracted from tissue, and uptake reported as a function of incubation time. The equilibrium binding time was chosen based on the greatest tissue uptake. For the concentration dependent binding, tissues sections were pretreated in PBST 0.5% and incubated at the equilibrium time in 4HPR PBST 0.5% solutions ranging from 1 to 250 μM (0.2 to 170 μg/mL). Tissue uptake was plotted as a function of free drug concentration.

4.4.2. Subcellular Component Binding

The binding of 4HPR to lipid cell membranes method was adopted from NIMH-PDSP assay protocol book.[16] Cell membrane fractions were isolated from fresh porcine buccal epithelium (~ 70 mg, n=5), 1 mL of ice cold RIPA lysis buffer added, and tissues were homogenized at 10,000 rcf for 2 min. The tissue homogenates were centrifuged at 1000 rcf x 10

min, and the supernatant containing the whole cell lysate was transferred to a new tube. The cell membrane fraction was isolated from the whole cell lysate by centrifuging the supernatant at 21,000 rcf x 20 min, yielding a pellet. The cell membrane pellet was washed 2x's with 1 mL of ice cold RIPA buffer, and centrifuged at 21,0000 rcf x 20 min, supernatant was discarded, yielding a purified pellet of cell membrane components. The mass of the purified cell membrane pellet was recorded, then incubated with varying volumes (500, 1000, or 250 μL) of 100 μM 4HPR in PBST 1% for 24 h at 37 °C on a shaking platform. The fraction of unbound (f_u) 4HPR after incubation with cell membrane fractions was determined by assaying the amount of 4HPR in incubation media by UPLC prior to and after 24 h. 4HPR uptake was reported as μg 4HPR per g of cell membrane fraction as a function of free drug concentration.

$$f_u = \frac{C_f}{C_i}$$

$$f_b = 1 - f_u$$

$$Amount\ Bound\ =\ f_b\ \times\ \frac{C_i \times Volume\ media}{g\ tissue\ or\ cell\ fraction}$$

4.4.3. 4HPR Aqueous Phase- Tissue Partitioning (Kp_u)

From the *in vitro* tissue binding experiments, 4HPR aqueous phase-tissue partition coefficients (Kp_u) were calculated, which refer to the ratio between drug concentration in tissue (C_t) and unbound drug ($C_{u,aq}$) in incubation media at equilibrium:

$$Kp_u = \frac{C_t}{C_{u,aq}}$$

Because 4HPR is a weak acid with pKa=9.76, ionization contributions at pH 7.4 are negligible. For physiological relevant calculations, the unbound fraction of drug in plasma (fu_p) is needed to extrapolate drug levels in media to plasma (17).

$$Kp = Kp_u \cdot fu_p$$

4.4.4. Tissue and Plasma Extraction Assays

4HPR was extracted from tissue and tissue homogenates. The wet masses of tissues were recorded, internal standard (5 μL of 0.5 mg/mL acitretin) was spiked into tissue samples, 200 μL of ice cold ACN added, sonicated on ice for 10 min, then clarified by centrifuging at 12,000 rcf for 5 min, and the amount of 4HPR in supernatant was determined by UPLC assay.

4.4.5. Statistical Analysis

Due to the relatively small sample sizes which prohibited determination of normality, nonparametric analyses were used. The Kruskal Wallis analysis of variance, followed by the Dunns multiple comparison test was used to assess the effects of time, and tissue status on 4HPR uptake (Fig. 5-1) and competitive binding with acitretin (Fig. 5-2). The Pearson correlation was used to evaluate the effects of 4HPR levels on tissue uptake (Fig. 5-5) and impact of solubilizing media (Fig. 5-6).

4.5. Results

4.5.1. Tissue Binding

Binding time, but not levels of solubilizing agent or tissue state, affects 4-HPR uptake.

4.5.1.1. 4HPR Uptake in Buccal Tissue (Bulk and Homogenates) as a Function of Solubilization by Tween

The results of the 4HPR uptake in intact porcine buccal epithelia are shown in Figure 4-1. These data show a time dependent drug uptake i.e. increased 4-HPR binding at 24h relative to 6 h (~180 vs. 80 μg 4HPR/g tissue respectively), with significant differences at these time points ($p<0.05$). In contrast, 4HPR uptake was independent of Tween levels as comparable micellar solubilization was obtained with 0.5, 1 or 2% Tween. Also, the tissue homogenate (0.5% Tween) and the intact tissue uptakes were comparable. After 24 h, ~75% 4HPR was bound to both tissue and homogenates (See Fig. 4-1b.) Although 100 μM 4HPR was insoluble in PBS + 0.02% Tween80, tissue components (lipids, proteins) actually increased 4HPR solubility in PBS 0.02% Tween80 incubation media from 0.33 μg/mL initially, to 1.83 ±1.38 μg/mL after 24 h. The results from Figure 1 show:

a) Time significantly affects drug uptake, even when PBST concentrations are the same.

b) These time differences are seen within the same PBST groups.

c) No real appreciable differences among PBST levels and homogenates.

d) Perhaps most importantly of all, the tissue doesn't appear to get "saturated" with 4HPR, uptake keeps increasing with time.
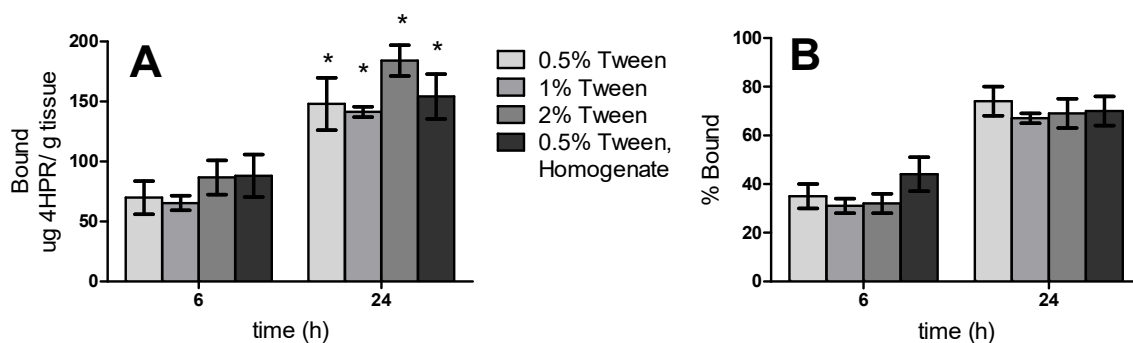
Figure 4-1. 4HPR uptake in porcine buccal intact tissue and tissue homogenates after incubation with 100 μM 4HPR in PBS + Tween80 (0.5, 1, 2%) after 6 and 24 h as represented by a) μg 4HPR/g tissue and b) Percent 4HPR bound to tissue (n=5, mean ± SE, *indicates $p < 0.05$). Only time, but not Tween level in PBST or homogenization affected 4HPR uptake.

4.5.2. 4HPR uptake in Intact s.c. Tissue with Solubilizers, Permeation Enhancers, and Competitive Ligands

Effect of PBST 2% + 0.1% DMSO on Uptake, and Competition with Acitretin

Results of the 4HPR SC tissue binding in PBST 2% + 0.1% DMSO incubation media (Fig. 4-2) show a linear increase in uptake as the free drug concentration increases (r^2=0.9875), while tissue saturation was not reached at 38 μg/mL 4HPR. Each data point is average of 6x60 μm sections, equating to a penetration depth profile of 360 μm, with no significant difference at each concentration, indicating homogeneous permeation. Each retinoid-distinguish e.g. 4HPR and acitretin exhibited 44% and 46% binding respectively. When 4HPR was coincubated with the same concentration of acitretin, binding of both retinoids decreased to 38% and 21%, respectively (but total retenoid uptake equated to 59%) (indicating that acitretin significantly ($p < 0.05$) inhibits 4HPR binding when both drugs added concurrently. These data imply a 1.8 fold prefence of 4HPR for non-specific binding, including lipid and protein binding.
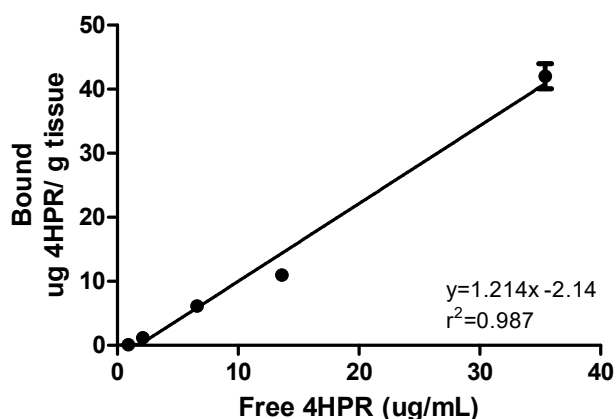
Figure 4-2. 4HPR binding to rat SC tissue after 24 h incubation in a solubilizing media of PBS+ 2% Tween80+ 0.1% DMSO. Each data point is average of 6x60 μm sections, equating to a penetration depth profile of 360 μm.

Effect of PVP-4HPR Solubilization on s.c. tissue uptake

Intact SC tissue 4-HPR uptake in super-saturated PVP-4HPR 9/1 solutions (Fig. 4-3a) showed similar drug uptake to tissues incubated with PBST 2% + 0.1% DMSO (Fig. 4-2). Both solutions provided comparable tissue uptake (10 μg 4HPR/g of tissue) when incubated in 10 μg/mL 4HPR solutions, equating to a ~1:1 4HPR/tissue mass ratio (a full Kp comparison proceeds this section). There is a linear increase in tissue uptake as free drug concentration increases, with a lag phase existing up to 7 μg/mL free 4HPR, yet tissue is still not saturated after 10 μg/g tissue. Appreciable 4-HPR precipitation from the supersaturated PVP-4HPR solution was observed after the incubation, where the initial 4HPR concentrations of 5-150 μg/mL had only yielded free drug levels 0.2-10 μg/mL after. This is shown in the mass balance in Figure 4-3b, where the amount 4HPR recovered in tissue + media is much lower than the amount dosed, suggesting that PVP-4HPR is not a stable complex in the presence of tissue components (likely salt).
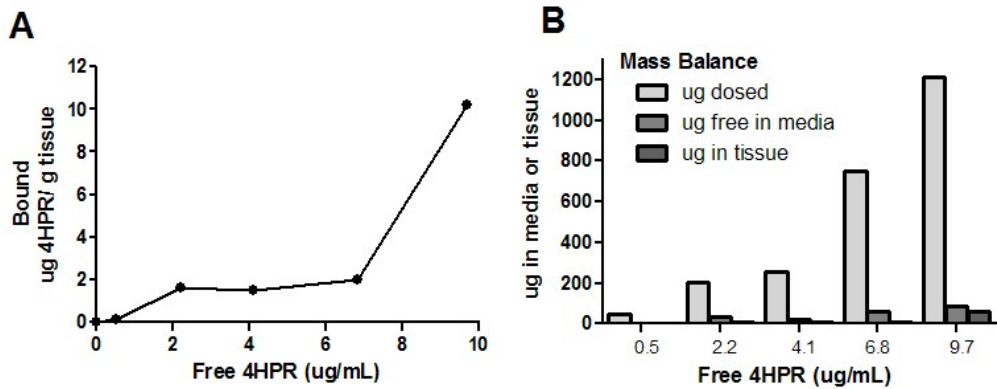
Figure 4-3. A) 4HPR binding to rat s.c. tissue after 24 h incubation in PVP-4HPR 9/1 solutions. B) Mass balance of 4HPR from the PVP-4HPR tissue incubations shows that the amount 4HPR recovered in tissue + media is much lower than the amount dosed, indicating the extent of 4HPR precipitation from the supersaturated solutions.

4HPR uptake in s.c. Thin Tissue Sections: Time and Concentration Dependence

The results of tissue uptake to determine equilibrium binding time after incubating thin s.c. tissue sections (20 μm) in PBST 0.5% drug solutions is shown in Fig. 4-4a. The equilibrium binding time was determined to be 4 h, due to greatest tissue uptake in the 100 μM 4HPR solution, while at low 4HPR level of 10 μM, equilibrium binding time was 2-6 h. At the later times points, the tissue was more apt to detach from the glass slide in the incubation media, which occurred in the 10 μM 4HPR level at 24 h. The results from the concentration dependent uptake of 4HPR is shown in Fig. 4-4b show linear (r2=0.9761), unsaturated, uptake at 170 ug/mL 4HPR which had bound 144 μg 4HPR/g tissue. This lack of tissue uptake saturation at this high drug levels is a rather unique finding.
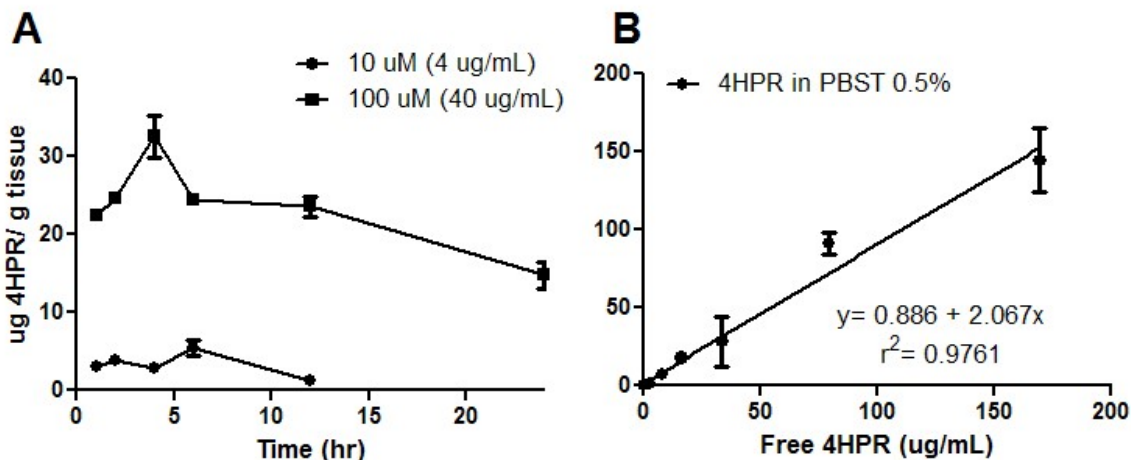
Figure 4-4. 4HPR binding kinetics with thinly sliced (20 μm) rat s.c. tissue in PBST 0.5%. A) Determination of equilibrium binding time by at two concentrations of 4HPR. B) Concentration dependent uptake of 4HPR after 4h incubation time.

4.5.3.   Cell Membrane Lipid Components Binding

The subcellular membrane component faction isolated from porcine buccal epithelial yielded 1-7% of the initial mass (< 5mg from 70 mg respectively). The results of 4HPR binding to subcellular cell membrane components are shown in Fig. 4-5. When the amount of 4HPR dosed is normalized to the mass of the cell membrane component (Fig 4-5a), we see a linear uptake, with no saturation of binding occurring at the free drug level of 34-38 μg/mL (~100 μM, Fig 4-5b). Statistics revealed a strong positive correlation between 4HPR levels and uptake. When top data point was removed (highest 4HPR level), the linearity decreased, implying that the highest 4HPR level was still linear, and the tissue not yet saturated. Table 4-3 summarizes these data, and shows 5-12% 4HPR in solution had bound to the isolated cell membrane fraction. To determine if buccal tissue binding was due to lipid interactions, we compared uptake in intact buccal to that of the cell membrane fraction. As shown in Table 4-4, the uptake in buccal cell membrane fraction was 500-2200 μg 4HPR/g cell membrane fraction, and could be back extrapolated to uptake per total tissue (based on 1-7 % w/w cell membrane fraction in tissue) to

5-155 µg 4HPR/g tissue. Comparing this value to the intact buccal uptake in of 144 µg 4HPR/g

tissue (in PBST 1%), we can see that the cell membrane components (lipids) are largely

responsible for the binding of 4HPR.

Table 4-2. 4HPR binding to cell membrane components in porcine buccal tissue homogenates

µg 4HPR spiked	Initial mass buccal tissue (mg)	Mass purified cell membrane pellet (mg)	µg 4HPR spike/mg pellet	µg 4HPR bound/ mg pellet	% Bound
20	75.3	1.57	13	1.42	11%
20	71.6	4.61	4	0.53	12%
20	71.3	0.87	23	1.53	7%
40	72.5	0.79	50	2.35	5%
10	73.0	1.06	9	0.70	7%
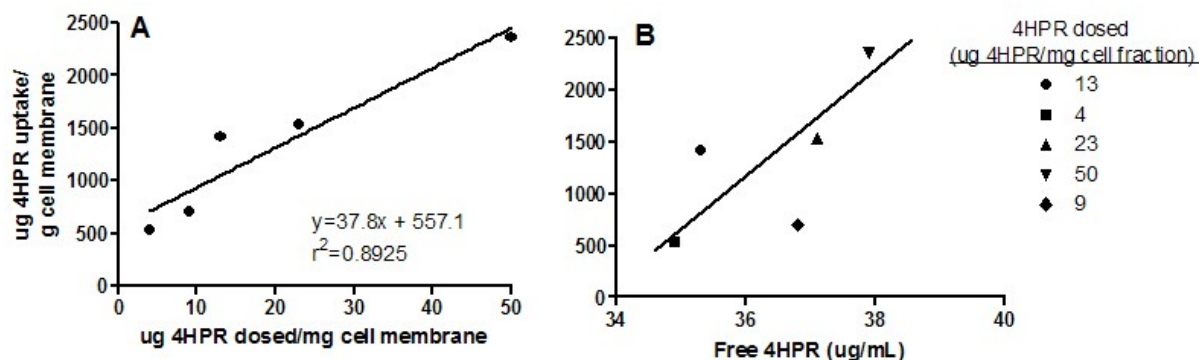
Figure 4-5. 4HPR binding to porcine buccal epithelia cell membrane components after 24 h: a) Normalized to mass of cell membrane, and b) as a function of free 4HPR in media after equilibrium. Varying volumes (250, 500, 1000 uL) of 10 µM 4HPR in PBS + 1% Tween 80 were spiked into the cell membrane pellet.

Table 4-3. 4HPR Uptake in Buccal tissues vs. Cell Membrane fraction

Tissue type	Uptake (µg 4HPR/g tissue)
Intact buccal	141 ± 4
Buccal cell membrane fraction	500-2200
Extrapolated buccal (based on 1-7% w/w cell membrane in tissue) *100 uM 4HPR in PBST 1%, 24h	5-155

4.5.4. Effects of Tissue Type on 4HPR Aqueous-Tissue Partitioning (Kp)

Comparison of 4HPR uptake in different tissues and media is shown in Fig. 4-6 and Kp

values in Table 4-6. Interestingly, all s.c. tissues had similar uptake despite type of preparation

(intact, thinly sectioned), or presence of solubilizing and permeation enhancing medias (Tween, PVP-4HPR, DMSO). Statistics reveal a positive correlation between 4HPR levels and uptake, with the exception of the intact s.c. tissue incubations with PVP, where a less linear relationship correlation of r^2=0.7393 was found. This lack of linearity may be due to the precipitation of 4HPR in the super-saturation solution, as indicated in Fig. 4-3. At lower free drug levels (<10 μM 4HPR) the s.c tissues exhibited Kp's of ~0.35-0.55, while 4HPR levels of 10-350 μM, Kp's were near 1. The most significant difference was tissue type, where uptake buccal epithelia had nearly 15-fold greater uptake than s.c. connective at free drug levels of 30 μM 4HPR.
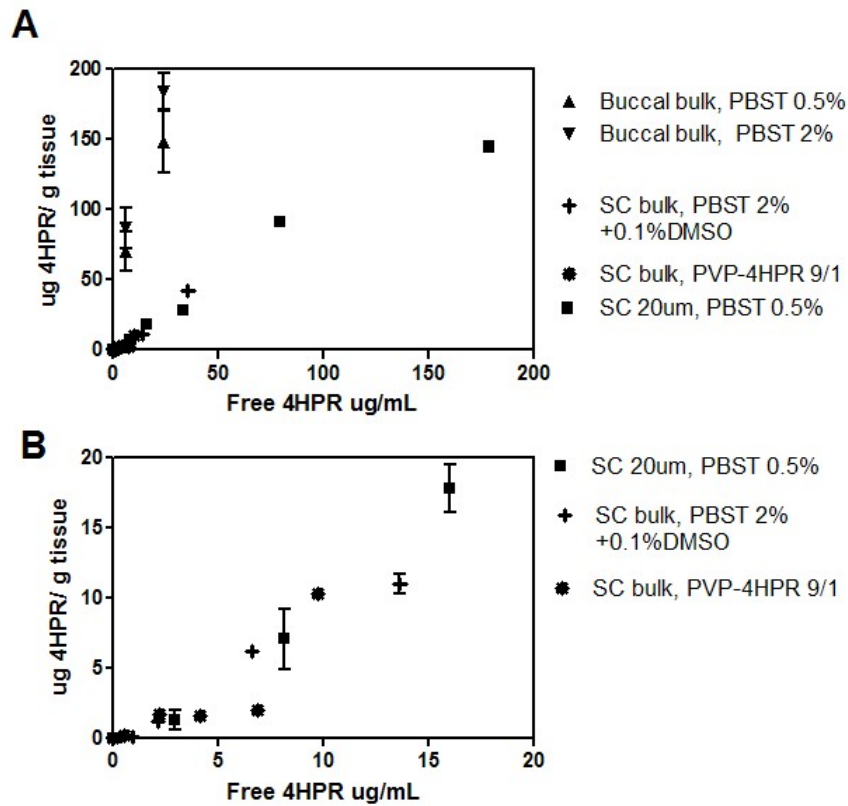
Figure 4-6. 4HPR tissue uptake comparison of buccal vs. s.c. in various media, intact and thinly sectioned tissues; a) all data points, and b) zoomed into lower concentration range.

Table 4-4. 4HPR Kp in buccal and s.c. tissues

Tissue Type	Tissue Preparation	Media	C_u, μM 4HPR	Kp
Buccal epithelia	Intact	PBST 0.5%	22	16.8 ± 2.5
		PBST 1%	29	12.4 ± 0.4
		PBST 2%	33	14.2 ± 1.0
	Homogenate	PBST 0.5%	25	15.2 ± 1.8
s.c.	Intact	PBST 2% + 1% DMSO	2-5	0.35 ± 0.21
			10-100	0.97 ± 0.16
		PVP-4HPR	10-25	0.56 ± 0.30
	Thin sections	PBST 0.5%	0.4-5	0.52 ± 0.07
			10-350	0.96 ± 0.14

- Kp was calculated based on free drug concentration after tissue uptake at equilibrium.

4.6. Discussion

4HPR plasma levels, as opposed to assessment of drug target tissue and plasma interactions, were the pharmacokinetic aspects evaluated in previous 4HPR human clinical trials (19). While local drug delivery has numerous pharmacologic benefits, locally-delivered drugs are hampered by limited tissue penetration distance (10,11,20). In an effort to enhance drug solubility and diffusion and diminish 4HPR's tissue penetration-limiting lipid and plasma-protein binding, this study introduced solubilizers and permeation enhancers. Optimally, these studies would identify a binding 'sweet spot' which would prevent rapid drug clearance yet allow the active unbound drug to exert its pharmacological effects. Several studies have demonstrated 4HPR's chemopreventive efficacy levels range between 2-5 uM, while cell toxicity observed at 10 μM 4HPR (21). These binding experiments were therefore conducted within this chemopreventive therapeutic range.

Tween has Limited Effect on 4HPR Uptake in Buccal Epithelia

Our data revealed that 4HPR buccal epithelial uptake was comparable regardless of incubation media Tween levels (0.5, 1, or 2%). Although homogenization can expose additional binding sites as a result of protein disruption and binding site unmasking, this technique can also create artifacts (22). Nonetheless, similar binding was observed in our buccal epithelia regardless

of tissue state (intact or homogenates). Collectively, these data show buccal epithelia possesses a high 4HPR binding capacity with saturation not yet reached and/or incomplete tissue penetration. The observed high level 4HPR-epithelia binding likely reflects, at least partially, keratinocytes' active role in lipid synthesis (23). Furthermore, previous studies have shown retinoid challenge increased oral keratinocyte lipid production (24).

Solubilizing and Permeation Enhancers do not Significantly Affect 4HPR Uptake in s.c. Tissue

Previously we have shown that 4HPR solubility can be enhanced by addition of 2% Tween, while DMSO augments both solubility and tissue penetration. Formation of a 9/1 (w/w) PVP-4HPR amorphous solid dispersion resulted in a 50-fold 4HPR solubility increase (data not shown). Notably, 4HPR solubility in PBST + 0.5% is comparable to serum, while PBST + 2% resulted in 4HPR solubilization up to 500 μg/ml (25). The high level of Tween (2%) was shown in the buccal binding experiment to have little effect on extent of binding, and was necessary to enhance 4HPR levels in tissue incubation media during attempted tissue binding saturation studies. No significant 4HPR tissue uptake differences were detected in intact s.c. tissue incubation during comparison of a combination of a DMSO penetration enhancer + 2% Tween solubilizing solution relative to the PVP-4HPR amorphous dispersion, nor the s.c. sections incubated in PBST 0.5%. Results show that drug-tissue saturation was not achieved in these solutions at free drug levels near 170 μg/ml 4HPR, and thus the limiting factor in tissue disposition is the ability to solubilize the drug. Tissue sectioning results revealed a uniform penetration depth profile of 360 μm; findings consistent with inter-sample homogeneity.

While a Competitive Ligand Decreases 4HPR Tissue Binding at Low Concentrations, 4HPR Demonstrates a Higher Binding Affinity

Tissue co-incubation studies with the same level of 4HPR and another synthetic retinoid, acitretin, showed 14% reduction in 4HPR binding while also demonstrating a 1.8 fold greater 4HPR binding affinity. 4HPR's higher binding affinity may reflect 4HPR's greater lipophilicity (log P=6.31) relative to acitretin's (logP=5.59), whose negative ionic charge reduces its lipophilicity. Chemical structural differences may also be involved i.e. while acitretin retains the polyene chain, it lacks an amide linkage, a redox active phenol group, and replaces the trimethylcyclohexenyl group. Previous work has shown that 4HPR induces protein conformational changes (6) upon binding, which may positively influence additional 4HPR binding. Results from the thinly sectioned s.c. tissues studies, which failed to show saturation even at high 4HPR levels, support this premise.

4HPR has greater Partitioning in Buccal Epithelia relative to s.c. Tissue

When comparing tissue type, we observe that 4HPR uptake is 15-fold greater in buccal epithelia compared to s.c. tissue, largely due to the extent of keratinization by ceramides acting as a penetration barrier, which are increased in buccal epithelium. Additional factors affecting tissue partitioning (Kp) *in vivo* include: 1) non-specific lipid plasma and tissue binding, 2) binding to proteins or lipoproteins in plasma and tissue interstitial space, 3) contributions of solubility and pH gradient between intra- and extracellular aqueous phases, 4) rapid equilibrium between plasma and tissue (i.e. permeability), 5) uniformity in distribution, 6) no transporter effect, and 7) tissue saturation (17). Further, as only the aqueous phase free drug can bind to tissues and permeate cell membranes, determination of percent plasma binding is essential. Several attempts were made to measure plasma protein binding using spin filtration and dialysis methods, however, unsatisfactory results were due to 4HPR's high affinity for the cellulosic membranes in these devices. The pH gradient of blood (pH=7.4) and tissue (pH=7.0) can also

affect drug partitioning (26). Because 4HPR is a weak acid (pKa=9.75), the ratio of fraction unionized in blood/tissue is 0.997, which renders the ionization contribution negligible. Our data show that the Kp in s.c. tissue is ~0.5 when free 4HPR > 10 μM and ~0.3 when free 4HPR < 10 μM while buccal epithelia exhibit Kp's near 15 for free drug levels > 10 μM. The implications of this stoichiometry are quite significant, as treated tissues would bind high levels of 4HPR with drug solubility as the limiting factor. As efficacious 4HPR chemopreventive levels are ~2-5 μM 4HPR, the extent of solubilization may not be a crucial local drug delivery design element.

4HPR Exhibits High Binding Affinity for Cell-Membrane Lipids

To delineate the contributing factor(s) to the high levels of tissue binding, cell membrane component binding was measured. It is known that retinoids, including 4HPR exhibit extensive plasma protein binding (27). The majority of these interactions are likely non-specific and reflect 4HPR adherance to proteins or phospholipids protruding from cell membranes. Our results show 4HPR binding to cell membrane components is comparable to the extrapolated binding to intact buccal epithelia. These data support the premise that 4HPR binds via phospholipid cell membrane interactions, which is probable given 4HPR's high lipophilicity. Due to the high retention at local tissue site due to non-specific tissue binding (protein and lipids), the markedly reduced amount of drug necessary to deliver, and our previous studies(6) we anticipate negligible blood-plasma 4HPR levels.

4.7. Conclusion

In these experiments, we evaluated 4HPR binding kinetics *in vitro* in tissues, cell membrane components. For tissue uptake studies, both buccal and s.c. tissues were studied, along with effect of solubilizing and penetration enhancing media. The type of 4HPR

solubilizing media and type of tissue preparation (intact, sectioned, homogenized) had little effect on tissue uptake, but rather the ability to solubilize 4HPR levels was the limiting factor in tissue disposition. Buccal tissue was shown to have ~15-fold greater 4HPR uptake than SC connective tissue, possibly due to differences in lipid profiles. We also show that the extent of 4HPR non-specific tissue binding is predominately due to interactions with phospholipids in cell membranes. More importantly, these studies will aide in design and evaluation of local 4HPR delivery systems, which will aim to enhance drug-tissue penetration distance.

4.8. References

1. Berni, R.; Formelli, F., In vitro interaction of fenretinide with plasma retinol-binding protein and its functional consequences. *FEBS Letters* **1992,** *308* (1), 43-45.
2. (a) Uray, I. P.; Dmitrovsky, E.; Brown, P. H., Retinoids and rexinoids in cancer prevention: from laboratory to clinic. *Seminars in oncology* **2016,** *43* (1), 49-64; (b) di Masi, A.; Leboffe, L.; De Marinis, E.; Pagano, F.; Cicconi, L.; Rochette-Egly, C.; Lo-Coco, F.; Ascenzi, P.; Nervi, C., Retinoic acid receptors: from molecular mechanisms to cancer therapy. *Molecular aspects of medicine* **2015,** *41*, 1-115.
3. (a) Garaventa, A.; Luksch, R.; Lo Piccolo, M. S.; Cavadini, E.; Montaldo, P. G.; Pizzitola, M. R.; Boni, L.; Ponzoni, M.; Decensi, A.; De Bernardi, B.; Bellani, F. F.; Formelli, F., Phase I trial and pharmacokinetics of fenretinide in children with neuroblastoma. *Clinical cancer research : an official journal of the American Association for Cancer Research* **2003,** *9* (6), 2032-9; (b) Peng, Y. M.; Dalton, W. S.; Alberts, D. S.; Xu, M. J.; Lim, H.; Meyskens, F. L., Jr., Pharmacokinetics of N-4-hydroxyphenyl-retinamide and the effect of its oral administration on plasma retinol concentrations in cancer patients. *Int J Cancer* **1989,** *43* (1), 22-6; (c) Formelli, F.; Carsana, R.; Costa, A.; Buranelli, F.; Campa, T.; Dossena, G.; Magni, A.; Pizzichetta, M., Plasma Retinol Level Reduction by the Synthetic Retinoid Fenretinide: A One Year Follow-up Study of Breast Cancer Patients. *Cancer research* **1989,** *49* (21), 6149-6152.
4. (a) Radu, R. A.; Han, Y.; Bui, T. V.; Nusinowitz, S.; Bok, D.; Lichter, J.; Widder, K.; Travis, G. H.; Mata, N. L., Reductions in Serum Vitamin A Arrest Accumulation of Toxic Retinal Fluorophores: A Potential Therapy for Treatment of Lipofuscin-Based Retinal Diseases. *Investigative Ophthalmology & Visual Science* **2005,** *46* (12), 4393-4401; (b) Formelli, F.; Clerici, M.; Campa, T.; Di Mauro, M. G.; Magni, A.; Mascotti, G.; Moglia, D.; De Palo, G.; Costa, A.; Veronesi, U., Five-year administration of fenretinide: pharmacokinetics and effects on plasma retinol concentrations. *Journal of clinical oncology : official journal of the American Society of Clinical Oncology* **1993,** *11* (10), 2036-42.
5. Han, B. B.; Li, S.; Tong, M.; Holpuch, A. S.; Spinney, R.; Wang, D.; Border, M. B.; Liu, Z.; Sarode, S.; Pei, P.; Schwendeman, S. P.; Mallery, S. R., Fenretinide Perturbs Focal Adhesion Kinase in Premalignant and Malignant Human Oral Keratinocytes. Fenretinide's Chemopreventive Mechanisms Include ECM Interactions. *Cancer prevention research (Philadelphia, Pa.)* **2015,** *8* (5), 419-30.
6. Mallery, S. R.; Wang, D.; Santiago, B.; Pei, P.; Schwendeman, S. P.; Nieto, K.; Spinney, R.; Tong, M.; Koutras, G.; Han, B.; Holpuch, A.; Lang, J., Benefits of Multifaceted Chemopreventives in the Suppression of the Oral Squamous Cell Carcinoma (OSCC) Tumorigenic Phenotype. *Cancer prevention research (Philadelphia, Pa.)* **2017,** *10* (1), 76-88.
7. van Gelderen, P.; de Vleeschouwer, M. H. M.; DesPres, D.; Pekar, J.; van Zijl, P. C. M.; Moonen, C. T. W., Water diffusion and acute stroke. *Magnetic Resonance in Medicine* **1994,** *31* (2), 154-163.
8. Swanson, B. N.; Zaharevitz, D. W.; Sporn, M. B., Pharmacokinetics of N-(4-hydroxyphenyl)-all-trans-retinamide in rats. *Drug Metabolism and Disposition* **1980,** *8* (3), 168-72.
9. <UNRAVELING THE MECHANISM OF THE lightstruck flavor of beenr.pdf>.
10. (a) Fleming, A. B.; Saltzman, W. M., Pharmacokinetics of the carmustine implant. *Clinical pharmacokinetics* **2002,** *41* (6), 403-19; (b) Strasser, J. F.; Fung, L. K.; Eller, S.; Grossman, S. A.; Saltzman, W. M., Distribution of 1,3-bis(2-chloroethyl)-1-nitrosourea and tracers in the rabbit brain after interstitial delivery by biodegradable polymer implants. *The Journal of pharmacology and experimental therapeutics* **1995,** *275* (3), 1647-55.
11. Haller, M.; Saltzman, W. M., Localized Delivery of Proteins in the Brain: Can Transport Be Customized? *Pharmaceutical Research* **1998,** *15* (3), 377-385.
12. Eida, S.; Van Cauteren, M.; Hotokezaka, Y.; Katayama, I.; Sasaki, M.; Obara, M.; Okuaki, T.; Sumi, M.; Nakamura, T., Corrigendum: Length of intact plasma membrane determines the diffusion properties of cellular water. *Scientific reports* **2016,** *6*, 25681.

13. Sakharov, D. V.; Kalachev, L. V.; Rijken, D. C., Numerical Simulation of Local Pharmacokinetics of a Drug after Intravascular Delivery with an Eluting Stent. *Journal of Drug Targeting* **2002,** *10* (6), 507-513.

14. Shinkar, D. M.; Dhake, A. S.; Setty, C. M., Drug Delivery from the Oral Cavity: A Focus on Mucoadhesive Buccal Drug Delivery Systems. *PDA Journal of Pharmaceutical Science and Technology* **2012,** *66* (5), 466-500.

15. (a) Allen, J. G.; Bloxham, D. P., The pharmacology and pharmacokinetics of the retinoids. *Pharmacology & Therapeutics* **1989,** *40* (1), 1-27; (b) Urien, S.; Claudepierre, P.; Meyer, J.; Brandt, R.; Tillement, J. P., Comparative binding of etretinate and acitretin to plasma proteins and erythrocytes. *Biochemical pharmacology* **1992,** *44* (9), 1891-3.

16. Roth, B. L., National Institute of Mental Health Psychoactive Drug Screening Program (NIMH PDSP). In *Assay Protocol Book, Version II* [Online] University of North Carolina at Chapel Hill, Department of Pharmacology, 2013.

17. Poulin, P., Drug Distribution to Human Tissues: Prediction and Examination of the Basic Assumption in In Vivo Pharmacokinetics-Pharmacodynamics (PK/PD) Research. *Journal of Pharmaceutical Sciences* **2015,** *104* (6), 2110-2118.

18. Vratilova, J.; Frgala, T.; Maurer, B. J.; Patrick Reynolds, C., Liquid chromatography method for quantifying N-(4-hydroxyphenyl)retinamide and N-(4-methoxyphenyl)retinamide in tissues. *Journal of Chromatography B* **2004,** *808* (2), 125-130.

19. Holpuch, A.; Desai, K.-G.; Schwendeman, S.; Mallery, S., *Optimizing therapeutic efficacy of chemopreventive agents: A critical review of delivery strategies in oral cancer chemoprevention clinical trials*. 2011; Vol. 10, p 23-23.

20. (a) Fung, L. K.; Ewend, M. G.; Sills, A.; Sipos, E. P.; Thompson, R.; Watts, M.; Michael Colvin, O.; Brem, H.; Saltzman, W. M., Pharmacokinetics of Interstitial Delivery of Carmustine, 4-Hydroperoxycyclophosphamide, and Paclitaxel from a Biodegradable Polymer Implant in the Monkey Brain. *Cancer research* **1998,** *58* (4), 672-684; (b) Dedrick, R. L.; Flessner, M. F., Pharmacokinetic Problems in Peritoneal Drug Administration: Tissue Penetration and Surface Exposure. *Journal of the National Cancer Institute* **1997,** *89* (7), 480-487.

21. Holpuch, A. S.; Hummel, G. J.; Tong, M.; Seghi, G. A.; Pei, P.; Ma, P.; Mumper, R. J.; Mallery, S. R., Nanoparticles for local drug delivery to the oral mucosa: proof of principle studies. *Pharm Res* **2010,** *27* (7), 1224-36.

22. Pacifici, G. M.; Viani, A., Methods of determining plasma and tissue binding of drugs. Pharmacokinetic consequences. *Clinical pharmacokinetics* **1992,** *23* (6), 449-68.

23. Khnykin, D.; Miner, J. H.; Jahnsen, F., Role of fatty acid transporters in epidermis: Implications for health and disease. *Dermato-endocrinology* **2011,** *3* (2), 53-61.

24. Schuster, G. S.; Erbland, J. F.; Wyrick, S. D.; Singh, B. B., Oral epithelial cell lipid synthesis in the presence of retinoic acid or nitrosonornicotine. *Journal of oral pathology* **1986,** *15* (8), 430-3.

25. Desai, K. G.; Mallery, S. R.; Holpuch, A. S.; Schwendeman, S. P., Development and in vitro-in vivo evaluation of fenretinide-loaded oral mucoadhesive patches for site-specific chemoprevention of oral cancer. *Pharm Res* **2011,** *28* (10), 2599-609.

26. Berry, L. M.; Roberts, J.; Be, X.; Zhao, Z.; Lin, M.-H. J., Prediction of Vss from In Vitro Tissue-Binding Studies. *Drug Metabolism and Disposition* **2010,** *38* (1), 115-121.

27. Kokate, A.; Li, X.; Jasti, B., Transport of a novel anti-cancer agent, fenretinide across Caco-2 monolayers. *Invest New Drugs* **2007,** *25* (3), 197-203.

CHAPTER 5: Controlled release local fenretinide delivery systems enhance buccal drug distribution

5.1. Abstract

The work presented herein is the first time, to our knowledge that the 4HPR's tissue distribution has been analyzed. We have chosen to deliver 4HPR locally from long-acting release polymeric implants, and the release kinetics along with the drug-tissue distribution were evaluated. Three different millicylindrical implant formulations were evaluated including a water-soluble matrix implant that provided continuous release based on the dissolution of the hydrophobic drug entity, PLGA implants capable of providing very long-acting continuous release (1-2 months) and PLGA implants loaded with a solubilized, amorphous drug (polyvinylpyrrolidone [PVP] -4HPR). These implants were injected into rabbit buccal epithelia, and release and drug diffusion monitored after 1 and 14 days. Quantitative Raman spectroscopic imaging was utilized to measure drug-tissue concentration gradients in excised tissue sections. Our results showed that the implants released much faster in the mouth compared to our previous studies in s.c. tissue, and that the drug distribution in the buccal tissues was on the order of 0.5- 8 mm for all formulations. The solubilized drug diffused the furthest through the tissue, and this movement was the greatest through the same tissue plane, versus traveling through tissue planes toward mucosa or deep epithelium. This data will be useful for development of long-acting chemopreventive therapies for oral cancer.

Long-Acting Release Fenretinide Implants

PVA/sucrose (solid depot)

PLGA +MgCO$_3$ (very slow release)

PLGA +PVP-4HPR-TEAC (amorphous, solubilized drug)

0.8 mm

1 cm

Superficial layer
Intermediate layer
Basal layer
Lamina propria
Submucosa
Muscle

Implant Cross Section

Diffusion distance and concentration gradient measured by Raman Imaging

Fenretinide concentration (ug/g tissue)

Diffusion Distance

5.2. Introduction

Fenretinide (4HPR) has demonstrated significant chemopreventive promise, however the inability to effectively deliver it has been its mainstay dilemma. Limited efficacy in clinical trials with oral dosing was observed in part due to dose limiting toxicity. Unfortunately, researchers in the study did not identify the drug's disposition at the site of action. To overcome this limited efficacy with oral dosing route, local drug delivery route can be employed, which is capable of delivering a large amount of drug at target site while alleviating the undesirable side effects associated with oral dosing. However, the inability to achieve widespread drug-tissue distribution is the most prevalent challenge to overcome during local drug delivery [1, 2]. Not surprisingly, there are many factors that govern drug distribution in tissues including: rates of diffusion, convection, elimination, protein binding, cellular uptake, capillary permeation, degradation and permeability into cell and subcellular components (which may lead to bioaccumulation), and finally intracellular metabolism and efflux [3]. To maximize tissue

137

distribution, often penetration enhancers are added to the formulation such as solubilizing agents, bile salts, chelators, anionic or cationic polymers[4].

As part of our previous efforts in developing local long-acting chemoprevention strategies for oral cancer, we have designed millicylindrical implants loaded with fenretinide (4HPR), a drug shown to have chemopreventive properties [5-8]. Local delivery of hydrophobic 4HPR presents a significant challenge owing to its extreme water insolubility, with a logP of 6.31. Previous studies in our lab evaluated 4HPR plasma levels after subcutaneous (s.c.) injections from a controlled release poly (lactic-co-glycolic acid) (PLGA) vehicle, and found that after 2 weeks it was unclear whether the actual drug was exhibiting controlled release properties due to dissolution into surrounding interstitial fluid, or slow release from tissue lipid "reservoirs" where 4HPR could have accumulated after fast dissolution [10]. We have also shown that 4HPR has a high propensity for non-specific tissue binding, and that the ability to solubilize the drug was the limiting factor in tissue uptake, likely due to affinity for phospholipids and secondarily from protein interactions. We have shown that 4HPR can be released slowly over 6 weeks from water soluble matrix (poly-vinyl alcohol [PVA]/sucrose) millicylindrical implants *in vivo* in s.c. tissue, while the PLGA implants containing pore forming agents provide very long release profiles of > 2 mo. We have also found that 1000-fold 4HPR solubility enhancement by preparing PVP-4HPR (9/1 w/w) amorphous dispersion implants, which was sustainable for more than 1 week in water. These formulations were chosen to evaluate *in vivo* for their potential to improve 4HPR tissue penetration distance. For clinical translation of oral cancer chemoprevention, rabbit buccal epithelia was chosen to evaluate these implants, due to similarity in tissue permeability, thickness and degree of keratinization or oral epithelia to humans.

Several approaches can be taken to quantitate drug-tissue distribution depending upon the molecule's properties or duration of drug exposure. A fluorescent molecule can be easily imaged, however, conjugating a fluorescent moiety onto a drug can alter its tissue diffusion properties. One could also radio-label the drug and use PET imaging, however it is not suitable for long-term studies due to stability of the radio-isotope. For molecules not fitting these criteria, the gold standard for drug-distribution studies is tissue sectioning, which could mean hundreds of tissue sections per distributive analysis, followed by drug extraction from tissues, HPLC analysis, and data processing. Because this approach is quite laborious, and handling of large volumes of samples has the potential to introduce errors, we sought a different approach to measure drug distribution.

Herein, we propose novel analytical methodology for quantitative Raman imaging techniques to characterize 4HPR distribution in buccal tissue. Since Raman micro-spectroscopy can be used to analyze almost any organic compound and requires no artificial chemical labels, our methodology could feasibly be utilized to characterize the natural distribution patterns for a multitude of colorless small molecules in a variety of tissue types. The data presented in this paper discusses the interplay of controlled release local drug delivery of 4HPR, and how correlates the level of drug solubilizes, rate of release, physiology of local tissue environment on the extent of drug diffusion or dispersion into the tissue surrounding the implant. This is the first time that 4HPR's tissue penetration has been evaluated, and will be useful for development of successful oral cancer chemopreventive delivery systems, in particular long-acting 4HPR-PLGA millicylinder implants.

5.3. Materials and Methods

5.3.1. Materials

4HPR was generously supplied by Merck Co. Excipients and polymers used for millicylinders formulations included: PLGA (50:50, 24-38kDa, acid end-capped, Evonik), polyvinyl alcohol, (PVA, 9-10 kDa, 80% hydrolyzed, Sigma Aldrich), D-sucrose (Sigma-Aldrich), polyvinylpyrrolidone (PVP K30, 40 kDa, BASF), triethyl-acetyl-citrate (TEAC), and magnesium carbonate ($MgCO_3$). Silicon tubing (0.8 mm i.d., BioRad Laboratories) was used for implant extrusion. All other materials were reagent grade or better including ethanol (EtOH), and Tween 80. Solvents for UPLC/UV analysis were HPLC grade including acetonitrile (ACN), double distilled water (ddH_2O), and phosphoric acid (H_3PO_4). Tissues were sectioned using optimum cutting temperature compound (OCT, Tissue Tek), and adhered to poly-lysine coated glass slides prior to incubation. Phosphate buffer saline (PBS) was used for tissue incubation media. Oil-red-O and Harris hematoxylin stains were utilized in tissue histological examinations.

5.3.2. 4HPR Tissue Calibration Standards for Raman Imaging

Rabbit buccal epithelia was excised from female New Zealand Rabbits and frozen on dry ice. The tissue was cryosectioned (Leica 3050S crysotat) 20 μm in z-plane direction so that each section contained all layers of epithelia (mucosa, lamina propia, and epithelium), and was thaw mounted on poly-lysine coated glass slides. A representative tissue mass was recorded by averaging 3 tissue section masses collected intermittently throughout the relatively homogeneous tissue block. The tissues sections were pre-treated by incubating in PBS + 0.5% Tween for 30 min, then incubated in 4HPR/PBST 0.5% calibration solutions (n=4) ranging from 1-500 μg/mL for 4 h, followed by tissue wash PBS and ddH_2O. At each concentration level, 3 tissues were extracted and assayed for 4HPR uptake by UPLC, and 1 was reserved for Raman imaging analysis, such that Raman imaging calibration curve could be constructed from UPLC 4HPR-

tissue uptake results. Additionally, 4HPR tissue partitioning coefficient (Kp) was calculated

from the concentration of free drug in incubation media (C_{free}) and the tissue uptake (C_{tissue}).

$$Kp = \frac{C_{tiss}}{C_{free}}$$

5.3.3. Raman measurements

All Raman images were acquired by a WiTec alpha300R confocal Raman microscope

equipped with the 532nm solid-state sapphire excitation laser (tuned to ~35mW intensity) and a

10x air objective (Zeiss Epiplan-NEOFLUAR, NA (numerical aperature) = 0.25) coupled to a

CCD detector via a multi-mode fiber of 100μm diameter, serving as the confocal pinhole.

Calibration standard spectra were acquired by raster scanning over three separate 2000 x 200

micron regions of each drug-incubated buccal tissue; relatively high spatial resolution was

attained with a step-size of 20 microns and pre-bleaching of biological autofluorescence was

accomplished by programming laser focus to pause for 0.5 seconds at each point before

acquiring spectra over integration time of 0.5 seconds. In order to achieve reasonable acquisition

times over the test sample regions of interest, large area raster scans were performed with a step-

size of 50 microns, pausing for 0.4 seconds at each point before acquiring spectra over

integration time of 0.2 seconds. Depending on the spatial dimensions of tissue region scanned,

total acquisition times ranged from six to fourteen hours per test sample.

5.3.4. Raman data processing

Using WiTec Project FOUR Software, all Raman spectra were first cleared of cosmic

rays (filter size: 4, dynamic factor: 2) and noise was reduced via a moving average smoothing

matrix; baseline subtraction was performed by fitting a 9th order polynomial to spectral data

points in the following wavenumber ranges: 205-515, 840-900, 1345-1405, 1495-1530, 1770-

2690, and 3120-3750. To generate Raman images, data was exported to MATLAB and an in-house algorithm was developed to ultimately identify and integrate 4HPR's characteristic Raman peak at 1582 cm^{-1} at every pixel of the scanned tissue section. The glass background was first subtracted and a decision tree was employed to distinguish and remove spectral contributions from the naturally occurring biomolecule heme (which yields a strong interfering Raman signal at ~1588 cm^{-1}) from that of 4HPR. A signal-to-noise ratio of ≥ 3 was installed as the detection limit for a peak. Spectra were normalized to account for variation in tissue thickness, the 4HPR Raman peak at 1582cm^{-1} was integrated, and the drug/tissue mass ratio was calculated from the calibration curve. To optimize and verify algorithm parameters, test samples were generated and analyzed as per acquisition methodology, processed through the algorithm, and used to determine the rates of false positive and false negative 4HPR detection in different biochemical tissue environments. For all final *in vivo* 4HPR dosed tissue Raman images, algorithm result outputs were manually compared with unprocessed spectral images and regions where sample burning occurred were cropped out so as not to artificially influence drug distribution analysis.

5.3.5. 4HPR Millicylinder Formulations

Three 4HPR millicylinder formulations were evaluated for drug-tissue penetration enhancement including:

1. PVA/Sucrose +10% 4HPR (crystalline drug in a water-soluble matrix)
2. PLGA+ PVP/4HPR/TEAC (controlled release of an amorphous solid dispersion)
3. PLGA+ 10% 4HPR +3% $MgCO_3$ (porous, very-long acting release)

Millicylinder preparation processes have been described in detail in Chapter 2. Briefly, PVA/ D-sucrose (40%, 30% w/v respectively in ddH$_2$0) millicylinders were loaded with 10% 4HPR, extruded into silicone rubber tubing, dried in vacuum oven at room temperature for 2

days, then at 40 °C for 2 days, and cut from tubing into 1 cm lengths with an inner diameter of 0.8 mm. PLGA+ PVP-4HPR-TEAC implants were prepared as described previously in Chapter 3 by first preparing the amorphous solid dispersion of PVP-4HPR-TEAC (9/1/1 mass ratio) by dissolving in MeOH, pouring into a thin film, drying, then cryomilling particles (Retsch swing mill cryomill, PN 20.749.001) and sieving particles <90 μm. These particles were then loaded into PLGA (dissolved in acetone) at a ratio of 50/50 (PLGA to PVP-4HPR-TEAC particles), mixed, then extruded, dried and cut to size as described above. The third formulation, PLGA+ 10% 4HPR+3% $MgCO_3$ was prepared as previously described in Chapter 2. 4HPR loading levels were verified using the millicylinder extraction assays as described in following sections.

5.3.6. Implantation of 4HPR Millicylinders in Rabbit Buccal Epithelium

4HPR millicylinders were evaluated in rabbit buccal epithelia for their ability to enhance drug-tissue distribution and also their release rate. Female New Zealand rabbits 3 months of age were purchased from Charles River Laboratories. All experiments were conducted in accordance to University of Michigan's Institutional Animal Care and Use Committee. Prior to implantation, rabbits were anesthetized with 5% isoflurane inhalation via calibrated vaporizer, and pre-weighed implants were inserted into the buccal region via an 18G trocar. Each rabbit received 2 implants (1 per cheek), with 1 cheek utilized for Raman imaging analysis for drug distribution, and the other for determining the amount of drug released (n=3 per formulation per time point). Serum samples were collected prior to implantation and at the endpoints. On endpoint days 1 and 14 and rabbits were isoflurane anesthetized and then euthanized via intravenous injection of saturated potassium chloride solution. The buccal tissues were harvested and kept on dry ice until tissue sectioning. For the tissue distribution analysis, a ~15 mm length of buccal tissue containing a cross-section of the millicylinder was frozen onto a

cutting chuck with OCT, and a 20 μm section near the middle of the implant was placed on glass slide, and imaged via Raman spectroscopy. For drug release from the implants, the implants were carefully removed, and drug was extracted via the loading assay. The release data from the implants in rabbit buccal was compared to those administered in rats s.c. as described in Chapter 2.

5.3.7. Drug- Tissue Penetration by Raman Imaging

To prepare these 4HPR-tissue penetration curves, a 1 mm wide region containing the center of the implant was selected in both the y-plane (i.e. same tissue layer) and the z-plane (through different tissue layers). The z-layer penetration was expressed as the movement towards the epithelium and also towards the mucosa. The penetration distance was reported at the location where drug concentration decreased to 10% of its initial value (C_{10}).

5.3.8. 4HPR Millicylinder Loading and Release Digestion Assay

4HPR loading and release was determined via implant digestion assay. For the PLGA implants, one millicylinder was weighed, and PLGA and 4HPR were co-dissolved by addition of 0.5 mL THF, followed by precipitation of PLGA with addition of 9.5 mL EtOH. The samples were centrifuged, and supernatant was assayed by UPLC/UV. For the PVA/sucrose implants, the implant was dissolved in 10 mL of EtOH.

5.3.9 4HPR Serum Levels

4HPR sera levels were determined in rabbits. A 100 uL aliquot of serum was spiked with internal standard (5 μL of 0.5 mg/mL acitretin), extracted with 300 uL ACN by sonication on ice for 10 min, clarified by centrifuging at 12,000 rcf for 10 min, and the amount of 4HPR in supernatant was determined by UPLC assay, and extraction recovery normalized by the internal standard.

5.3.10 4HPR UPLV-UV Assay

4HPR levels in millicylinder digests, serum were measured by UPLC/UV. The reverse phase UPLC/UV analysis was carried out with a Waters Acquity UPLC system and Empower software under the following conditions: Acquity BEH C18 2.1x100 mm column, mobile phase 80:20 ACN: ddH$_2$0 + 0.1% phosphoric acid (H$_3$PO$_4$), isocratic flow rate of 0.65 mL/min, UV detection at 365 nm, and total analysis time of 2 min. 4HPR LLOQ is 0.05 µg/mL.

5.4. Results and Discussions

5.4.1   Raman 4HPR Tissue Calibration Standards

The first step in developing our quantitative Raman imaging method was to prepare a calibration curve with buccal tissue sections incubated in 4HPR dissolved in PBST 0.5% solutions (4 h previously determined to be the equilibrium binding time). As shown in Figure 1a, there was a linear increase in 4HPR tissue uptake as the concentration of 4HPR in incubation media increases, with correlation coefficient of r^2= 0.997. We calculated 4HPR partition coefficient from the PBST 0.5% media into buccal epithelium sections, and found consistent partitioning (Kp) that ranged from 1.9-2.2 over a wide concentration range of 3-91 ug/mL free 4HPR in media (Fig. 5-1b).

Calibration sections were analyzed as per acquisition methodology and 3000 Raman spectra were collected across all regions of each tissue section and individually processed using algorithm to determine the integrated intensity of the 4HPR peak at 1582 cm^{-1}. The average spectra for each calibration standard are reported in Figure 1c and the average (+/- SE) integrated intensity yielded a linear relationship with the actual drug/tissue mass ratio as determined by HPLC (r^2=0.985). The linear range was determined to cover 6.5 – 200.7 ug 4HPR/g tissue, and

tissue regions exceeding this range were considered to be saturated and colored white in the resulting Raman concentration images.

5.4.2   Raman Hyperspectral Image Processing Algorithm

To analyze 4HPR distribution throughout a single buccal tissue sample, at least 30,000 Raman spectra were required. Acquired in a raster pattern across the tissue section under investigation, each spectrum must be individually processed and interpreted to extract relevant chemical information, thus creating a necessity for automated algorithms that perform processing functions in a time-efficient manner. Developed in-house, our MALTAB algorithm wascapable of processing tens-of-thousands of spectra per minute with outstanding reliability. One major advantage of Raman is the non-destructive nature of the analyses; tissue sections undergo minimal preparation ensuring the natural distribution patterns of 4HPR are unadulterated and enabling quantitative characterization as such. Tissue sections are typically prepared on glass slides and, as was in our case, contained residual blood. The oxygen-carrying heme protein in blood gives rise to an enhanced resonance Raman signal at $1588cm^{-1}$ that partially overlaps the characteristic peak of 4HPR, making algorithmic distinction between the two difficult. Exploiting heme's unique Raman peak at $750cm^{-1}$, a decision tree was employed to identify spectral contributions from heme and using a scaled reference spectra obtained from pure blood, subtract the interference, leaving only spectral contributions from 4HPR and other tissue components to be quantified. No other chemical components present in our system, including millicylinder excipients, interfered with the 4HPR Raman peak at $1582cm^{-1}$ (see supplemental figure S1). To confirm the validity of algorithm functionality, Raman test datasets were acquired from dispersions of pure biochemical components or unadulterated buccal tissue on glass slides.

Since the intended Raman results for the test samples were known, they were used to experimentally determine the reliability of the algorithm.
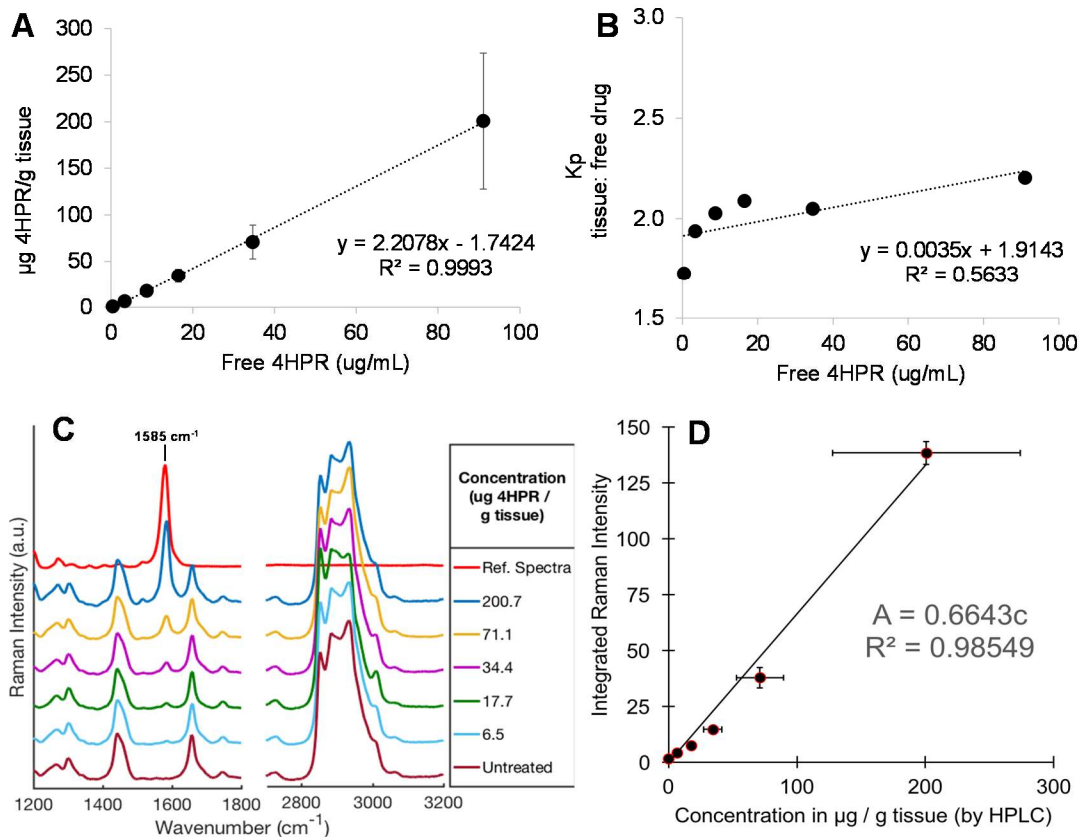
Figure 5-1. Excised buccal tissues (sectioned 20 μm thick) incubated in known concentrations of 4HPR (in PBST 0.5%) were assayed via HPLC, and served as calibration standards for quantitative interpretation of Raman spectra. A) 4HPR tissue uptake as a function of incubation media concentration b) 4HPR partitioning (Kp) from aqueous media to tissue, c) 4HPR Raman spectra showing limit of detection at 6.5 ug 4HPR/g tissue, and d) Raman 4HPR-tissue calibration curve shows Raman signal intensity as a function of tissue concentration by HPLC. (n=3, mean ± SE).

5.4.1 Evaluation of 4HPR Release and Distribution from Millicylinder Implants

Effect of Tissue Type on Release rates (Buccal vs. s.c.)

The three millicylinder formulations prepared with different polymer systems and drug-solubility enhancement were evaluated *in vivo* for their release rate as well as their drug-tissue distribution after 1 and 14 days. The effects of implantation sites on drug release rate was evaluated by comparing release into buccal epithelia vs s.c, which was previously evaluated in

our rat *in vivo* studies in Chapters 2 and 3. The immediately dissolving, water soluble matrix PVA/sucrose implant served as a benchmark for the dissolution controlled release of a hydrophobic solid drug depot. The PLGA + 10% 4HPR + 3%MgCO$_3$ formulation was shown to have very long-acting release in s.c. tissues (> 2 months release). The PLGA+ PVP-4HPR-TEAC formulation provided superior solubility enhancement due to formation of amorphous solid dispersion between PVP, 4HPR and TEAC, and served to test the premise that the ability to solubilize the hydrophobic drug is the limiting factor in tissue penetration.

The results for drug release from these implants are shown in Figure 5-2, and actual 4HPR implant loading is noted in the figure. All of the implants released faster in buccal compared to s.c., likely due to greater blood flow in the mouth compared to skin. In the PVA/sucrose formulation, the day 1 burst in buccal was almost double of the s.c. release. The PLGA-PVP-TEAC amorphous drug system also had a high burst release on day 1 in buccal (62%), while in s.c only 26% released, yet after 2 weeks, both released similar levels (69% and 77% respectively).   This fast release is likely due to only 50% PLGA in the initial implant composition. The very long-acting release PLGA formulation with pore-forming agent MgCO$_3$, released 4HPR twice as fast in buccal (29% vs 15%) after 14 days, and therefore was most capable of these formulations of providing long duration of release in the mouth, due PLGA's well characterized slow release properties.

100%
80%
60%
40%
20%
0%

% 4HPR Release

■ Day 1 Buccal
■ Day 14 Buccal
■ Day 1 s.c.
■ Day 14 s.c.

Sucrose/PVA+ 10% 4HPR   PLGA +PVP-4HPR-TEAC (10%)   PLGA+10% 4HPR+3% MgCO3

4HPR Actual Loading: *12.0 ± 0.5%*   *8.4 ± 0.1%*   *9.8 ± 0.1%*
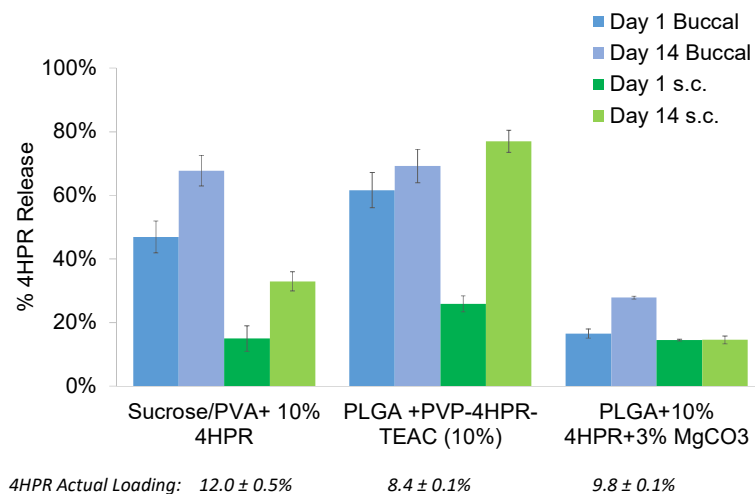
Figure 5-2 4HPR in vivo release from three millicylinder formulations after 1 and 14 days in rabbit buccal epithelia compared to rat s.c. tissue types (mean ± SE, n=3). The PVA/sucrose implant is an immediately dissolving, water soluble matrix, the PLGA+PVP-4HPR-TEAC implant provides controlled release of a solubilized form of 4HPR, while the PLGA+ 3% MgCO$_3$ provided very long-acting drug release.

4HPR Tissue Distribution

The drug-tissue concentration gradients were generated based on the Raman imaging methods and calibration curve shown in Figure 5-1. In Figure 5-3, a representative Raman image is shown for 4HPR dispersion in buccal epithelia after 14 days of release from the PLGA-PVP-4HPR-TEAC implant. The preparation of the tissue-penetration curves is clearly marked around the implant hot spot, and shows selected regions of z-plane diffusion, (through different tissue layers), and y-plane diffusion (along same tissue layer). For example, the y-diffusion distance (Fig. 5-4b), is measured at the edge of the saturation zone (200 µg 4HPR/g tissue at 6000 µm) to the C_{10} (20 µg 4HPR/g tissue at 200 um), and therefore equals 5.8 mm. A complete data set for all formulations, replicates, and time points including Raman images and tissue-

penetration curves, can be referenced in Supplemental Information Figure S5-3.
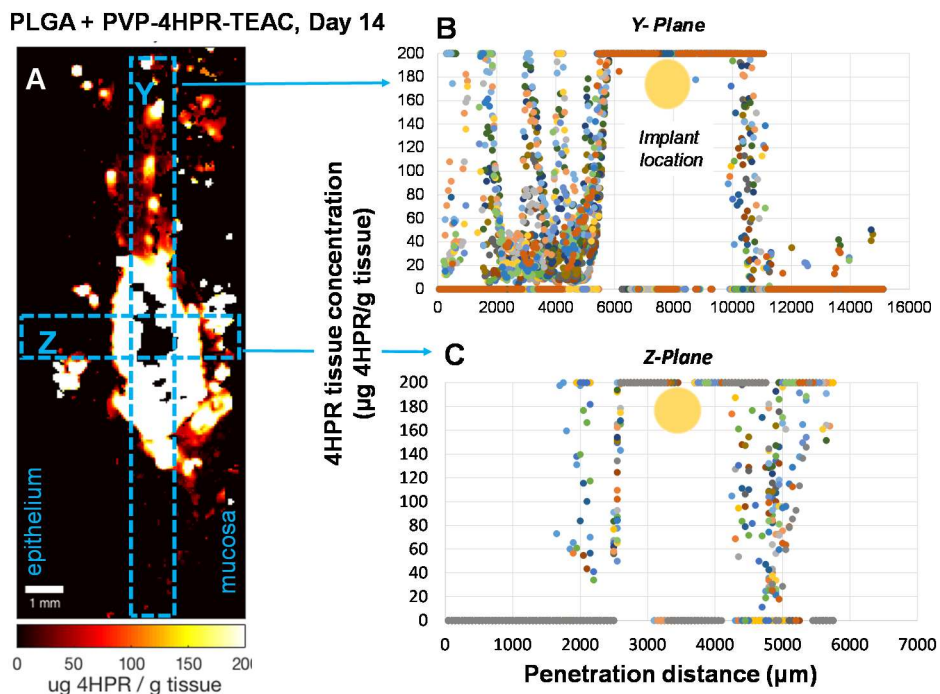
Figure 5-3 4HPR distribution in buccal epithelia after release from millicylinder implants. A) Representative Raman image of tissue dosed with PLGA+ PVP-4HPR-TEAC implants after 14 days detailing the process for generating drug-tissue penetration curves in both the b) y-plane (same tissue layer) and c) z-plane (towards epithelium or mucosa). Each data point represents a 50x50 μm pixel from the corresponding boxed region in (a), and the location of millicylinder is noted on plots with a yellow circle. Full data set for each sample replicate and times points can be referenced in Supplemental Information Fig. S3.

4HPR's tissue penetration from these implants is portrayed by distance by which 4HPR's

concentration decreased to 10% of initial (C_{10}). These distances were extracted from Raman

images in Supplemental Figures S5-3, and is shown in Figure 5-4 for both the z-plane

penetration towards the mucosa and towards the epithelium in addition to the y-plane

penetration. Most notably, the y-plane penetration along same tissue plane is much greater than

penetration through different tissue layers. Statistical analysis was performed within groups,

different directions within groups day 1 to day 14, and among the groups, different

directions. We used a nonparametric test due to the small n numbers, specifically the Kruskal

Wallis Analysis of Variance followed by a Dunn's Multiple Comparison post hoc test. It is

difficult to disseminate if there was preferential movements towards the epithelia or mucosa, as no trends could be determined with this sample size (n=3). All formulations and time points had an average z-plane diffusion distance of 0.3 to 2.0 mm. Pre-cancerous cells will proliferate from the basal cell membrane, a region close to the where the implants were dosed, and therefore these implantation depths and drug diffusion distances in z-plane should be satisfactory for oral cancer chemoprevention.

A better indication of the formulation's drug penetration enhancing performance, can be observed along the y-plane. The PVA/sucrose implants had an average penetration of 1.7 ± 0.6 mm after day 1, while that value decreased to 1.1 ± 0.6 mm after 14 days. This could be attributed to clearance of the drug from the active site where after 1 day they released 47% 4HPR, and 68% after 14 days. Perhaps the large burst release of crystalline drug was itself a barrier to drug movement. Next, we see that the very slow releasing PLGA+ $MgCO_3$ formulation enabled greater drug penetration than the solid depot, whereby 4HPR moved on average 1.7 ± 0.6 mm and 2.8 ± 1.0 mm from implant after 1 and 14 days respectively. Finally, the PLGA + amorphous, solubilized drug (PVP-4HPR-TEAC), had far surpassed the other formulations in tissue penetration enhancement, such that 4HPR penetrated on average of 2.6 ± 1.0 mm and 5.8 ± 1.7 mm after 1 and 14 days respectively. As hypothesized, the ability to deliver a solubilized form of the drug into the aqueous tissue environment was the limiting factor in the ability to achieve widespread tissue distribution. As the oral cavity is a curved surface with interruption of the mucosa surface by the rabbit's lip pomenture, some of the diffusion variability could be attributed to differences in implantation angles or depths, and therefore cross-sections may have captured slightly different diffusion planes. For all formulations, there was no detectable 4HPR in serum, which is a favorable aspect with local delivery systems, such that the

undesired side effects associated with systemic drug delivery could be alleviated with these
implants.
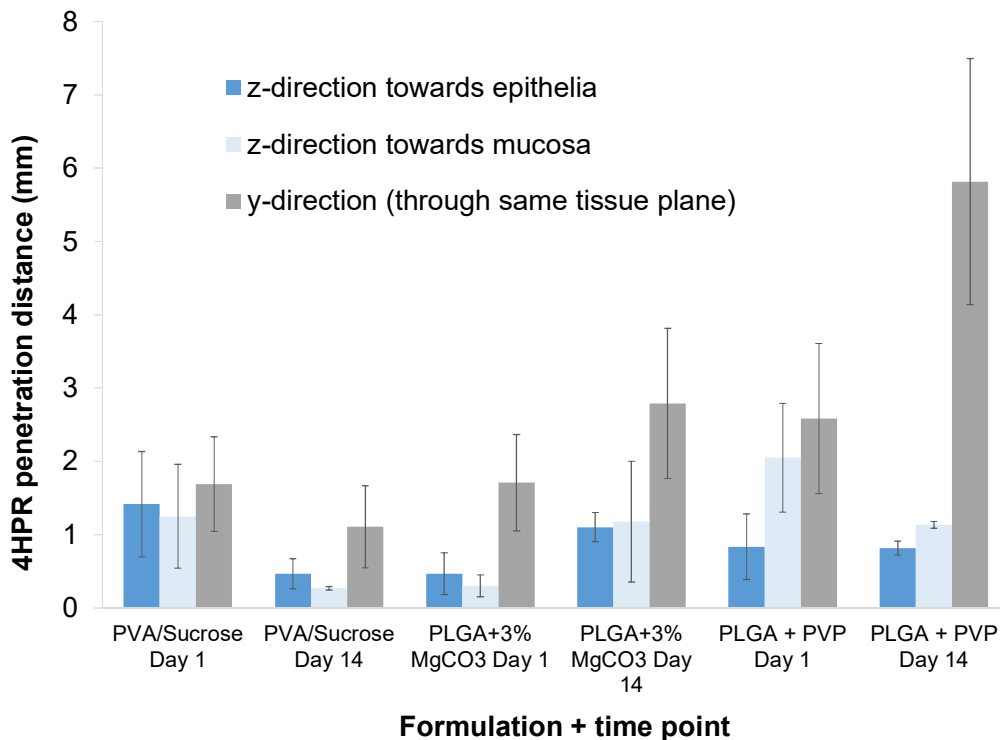
Figure 5-4 4HPR penetration distances in buccal epithelia from millicylinder formulations after day 1 and 14
determined by concentration gradients in tissue sections measured by semi-quantitative Raman spectroscopy.
Penetration distance represents distance by which drug concentration decreased to 10% of starting value, which was
20 μg 4HPR/g tissue, given that Raman signal intensity was saturated at perimeter of implant, giving initial
concentration at edge of implant of 200 μg 4HPR/g tissue. (Mean ± SE, n=3).

Effect of Tissue Environment (Tissue layer, lipid profiles) on 4HPR dispersion

Our results shown in Figure 5-4 are evidence that successful formulations can enhance
4HPR tissue distribution by solubilization of the drug. However, other physiological factors may
be either enhancing distribution or acting as a diffusion barrier, such as local blood flow, degree
of keratinization of tissue, and local protein/lipid levels to name a few. To further examine this, a
histological examination of the tissue environment surrounding the implant was performed

which included staining with oil-red-o for lipids + Harrison hematoxylin stain, and evaluation of

tissue bio-composition by Raman mapping of proteins and lipids in epithelium, submucosa, and

mucosa. In Figure 5-5a, we see that the red lipid-specific stain has the greatest uptake in the

submucosa region, ie, the implantation site. An attempt was made to correlate the amount of

lipid and y-plane diffusion distance (along same tissue layer), for each of the 3 formulations

(time points were combined). As shown in Figure 5-5b, the level of lipids does not appear to

affect the diffusion distance for the PVA/sucrose and PLGA+MgCO$_3$ formulations, however we

see a positive effect of diffusion distance increase as local lipid levels increase for the solubilized

PLGA+PVP formulation. In Figure 5-5c, we see that Raman mapping shows the highest levels

of protein and lipid in the sub-mucosa region, ie, implantation region, and is consistent with the

oil-red-o staining (Fig. 5-5a). Further tissue pathological investigations may prove insightful for

enhancing drug penetration distance for local delivery systems.
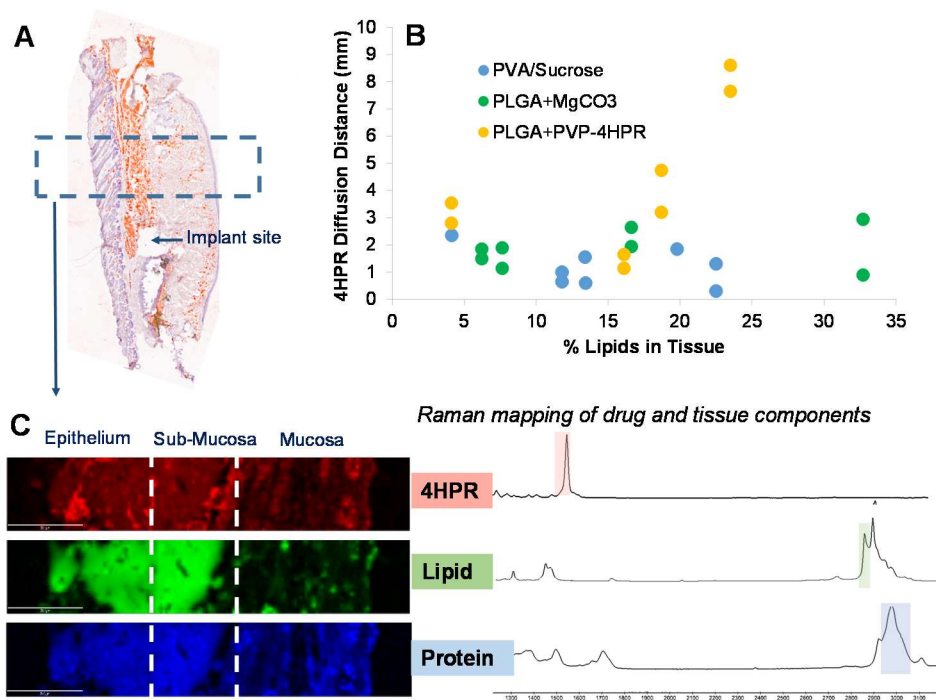
Figure 5-5 Correlation of tissue composition with 4HPR penetration distance in buccal tissue. A) Representative oil-red-o stained tissue (specific for lipids), b) 4HPR diffusion distance as a function of lipid level for each formulation, and c) Raman mapping of 4HPR, lipid, and protein in a tissue section incubated in 4HPR/PBST solution, and co-localization of the biocomponents in the different tissue sections (epithelium, submucosa, mucosa).

5.5. Conclusion

Here, we have published for the first time, the tissue penetration behavior of 4HPR after local delivery in buccal epithelia from long-acting release implants. We have developed quantitative Raman imaging and spectral processing methods to obtain high resolution of drug distribution in tissue sections. We have shown that 4HPR diffusion distance can be enhanced 4-fold by delivering an amorphous form of 4HPR from PLGA implants, compared to the solid dispersion control prepared in a PVA/sucrose matrix. Therefore the ability to solubilize this hydrophobic drug is likely a limiting factor in its tissue distribution. Furthermore, we have shown that the tissue type, ie buccal vs. s.c has a significant impact on the rate of drug release from these implants, such that nearly 2-fold increase in amount of drug released occurred in the buccal epithelia, likely due to greater blood flow. There are other physiological factors that may contribute to the 4HPR diffusion, including lipid and protein level, or depth of implantation, and deserve further examination for future evaluation of the drug system's performance. We have shown that these implants are capable of delivering 4HPR to the basal cell membrane tissue regions to target the pre-cancerous cells that may arise, and may be a beneficial strategy for secondary oral cancer chemoprevention.

5.6. Supplemental Information

A. The following figures support the quantitative Raman imaging method development and validation.

B. Additional figures show all of the raw Raman imaging data from the each formulation and time point, along with the corresponding concentration-diffusion gradient curves.

Preparation of pure component algorithm test samples

To assess automated algorithm reliability and probability of false negative and positive interpretations, the most abundant chemical components in the system were identified and utilized to create test sample sets. The components of interest were 4HPR, protein, lipid, residual blood, and glass. For representative protein and lipid materials, albumin (MP Biomedicals; cat. #810033) and 1,2-dioleoyl-*sn*-glycero-3-phosphocholine (Avanti Polar Lipids, Inc.; cat. #850375P) were used. Each component was dissolved in an appropriate solvent (4HPR/lipid in methanol and protein/blood in water), transferred to glass slide, and allowed to evaporate dry as pure component dispersions. Additionally, an untreated tissue section containing residual blood and an untreated tissue section washed free of blood (with PBS) were analyzed on glass to determine reliability of algorithm's scaled glass and blood subtraction. Large area Raman scans were acquired from the resulting test samples using the Raman acquisition methodology. These test datasets were processed through the algorithm and the error frequency was determined based on fraction of pixels interpreted as 4HPR-positive or 4HPR-negative.

Table S1. Algorithmic error probability testing determined from test datasets.

Spectral components present in test dataset	Glass				
	Tissue				
		Blood			
			4HPR		
				Protein	
					Lipid
# Spectra acquired	9600	625	625	625	625
# 4HPR-positive	6	1		0	0
# 4HPR-negative			0		
% False (+)	0.063	0.160		0	0
% False (-)			0		
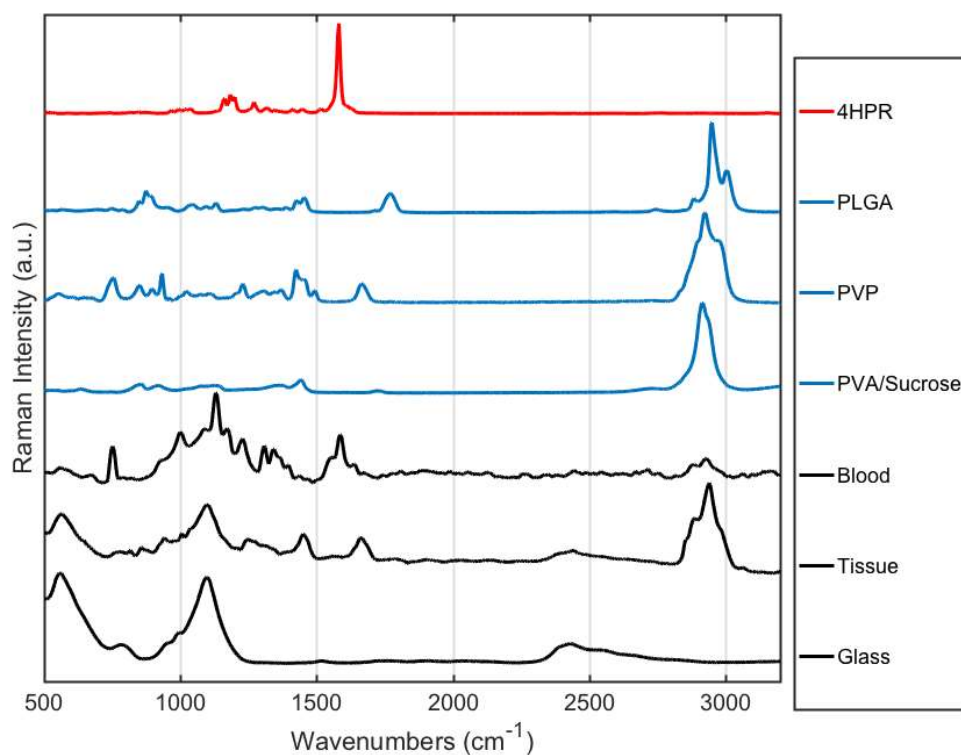
Figure S5- 1 Millicylinder excipients and biocomponent Raman reference spectra show no interference with 4HPR's peak at 1582 cm-1 except from blood. Spectral contributions from glass are apparent in unprocessed tissue spectra. Spectra are shown for 4HPR, PVP, PLGA, PVA/Sucrose, rabbit blood, and untreated tissue.
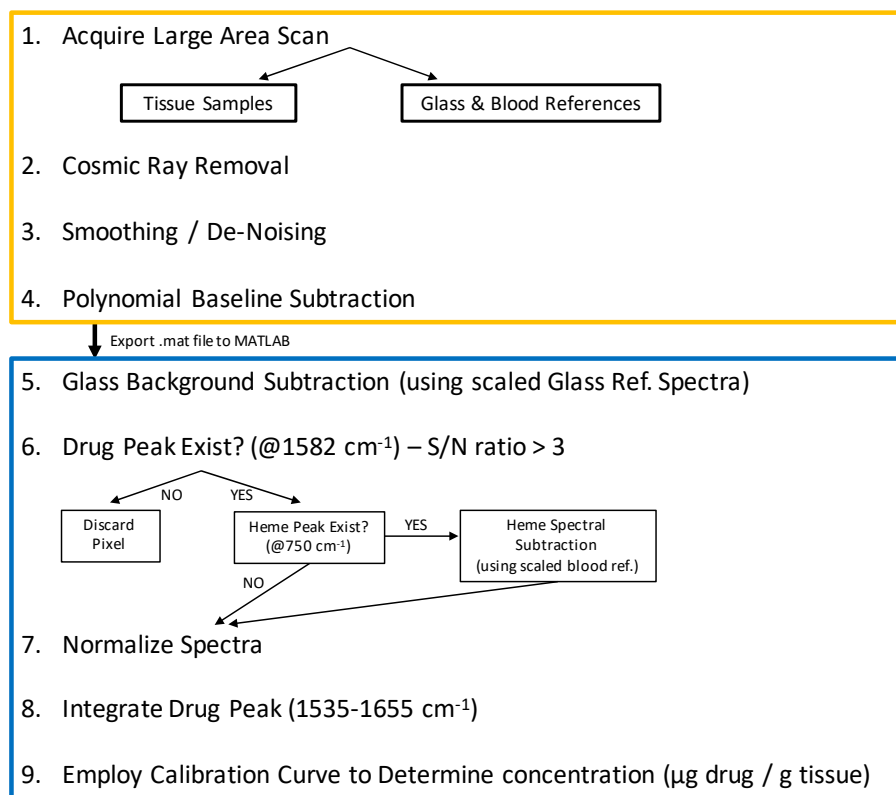
Figure S5- 2 Raman hyperspectral image processing algorithm overview. Data acquisition and initial pre-processing performed using WiTec ProjectFOUR software (shown on top in yellow); automated MATLAB algorithm processing steps (shown on bottom in blue).

The following pages contain **Supplemental Figure S5-3:**

Figure S5- 3 Shown below are Raman images of 4HPR distribution in buccal epithelium section after release from long-acting implants after days 1 and 14, n=3. Shown for each formulation and time point is the Raman heat map of 4HPR concentration in tissue section, oil-red-o (lipid specific) and hematoxylin stain to visual pathological features, and concentration –distance profiles in both the z-plane (through different tissue layers) and y-plane (through same tissue section).

Day 1: Sucrose/PVA + 10% 4HPR

Z-plane

Y-plane

4HPR Tissue Concentration (µg 4HPR/g tissue)

Distance (µm)

Day 14: Sucrose/PVA + 10% 4HPR

Z-plane

Y-plane

4HPR Tissue Concentration (µg 4HPR/g tissue)

Distance (µm)
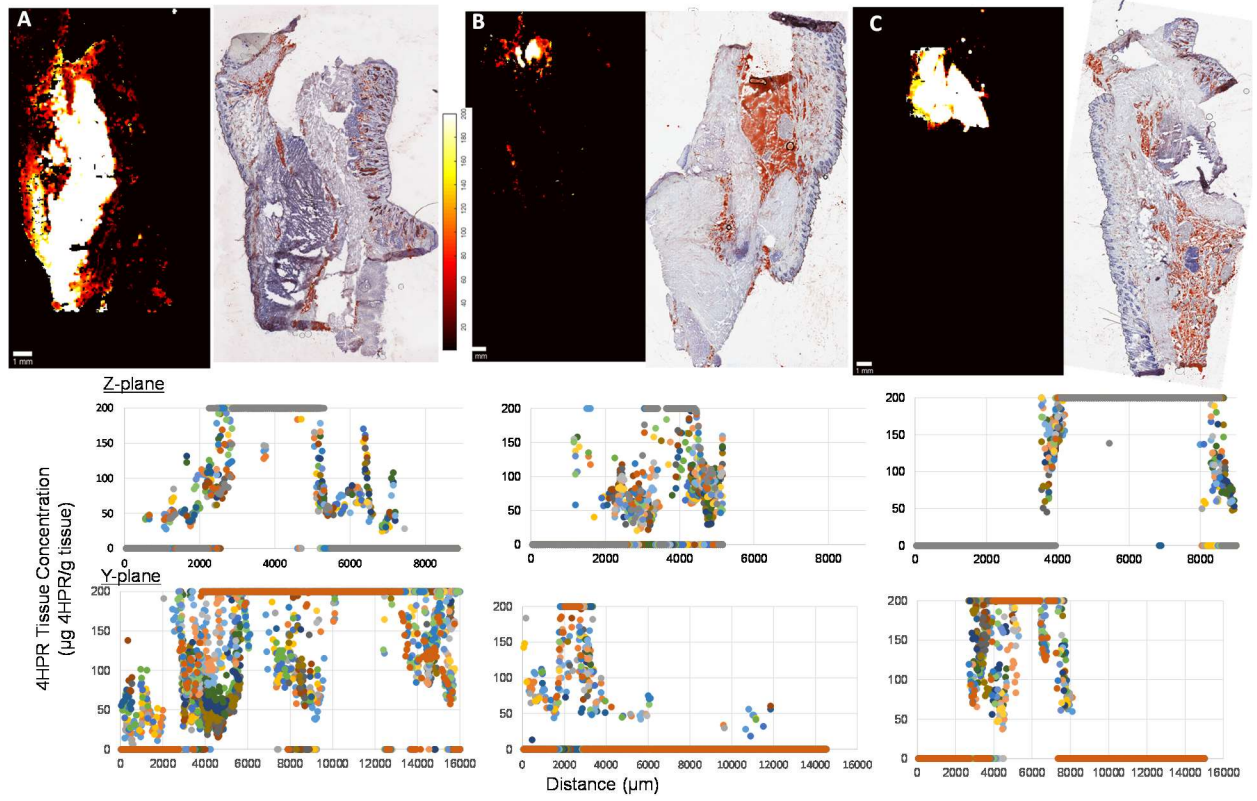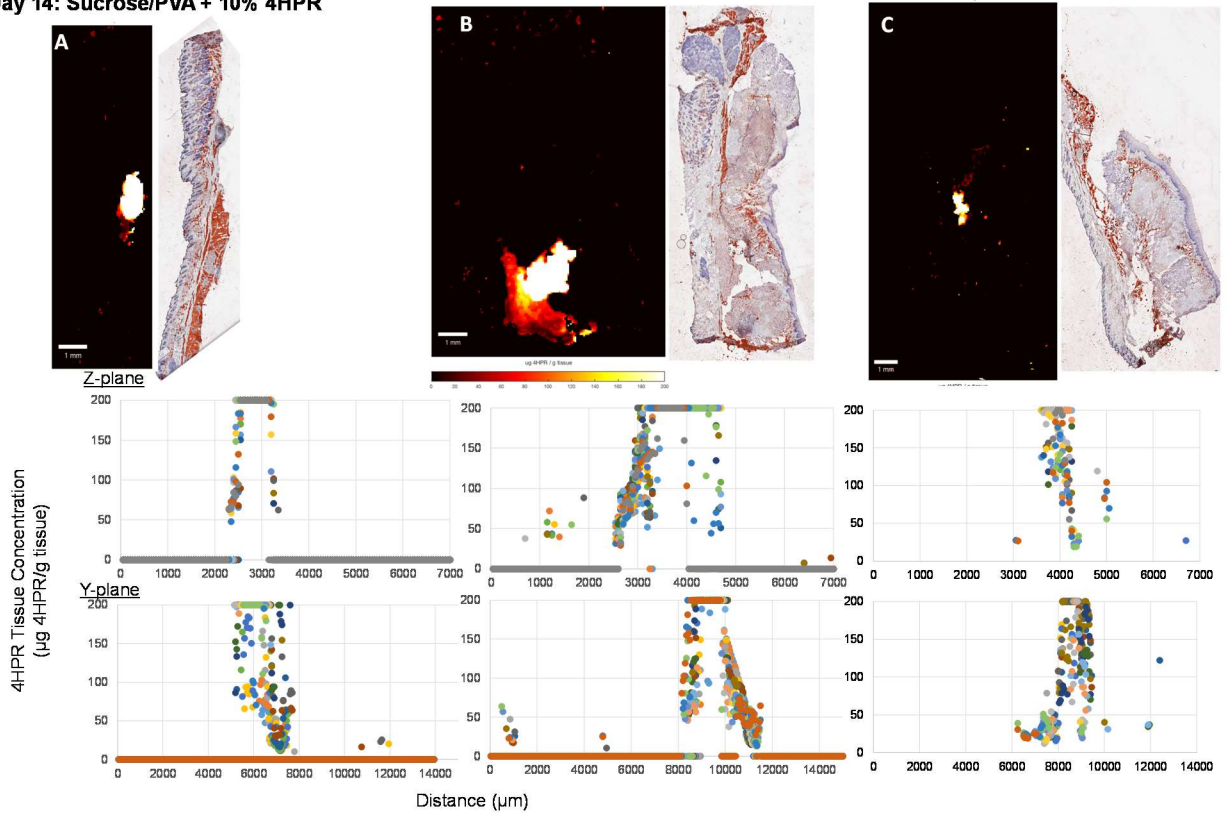
Day 1: PLGA+ 10% 4HPR +3% MgCO₃
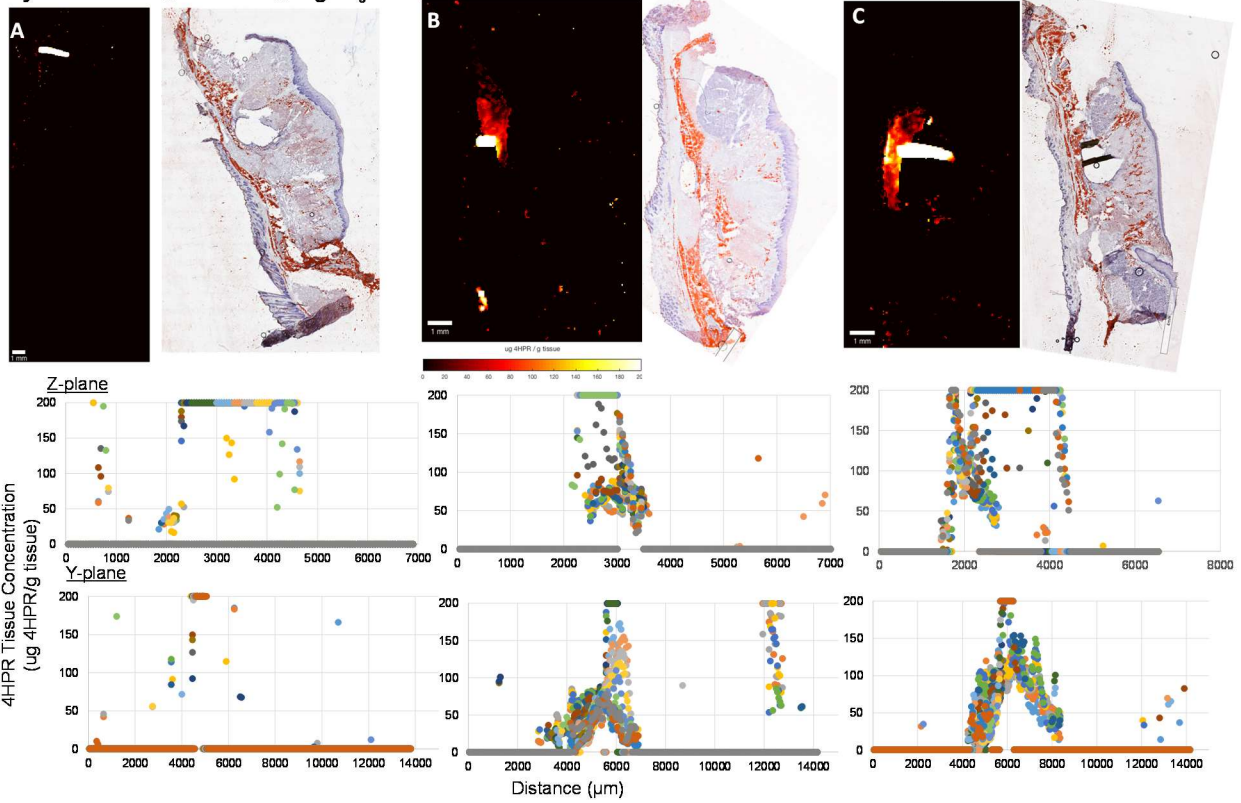
Day 14: PLGA+ 10% 4HPR +3% MgCO₃

159

Day 1: PLGA+ PVP-4HPR-TEAC

Z-plane

Y-plane

4HPR Tissue Concentration (µg 4HPR/g tissue)

ug 4HPR / g tissue

Distance (µm)

Day 14: PLGA+ PVP-4HPR-TEAC

Z-plane

Y-plane

4HPR Tissue Concentration (ug 4HPR/g tissue)

µg 4HPR/ g tissue

Distance (µm)
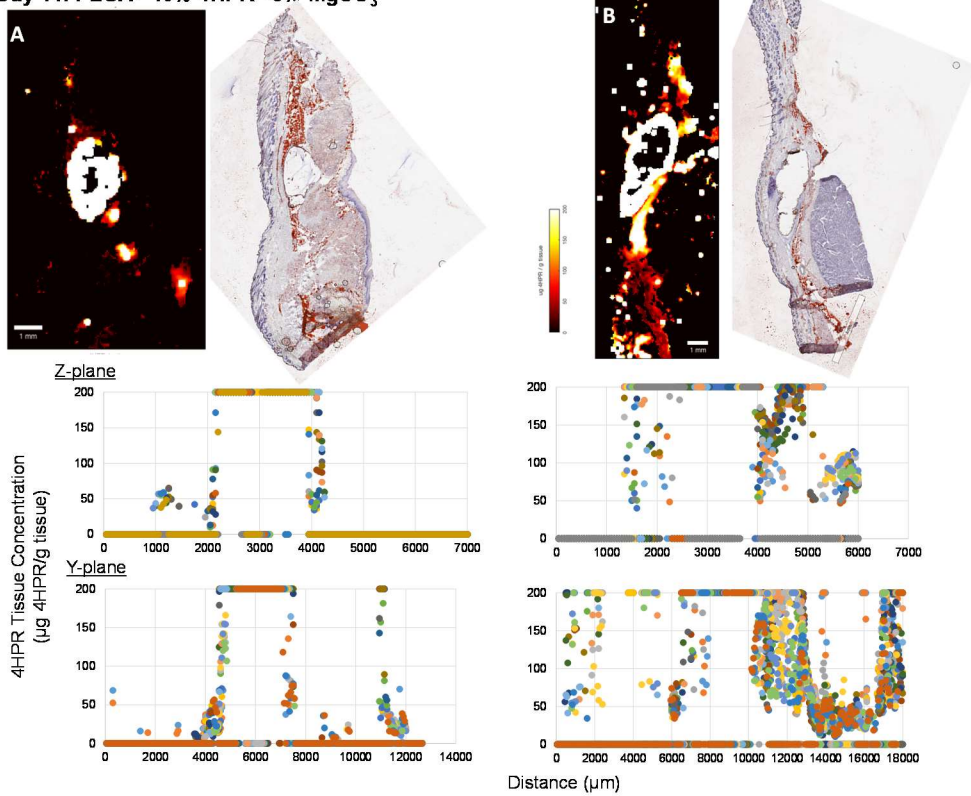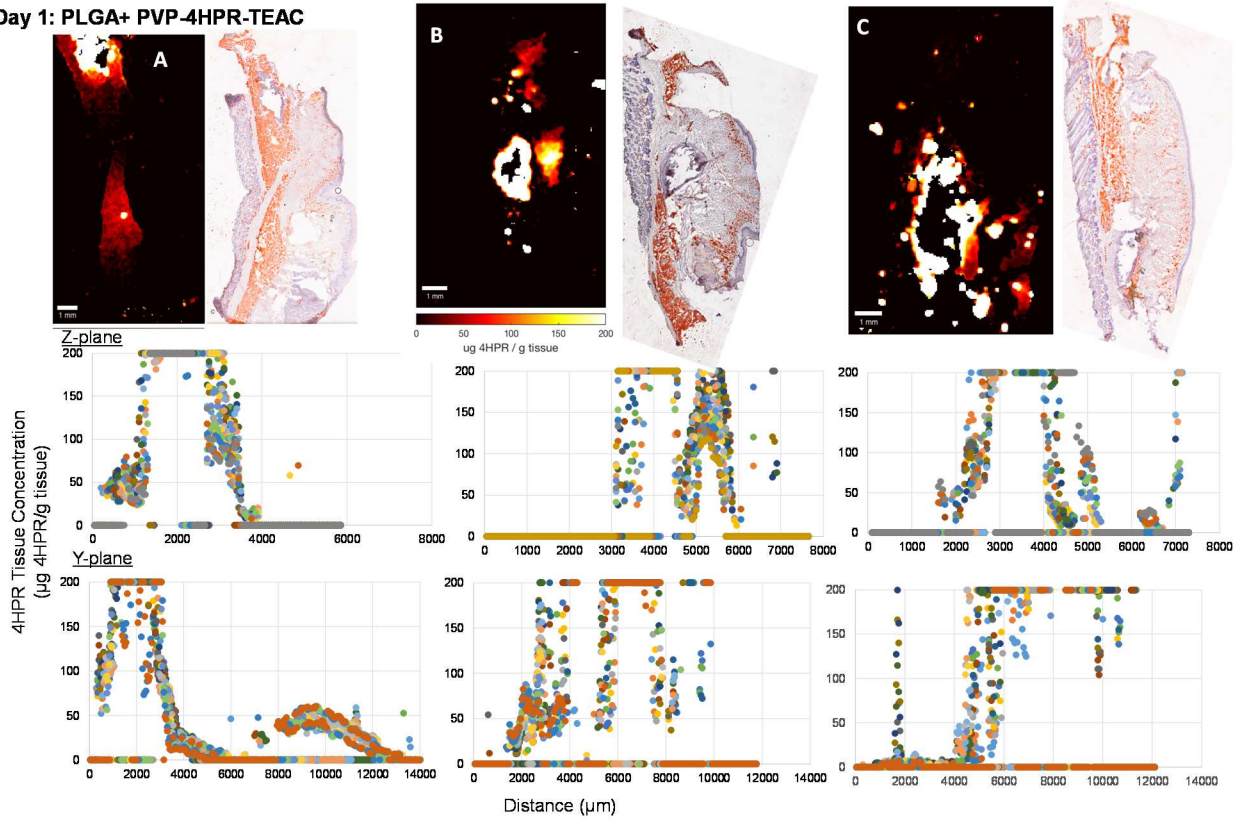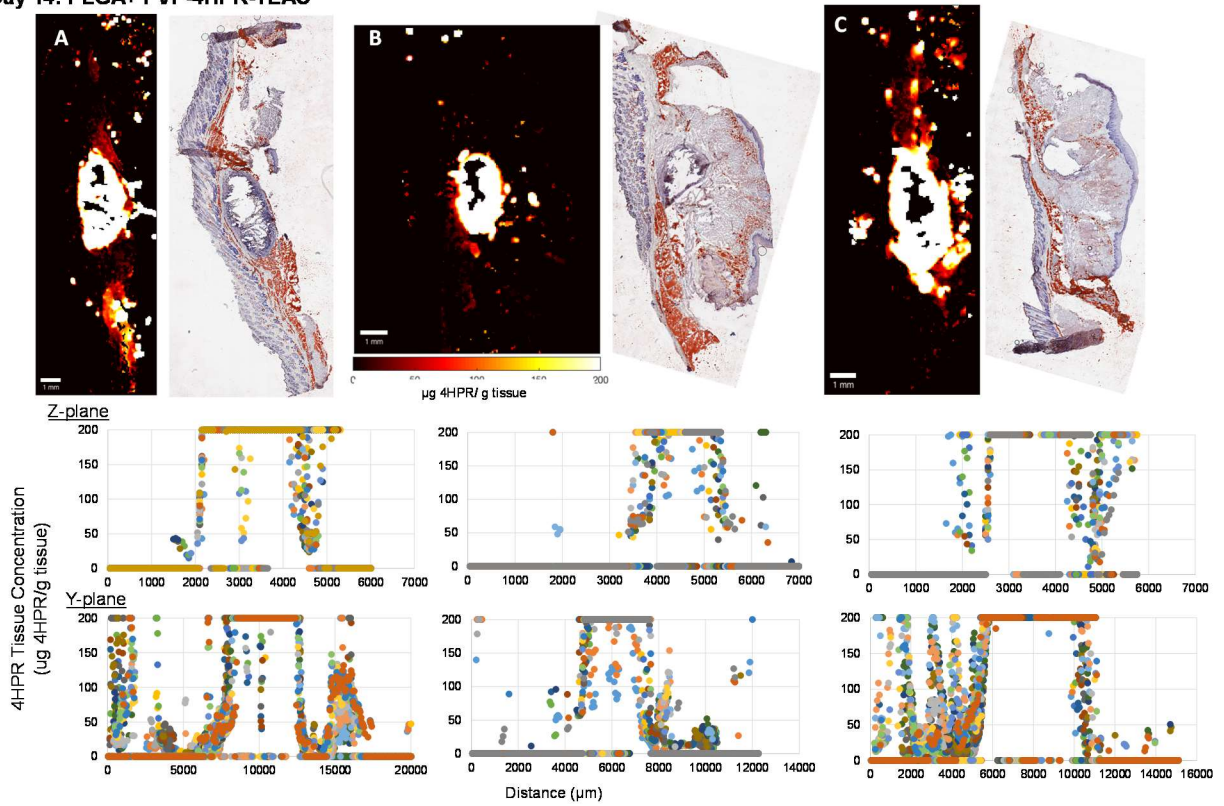
5.7. References

[1] A.B. Fleming, W.M. Saltzman, Pharmacokinetics of the carmustine implant, Clinical pharmacokinetics, 41 (2002) 403-419.

[2] J.F. Strasser, L.K. Fung, S. Eller, S.A. Grossman, W.M. Saltzman, Distribution of 1,3-bis(2-chloroethyl)-1-nitrosourea and tracers in the rabbit brain after interstitial delivery by biodegradable polymer implants, The Journal of pharmacology and experimental therapeutics, 275 (1995) 1647-1655.

[3] M. Haller, W.M. Saltzman, Localized Delivery of Proteins in the Brain: Can Transport Be Customized?, Pharmaceutical Research, 15 (1998) 377-385.

[4] R. Strickley, Solubilizing Excipients in Oral and Injectable Formulations, Pharmaceutical Research, 21 (2004) 201-230.

[5] B.B. Han, S. Li, M. Tong, A.S. Holpuch, R. Spinney, D. Wang, M.B. Border, Z. Liu, S. Sarode, P. Pei, S.P. Schwendeman, S.R. Mallery, Fenretinide Perturbs Focal Adhesion Kinase in Premalignant and Malignant Human Oral Keratinocytes. Fenretinide's Chemopreventive Mechanisms Include ECM Interactions, Cancer Prevention Research, 8 (2015) 419-430.

[6] S.R. Mallery, D. Wang, B. Santiago, P. Pei, S. Schwendeman, K. Nieto, R. Spinney, M. Tong, G. Koutras, B.B. Han, A.S. Holpuch, J.C. Lang, Benefits of Multifaceted Chemopreventives in the Suppression of the Oral Squamous Cell Carcinoma (OSCC) Tumorigenic Phenotype, Cancer Prevention Research, (2016).

[7] F. Formelli, M. Clerici, T. Campa, M.G. Di Mauro, A. Magni, G. Mascotti, D. Moglia, G. De Palo, A. Costa, U. Veronesi, Five-year administration of fenretinide: pharmacokinetics and effects on plasma retinol concentrations, Journal of clinical oncology : official journal of the American Society of Clinical Oncology, 11 (1993) 2036-2042.

[8] D. Moglia, F. Formelli, G. Baliva, A. Bono, M. Accetturi, M. Nava, G. De Palo, Effects of topical treatment with fenretinide (4-HPR) and plasma vitamin A levels in patients with actinic keratoses, Cancer letters, 110 (1996) 87-91.

[9] N. Tradati, F. Chiesa, N. Rossi, R. Grigolato, F. Formelli, A. Costa, G. de Palo, Successful topical treatment of oral lichen planus and leukoplakias with fenretinide (4-HPR), Cancer letters, 76 (1994) 109-111.

[10] C.W. Ying Zhang, Sachin Mittal, Amitava Mitra, Steven P. Schwendeman, Design of controlled release PLGA microspheres for hydrophobic fenretinide, Molecular Pharmaceutics, (in press).

[11] K. Galler, R.P. Requardt, U. Glaser, R. Markwart, T. Bocklitz, M. Bauer, J. Popp, U. Neugebauer, Single cell analysis in native tissue: Quantification of the retinoid content of hepatic stellate cells, Scientific reports, 6 (2016) 24155.

Chapter 6: Conclusions, Significance, and Future Work

The work presented in this thesis details successful 4HPR millicylinder implant formulations capable of providing 1 mo, 2mo, or > 2mo. release *in vivo* depending upon choice of polymer and excipients, including solubilizers. This represents and important step towards translation into clinical applications for oral cancer chemoprevention, by improving patient compliance and survival with less frequent dosing, and greater therapeutic efficacy due to wide spread tissue penetration. The challenges associated with local delivery of 4HPR, an extremely aqueous insoluble drug, included incomplete release from the implant, high non-specific tissue binding, and limited tissue dispersion, were addressed and overcome.

In Chapter 2, local, long-acting release 4HPR millicylindrical implants were prepared from both PLGA and water soluble matrices with and without solubilizers and crystallization inhibitors. The implants were evaluated *in vitro* and *in vivo* over 1-2 mo. Addition of the high levels of pore forming agent ($MgCO_3$) and bile salt were added to improve the release, leaving only 40% PLGA in the implant system to govern the release. The 4HPR *in vivo* release from PLGA only marginally improved by addition of solubilizers, where extremely long release duration (less than 50% 4HPR released after 2 mo.) was observed, which indicated a lack of PLGA erosion controlled release. These PLGA implants exhibited a burst release, followed by a 3 week lag period, and increased drug release rate from day 21-56, likely due to PLGA erosion. It was suspected that 4HPR release at the later stages was governed by the slow dissolution of the hydrophobic drug, and therefore the *in vivo* release was compared to an immediate

162

dissolving, water soluble matrix implant. The water soluble implants were capable of providing controlled release up to 6 weeks. These studies led us to conclude that 4HPR release was governed by dissolution of the hydrophobic drug. These results are consistent with previous PK studies that compared s.c. dosing of 4HPR microspheres to a drug suspension, which showed similar controlled release of drug into plasma after 2 weeks. We suggest possibly combining the PLGA and water soluble implants to provide continuous dosing over 2+ mo. In our initial tumor efficacy studies in oral cancer xenograph mice, we found our 4HPR-PLGA millicylinders were effective at reducing rate of tumor growth relative to no-drug controls.

The limitations of the initial PLGA-4HPR millicylinder formulations were realized in Chapter 2, and therefore creation of amorphous drug systems for solubility enhancement was investigated in Chapter 3. A robust PVP-4HPR ASD showed incredible 50 to 1000-fold solubility enhancement over 1 week, and was loaded into PLGA millicylinders, and release was evaluated *in vitro* and *in vivo*. One of the drawbacks of using this solubility enhancing ASD system, is the large quantity of excipient necessary relative to the drug, and thereby decreases the drug dose that can be delivered. The optimal PVP-4HPR ratio was determined to be 9/1, and therefore if loaded 50/50 into PLGA, the total 4HPR loading is only 5%. The *in vitro* release with the 9/1 PVP-4HPR was not satisfactory, and after careful literature review, addition of the plasticizer TEAC to the PVP-4HPR ASD substantially improved release nearly 6-fold. The *in vivo* release study with the solubilized amorphous PVP-4HPR immediate dissolving and PLGA + PVP-4HPR-TEAC implants showed large release enhancement compared to our previous PLGA and PVA/sucrose crystalline drug formulations where slow, continuous, and nearly complete release was achieved over 30 days. These results are useful for tailoring formulations

to target a wide range of release durations based on selection of polymer matrix and level of solubility enhancement.

In Chapter 4, we evaluated 4HPR's tissue binding and lipid cell membrane binding to predict the factors responsible for 4HPR tissue dispersion. These results show that time of exposure, but not solubilizer or permeation enhancers, affected tissue uptake. Furthermore, 4HPR exhibited a fifteen-fold greater binding affinity to buccal epithelia relative to SC connective tissues. Most notably, obtaining 4HPR solubility in aqueous solutions was the limiting factor for tissue uptake. While the majority of non-specific tissue binding likely reflects lipid interactions, it is well known that 4HPR also demonstrates high affinity protein binding. Therefore, future 4HPR injectable formulations should aim to maximize drug solubility to achieve widespread distribution at the local lesioned site.

In Chapter 5, we have made significant headway in developing quantitative Raman imaging methods to determine 4HPR spatial distribution after dosed into rabbit buccal epithelia. This is the first time the 4HPR's tissue distribution has been mapped, and the imaging methods are hugely advantageous over the traditional tissue sectioning and extraction methods. With it, we can see the drug's partitioning into the various layers of tissue, such as the mucosa epithelium, sub-mucosa, or deep muscle layers. In tandem, lipid staining allowed us to visualize the drug's affinity for lipid rich regions, where we had hypothesized 4HPR's high lipid affinity limits its penetration. The millicylinders were implanted in rabbit buccal epithelia and drug release and distribution were evaluated over 14 day, including the formulations: crystalline drug control in an immediate dissolving sugar matrix, 4HPR-PLGA, and the extremely solubilized PVP-4HPR-TEAC ASD in PLGA implants. The results from the tissue distribution revealed that the amorphous drug had the greatest tissue penetration, results which are consistent with the

conclusions from the ex-vivo tissue uptake study that found drug solubility was the limiting factor in uptake. Without the solubility enhancement, there is no driving force to move hydrophobic 4HPR from the depot into the surrounding aqueous tissue environment.

To conclude, we have shown that formulation challenges of local delivery of this hydrophobic, high protein and lipid binding drug 4HPR, can be overcome. For the first time, 4HPR's local tissue interactions and distributions were evaluated. Also novel is the quantitative Raman imaging method. These formulations will be of great value and importance for those patients who have suffered the debilitating effects of oral cancer, and will serve to provide them with effective and worry free cancer prevention therapies, which will be necessary for the remainder of their lives. These formulation strategies can also be applied for local delivery of other hydrophobic drug molecules as well.

Future studies should investigate the use of other penetration enhancing excipients to further move the drug into surround tissue to treat a larger lesional area, for example, propylene glycol, tweens, menthol, chitosan polymers, bile salts, and hyaluronidase enzyme for tissue spreading. Alternatively, other depot forms such as in situ forming implants, hydrogels, or microparticles could be investigated. The toxicity of these excipients should be evaluated locally and systemically, with inflammation at the implantation site being the most likely pitfall. Additionally, the translational aspect could evaluate the effects of radiation therapy on the stability or release of 4HPR from the implants, as patients maybe be concurrently preventing cancer regrowth while removing new lesions. Future studies could also investigate the drug release and distribution at different implantation sites in mouth, including tongue, or floor of mouth, which have different levels of keratinization and tissue thickness.

Appendix 1: Excipients and solvents used for solubilization of 4HPR

Compilation of experimental data and literature reviews

Solvent	Solvent/Solubilizer classification	Solubility (mg/mL)
Literature Data From our Lab		
Dichloromethane (DCM)	Organic solvent (Hansen's solubility calc.)	2.5
Ethyl acetate (EtOAc)	Organic solvent	21
Chloroform	Organic solvent	7
Methanol (MeOH)	Organic solvent	36
Ethanol (EtOH)	Organic solvent	47
1-Propanol	Organic solvent	36
2-Propanol	Organic solvent	37
Acetone	Organic solvent	100
Acetonitrile (CAN)	Organic solvent	3.8
THF	Organic solvent	>200
Dimethylformamide (DMF)	Organic solvent	>99
Dimethylsulfoxide (DMSO)	Organic solvent	>95
N-Methylpyrrolidone (NMP)	Organic solvent	150
Phosphate buffer solution (PBS)	Aqueous solvent	0.000023
PVA (5% in water)	Aqueous solvent, water	0.0008
Tween 80 (1% & 3% in PBS)	Aqueous solvent, PBS	0.2, 0.6
Sodium deoxycholate (NaDC) 5%	Bile Salt (In Simulated Saliva Solution, pH 6.8)-Buccal Mucosa patch study	0.403
Sodium cholate (NaC) 5%	Bile Salt (In Simulated Saliva Solution, pH 6.8)	0.264
Sodium taurocholate(NaTC) 5%	Bile Salt (In Simulated Saliva Solution, pH 6.8)	0.203
Sodium glycholate (NaGC) 5%	Bile Salt (In Simulated Saliva Solution, pH 6.8)	0.166
Tween 20 (5%)	Non-ionic Surfactant (In Simulated Saliva Solution, pH 6.8)	0.404
Tween 80 (5%)	Non-ionic Surfactant (In Simulated Saliva Solution, pH 6.8)	0.457
Brij 35 (5%)	Non-ionic Surfactant (In Simulated Saliva Solution, pH 6.8)	0.150
Brij 98 (5%)	Non-ionic Surfactant	0.505

	(In Simulated Saliva Solution, pH 6.8)	
Soluplus (5%)	Polymer (In Simulated Saliva Solution, pH 6.8)	0.200
Lecithin (5%)	Lipid (In Simulated Saliva Solution, pH 6.8)	0.098
		µg/mL
Brij 98 (0.1, 0.5, 1 %w/w)	PBS (From Merck Report)	15, 60, 130
Brij 35(0.1, 0.5, 1 %w/w)	PBS (From Merck Report)	15, 40, 70
Tween 80(0.1, 0.5, 1 %w/w)	PBS (From Merck Report)	15, 85, 170
PluronicF127(0.1, 0.5, 1 %w/w)	PBS (From Merck Report),	15, 60, 70
DI	DI (hydrophobic fenret Inj), 3 days	0.023
Tween 80 (0.02, 0.1, 0.5, 1, 2%)	PBS, (hydrophobic fenret. Inj), 3 days	6, 22, 100, 200, 625
Experimental Data		µg/mL
Water	Water	0.2
Tween 80 (2%)	PBS day 1, 7	Day 1: 300 Day 7: 499
PEG400	Potential osmotic pump solution	941
NMP (12.5%) in PBS	ISFI solvent	0.25
NMP (12.5%) in PBS 2% Tween	ISFI solvent/in vitro release media	624
5% PG + 2.5% Menthol in PEG 400	Potential Osmotic pump solution	896
5% NaDC in 2% Tween 80 PBS	PBS	638
NaDC (1, 2, 5, 10, 20 %)	Water, Day1, 7 sampled	<u>Day 1</u>: 22,142,396,617 <u>Day 7</u>: 32, 56, 157, 567, 1038
B-CD (1, 2, 5, 10, 20 %)	Water, Day1,7 sampled, similar data	7, 13, 23, 34, 40
HP-B-CD (1, 2, 5, 10, 20 %)	Water, Day1, 7 sampled, similar data	0.06,0.09, 1.6, 7, 32
TA-B-CD (1, 2, 5, 10, 20 %)	Water	Insol.
PVP (1, 2, 5, 10, 20 %)	Water, Day1, 7 sampled, similar data	0.04, 0.04, 0.36, 0.66
HPMC (1, 2, 5, 10, 20 %)	Water	Insol.
PEG4600 (1%)	Nonionic surfactant. In DI. N.d. at 2,5,10, 20%	0.25
PEG800 (1, 2, 5%)	Nonionic surfactant. In DI. N.d. at 10, 20%	0.25 in all
Pluronic F127 Prill (1,2,5,10%)	Non-ionic surfactant, PEG-PG-PEG Mn=5800, water	2, 8, 45, 115
Phosphatidyl Choline (1, 5%)	Lipid, in water, day 1,7	314, 946
Serum	day 1, 7	57, 67

Na 4HPR salt in DI	day 1, 7—(Prepared by kneeding in EtOH, or acetone rxn solvent)	EtOH- 19, 104 Acetone- 32, 112
Na 4HPR salt	PBST 0.02%, day 1, 7	56, 103
Na 4HPR salt	PBST 0.5%, day 1, 7	264, 295
Na 4HPR salt	PBST 2%, day 1, 7	632, 79
Na 4HPR salt in serum	day 1, 7 (prepared from kneeding in acetone)	228, 126

*Solvent solubilities measured at 25 ˚C, while all others at 37 ˚C. All percentages are expressed as w/v %.

*Insol. =insoluble

*N.d.=Not detected

Appendix 2: Elucidation of Physicochemical interactions of Fenretinide with Poly(lactic-co-gylcolic acid) in Long-acting release implants

A2.1 Abstract

Poly(lactic-co-glycolic acid) (PLGA) is an FDA approved bio-erodible polymer used for long-acting release drug delivery, whose chemical properties can easily by tailored to the intended target dosing frequency. Fenretinide (4HPR), a synthetic retinoid molecule, has been exploited for its chemopreventive properties, in particular, oral cancer. In our recent studies, we had developed 4HPR-PLGA delivery systems, however, we found extremely slow and incomplete drug release from our polymer matrix both in vitro and in vivo. We had suspected that 4HPR was interacting with PLGA in such a way that prevented its release or facilitated degradation once released. 4HPR is a hydrophobic molecule, and also known to be subject to photo-and oxidative degradation due to its high degree of conjugation. Our studies found that 4HPR was stable within the PLGA matrix after months of incubation in vitro, however, once released into aqueous media, had shown both photo-and oxidative degradation. Mechanisms of PLGA-4HPR interactions were investigated including release in solubilizing/non-solubilizing media, LC-MS of degradation products in release media, polymer glass transition temperature, effects of residual carrier solvent, FTIR for carbonyl chemistry interactions, and Raman spectroscopy for π- electron interactions. These data suggest that PLGA carboxylate groups are interacting with 4HPR's amide bond, and prompting 4HPR hydrolysis into its parent retinoic acid structure, similar to known acylation reactions with PLGA and peptides. Also, the acetone carrier solvent appears to have an effect on the adhesion of 4HPR to the PLGA, and remains

traps within the millicylinders prior to release. Interestingly, we have also shown a direct correlation between the level of residual solvent, polymer Tg, and the amount of drug released. These data will be useful for designing future long-acting release 4HPR-PLGA systems or other hydrophobic drugs or those containing amide bonds loaded into PLGA.

A2.2. Introduction

Retinoids are a group of endogenous and exogenous molecules synthesized *in vivo* from carotenoid molecules or synthetically from Vitamin A (or retinol) and have important physiological roles including growth and development, reproduction, and cellular differentiation. Synthetic derivatives of Vitamin A have been utilized to treat a variety of skin disorders, and one of particular interest to us is fenretinide (4HPR), a highly active and promising therapeutic and chemopreventive agent for epithelial and neural origin cancers[1]. It is known that retinoids, including 4HPR, are highly photo-sensitive leading to many types of isomerization reactions, which can be increased in the presence of organic solvents due electron transitions during conversion of singlet and triplet energy states[2]. Retinoid structural rearrangement can also occur by reduction of the carbon-carbon double bonds in the presence of free radicals or light initiation. The propensity of retinoids to capture light is the property by which renders them useful for photon capture and light sensing in the eye's opsin protein domains[2].

Due 4HPR's lack of efficacy and dose-limiting toxicities by oral route, we have chosen to formulate 4HPR for local delivery using poly(lactic-co-glycolic acid) (PLGA) implants for long-acting release. PLGA has been widely used as a choice polymer for controlled release drug delivery application due to its FDA approval, safe, predictable, and tailorable release properties based on ratio of lactide: glycolide monomers, molecular weight, and end-group capping. The selection of the type of PLGA is largely dependent upon the duration of release (30 days to 9

170

months) and the drug properties. The polyester undergoes hydrolysis into its lactic and glycolic acid monomers, giving rise to an acidic microenvironment and has shown to lead to autocatalyis of peptides[3]. While PLGA is often utilized for stability enhancement of peptides or proteins, it is known that the hydrolysable ester bonds are subject to nucleophilic interactions with the encapsulated drugs.

In our long-acting release 4HPR-PLGA millicylinder systems, we have found incomplete release of this hydrophobic drug even after 2 months in a solubilizing buffer. The aim of this work is to address the reasons for incomplete release, which go beyond the drug's obvious limited aqueous solubility, and addresses the drug-polymer interactions. We suspect that 4HPR is interacting with PLGA similarly to peptides[4], due to similar amide functional groups. Mechanisms of PLGA-peptide interactions that have been reported include acid-catalyzed reactions, such as deamidation and chain cleavage, drug-polymer acylation reaction and protein denaturation or degradation[5,4,6,7]. 4HPR is a weak acid, with a hydrolysable amide bond, which yields a reactive amino-phenol by-product. Results from our study shows that 4HPR does not appear to be hindering PLGA erosion, where nucleophilic attack of the amino-phenol would facilitate PLGA hydrolysis similarly to water. This paper considers the possible mechanisms of PLGA-drug interactions that causes incomplete drug release by inspection of 4HPR degradation products via mass spectrometry, carbonyl chemistry via FTIR spectroscopy, and π-π interactions via Raman spectroscopy. Additionally, the effect of the protic acetone solvent used for millicylinder preparation was assessed. These studies will help guide further preparation of 4HPR-PLGA millicylindrical implants for long-acting release drug delivery for oral cancer chemoprevention. The utility of this research will also aid in troubleshooting PLGA delivery

systems where loading amide, amine, or phenolic compounds have resulted in incomplete release.

A2.3. Methods

A2.3.1 4HPR in vitro release from PLGA millicylinders and PLGA Erosion

4HPR *in vitro* release from PLGA millicylinders was determined by placing one millicylinder (5-7 mg) in 5 mL Eppendorf tube containing 4 mL PBS pH 7.4 + 0.02% or 2% Tween 80, incubating at 37 °C on a shaking platform (200 rpm) and tubes protected from light by foil. The solutions were sampled by complete media replacement, 4HPR levels quantified by UPLC-UV, while 4HPR degradation products qualitatively determined by UPLC-MS. PLGA implant erosion was performed after incubating implants in PBST 2%, and measuring PLGA mass loss after drying over 28 days. A drug-loading and mass balance determination after *in vitro* release by digesting PLGA-4HPR millicylinders in THF, then precipitating PLGA with EtOH.

A2.3.3 Identification of 4HPR Degradation products by LC-MS and MS/MS

The extent of 4HPR degradation after *in vitro* release from PLGA millicylinder (10% 4HPR+ 3% $MgCO_3$) into PBST 2% was compared to the drug's degradation in individual millicylinder components including PBST 2 % media, PBST 2% + 10% acetone, PBST 2% + PLGA + 10% acetone, PBST 2% + PLGA, PBST 2%+ PLGA + 10% acetone + 3% $MgCO_3$. The solutions were analyzed by LC-MS using Waters Acquity UPLC-MS (quadrupole mass analyzer, QDa Acquity) system and Empower software under the following conditions: Acquity BEH C18 2.1x100 mm column, mobile phase 80:20 ACN: 0.1% formic acid, isocratic flow rate 0.65 mL/min, and total analysis time of 2 min. MS was operated in both positive and negative ion mode, and 4HPR's molecular ion [M+H$^+$] m/z 392 was detected, and degradation products

after in vitro release from 4HPR-PLGA millicylinders and buffers were identified based on literature mass spectra of retinoid molecules. The MS/MS fragmentation was performed on ions observed in LC-MS using with Sciex 5500 Qtrap MS.

A2.3.2 Microcalorimetry

The amount of residual solvent trapped in PLGA-4HPR millicylinders after drying was determined by Thermogravimetric Analysis (TGA, Discovery, TA instruments). The following temperature ramping profile was used: 10 °C/min until 300° C, then 20 °C/min till 600° C. The percent mass loss after 150 °C was used to estimate both residual acetone and water removal during the TGA analysis. The heating curves of the drug loaded (10, 20%, or 30% 4HPR) PLGA implants containing 3% $MgCO_3$ were compared to no drug implants and starting materials.

The glass transition temperature (Tg) of the dried PLGA-4HPR millicylinders (prepared in previous reports, and could contain 5-30% 4HPR, 20% sodium deoxycholate, or 3-15% $MgCO_3$) was measured to correlated with amount of 4HPR released *in vitro* release after 28 days. For the differential scanning calorimetry (DSC) analysis (Discovery, TA instruments), 2-3 mg of the millicylinder was added to a hermetic pan, and samples were heated under modulating temperature from -10 °C to 70 °C, and Tg was determined.

A2.3.4 FTIR and Raman Analysis of PLGA-4HPR Films

PLGA-4HPR films were composed of 5% PLGA 503H + 4HPR (5, 10, 20 or 30%) + 3% $MgCO_3$ dissolved in acetone and physical mixtures. Individual FTIR spectra were acquired for acetone, 4HPR (solid), 4HPR (in acetone), PLGA, and PLGA + $MgCO_3$. FTIR spectra were acquired with Perkin Elmer Spectrum BX spectrophotometer equipped ATR crystal accessory, 20 uL of the polymer-drug solution dropped onto ATR, allowed to dry, then spectra acquired in 400-4000 cm^{-1} range, 20 scans, and percent absorbance was reported.

Raman spectra was acquired of PLGA-4HPR films prepared as described in FTIR analysisby placing 50 μL of film, solid or solutions onto a silicon wafer and allowing to dry. Spectral acquisitions were performed using a WiTec Confocal Raman spectrometer, 532 nm laser in 400- 3500 cm^{-1} range, 20X objective, 35 accumulations per spectra, with 1 sec accumulation time.

A2.4 Results and Discussion

A2.4.1 4HPR-PLGA millicylinder *in vitro* release and polymer erosion

4HPR was encapsulated in PLGA 503H millicylinders containing 3% $MgCO_3$ for controlled release of 4HPR based on our previous work with formulating 4HPR into microspheres and ISFIs.[8] The free-acid low molecular weight PLGA continuously erodes at physiological conditions to allow continuous release[9]. Also, we have found a positive effect upon addition of a poorly soluble basic salt (i.e. solubilizes upon pH lowering like antacids) on release of proteins and hydrophobic small molecules from PLGA millicylinders, which is attributed to pore formation and neutralization of PLGA monomers that have degraded within the bulk polymer[10,11].

The *in vitro* release of 4HPR from PLGA millicylinders was performed in both solubilizing (PBST 2%) and non-solubilizing (PBST 0.02%) buffers to determine if maintenance of sink conditions (with high level of solubilizer) could facilitate complete release of hydrophobic 4HPR from the implant. 4HPR solubility in PBS +0.02% and 2% Tween is 0.02 and 500 μg/mL respectively. In Figure 1a, we observed that release is accelerated in presence of high levels of Tween solubilization, resulting in 40% vs. 4% 4HPR released by day 56 for PBST 2% and PBST 0.02% respectively. Clearly, the level of solubilization by Tween in the release media greatly dictates release of the hydrophobic drug. A mass balance for the PBST 2% media revealed an incomplete accounting of drug, such that $42 \pm 4\%$ 4HPR was released and $35 \pm 3\%$

4HPR was remaining in millicylinder, equating to $77 \pm 4\%$ 4HPR recovered. The initial drug

loading in the implant was close to 100%, indicating that the drug is stable initially inside of the

PLGA, and therefore degradation must be occurring after being released from the implant into

the aqueous media. The SEM of the implant cross-section (Fig. 1c) prior to *in vitro* release shows

that 4HPR is soluble in the PLGA. This incomplete drug release is unusual given that PLGA

503H typically is mostly eroded after 1 month, and after 2 months it should be completely

hydrolyzed into its glycolic and lactic acid monomers. It was suspected that 4HPR may be

interacting with PLGA and inhibiting PLGA erosion, leading to a delayed release profile.

However, this was not observed (Fig. 1b), where 10% and 20% 4HPR loaded implants

containing 3% $MgCO_3$ did not significantly alter polymer erosion compared to the PLGA+ 3%

$MgCO_3$ control, and by 28 days 50-60% PLGA had eroded. We do see that the basic pore-

former $MgCO_3$ significantly delayed erosion at 15% compared to 3%, likely due to electrostatic

interactions between magnesium cations and PLGA's carboxylate groups.
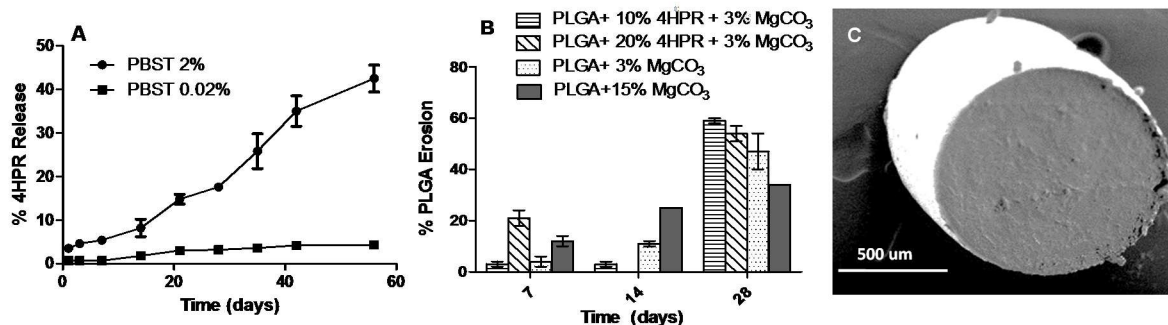

Figure A2- 1: a) 4HPR in vitro release from PLGA millicylinders (20% 4HPR + 3% MgCO3) in solubilizing PBST 2% and non-solubilizing PBST 0.02% media. B) Effect of drug loading and MgCO3 level on PLGA erosion in millicylinders in PBST 2%. C) SEM of 10% 4HPR in PLG PLGA millicylinder +3% $MgCO_3$ shows 4HPR solubility in the PLGA polymer phase. (Mean $\pm$ SE, n=3)

A2.4.2 Mass Spectrometric analysis on 4HPR degradation in *in vitro* release media and PLGA implant

The mass balance showed that that ~25% of 4HPR degraded either within the PLGA matrix or in the aqueous release media after 2 months, therefore, the stability of 4HPR in the *in vitro* release media (PBST 2%) was evaluated and compared to the stability of 4HPR within the PLGA implant, and also in the presence of individual millicylinder components to delineate source of 4HPR degradation. A qualitative LC-MS/MS analysis was performed to identify these degradation products, based on literature data. As shown in Table 1, the addition of acetone, PLGA, and $MgCO_3$ to the PBST 2% media have little effect on the degradation compared to 4HPR in the control PBST 2% solution. However, substantial drug degradation occurs after 4HPR is released from PLGA millicylinder, and after 1 week, the 4HPR peak was reduced to 82%, while the peak at RT=0.9 increased to 17.2% of total chromatogram peak area. Yet, the drug was 100% stable within the PLGA. These results show that 4HPR stability is compromised in presence of PLGA even early on in release profile, and the identification of degradation products in the release media (RT=0.9 and 1.7 min) will be helpful to determine what may be driving the reaction. The pathway of this degradation is therefore the subject of this investigation.

Table A2- 1. Evaluation of 4HPR degradation in dissolved in solubilizing media in presence of millicylinder components compared to 4HPR release from PLGA millicylinder and within the implant.

Media Composition	RT= 1.8(4HPR)		RT= 1.7 (4HPR cis)		RT=0.9 (retinoic acid oxidzation & isomers)	
	D1	D7	D1	D7	D1	D7
PBST 2% media only	100%	96%	-	0.3%	-	3.8%
PBST 2%+ acetone	99%	97%	0.1%	0.3%	0.7%	2.6%
PBST 2%+ acetone+ PLGA	100%	98%	0.1%	0.2%	0.4%	1.7%
PBST 2%+ PLGA	99%	98%	-	0.1%	1.4%	2.3%
PBST 2%+ acetone+ PLGA+ MgCO$_3$	99%	98%	0.1%	0.3%	0.4%	1.4%
Release from PLGA implant, PBST 2%	95%	82%	0.8%	0.6%	4.4%	17.2%
Extracted from PLGA implant	-	100%	-	-	-	-

Days 1 and 7 reflect the extent of degradation at retention times (RT, min) in UPLC-UV % peak area percentages, 365 nm.

Figure 2 shows UPLC-UV (365nm) chromatogram traces with 3 abundant peaks present at RT's ~1.8 (parent 4HPR), 1.7, and 0.9 min, which are indicative are indicative of the parent retinoid structure, and abundant ions identified by MS of 4HPR in PBST 2%, 4HPR release from PLGA millicylinders in PBST 2%, and 4HPR extracted from PLGA millicylinders. Reference LC-MS/MS spectra of 4HPR and its oxidized/metabolic derivatives have previously been reported, and served as a reference for identification[12],[13]. Per AIST database, 4HPR's most abundant MS/MS ions include m/z 283 (after neutral loss of 4-amino-phenol), m/z 270 (minus C-H), and m/z 255 (minus CH$_3$), while the oxidization on the hexenyl ring (after loss of 4-amino-phenol) yields ions m/z 281 and 253. No p-amino-phenol fragment is detected in LC-MS extracted ion chromatogram, and therefore it is plausible that it is adhering to PLGA due to its strong nucleophilic character, whose attractions are favorable for 4HPR's amide bonds cleavage, similar to those reported for PLGA and peptide interactions [4],[7],[5]. Additionally, the negative ion MS detected m/z 313 in only the 4HPR-PLGA millicylinder release, which is identified as 4-

oxo-retinoic acid. The positive ion m/z 253 is only detected in the PBST release, and based on

MS/MS fragments, does not appear to be 4HPR, but rather an isoprene unit (68 Da) with 4 CH_2

groups (14 Da). Positive ion m/z 461 and 483 are likely some adduct of 4HPR given its similar

MS/MS fragmentation pattern as 4HPR. Further analysis of these interactions will be

investigated through FTIR and Raman analysis in the following sections.

A. 4HPR release from PLGA millicylinder in PBST, Day 7
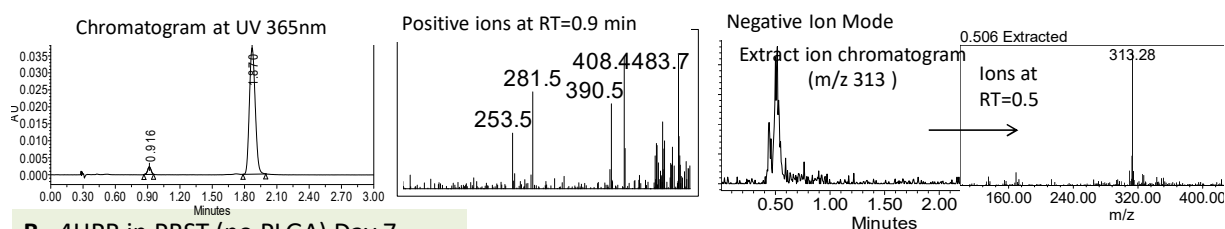
B. 4HPR in PBST (no PLGA) Day 7
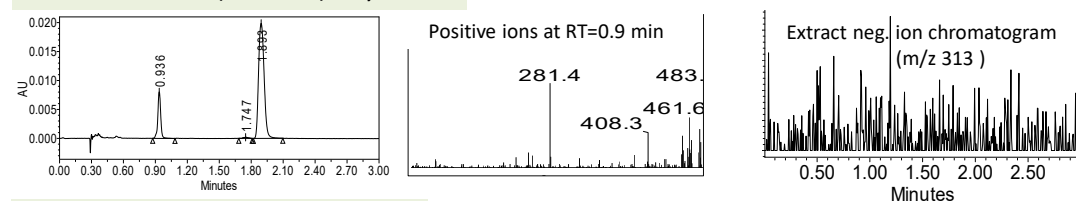
C. PLGA millicylinder digest, Day 7

4HPR stable
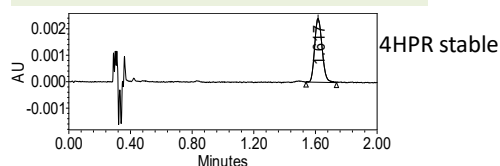
D. p-amino phenol standard, M+H+ 110Da @ RT=0.3min

Not detected in any sample

E.
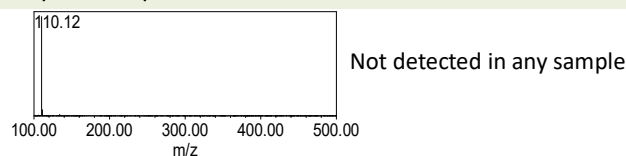
RT	m/z [M+H+]	MS/MS ions	Proposed Compound		PLGA Digest	PLGA Release	PBST
0.9	281	**177,133,89***	Retinaldyde, oxidized			✓	✓
	253	191,123,109,95,81,67					✓
	461	415,371,327,309,**177,133,89***					
	483	**133,89**					
1.7	392	281,270,255	4HPR cis-isomer			✓	✓
1.8	392	281, 270,255	4HPR		✓	✓	✓
	m/z [M-H+]						
0.5	313		4-oxo-retinoic acid				✓

Figure A2- 2 Qualitative LC-MS investigation of 4HPR degradation products after a) in vitro release from PLGA millicylinders compared to b) 4HPR in PBST, and c) stability in PLGA polymer matrix. Chromatogram traces at 365 nm and mass spectra of positive ions at those peaks. The negative ion m/z 313 only detected in 4HPR-PLGA release sample. The suspected degradation products after 4HPR amide hydrolysis, p-aminophenol, was not detected

in any sample (standard MS in (d)). The suspected retinoic acid derivative degradation products at given RT's 0.5, 0.9, 1.7, and 1.8 min are shown in (e) and their presence in samples indicated.

A2.4.3 FTIR analysis of 4HPR-acetone and 4HPR-PLGA interactions

Fourier-Transformed Infrared (FTIR) spectroscopy is useful to assess functional groups that exhibit asymmetrical stretching giving rise to a net change in dipole moment, and ultimately ionic interactions, and is due to absorption of light by vibrating molecules. Raman spectroscopy is useful to assess functional groups that exhibit symmetrical stretching, polarization, covalent interactions, and the principle guiding the detection of these interactions is due to scattering (elastic and inelastic, stokes shift) of light by the vibrating molecules. Coupled together, Raman and FTIR can be used in tandem to elucidate interactions. In both Raman and FTIR spectroscopy, molecular vibrations are influenced by neighboring atoms via vibronic coupling, potential energy surfaces, and masses of atoms.

It was suspected that interactions were occurring between PLGA, acetone, and 4HPR in the millicylinder (PLGA 503H + 20% 4HPR + 3% $MgCO_3$ using acetone as carrier solvent) leading to slow drug release. The results from the FTIR analysis are shown in Fig. 3 and a detailed peak assignment can be referenced in supplemental material Table S1. It should be noted that electron withdrawing groups can shift the frequency higher and conjugation shifts the frequency lower. It was suspected that protic polar acetone carrier solvent was a player in the chemistry occurring within these PLGA-4HPR films, yet it is also known that organic solvents can accelerate 4HPR's photo-degradation. In Fig. 3a, the FTIR of 4HPR solid is compared to that of 4HPR dissolved in acetone (which was allowed to evaporate prior to analysis). Acetone (characteristic ketone peak at 1709 and 1749 cm-1) altered 4HPR's (dry) spectra, and split 4HPR's carbonyl region peak from amide at 1630 cm-1 into 1606 and 1641 cm-1, indicating 4HPR and acetone's solvate interactions at 4HPR's carbonyl. This solvent effect on 4HPR is also

observed in the PLGA-4HPR-MgCO₃ acetone film when compared to the physical mixture (see Supplemental Table S1).

Next, the interactions between PLGA and 4HPR in the PLGA-4HPR-MgCO₃ acetone films were examined (Fig 3b). The MgCO₃ did not alter the spectra of the PLGA films (data not shown). The acid end-capped PLGA's characteristics FTIR peaks include C-H stretches at 2950 cm-1 and an intense C=O stretch at 1749 cm-1 from the carbonyls on lactic and glycolic acid monomers. PLGA does not contain any peaks in the 1600-1500 cm-1 region, where 4HPR has strong absorptions due to amide and ring bonds. 4HPR has characteristic peaks at 3500 and 3300 (N-H stretch, 2° amide), 1629 (C=O, strong, amide), 1575 (C=C ring stretch), 1543 and 1505 cm-1 (N-H bending). The most significant change in 4HPR's spectra in the presence of PLGA is the disappearance of peaks at 1311 and 1245 cm-1, corresponding to C-O from phenol or acyl C-O, suggesting that either 4HPR's phenolic group is interacting with PLGA. When examining 4HPR's characteristic 1500-1600 region in PLGA, we see slight blue shifts, potentially due to H-bonding. Also in the 4HPR-PLGA films, 4HPR's N-H stretching peaks at 3300, 3500 cm-1 are much less intense, possibly due to either dilution by PLGA matrix that masks this N-H bond, or due to hydrogen bonding between PLGA and/or acetone. 4HPR's effect on PLGA's FTIR spectra was examined (PLGA vs. 4HPR-PLGA) show identical traces, except in the aforementioned 1500-1600 range, indicating that PLGA structure was not altered by 4HPR. To conclude, the results from this FTIR analysis suggests that acetone interacts with 4HPR at its carbonyl group, and PLGA is interacting 4HPR's phenolic group. Further investigation into 4HPR's π-electron chemistry will be investigated by Raman spectroscopy in the following section.
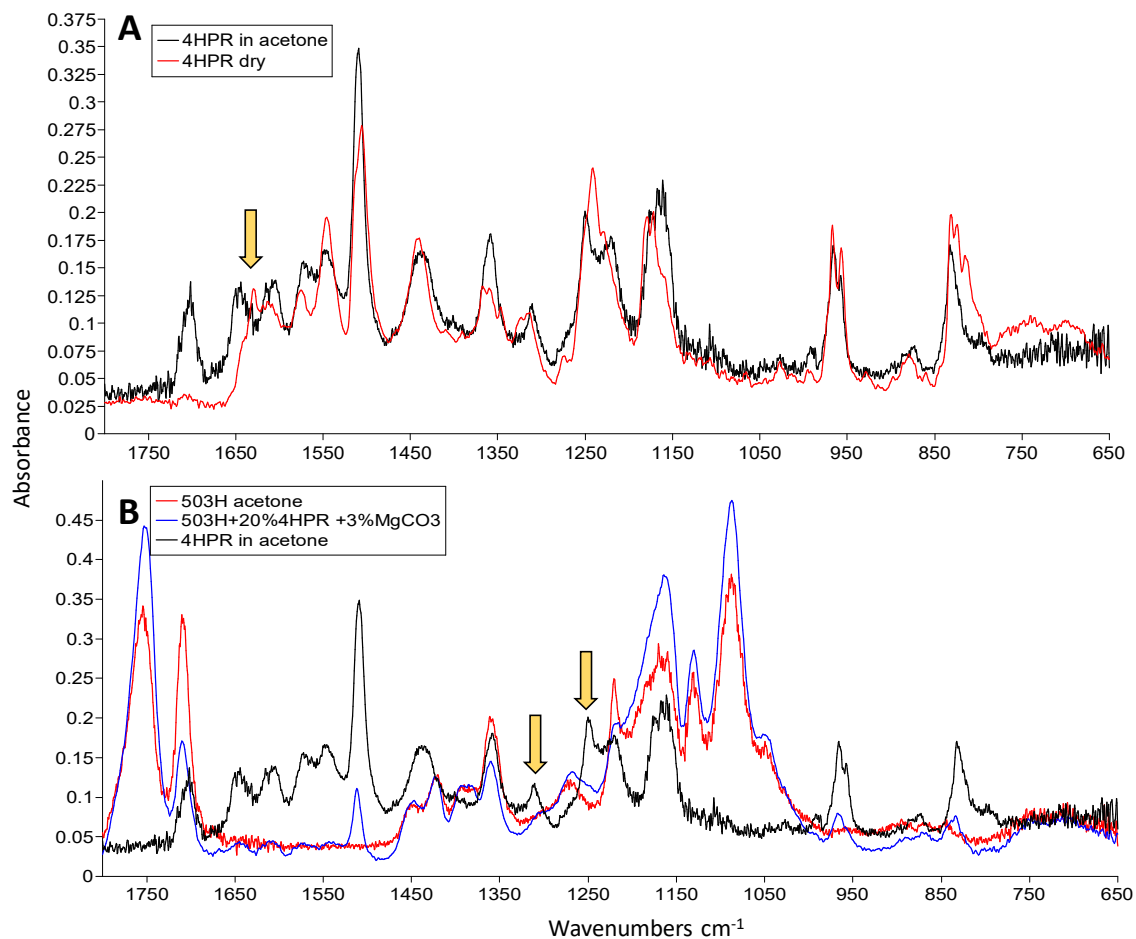
Figure A2- 3 FTIR spectra depicting carbonyl chemistry of 4HPR interactions with (a) acetone and (b) PLGA by comparing 4HPR spectra in acetone, PLGA 503H in acetone and PLGA 503H + 20% 4HPR+ 3% MgCO3 film in acetone. Spectral differences are noted with arrows.

A2.4.4 Raman Spectra show 4HPR's π-electrons not altered in PLGA matrix

Raman spectroscopy is a useful tool to measure π-π interactions between substances, due to the intensities of C=C bonds, and is often used in tandem with FTIR for structural elucidation. 4HPR's conjugated retinoid backbone contains a large cloud of π-electrons that could interact with PLGA. To test this, Raman spectra of both 4HPR and PLGA +20% 4HPR + 3% MgCO$_3$ film were compared as shown in Figure 4. There is no difference in the spectra, and therefore it can be concluded that 4HPR's backbone is not reactive toward neither PLGA nor magnesium ions.
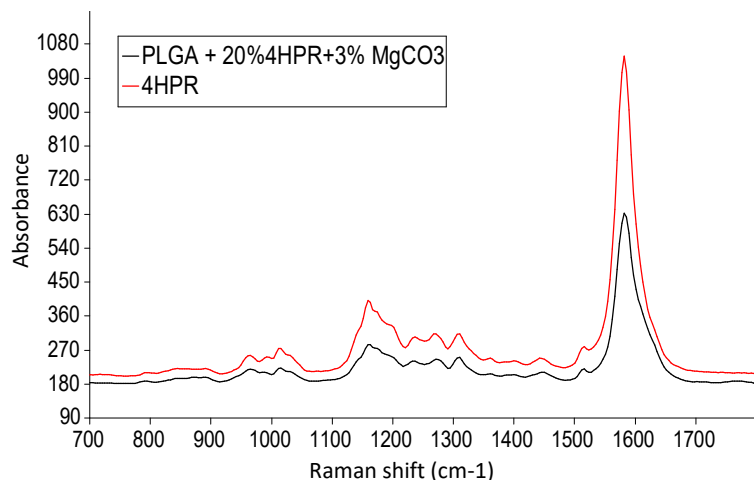
Figure A2- 4. Raman spectra of 4HPR (red) and PLGA +20% 4HPR + 3% MgCO$_3$ film (black) shows that 4HPR's conjugated π electrons are not interacting with PLGA.

A2.4.5 Microcalorimetric analysis reveals residual acetone trapped in PLGA millicylinder affects 4HPR release

As deduced from the FTIR analysis, the protic acetone solvent used during millicylinders preparation may have contributed to the drug-polymer interactions. TGA was used to measure the amount of residual acetone remaining in the PLGA-4HPR and PLGA millicylinders after drying. Melting thermograms (Fig.5 a-c, Table 2) show solvate entrapment within PLGA millicylinders, which could not escape until heated to 150 ˚C, well above acetone's boiling temperature, suggesting that acetone is either interacting with the millicylinder components, or the diffusion from bulk matrix is very slow. Here, all 4HPR (10,20,30%) PLGA + 3% MgCO$_3$ milliyclinders had residual solvent levels near 3-4%, while the no drug PLGA + 3% MgCO$_3$ millicylinder contained 5.8% residual solvent. Since both drug loaded and unloaded implants had similar levels of residual solvent, we suspect that acetone entrapment is likely due to its slow diffusion through the bulk PLGA millicylinder, rather than complexation with 4HPR-PLGA. Nonetheless, the presence of acetone in the implants may accelerate the drug degradation

process, and potentially alter the chemistry occurring within the bulk implant, or act as a polymer plasticizer.

It is known that the glass transition temperature (Tg) of a polymeric substance affects the drug release rate.[14], [15] The percent 4HPR release by day 28 was plotted as a function of the implant Tg for all of our PLGA 503H formulations (Fig. 5d), and found that more drug was released at lower Tgs. This can be attributed to greater mobility of polymer chains, which allows for faster drug diffusion through the polymer matrix. Also, we had suspected that residual acetone or water could be trapped inside millicylinder prior to the start of release study and may influence the Tg. We found that there was an exponential relationship between the percent of residual solvent in implant and the Tg, with greater solvent yielding lower Tg's (Fig. 5e). Although all implants were subject to the same drying methods, the differences in residual solvent level may be due to solvate formations with agents within the millicylinder.
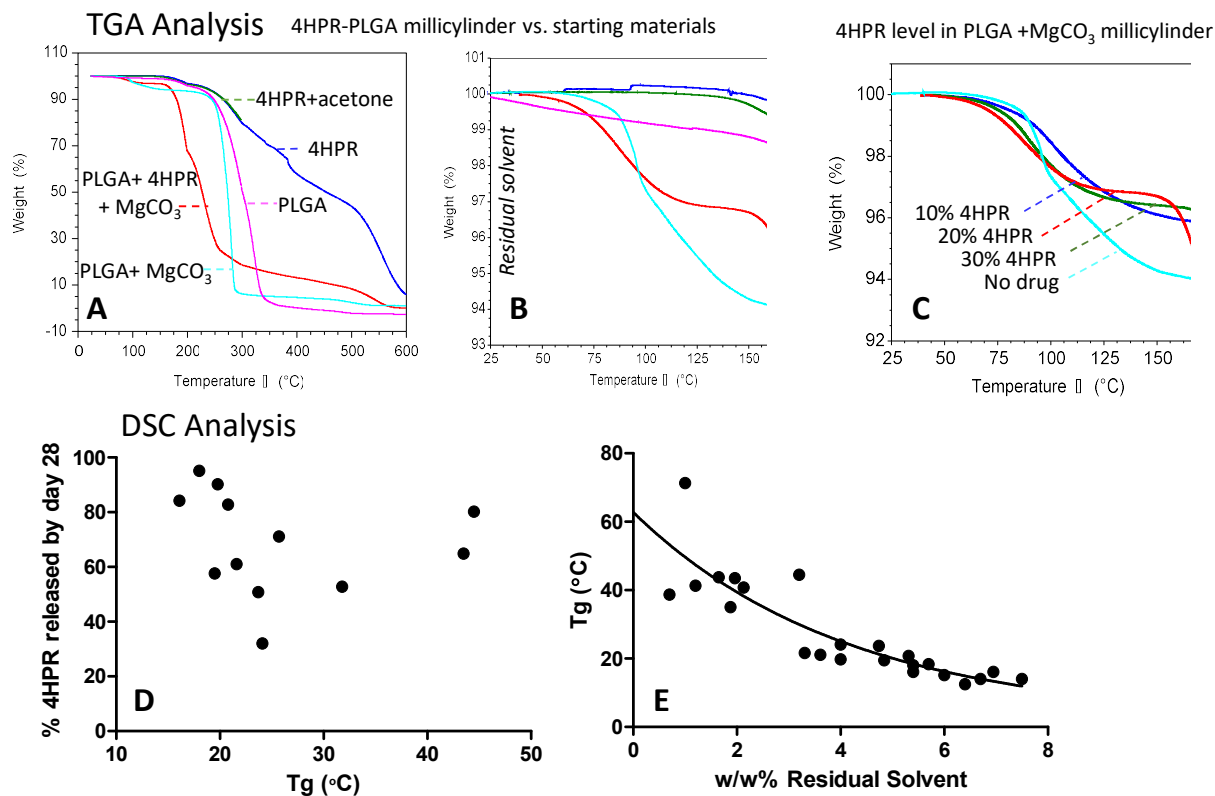
Figure A2- 5. Microcalorimetric measurements by TGA and DSC reveal effects of formulation variables on Tms and Tgs of 4HPR PLGA (503H) millicylinders containing 3% $MgCO_3$. A, b,c) TGA analysis of PLGA-4HPR millicylinders and starting materials depicting residual solvent entrapments, a) at full temperature range, b) zoomed into 25-175 °C for residual solvent determination, c) effect of 4HPR loading in PLGA implants on solvent entrapment. See Table 2 for mass loss weights at 150 °C. d,e) DSC data correlating the dependence of Tg of PLGA in millicylinder implants (which could contain up to 15% $MgCO_3$ and 20% NaDC and 10-30% 4HPR) with d) percent 4HPR released after 28 days *in vitro*, and e) The effect of residual solvent initially present in implants on Tg.

Table A2- 2. TGA analysis of 4HPR-PLGA millicylinders for residual solvent initially present

Compounds/ formulations	Weight % remain @150 °C	% Residual Solvent
4HPR	99.7	0.3
4HPR+acetone	99.9	0.1
PLGA	98.7	1.3
PLGA +3% $MgCO_3$ millicylinder	94.2	5.8
PLGA+ 10% 4HPR +3% $MgCO_3$ millicylinder	95.8	4.2
PLGA+ 20% 4HPR +3% $MgCO_3$ millicylinder	96.6	3.4
PLGA+ 30% 4HPR +3% $MgCO_3$ millicylinder	96.2	3.8

A2.4.6 Comprehensive Deductions of 4HPR Behavior in PLGA implants

In this paper, we have shown that 4HPR release from PLGA millicylinders is faster in presence of solubilizers, and that 4HPR does not appear to be altering PLGA erosion, but rather the magnesium ions from the basic $MgCO_3$ salt slow the erosion. PLGA is solubilizing and stabilizing 4HPR inside the millicylinder, yet once released into aqueous media 4HPR degrades by hydrolysis of the amide linkage into the retinoid backbone and phenol molecules. To tease out what may be catalyzing this degradation, we incubated 4HPR in solubilizing media in presence of various millicylinder components, and the UPLC analysis revealed that release from PLGA millicylinder, not acetone or other millicylinder components, was responsible for the degradation. Despite the presence of sink conditions, only 50% 4HPR released after 2 months, a release that is inconsistent with the typical PLGA 503H erosion patterns. To address this, we considered the potential interactions between 4HPR, 4HPR degradation products, acetone, $MgCO_3$, and PLGA. We have shown in the FTIR spectra that 4HPR's carbonyl region is altered in presence of acetone, indicating solvate-drug interactions near the amide bond. We also see differences in 4HPR's FTIR spectra in the presence of PLGA, namely the disappearance of peaks in the 1300 cm^{-1} region, likely due to interactions with 4HPR's phenol group and PLGA carboxyl groups. The Raman analysis revealed that 4HPR's π-electrons are not altered by PLGA. The microcalorimetric analysis showed that residual solvent (acetone or water) was trapped in the PLGA-4HPR millicylinder and this increased level of residual solvent increased its PLGA's Tg, leading to a greater amount of drug released after 28 days. Further chemical explanations proceed.

It is known that PLGA is subject to hydrolysis due to nuclephilic attack of water on the ester carbon, resulting in the formation of a primary alcohol and carboxylic acid[5]. Further explanations of PLGA autocatalysis and mechanisms of drug release can be referenced elsewhere[5, 16,17]. First, the most obvious reactive group is 4HPR's phenolic group, or its degradation product, 4-amino-phenol after hydrolysis of 4HPR's amide bond. This contains a nucleophilic hydroxyl group and a basic amino group, where in a neutral environment the amine is more reactive, while in both acidic and basic environment the hydroxyl is more reactive. Given that PLGA's microclimate pH is near 3.5^{18} the chemistry is more likely to occur with the hydroxyl group nucleophilic attack on PLGA's carboxylate group, as shown in Figure 8. The basic salt $MgCO_3$ may play a role in activating either 4HPR (pKa 9.75) or its amino-phenol's nucleophilic reactivity, by abstraction of the acidic hydrogen on the hydroxyl group. Yet in the FTIR spectra, $MgCO_3$ did not alter the spectra of the PLGA films indicating a chemical reaction had not occurred, yet ionic pairing could exist between PLGA's carboxylate groups and magnesium ions, as evident in Figure 1b, where elevated levels of $MgCO_3$ decreased PLGA erosion. To summarize these experimental outcomes to describe 4HPR's behavior in PLGA (depicted in Fig. 6):

- Incomplete 4HPR release from PLGA after 2 months indicate PLGA-4HPR interactions are more favorable than 4HPR's partition into a solubilizing tween micelle
- PLGA environment is acidic, and typical erosion pattern not affected by presence of 4HPR, but rather presence of the basic pore-forming salt $MgCO_3$.

- Indeed the PLGA polymer is stabilizing 4HPR, however, it degrades upon release into the aqueous media into retinoic acid isomerization products, which have lower affinity for PLGA than 4HPR.

- FTIR analysis revealed PLGA interacting with 4HPR carbonyl or phenol, as evident by disappearance of C-O peak, and blue shifts of 4HPR's amide region indicate hydrogen bonding with PLGA.

- Residual acetone solvent is trapped within PLGA-4HPR millicylinder prior to release studies, and greater levels lead to faster drug release likely due to plasticization of PLGA.

- This residual acetone solvent interacts with 4HPR's carbonyl via hydrogen bonding, as evident by FTIR, making it more electron withdrawing, further activating the hydrolysis of the amide bond.

- 4HPR's suspected degradation product, p-amino-phenol, is acting as nucleophile for PLGA hydrolysis and is also a driving force for 4HPR's amide hydrolysis. Lack of detection of p-amino-phenol in release media and presence of cleaved retinoic acid by-products confirms this premise.

Proposed Mechanism of 4HPR behavior after release from PLGA millicylinders
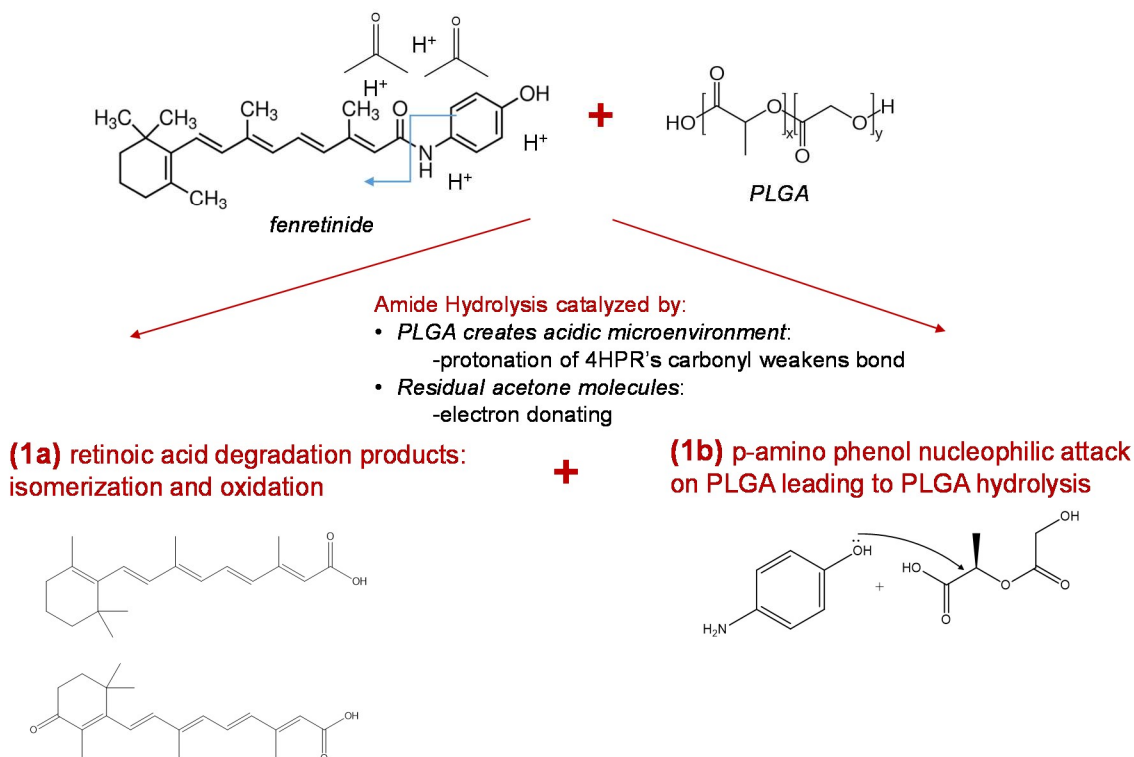
Figure A2- 6. Proposed mechanisms of 4HPR behavior within a PLGA polymer matrix in presence of acetone carrier solvent.

A2.5 Conclusion

We have utilized PLGA to formulate long-acting release depots to locally deliver 4HPR. The prolonged drug release *in vitro* (2+ months) in a solubilizing buffer was uncharacteristic of the selected PLGA's typical erosion pattern. The polymer was stabilizing 4HPR, however the drug release from the PLGA indicated degradation by LC-MS, and mass balance accounted for roughly 20% in the release media. Here we have elucidated 4HPR's interactions with PLGA similar to peptides' acylation reaction with PLGA, including hydrolysis of 4HPR's amide bond into retinoic acid isomerization products. Future work for utilizing the favorable PLGA polymer for controlled release 4HPR delivery may involve investigation of stability enhancement of

4HPR by inclusion of different salts, solvent systems, or increasing stability of amide bond by bioisosteres conversions.

Supplemental Information

Table A2- 3. FTIR Peak Assignments for 4HPR and 4HPR-PLGA Films

4HPR, solid		4HPR in acetone		PLGA 503H, in acetone		PLGA- 4HPR +3% MgCO₃ Films		PLGA- 4HPR +3% MgCO₃ Physical Mixture		Acetone	
cm-1	Assignment	cm-1	Assignment	cm-1	Assignment	cm-1	Assignment	cm-1	Assignment	cm-1	Assign.
3500, 3200	N-H stretch, amide, 2 indicates 1° amine	Same as solid, except where noted								3414	O-H stretch
										3005	
2930	C-H Stretch (alkane)			2998	C-H stretch (alkane)	2950	C-H stretch (alkane)	2952	C-H stretch	2966, 2926	C-H stretch
								2360			
						2161		2161			
				1749, 1709	C=O stretch, Carboxylic acids	1749, 1709	C=O stretch,	None at 1709, therefore this is from acetone		1749	
										1709	
		1709									
1629	C=O, amide	1641	Acetone is splitting			1641	C=O, amide	1652			
		1606				1606	N-H Bend, 1° amines	Doesn't split in physical mix			
1575	C=C stretch, amide					1571	C=C stretch, amide	1576			

1546	N-H bend, amide				1541	N-H bend	1557	
1505	N-H bend, amide				1511 blue shift	N-H bend, amide	1505	
1440	-C-C stretch (in ring), aromatics		1421	C-C stretch (in ring), aromatics, or C-H bend, alkanes	1421	C-C stretch (in ring), aromatics, or C-H bend, alkanes	1422	1434
1367	C-H rock, Alkanes		1384, 1361	C-H rock, alkanes	1384, 1361	C-H rock, alkanes	1393	1363
1313	C-O, phenol, or acyl	Absent	Absent			Absent	Absent	
1241	C-O stretch (ROH, COOH	Absent	Absent			Absent	Absent	1223
1172	COOR, COR)		1269 1163 1130	C-O stretch (ROH, COOH, COOR, or COR)	1269 1163 1130	C-O stretch (ROH, COOH, COOR, or COR)	1167 1128	
			1086		1083		1083	1093
967 956	=C-H bend (alkenes)						968	
831			867		867		832	903
740	C-H Rock (alkanes)		712	C-H Rock (alkanes)	712	C-H Rock (alkanes)	714	
								531

A2.6 References

1. (a) Desai, K. G.; Mallery, S. R.; Holpuch, A. S.; Schwendeman, S. P., Development and in vitro-in vivo evaluation of fenretinide-loaded oral mucoadhesive patches for site-specific chemoprevention of oral cancer. *Pharm Res* 2011, *28* (10), 2599-609; (b) Chiesa, F.; Tradati, N.; Grigolato, R.; Boracchi, P.; Biganzoli, E.; Crose, N.; Cavadini, E.; Formelli, F.; Costa, L.; Giardini, R.; Zurrida, S.; Costa, A.; De Palo, G.; Veronesi, U., Randomized trial of fenretinide (4-HPR) to prevent recurrences, new localizations and carcinomas in patients operated on for oral leukoplakia: Long-term results. *International Journal of Cancer* 2005, *115* (4), 625-629; (c) Tradati, N.; Chiesa, F.; Rossi, N.; Grigolato, R.; Formelli, F.; Costa, A.; de Palo, G., Successful topical treatment of oral lichen planus and leukoplakias with fenretinide (4-HPR). *Cancer letters* 1994, *76* (2-3), 109-11.
2. Kiser, P. D.; Golczak, M.; Palczewski, K., Chemistry of the Retinoid (Visual) Cycle. *Chemical Reviews* 2014, *114* (1), 194-232.
3. Shenderova, A.; Burke, T. G.; Schwendeman, S. P., The acidic microclimate in poly(lactide-co-glycolide) microspheres stabilizes camptothecins. *Pharm Res* 1999, *16* (2), 241-8.
4. Sophocleous, A. M.; Desai, K.-G. H.; Mazzara, J. M.; Tong, L.; Cheng, J.-X.; Olsen, K. F.; Schwendeman, S. P., The nature of peptide interactions with acid end-group PLGAs and facile aqueous-based microencapsulation of therapeutic peptides. *Journal of Controlled Release* 2013, *172* (3), 662-670.
5. Houchin, M. L.; Topp, E. M., Chemical Degradation of Peptides and Proteins in PLGA: A Review of Reactions and Mechanisms. *Journal of Pharmaceutical Sciences* 2008, *97* (7), 2395-2404.
6. Sophocleous, A. M.; Zhang, Y.; Schwendeman, S. P., A new class of inhibitors of peptide sorption and acylation in PLGA. *Journal of controlled release : official journal of the Controlled Release Society* 2009, *137* (3), 179-84.
7. Zhang, Y.; Sophocleous, A. M.; Schwendeman, S. P., Inhibition of peptide acylation in PLGA microspheres with water-soluble divalent cationic salts. *Pharm Res* 2009, *26* (8), 1986-94.
8. Wischke, C.; Zhang, Y.; Mittal, S.; Schwendeman, S. P., Development of PLGA-based injectable delivery systems for hydrophobic fenretinide. *Pharm Res* 2010, *27* (10), 2063-74.
9. Hirota, K.; Doty, A. C.; Ackermann, R.; Zhou, J.; Olsen, K. F.; Feng, M. R.; Wang, Y.; Choi, S.; Qu, W.; Schwendeman, A. S.; Schwendeman, S. P., Characterizing release mechanisms of leuprolide acetate-loaded PLGA microspheres for IVIVC development I: In vitro evaluation. *Journal of Controlled Release* 2016, *244, Part B*, 302-313.
10. Kang, J.; Schwendeman, S. P., Comparison of the effects of Mg(OH)2 and sucrose on the stability of bovine serum albumin encapsulated in injectable poly(d,l-lactide-co-glycolide) implants. *Biomaterials* 2002, *23* (1), 239-245.
11. Desai, K. G. H.; Mallery, S. R.; Schwendeman, S. P., Effect of formulation parameters on 2-methoxyestradiol release from injectable cylindrical poly(dl-lactide-co-glycolide) implants. *European Journal of Pharmaceutics and Biopharmaceutics* 2008, *70* (1), 187-198.
12. Cooper, J. P. Fenretinide Metabolism in Humans and Mice: Utilizing Pharmacologic Modulation of its Metabolic Pathways to Increase Systemic Exposure. Texas Tech University, Lubbock, TC, 2014.

13. Bempong, D. K.; Honigberg, I. L.; Meltzer, N. M., Normal phase LC-MS determination of retinoic acid degradation products. *Journal of Pharmaceutical and Biomedical Analysis* 1995, *13* (3), 285-291.
14. Alhnan, M. A.; Basit, A. W., In-process crystallization of acidic drugs in acrylic microparticle systems: influence of physical factors and drug-polymer interactions. *J Pharm Sci* 2011, *100* (8), 3284-93.
15. Yao, J.; Shi, N. Q.; Wang, X. L., [The development of co-amorphous drug systems]. *Yao xue xue bao = Acta pharmaceutica Sinica* 2013, *48* (5), 648-54.
16. Fredenberg, S.; Wahlgren, M.; Reslow, M.; Axelsson, A., The mechanisms of drug release in poly(lactic-co-glycolic acid)-based drug delivery systems—A review. *International Journal of Pharmaceutics* 2011, *415* (1–2), 34-52.
17. Ford Versypt, A. N.; Pack, D. W.; Braatz, R. D., Mathematical modeling of drug delivery from autocatalytically degradable PLGA microspheres — A review. *Journal of Controlled Release* 2013, *165* (1), 29-37.
18. Liu, Y.; Schwendeman, S. P., Mapping microclimate pH distribution inside protein-encapsulated PLGA microspheres using confocal laser scanning microscopy. *Molecular Pharmaceutics* 2012, *9* (5), 10.1021/mp200608y.